



Accessing the metabolic potential of *Pseudomonas putida* through dedicated synthetic biology tools

Kozaeva, Ekaterina

Publication date:
2021

Document Version
Publisher's PDF, also known as Version of record

[Link back to DTU Orbit](#)

Citation (APA):
Kozaeva, E. (2021). *Accessing the metabolic potential of Pseudomonas putida through dedicated synthetic biology tools*. Technical University of Denmark.

General rights

Copyright and moral rights for the publications made accessible in the public portal are retained by the authors and/or other copyright owners and it is a condition of accessing publications that users recognise and abide by the legal requirements associated with these rights.

- Users may download and print one copy of any publication from the public portal for the purpose of private study or research.
- You may not further distribute the material or use it for any profit-making activity or commercial gain
- You may freely distribute the URL identifying the publication in the public portal

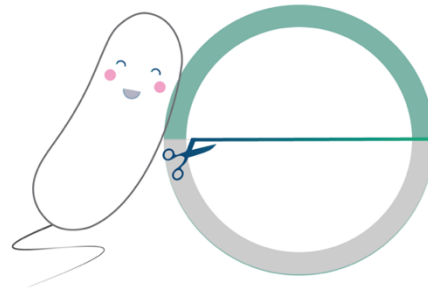
If you believe that this document breaches copyright please contact us providing details, and we will remove access to the work immediately and investigate your claim.



Accessing the metabolic potential of *Pseudomonas putida* through dedicated synthetic biology tools

Ph.D. Thesis

Ekaterina Kozaeva



The Novo Nordisk Foundation Center for Biosustainability
Technical University of Denmark

November 2021

Accessing the metabolic potential of *Pseudomonas putida* through
dedicated synthetic biology tools

Ph.D. thesis written by Ekaterina Kozaeva

Supervised by Senior Researcher & Group Leader Pablo Iván Nickel

© **PhD Thesis 2021 Ekaterina Kozaeva**
Novo Nordisk Center for Biosustainability
Technical University of Denmark
All rights reserved



**Technical
University of
Denmark**

Dedicated to my grandparents

Посвящается
моим дорогим и самым
вдохновляющим людям:
Залыгиной Дине Андреевне
Гучмазовой Екатерине Ильиничне
И светлой памяти
Козаева Авксентия Ильича

Science is made up of imaginations
that ran wild and dreamed magical things
that actually became achievable.

— L. A. Jones, *Professional troublemaker*

Controls are the best friends of a researcher.
Sometimes they confirm your beliefs,
sometimes they tell you an inconvenient truth,
but there is no science without controls.

— M. J. Nieto-Domínguez, *Benchling notes*

PREFACE

This thesis is written as partial fulfillment of the requirements to obtain a Ph.D. degree at the Technical University of Denmark. The work presented in this thesis was carried out between September 2018 and November 2021 at the Novo Nordisk Foundation Center for Biosustainability at the Technical University of Denmark, Kongens Lyngby, Denmark. The work was supervised by Senior Researcher & Group Leader Pablo Iván Nikel and funding was provided by the Novo Nordisk Foundation through the Copenhagen Bioscience Ph.D. Programme, grant no. NNF16CC0020908.



Ekaterina Kozaeva
Kgs. Lyngby, November 2021



The Ph.D. thesis was evaluated by:

Professor Víctor de Lorenzo¹

Professor Claudia Vickers²

Senior Researcher Michael Krogh Jensen³

¹ Systems and Synthetic Biology Department, Centro Nacional de Biotecnología (CNB-CSIC), Madrid, Spain.

² CSIRO Future Science Platform in Synthetic Biology, Commonwealth Scientific and Industrial Research Organisation (CSIRO), Queensland, Australia.

³ Novo Nordisk Foundation Center for Biosustainability, Technical University of Denmark, Kgs. Lyngby, Denmark

ABSTRACT

Current chemical production processes rely almost exclusively on nonrenewable, fossil resources, resulting in environmental challenges, such as global warming, pollution, and a decrease of biological diversity. Thus, establishing sustainable alternatives to oil-based manufacturing is critical to mediate a green transition towards sustainability. Recent scientific advances within genetic engineering, DNA sequencing, and gene, genome manipulation opened up new avenues towards green manufacturing in the form of cell factories. Every living cell can be represented as a miniature factory, where various molecular machines orchestrate chemical processes. By rewiring microbial metabolism, we can establish cell factories for sustainable synthesis of chemicals, fuels and materials from renewable resources. The soil bacterium *Pseudomonas putida* continues to gain increased attention as a host for bioproduction due to its remarkable capacity to handle chemical stress and perform well under harsh operating conditions.

This Ph.D. thesis aims to exploit these features of *P. putida* for bioproduction through implementation of a dedicated CRISPR-based synthetic biology toolset. Approaches for genome editing, counter-selection, gene-silencing and base-editing were designed, established *in vivo*, and characterized. This toolbox was implemented to assist bioproduction in *P. putida*. Hence, central metabolism was rewired to establish biosynthesis of desired products by combined genome modifications, integration of heterologous pathways, and engineered cell morphology. In particular, strains with increased acetyl-coenzyme A availability – key precursor for a variety of added-value compounds, showed increased accumulation of the biopolymer poly(3-hydroxybutyrate). Moreover, platform strains for production of methyl-ketones were established, and the potential of chromosome-free cell systems was demonstrated. This synthetic biology toolset facilitates engineering efforts of Pseudomonads, taking us a step closer to economically-competitive, bio-based production processes.

DANSK RESUME

Nuværende kemiske produktionsprocesser er næsten udelukkende afhængige af ikke-vedvarende, fossile ressourcer, hvilket resulterer i miljømæssige udfordringer, såsom global opvarmning, forurening og et fald i biologisk mangfoldighed. Hvorfor etablering af bæredygtige alternativer til oliebaseret produktion er afgørende for at frembringe en grøn omstilling til bæredygtighed. Nye videnskabelige fremskridt inden for genteknologi, DNA-sekventering og gen- og genom manipulation åbnede nye veje for grøn fremstilling i form af cellefabrikker. Hver levende celle kan repræsentere en miniaturefabrik, hvor forskellige molekylære maskiner orkestrerer kemiske processer. Ved at ændre i den mikrobiel metabolisme kan vi etablere cellefabrikker som kan udføre bæredygtig syntese af kemikalier, brændstoffer og materialer fra vedvarende ressourcer. Jordbakterien *Pseudomonas putida* vinder fortsat øget opmærksomhed som vært for bioproduktion på grund af dens bemærkelsesværdige evne til at håndtere kemisk stress og præstere godt under barske forhold.

Denne Ph.D. afhandling har til formål at udnytte *P. putidas* egenskaber til bioproduktion gennem implementering af et dedikeret CRISPR-baseret syntetisk biologisk værktøjssæt. Redskaber til genom-redigering, mod-selektion, gen-dæmpning og base-redigering blev designet, etableret *in vivo* og karakteriseret. Denne værktøjsskabe blev implementeret for at hjælpe bioproduktion i *P. putida*. Derfor blev den centrale metabolisme omdannet for at facilitere målrettet biosyntese af produkter ved at kombinere genom modifikationer, integration af heterologe reaktionsveje og rekonstrueret cellemorfologi. Især stammer med øget acetyl-coenzym A tilgængelighed – en nøgleprecursor for en række værditilvækstende komponenter – viste øget lagring af biopolymeren poly(3-hydroxybutyrat). Desuden blev platformstammer til produktion af metylketoner etableret, og potentialet for kromosomfrie celledsystemer blev demonstreret. Dette syntetisk biologiske værktøjssæt leder den tekniske indsats for Pseudomonader og tager os et skridt tættere på økonomisk konkurrencedygtige, biobaserede produktionsprocesser.

ACKNOWLEDGEMENTS

Since I was a kid, I have loved reading books. Best ones were those including adventures and hopefully a bit of magic. At night you could have found me hiding under the blanket with a flashlight diving in the world created by beloved S. L. Clemens, J. G. London, J. K. Rowling, and J. R. Tolkien. But the greatest adventure I had experienced, with a bit of magic of course, was my Ph.D. journey. How grateful I am to be at the stage of writing the acknowledgements section already. It feels thrilling to complete this part of my life, shared with a number of fantastic people. So, let me start!

First of all I would like to thank Copenhagen Bioscience Ph.D. Programme: for giving me the ticket for this ride, for choosing me among hundreds of other talented candidates, for supporting me during these years and for building up a beautiful community of young scientists within several NNF Centers. My special gratitude goes to the program coordinators Amelia and Moreno; selection committee members: Morten Nørholm and Michael K. Jensen; and the student community: Daria, David, Jenny, Jan, Alex, Denis, Sveta, Petar, Nicole, Bettina, Anja, Philip, Sam, and many others.

And for the part of my Ph.D. which truly felt as if a family adapted me like their own, I would like to thank my supervisor Pablo. Your passion for science is truly exceptional and inspiring. Thank you for enlightening talks, for troubleshooting sessions, but also for every question you asked about the Russian ballet and cuisine. Thank you for panettone every Christmas. Thank you for providing me with independence and intellectual freedom. Thank you for the warm environment you have created in the SEM group.

As for my labmates, SEMsters, how lucky I am meeting those amazing people and sharing these 4 years. I am truly thankful to every past and present member of the group! You are wonderful human beings. And let me just mention some of those, who played crucial role in my progress and happiness. Thank you to the role model of my first years, Patricia, for bringing so much joy and light in the group, for answering my every single question, for always making time and being ready to help. Thank you, Nicolas Wirth, for being a good and supportive friend and inspiring

passionate colleague, I truly admire your talent and grateful for being able to work by your side. Thank you, Antonin, for being always there for me, for always offering help, for inspiring Illustrator skills. Thank you for sharing stories about random facts, for being calm, positive and making me laugh so many times. Thank you, Justine, for sharing everything with me. Thank you for amazing experience of working together, you are the most caring, responsible and bright scientist. Thank you for making me fall in love with champagne, for bringing a lot of fun not only in the lab but also outside. I am also thankful to your family, for sharing your childhood memories and experiencing true French village adventure. Thank you, Manuel, for literally carrying my mental health through the last several months of Ph.D., for helping out with experiments and taking over my project to answer that last question I dreamt of. Thank you for working 12 hours a day and answering my texts midnight, thank you for running extra mile to make things happen. Thank you for being a great friend and a truly good person.

For making a lot of my days brighter in the lab and during the lunch breaks thank you to Rob, Carlos, Nico G, Nico K, and Alberto.

I am also grateful to Daniel for my rotation experience, as well as to labs of Morten Sommer (thanks to Ruben and Mareike) and Alex Nielsen (thanks to Hemanshu and Jenny). To Alex, as my cosupervisor, I am especially thankful for being on my side and those kind words which made me going on. It was always a pleasure to talk to you, to be guided by you and to feel your support!

I would like to thank some other talented scientists who happened to be my friends during these years. Thank you, Max, for salsa dancing, for Werevolves, for Alicante and all those jokes. Thank you, Sara, for cheering me up, strawberries and a little piece of Portugal in Denmark. Thank you to Nick, you are so much fun, and sorry for being a bit mean to your model. Thank you, Jasper, for being a phantom of the opera, for making the best summer house trip, for singing Ekaterina in my office, for many more things we shared together. Thank you Niko for your support, for being grumpy sometimes, for the Oktoberfest, for making things happen, for the couch welcome box and the best carbonara. Thank you Viviënne for being so cheerful, for your driving skills, for Georgian food and some great Dutch experience. Thank you Bram for being always so welcoming, politically correct, supportive and for 15 minLeffe.

Thank you to Chris for the CRISPR inspiration, piano and jazz, for 28th floor experience. Thank you Arrate for sharing the room together and telling me legends of the Busque country. And cheers to the Ph.D. Club!

Thank you to my dear friends from back home: Tania, you have been there daily, I am so grateful. Julia, Ivan, thank you for staying always by my side. Thank you for visiting me in Denmark and sharing this journey together. You were with me at every moment I needed no matter the distance. Rita and Anastasia, all the fun we shared together during my first years here and having you in my life is fantastic.

It is hard to describe how much the distance feels like when you are apart from your family. It is harder to describe how truly grateful I am to my parents for always believing in me. Спасибо моим родителям за любовь, поддержку и поощрение самостоятельности. Сколько я себя помню, вы всегда были уверены в моих силах. Я всегда чувствую, что вы рядом. Вы самые лучшие. Thank you!

And I would like to thank Denmark, and Mikkell as its beautiful representation, for being the most welcoming, caring and hyggelig. Thank you for making my life bright even in the dark days. Thank you for the walks by the seaside and the countryside roads, for the Julecalendar and pebernodder, thank you for the feeling of home.

And some great closing is needed here, but I would be happy to submit this beautiful thesis in 10 min, so maybe let's leave it here as it is.

PUBLICATIONS

- I. Nicolas T. Wirth, Ekaterina Kozaeva, and Pablo I. Nickel. Accelerated genome engineering of *Pseudomonas putida* by I-SceI-mediated recombination and CRISPR-Cas9 counterselection. *Microbial Biotechnology* (2020) 13(1): 233-249.
- II. Ekaterina Kozaeva[§], Christos Batianis[§], Stamatios G. Dalamas[§], Maria M. Pascual, Daniel C. Volke, Pablo I. Nickel, Vitor A. P. Martins dos Santos. An expanded CRISPRi toolbox for tunable control of gene expression in *Pseudomonas putida*. *Microbial Biotechnology* (2020) 13(2): 368-385.
- III. Ekaterina Kozaeva, Zacharias S. Nielsen, and Pablo I. Nickel. pAblo pCasso vectors for unconstrained CRISPR-SpRY cytidine and adenosine base-editing and self-curing in *Pseudomonas putida*. *Manuscript in preparation*.
- IV. Ekaterina Kozaeva, Svetlana Volkova, Marta R. A. Matos, Mariela P. Mezzina, Tune Wulff, Daniel C. Volke, Lars K. Nielsen, and Pablo I. Nickel. Model-guided dynamic control of essential metabolic nodes boosts acetyl-coenzyme A-dependent bioproduction in rewired *Pseudomonas putida*. *Metabolic Engineering* (2021) 67: 373-386.
- V. Ekaterina Kozaeva, Kent K. T. Yang, and Pablo I. Nickel. Pathway and morphology engineering towards 2-pentanone biosynthesis in whole- and mini-cells of *Pseudomonas putida*. *Manuscript in preparation*.
- VI. Ekaterina Kozaeva[§], Viviënne Mol[§], Pablo I. Nickel, and Alex T. Nielsen. High-throughput colorimetric assays optimized for ketone and aldehyde detection produced by microbial cell factories. *Manuscript in preparation*.

[§] These authors contributed equally.

Publications not included in this thesis

- I. Ekaterina Kozaeva[§], Manuel J. Nieto-Domínguez[§], Abril D. Hernández, Kasper Enemark-Rasmussen, and Pablo I. Nickel. Mechanistic insights of enzymatic dehalogenation during fluorinated biocatalysis. **Manuscript in preparation.**
- II. Daniel C. Volke[§], Román A. Martino[§], Ekaterina Kozaeva, Andrea Smania, and Pablo I. Nickel. Modular (de)construction of complex bacterial phenotypes by CRISPR-nCas9–assisted, multiplex cytosine editing. **Manuscript in preparation.**
- III. Nora Lisa Bitzenhofer, Luzie Kruse, Stephan Thies, Benedikt Wynands, Thorsten Lechtenberg, Jakob Rönitz, Ekaterina Kozaeva, Nicolas T. Wirth, Christian Eberlein, Karl-Erich Jaeger, Pablo I. Nickel, Hermann J. Heipieper, Nick Wierckx, and Anita Loeschcke. Towards robust *Pseudomonas* cell factories to harbour novel biosynthetic pathways. *Essays in Biochemistry*. (2021) 65(2): 319-336.

[§] These authors contributed equally.

Patents not included in this thesis

- I. Justine Turlin, Ekaterina Kozaeva, Pablo I. Nickel. (2021). Engineering C1-dependent growth in *Pseudomonas putida* and chemical production. **Patent in preparation.**

CONTENT

Preface	V
Abstract	VII
Dansk resume	VIII
Acknowledgements	IX
Publications	XII
Content	1
PhD thesis outline	2
Chapter 1 Towards Sustainable Revolution: current advances in cell factory engineering	5
Chapter 2 Genome engineering of <i>Pseudomonas putida</i> using homologous recombination assisted by CRISPR-Cas9 counterselection.	35
Chapter 3 An expanded CRISPRi toolbox for tunable control of gene expression in <i>Pseudomonas putida</i> .	80
Chapter 4 Unconstrained CRISPR-editing: cytidine and adenosine base-substitution under conditional replication.	127
Chapter 5 Model-guided dynamic CRISPRi control boosts bioproduction in rewired <i>Pseudomonas putida</i> strains.	159
Chapter 6 Pathway and morphology engineering towards 2-pentanone biosynthesis in whole- and mini-cells.	263
Chapter 7 High-throughput colorimetric assays optimized for ketone and aldehyde detection produced by microbial cell factories.	292
Conclusions and outlook	316
Appendix: Co-authorship declarations	320

PHD THESIS OUTLINE

Since the Industrial Revolution in XVIII century, antropogenic influence took a heavy toll on the environment, with consequences lasting through the century and beyond. In XXI, our planet craves for the Sustainable Revolution, reducing the climate impact that fossil fuel usage has had, and providing sustainable solutions for our industrial needs. Bio-based manufacturing of chemicals and fuels using microbial cell factories could provide an alternative to petroleum-derived industry.

A multibillion dollar industry already exists making various compounds of interest (including drugs, probiotics, fertilizers, and textiles) with engineered cells. Although a number of bioprocesses have been established thus far, some limitations are still to be addressed in cell factories to become economically-competitive. Among these, the existing conversion technologies, lack of political incentives, and high costs compared to oil-based production constitute the main hurdles to solve. To improve economic feasibility of bio-based production, scientists around the world work on expanding the knowledge on the mechanisms ruling metabolism and strain engineering, developing more robust and streamlined methods for cell manipulation. Synthetic biology and metabolic engineering advances continue to provide approaches to establish green manufacturing, while decreasing the cost of the strain development processes, enforcing the blossoming of Sustainable Revolution.

The aim of this Ph.D. thesis is to develop synthetic biology tools that can be used to unleash the metabolic potential of the Gram-negative, non-pathogenic bacterium *Pseudomonas putida* as a superior cell factory for bioproduction. The developed approaches are deployed to ease genome manipulations in environmental bacteria, helping to improve bio-based chemical synthesis, and providing insights on engineering metabolism. On this background, the thesis is divided in the following seven chapters.

Chapter 1 provides a general introduction to bio-based manufacturing by microbial cell factories and synthetic biology tools used to construct them. The chapter comprises an overview of *P. putida* as a

bioproduction *chassis*, including specifics about the host metabolism followed by a discussion of metabolic engineering principles, and highlighting the development and application of CRISPR approaches for microbial biotechnology.

Chapter 2 describes a genome-engineering approach for *P. putida* based on I-*Sce*I-mediated recombination assisted by CRISPR-Cas9 counterselection. Guidelines presented in this chapter ease genome manipulation and allow to generate insertions, gene deletions or any desirable exchange of genetic parts in the chromosome. The mechanism is based on DNA recombination forced by double-stranded DNA cuts (by the I-*Sce*I endonuclease) followed by highly efficient CRISPR-Cas9 mediated counterselection of mutants. Optimized workflow is demonstrated in action by deleting selected genes and integrating fluorescent reporter genes in the chromosome of *P. putida* KT2440.

Chapter 3 presents an expanded CRISPRi toolbox for tunable control of gene expression in *P. putida*. This system relies on a single-plasmid CRISPR-interference (CRISPRi), and enables tunable, tightly controlled gene repression of chromosomally-expressed genes encoding fluorescent proteins, either individually or simultaneously. Additionally, this method allows for suppressing the expression of the essential genes, resulting in significantly low growth rates or morphological changes. This versatile system expands the capabilities of the current CRISPRi toolbox for efficient, targeted and controllable manipulation of gene expression.

Chapter 4 describes unconstrained CRISPR-editing in *P. putida* via cytidine and adenine base-substitution. Different base-editing systems were adapted to establish plasmid-borne, efficient nucleotide substitution using a novel protospacer adjustment motif (PAM)-relaxed nCas9 variant, which makes the vast majority of the bacterial genome targetable by this technology. In addition, a set of induction-dependent, self-curing vectors was created to enable efficient curing of the plasmids. Presented strategy eases complex strain engineering, making quick and easy base-editing and gene manipulation possible.

Chapter 5 shows an example of application of the tools developed, by demonstrating how model-guided dynamic CRISPRi control boosts acetyl-CoA-dependent bioproduction in rewired *P. putida* strains. Dynamic CRISPRi gene expression of key targets mediated an increase in the acetyl-CoA content of engineered strains, allowing for improved poly(3-hydroxybutyrate) production. By manipulating the cell morphology of these engineered strains, biopolymer accumulation was further improved, and proved to be consistent in bioreactor cultures. This strategy of rationally redirecting metabolic fluxes in the central metabolism of *P. putida* towards product biosynthesis-especially is relevant when deletion of essential pathways is not an option.

Chapter 6 describes sustainable alternatives to methyl ketone synthesis, by demonstrating pathway and morphology engineering towards 2-pentanone production in whole- and mini-cells. Using CRISPR-approaches previously developed in the thesis, we engineered *P. putida* to produce chromosome-free, catalytically active mini-cells that retained the ability to produce 2-pentanone with stable yields. This underscores the value of *P. putida* as host for biosynthesis of ketones, illustrating how the combined engineering of pathways and synthetic morphologies enables stable production phenotypes in bacterial cell factories.

Chapter 7 highlights the development and application of high-throughput colorimetric assays optimized for ketone and aldehyde detection produced by microbial cell factories. To further improve microbial cell factory performance, strain and pathway engineering is critical, demanding the development of high-throughput screening and selection systems. Such assays were applied to analyze acetone production in an engineered *Escherichia coli* MG1655 strain. The proposed fast, colorimetric assays may allow iterative rounds of (automated) randomized strain and pathway mutagenesis and screening, to facilitate further improvement of production titers for the industrially relevant chemical class of ketones and aldehydes through microbial cell factories.

INTRODUCTION

Chapter 1

Towards Sustainable Revolution: Current advances in cell factory engineering

A tiny microbe is capable to do fascinating inventions: from changing the Earth's atmosphere millions of years ago to sparkling wines nowadays. In 1991, a discipline of refining those living organisms to produce desired products, called *metabolic engineering*¹, was defined. Here, metabolic fluxes are redirected towards formation of a specific product. Over more than 30 years of rapid development, the capability of green manufacturing was illustrated by bioproduction examples of hundreds of different chemicals from renewable raw materials^{2,3}.

Current chemical processes, however, continue to rely almost exclusively on non-renewable fossil feedstock and an oil-dependent industry, resulting in environmental challenges, including global warming, pollution, and a rapid decrease of biological diversity⁴. Exploring alternative sustainable processes and their immediate application is one way to tackle these problems. Compared to traditional oil-derived manufacturing methods, biotechnological production reduces greenhouse gases emission and environmental pollution, allows waste recycling, and often results in biodegradable chemicals⁵⁻⁷ (**Figure 1.1.**). Implementing solid biorefinery strategies for production helps establishing a sustainable circular bioeconomy and allowing for a responsible utilization of biological materials by reducing the load on non-renewable resources⁶.

To achieve green manufacturing via biological production, it is essential to expand the biochemical repertoire of living organisms. Recent advances in the fields of omics⁸, genome-scale metabolic modelling⁹⁻¹¹, automation¹², and genetic engineering assisted by evolution¹³ have expanded the tools and strategies of metabolic engineering, enabling increasingly massive systematic engineering² of microbes toward achieving their outstanding performances.

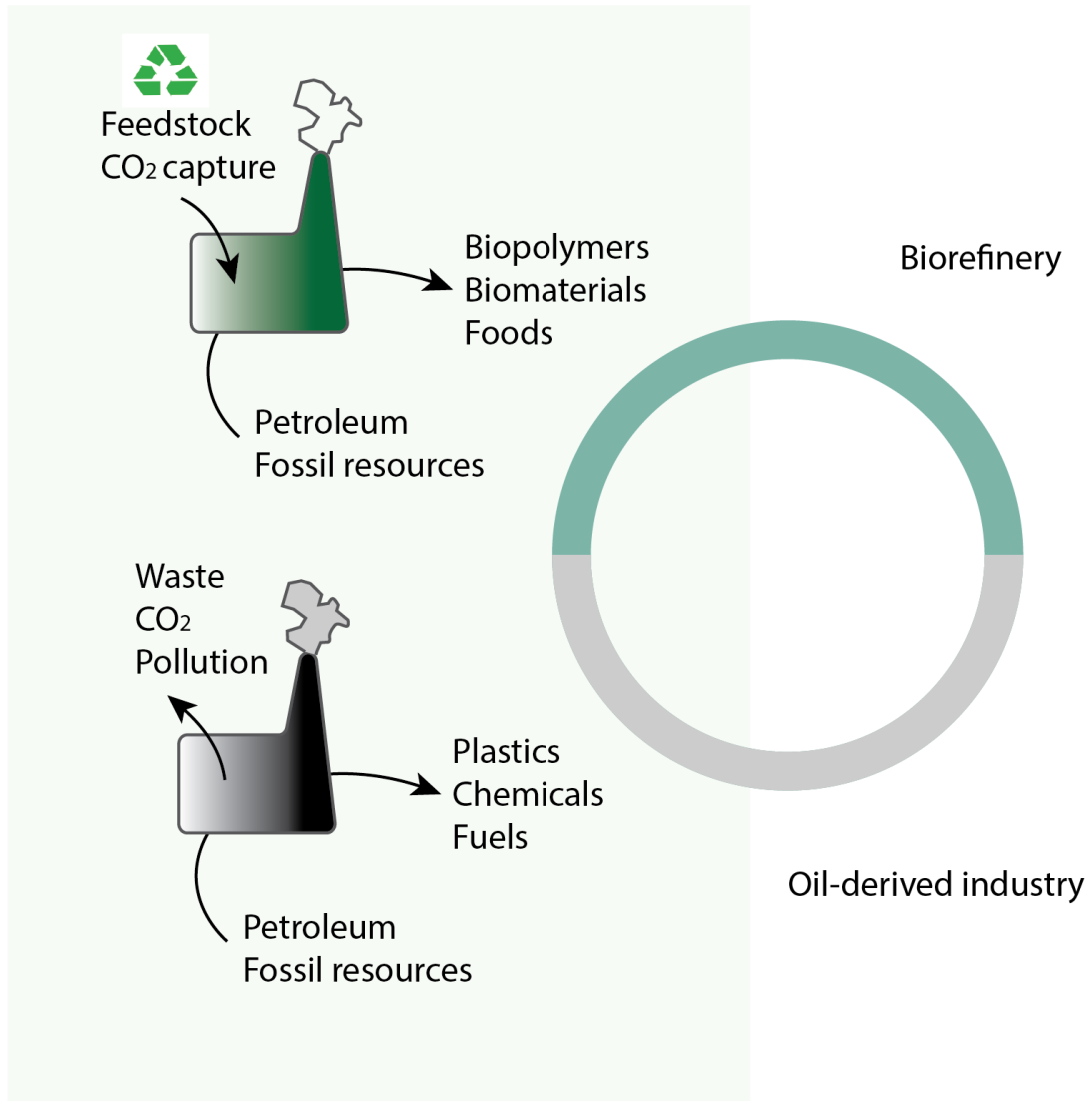


Figure 1.1. Replacing oil-derived industry with biorefinery (green manufacturing). Currently, industrial production of chemicals heavily relies on the use of petroleum and fossil resources for production of various materials, including plastics, chemicals, and fuels. Oil-based refinery causes environmental challenges by generating waste, emission of CO₂ and pollution by often non-degradable chemicals. Green manufacturing already provides a variety of products using renewable feedstock and CO₂ capturing technologies, bring to the market biopolymers, biomaterials, and foods.

Expanded knowledge of microbial physiology, direct access to influence the biochemical machinery and generation of desirable metabolic functions allows scientists to create microbial cell factories. Can those bring humanity to sustainable production of materials, chemicals, and fuels?

1.1. Microbial cell factories

A living cell can be viewed as a miniature factory having a diverse collection of dedicated molecular machines. Optimized by billions of years of evolution, these machines orchestrate nearly every major biochemical process in the cell. Nowadays, scientists engineer designer cell factories for the target compound production by adopting a combination of metabolic engineering and synthetic biology tools and choosing a suitable host¹⁴⁻¹⁶. Those can include mammalian and insect cells, fungi, yeast, and bacteria¹⁷. The list of the microbial hosts that can serve as efficient cell factories is expanding rapidly¹⁸, providing suitable options for biosynthesis of potentially any molecule of choice. In this Ph.D. thesis, the non-pathogenic soil bacterium *Pseudomonas putida* – a rising star of the industrial biotechnology¹⁹, was explored as a cell factory.

Pseudomonas putida as a host for bioproduction

P. putida is a Gram-negative bacterium increasingly used as a production host for applications involving harsh operation conditions (**Figure 1.2.**). Naturally facing stressful physicochemical surroundings, it could satisfy many bioproduction requirements. Strain *P. putida* KT2440, isolated in 1981^{20,21}, followed by genome sequencing and annotation in 2002²², is the most studied member within Pseudomonads^{23,24} and broadly applied for industrial biotechnology²⁵. It is a robust host with a fast growth, low nutritional requirements, safe to operate in the lab [host-vector (HV1) certified organism²⁶], with established tools for genome manipulation, cloning and expressing heterologous genes²⁷.

One of the challenges for microbial production is chemical stress caused by industrial bioprocesses. The target compound of interest, pathway intermediates, or a medium components (could be a byproduct of feedstocks, biomass hydrolysates) could be toxic for the cell, influencing bacterial growth and strain performance¹⁴.

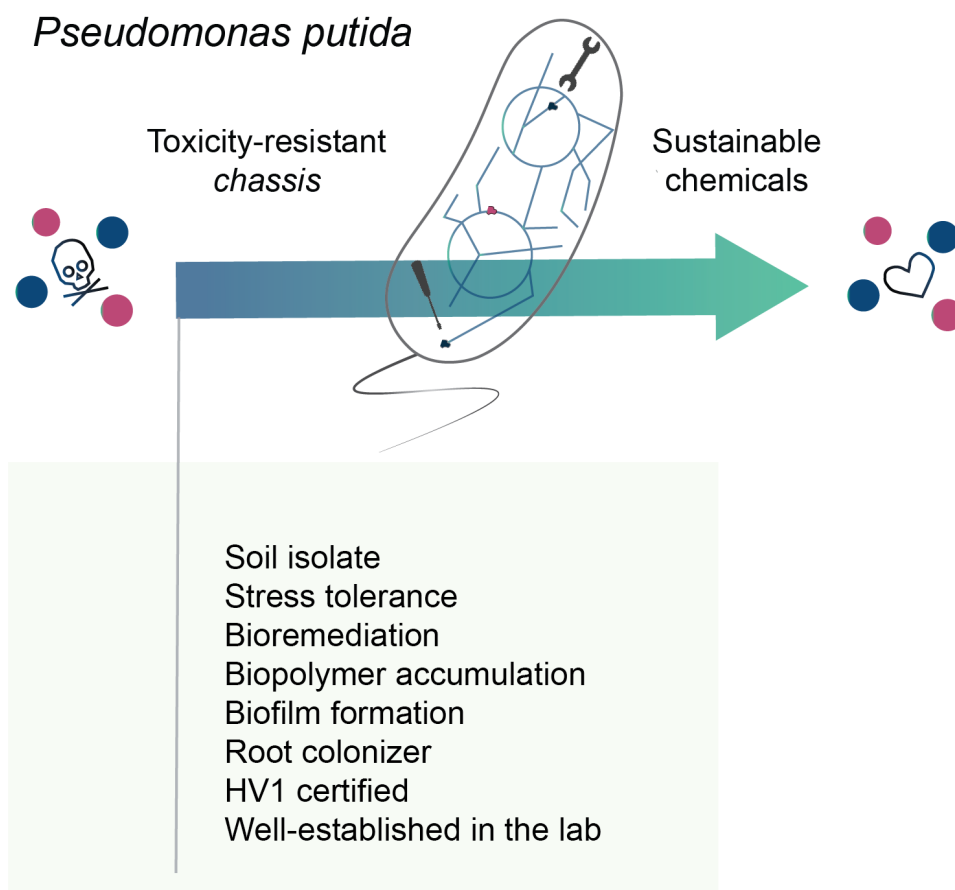


Figure 1.2. Replacing oil-derived industry with biorefinery (green manufacturing). Currently, industrial production of chemicals heavily relies on the use of petroleum and fossil resources for production of various materials, including plastics, chemicals, and fuels. Oil-based refinery causes environmental challenges by generating waste, emission of CO₂ and pollution by often non-degradable chemicals. Green manufacturing already provides a variety of products using renewable feedstock and CO₂ capturing technologies, bring to the market biopolymers, biomaterials, and foods.

As *P. putida* is naturally thriving in harsh environments, it exhibits increased tolerance towards oxidative stress, especially relevant to withstand high concentrations of chemicals, including solvents²⁸. It is extensively studied for bioremediation^{6,23,29} and is also able to use a wide range of carbon sources, such as organic acids, glycerol, various sugars^{25,30,31}.

While using hexoses as a carbon source, *P. putida* exhibits high rates of NADPH regeneration relying on the Entner-Doudoroff (ED) and pentose phosphate pathways, and Embden-Meyerhof-Parnas route¹⁹. Such metabolic architecture (**Figure 1.3.**) allows robust expression of heterologous enzymatic pathways and high tolerance to stressful conditions^{18,32-35}.

Sequenced and annotated genome^{22,23} allowed to develop a range of bioinformatic tools for *P. putida* KT2440. Those include databases with genetic information³⁶ or protein interaction³⁷ (*Pseudomonas* database, *PutidaNET*), genome-scale metabolic models³⁸⁻⁴¹, as well as large-scale kinetic models⁴². Developed computational approaches facilitate cell factory design and allow rational metabolic engineering of the host.

The toolbox for genome engineering and manipulation of heterologous pathways is well established in *P. putida*. These efforts were made easy to set by adopting the standardized and modular vector framework SEVA (*Standard European Vector Architecture*)⁴³, which is constantly being updated⁴⁴⁻⁴⁶. A broad selection of expression systems⁴⁷, promoters, terminators, translational couplers⁴⁸, and transposons^{49,50} have been characterized for *Pseudomonas* and particularly in strain *P. putida* KT2440⁵¹. Various genome refactoring techniques are constantly being developed and already allow any desired modification of the host⁵²⁻⁵⁴. One of the highlight homologous recombination-based technologies for genome manipulation in *P. putida* is adapting the endonuclease I-*SceI* from *Saccharomyces cerevisiae*. Upon conditional expression in bacterial cell, it introduces double strand break in DNA sequence, forcing recombination⁵⁵. This homing endonuclease I-*SceI* allows deleting large genomic fragments⁵⁴, and was implemented to create the reduced-genome *P. putida* EM42 strain, where the flagellar machinery as well as some key insertion sequences and transposons were eliminated, proving improved ATP and NAD(P)H availability. Further developing synthetic biology tools for *Pseudomonas* in the near future, e.g., increasing the efficiency of DNA recombination and genome editing, is progressing by days leading towards more precise and efficient engineering, speeding-up cell factory establishment.

Metabolic engineering of cell factories

Various approaches are available for metabolism refactoring towards the overproduction of target molecule^{1,56-58}. Increased biochemical productivity of the cell factory can be achieved by overexpressing of heterologous enzymes, decreasing byproduct formation, and enforcing product accumulation^{3,59,60}. Established platform strains usually show optimized metabolic flux toward key precursor compounds⁶¹. However, bridging the gap between strain development and commercial scale cell factory is a long process. On average, it takes 5-8 years, and around \$50 million to establish the whole process.⁶² Around the world researchers in metabolic engineering are working on cutting down those costs by speeding up the **Design-Build-Test-Learn** (DBTL) cycle (**Figure 1.4**), the most common approach for biological engineering⁶³.

Design. At this stage the cell factory design is developed, target molecule for production is defined and suitable strategies for its synthesis are explored. The choice of the host organism is based on the strain physiology and naturally built-in properties for product formation, as well as feedstock utilization capacity to ensure economically feasible process, and tolerance to the bioprocess conditions. To produce the compound of interest, the pathway and its enzyme components can be selected using databases, such as KEGG⁶⁴, MetaCyc, BioCyc^{65,66} and BRENDA⁶⁷. Biosynthetic gene clusters and pathways can be identified and built *de novo* through a retrosynthetic approach⁶³. Balancing of the selected pathway can be achieved by using characterized promoters, terminators, ribosome binding sites and plasmid backbones that can be used for cell factory design and diverse synthetic biology toolsets^{2,3,68}. Metabolic modelling can help to evaluate metabolic fluxes, predict knockouts for the by-product elimination, analyse biomass formation, substrate consumption and simulate fermentations^{10,11,59,69-72}.

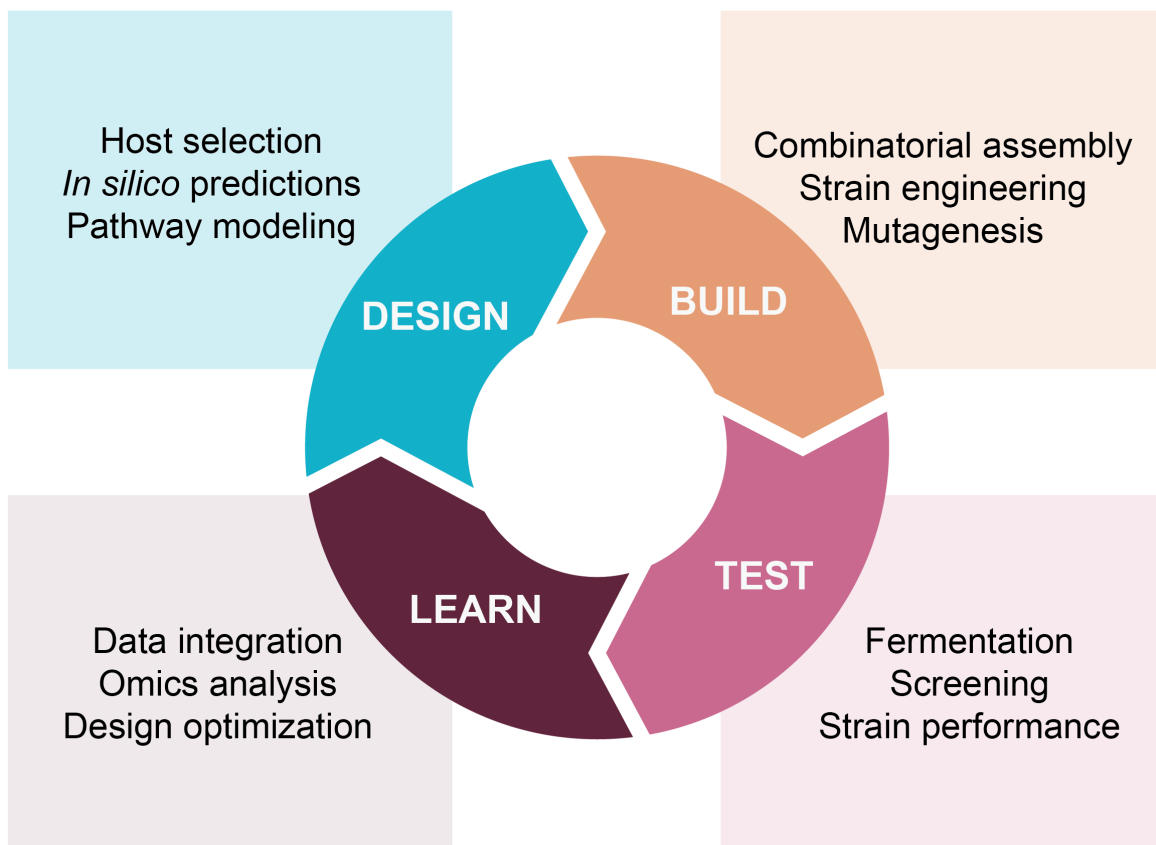


Figure 1.4. The Design-Build-Test-Learn (DBTL) cycle for cell factory engineering. **Design** stage, assisted by computational tools, databases, and modelling, defines the problem, and establishes the initial design. **Build** stage includes synthesis and assembly of genetic elements followed by their integration into selected host. **Test** stage involves characterization of the constructed cell factory and validation of the predicted design. **Learn** stage summarizes all the obtained data, analysing the ways to improve strain performance. Gained learnings assist further iterations of the cycle. Adapted from Petzold et al.⁶³

Moreover, recent development of artificial intelligence opens a new era of metabolic engineering and cell factory design, assisted by machine learning^{73,74} (e.g. based only on the sequence AlphaFold⁷⁵ is able to highly-accurate predict the structure and define potential function of any protein of choice). The availability of computational tools is growing fast assisting the design phase.

Build. At this stage the cell factory is constructed: genetic elements are synthesized, assembled, and installed into the preferred host. Dropping costs for sequencing and DNA synthesis (from oligonucleotides to synthetic genomes⁷⁶), as well as continuing to advance synthetic biology technologies are fuelling up the development of this stage⁷⁷.

The behaviour of assembled biological parts, especially during integration of novel enzymes and complex pathway engineering, is not always predictable. A powerful approach to generate synthetic libraries can be implemented to select the best variants and can include millions of gene combinations together with various genetic elements, resulting in either plasmids or genome integrations⁷⁸⁻⁸⁰. In 2020, the Nobel Prize in Chemistry was awarded to Emmanuelle Charpentier and Jennifer Doudna for the development of genome editing technologies based on Clustered Regularly Interspaced Short Palindromic Repeats (CRISPR) and associated proteins^{81,82}. Their further applications for cell factory engineering continue to revolutionize the field^{83,84}. Another remarkable feature of the build stage approach is adapting directed evolution, which was demonstrated to create enzymes with improved or novel functions by Frances Arnold, a winner of Nobel Prize in Chemistry in 2018^{85,86}. Cell factories can be evolved (adaptive laboratory evolution - ALE)¹³ under selection pressure to obtain better performing mutants with improved features of interest; those can include substrate assimilation, bioremediation, and chemical tolerance⁸⁷.

Test. At this stage constructed cell factory is validated. Advances in omics technologies allow testing modified and synthesized genomes, as well as analysis of the transcriptome, proteome, and metabolome. It helps to evaluate genome engineering efforts and access metabolic information about desired function or phenotype⁶³. A broad range of precise analytical methods for metabolite analysis was developed based on chromatography and mass spectrometry, however it might be limiting for high-throughput screenings due to the long run of the sample. In this case, screen could be assisted by coupling product to growth of fluorescent output (biosensors). Selection of the best producing variants can be assisted by microfluidics technologies, microtiter plate screens or flow cytometry cell sorting^{79,88}. Production strain performance is also evaluated during upscaling and down-stream processing.

Learn. At this stage, gathered data and established cell factory design is thoroughly analysed. Resulting information can be implemented to further optimize pathway design, adjust host modifications, improve metabolic fluxes, and maximize product titres, rates, and yields. Computational approaches can be used to integrate obtained datasets in metabolic models, to analyse fluxes and generate new design rules. Recent development of machine learning algorithms, as well as improved quality of datasets from the test stage provides more opportunities to make cell factory engineering more efficient, cheap, and predictable^{73-75,89}.

With advances in bioprocess engineering, and further development of bioinformatics methods data processing, as well as synthetic biology tools the possibilities for green manufacturing will continue to expand. Synthetic biology tools allowed biological engineers to approach cell factory optimization in new ways. Some of the beautiful examples include: expanding of the genetic code and production of proteins with novel properties^{90,91}, synthetic chromosomes^{92,93}, minimal⁹⁴⁻⁹⁷ and recoded⁹⁸ genomes, or even chromosome-free cells⁹⁹. There is no doubt that CRISPR is one of the breakthroughs of the decade for synthetic biology, bringing us today to genome editing technologies which allow to build, write, edit, and manipulate DNA code better than ever.

1.2 CRISPR-Cas9 and microbial biotechnology

A new era for biology was opened by the advent of recombinant DNA technology just 50 years ago, when reprogramming and manipulation of the genetic code became possible. What is most striking is how the molecular biology tools and methods for DNA manipulation changed through the next decades⁷⁷. As building of a genetic construct was slow and typically unpredictable inside the cell, more efficient and high-throughput techniques for genome engineering were severely lacking. That is why development of CRISPR-based technologies have revolutionized biosciences, as first appeared only in 2011, and continue to further advance (**Figure 1.5**) until nowadays.

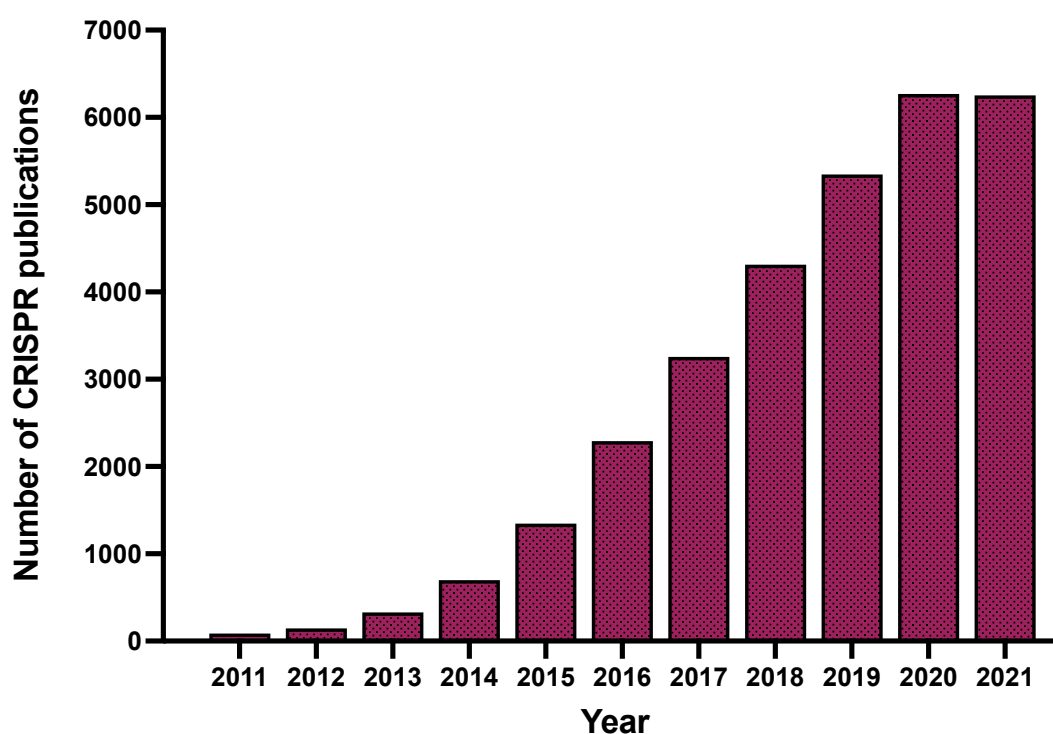


Figure 1.5. Number of publications mentioning “CRISPR” in the last 10 years. The dataset is generated using the search engine PubMed, and the graph was visualized with Prism 9.1 Software (GraphPad, California, USA).

In 1809, Jean-Baptiste Lamarck described a theory of acquired characteristics, representing the ability of the organism to immediately adapt to the environmental force¹⁰⁰. A couple of centuries later, we could witness an example of such adaptation in bacteria. Used by many prokaryotes, CRISPR acts like an immune system, protecting the cell from foreign nucleic acids. Most archaea (about 85%) and bacteria (about 50 %) carry this system in their genome¹⁰¹.

Appeared for the first time in 1987 as “five highly homologous sequences of 29 nucleotides arranged as direct repeats with 32 nucleotides as spacing”¹⁰², it was only 15 years later that the name CRISPR (Clustered Regularly Interspaced Short Palindromic Repeats) appeared for the first time¹⁰³. CRISPR-Cas systems are diverse and their classification is constantly being updated. The most recent one include: (i) the wide-spread Class 1 that works with multisubunit complexes of Cas proteins (such as Cascade); (ii) more rare Class 2, which uses a single effector protein (such as Cas9, **Figure 1.6**). The simplicity of the Class 2 CRISPR-Cas systems was adapted for a new generation genome editing approaches and applied for various species, including bacteria, yeast, mammalian cells and plants.^{82,83,104-106}

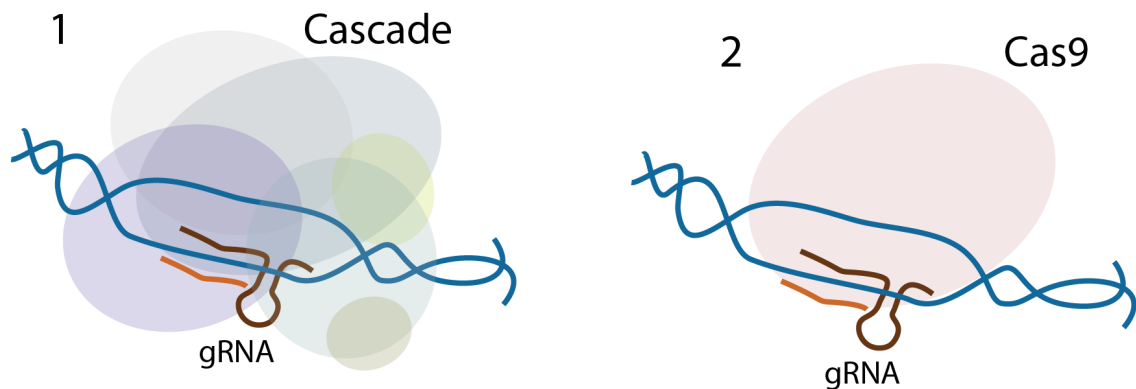


Figure 1.6. Class 1 and 2 of CRISPR-Cas systems representation. Class 1 adapts multisubunit complexes consisting of 4-7 subunits of Cas proteins to bind the target sequence (Cascade), while Class 2 systems for the same purpose use just one multidomain protein (Cas9).

Mysterious repeated sequence

Groundbreaking scientific discoveries are often based on decades of many great minds combined efforts. This story starts in 1987, with a difficult to define sequence of a region in *Escherichia coli* chromosome. It took scientists several months to sequence it using Klenow fragment and autoradiography^{102,107} (nowadays DNA sequencing progress allows to perform the same task in just a day). The sequenced area was especially hard to read due to secondary structures formed by the palindromic repeating sequences. The feature of those sequences was so mysterious (not detected in any databases) and unexpected that it was reported in the paper as a remarkable observation. Soon after that, similar sequences were demonstrated for a variety of bacteria and archaea¹⁰⁷.

In 2002, the term CRISPR was introduced, defining characteristics of those sequences: (i) placed into intergenic regions, (ii) contain multiple conserved short direct repeats, (iii) the repeats are interspersed with nonconserved sequences, and (iv) on one side of the repeat cluster there is a leader sequence¹⁰⁸. Around the same time, CRISPR associated proteins (Cas nucleases) were identified and systematically analysed¹⁰⁹, however the function of the CRISPR-Cas system remained unknown.

In 2007, Danish bio-based company Danisco¹¹⁰ (now DuPont, as a part of International Flavors and Fragrances, IFF) was able to finally prove its function. The study published in *Science*¹¹⁰ showed that the lactic acid bacterium *Streptococcus thermophilus* uses CRISPR as an acquired immune system. Later, originally discovered in 1987 mysterious sequence was reconstituted for *E. coli*, demonstrating, and validating its function¹¹¹, thus **solving the mystery**.

The simplified illustration of the CRISPR-Cas immunity is presented in **Figure 1.7**. It involves 2 major phases: adaptation (development of the immune memory by spacer acquisition) and interference (immune response and foreign DNA elimination).

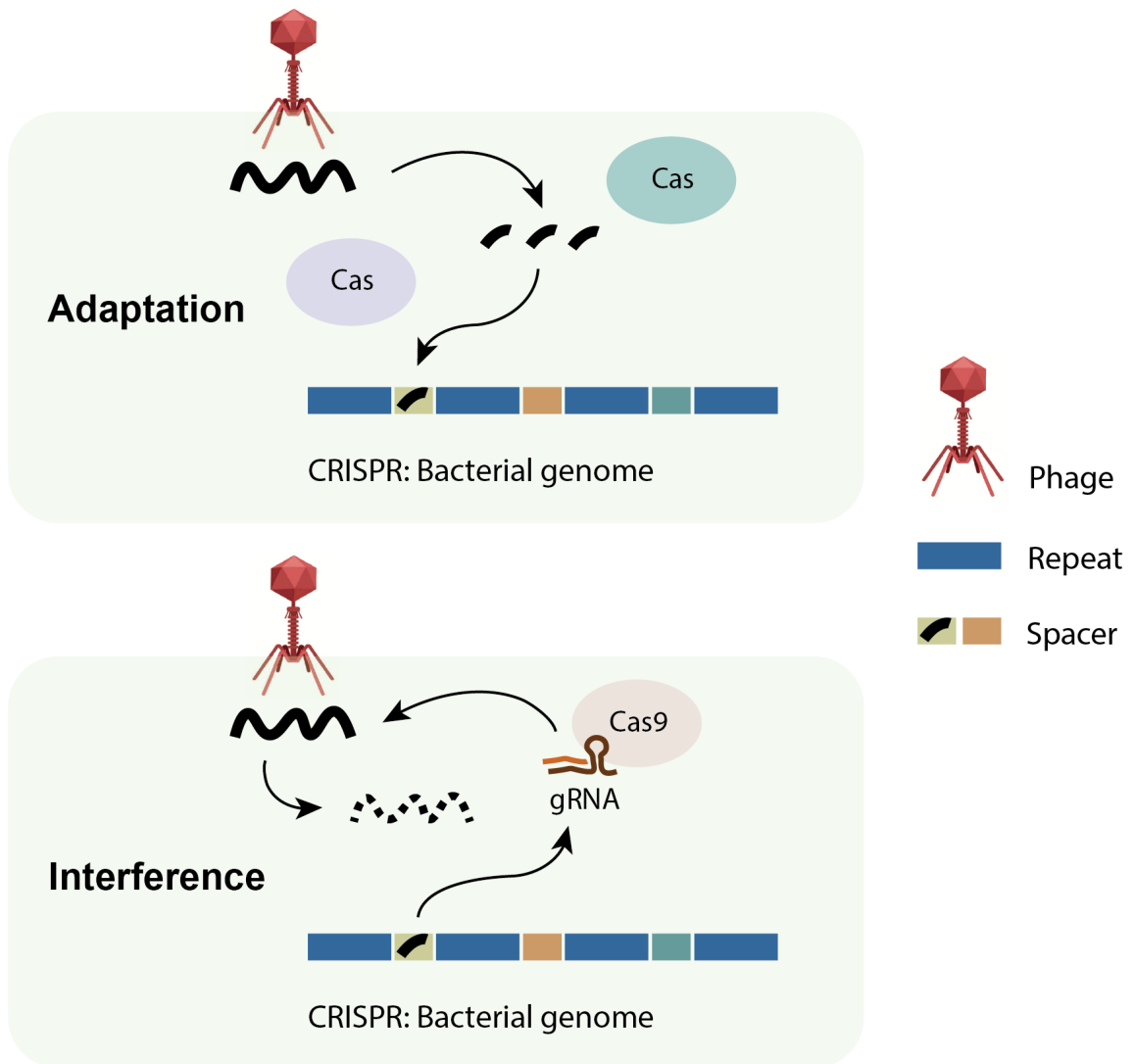


Figure 1.7. Simplified illustration of the functioning CRISPR-Cas acquired immunity. During **Adaptation** phase, the foreign DNA (injected by the phage for example) is recognized by Cas proteins, and processed in small fragments, which then are getting inserted in the CRISPR locus of bacterial genome as spacers. It allows acquiring the immunity against similar invasion. During **Interference** phase, the foreign DNA is being eliminated by Cas9 cleavage. Homologous to the spacer sequence gRNA (guide RNA) forms a complex with Cas9 ensuring precise binding to the target sequence.

Cas nucleases driving the bacterial immunity. Those enzymes can bind and create double-stranded breaks (DSBs) in DNA, generating a little piece of foreign DNA called protospacers. Those fragments can be stored in the bacterial genome between repeated palindromic sequences, and this arrangement serves as an immune memory: upon reinfection with same DNA sequence, it gets recognised and eliminated.

Several important observations paved the way towards CRISPR genome-editing technologies. Among others, some key findings include: (i) DNA catalytic activity of Cas9, resulting in double strand break in *S. thermophilus*¹¹², (ii) presence of protospacer-adjacent motifs (PAMs) and its crucial role in sequence recognition¹¹³, (iii) gRNA requirement for Cas9 action¹¹⁴, (iv) portability of the system into different bacterial strains¹¹⁵, and (v) demonstration that Cas9 can target any desired DNA sequence in bacteria⁸². Since then, CRISPR-Cas approaches are gradually developing to engineer and manipulate genomes of almost all domains of life.

In a living cell, DNA double-strand break is a serious damage which needs to be repaired at any cost to ensure survival. Two main repair mechanisms can assist the cell to heal quickly: non-homologous end joining (NHEJ) and homology-directed repair (HDR). NHEJ is present in most of the eukaryotic cells. It is sequence-nonspecific and ligates both ends of DNA with a potential of random deletion/insertion in the targeted site. HDR requires homologous template to repair the cleavage site, although it is less efficient. In most prokaryotes, DSBs is highly lethal, due to absent NHEJ activity. Thus, conventional CRISPR-Cas applications rely on HDR-mediated repair and donor templates, often assisted with co-introducing of recombination factors to boost efficiency (λ -red recombineering). As genome editing heavily relies on the DNA repair mechanisms and activities, its effectiveness of CRISPR-engineering differs depending on the cell type⁸³. Beyond genome editing applications, CRISPR-Cas systems can be used as an antimicrobial agent (chromosome cleavage) for pathogenic bacteria, assisting the control of antibiotic resistance. Moreover, immunity engineering in specific strains towards phage resistance can be relevant in the fermented food industry, protecting strains from phage infection during production processes¹¹⁶.

It is not all about the cleavage: tools revolutionising microbial biotechnology

The *Streptococcus pyogenes* Cas9 is the most commonly used Cas enzyme for engineering purposes¹⁰⁷. CRISPR-Cas9 gene editing works by creating double-stranded breaks in the DNA and then taking advantage of cellular previously mentioned DNA repair pathways⁸³.

And as all scissors need a hand to guide them through the cutting process, for Cas9 to be active, it needs to bind with a complex of complementary protospacer CRISPR RNA (crRNA) and a scaffold trans-activating CRISPR RNA (tracrRNA). These two RNAs can be synthetically fused into one a single guide RNA (sgRNA). Before cutting, the Cas9 is also examines if the DNA contains the protospacer adjacent motif (PAM), a short sequence downstream the target site. It will only create a double-stranded break upon its recognition, ensuring the stability of its own DNA. PAM availability, however, remains a common limitation even with the use of different Cas protein orthologs. Because of these challenges, many researchers have engineered or evolved Cas9 variants with less restrictive PAM compatibilities^{84,117}.

Without introduction of the DSBs, CRISPR-Cas9 system can be used to alter target gene expression by either repressing or enhancing transcription. To repurpose the CRISPR system as a regulator of gene expression, catalytically inactive version of Cas9 (dCas9) is used. The dCas9 lacks endonucleolytic activity, which is caused by two point mutations in the domains allowing DNA cleavage: RuvC-like (D10A) and HNH (H840A). Binding of dCas9 to DNA blocks and inhibits transcription, which was called CRISPR interference (CRISPRi)¹¹⁸. Repression of the gene is more effective when targeting non-template strands, and can reach more than 99% reduction of gene expression in bacteria (and not as efficient in eukaryotes). dCas9 can be also fused with a transcriptional activator to enhance transcription of the targeted region, resulting in CRISPR activation (CRISPRa)¹¹⁹. Inducible control of sgRNA and dCas9 expression allows regulation of transcription at a desired timepoint, which can be highly useful for dynamic metabolic

engineering purposes, while simultaneous repression and activation of different gene targets^{105,120}.

Another type of catalytically impaired Cas9 variant is widely used in genome editing applications. This variant contains only a single point mutation (either in the RuvC-like domain (D10A) or in HNH domain (H840A), resulting in a nCas9 which is only able to create a single strand break. This nCas9 nuclease can be fused to variety of proteins that manipulate DNA repair machinery. Some of the emerging approaches include: (i) prime editors, where nCas9 is fused to reverse transcriptase, allowing to directly copy the edited sequences into target sites instead of the original DNA sequence, and (ii) base editors, where nCas9 fused to deaminase, allowing to precisely incorporate point mutations without DSBs or donor templates⁸⁴. Even though prime editing was not set up in prokaryotes yet, the development and application of the base-editors is advancing rapidly¹²¹.

Base editors can be divided in two categories, depending on the type of deaminase: cytosine base editors (CBEs, cytosine deaminase), converting C•G base pairs to T•A base pairs; and adenine base editors (ABEs, adenosine deaminase), catalysing A•T-to-G•C substitutions. Thus, CBEs and ABEs can mediate all possible nucleotide mutations (C→T, A→G, T→C, G→A). Deamination of substrate nucleotides initially generates uracil and inosine, creating a mismatched base pair on the non-deaminated strand, which is then repaired by cellular DNA repair systems, resulting in desirable substitution. Uracil excision (which is much more efficient to compare with inosine excision) may happen in the DNA sequence before the editing event, influencing editing efficiency. To avoid that, cytosine deaminase is fused with two copies of uracil glycosylase inhibitor proteins (UGIs) that substantially increase editing yield and precision¹²²⁻¹²⁴.

Moreover, among other interesting applications of CRISPR-Cas9 is a tool for targeted mutagenesis. A fusion of nicking variant of Cas9 and an error-prone DNA polymerase I, results in a directed evolution system called EvolvR¹²⁵. It allows diversification of the desired loci and useful for a range of biotechnological purposes¹²⁵. All discussed CRISPR-Cas9 technologies, especially relevant for bacterial engineering are presented in **Figure 1.8**.

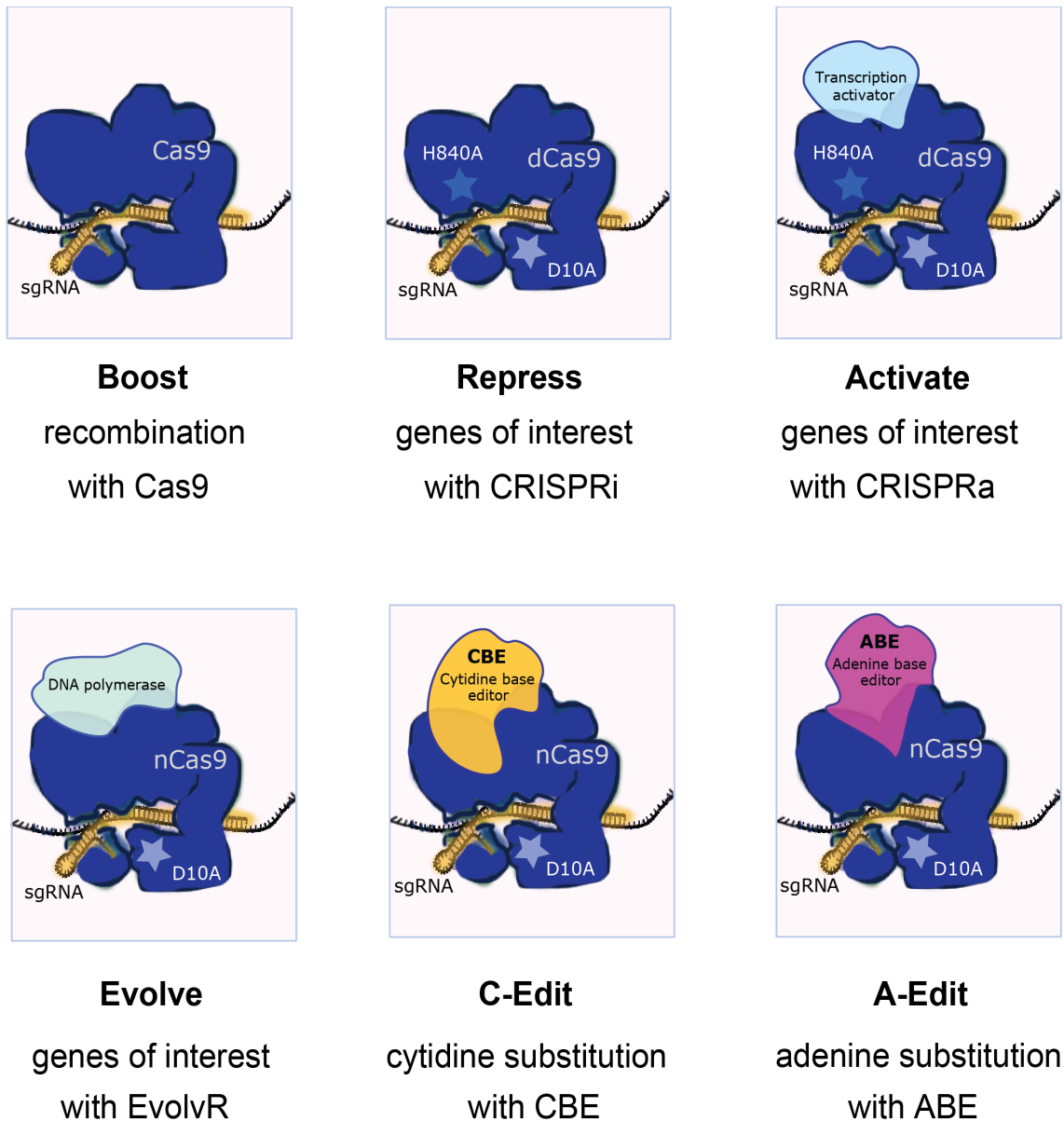


Figure 1.8. Key CRISPR-Cas9 applications used in bacterial biotechnology. Cas9-assisted recombineering help to enforce homologous recombination and eliminate undesirable sequences. CRISPRi and CRISPRa help to regulate transcription of the target gene. EvolvR mutagenesis tool allows to randomly mutate desired genome region. Base-editors (CBEs and ABEs) make possible the substitution of any nucleotide in the genome.

CRISPR-Cas9 approaches help us in strain development and overcoming some of the microbial production limitations. Future research efforts in the field may will enforce the establishment of economically feasible cell factories and sustainable replacement of currently prevalent oil-derived chemical industry.

This Ph. D. thesis builds on the developments in the CRISPR-Cas9 technologies, as well as target engineering of *Pseudomonas* cell factories. Such efforts in broadening of the CRISPR-based synthetic biology toolbox aim to ease genome manipulation and achieve better yields and productivities for more efficient biosynthesis processes.

References

- 1 Bailey, J. E. Toward a science of metabolic engineering. *Science* **252**, 1668-1675, doi:10.1126/science.2047876 (1991).
- 2 Choi, K. R. *et al.* Systems Metabolic Engineering Strategies: Integrating Systems and Synthetic Biology with Metabolic Engineering. *Trends Biotechnol* **37**, 817-837, doi:10.1016/j.tibtech.2019.01.003 (2019).
- 3 Dai, Z. & Nielsen, J. Advancing metabolic engineering through systems biology of industrial microorganisms. *Curr Opin Biotechnol* **36**, 8-15, doi:10.1016/j.copbio.2015.08.006 (2015).
- 4 Malhi, Y. *et al.* Climate change and ecosystems: threats, opportunities and solutions. *Philos Trans R Soc Lond B Biol Sci* **375**, 20190104, doi:10.1098/rstb.2019.0104 (2020).
- 5 in *Industrialization of Biology: A Roadmap to Accelerate the Advanced Manufacturing of Chemicals* (2015).
- 6 Leong, H. Y. *et al.* Waste biorefinery towards a sustainable circular bioeconomy: a solution to global issues. *Biotechnol Biofuels* **14**, 87, doi:10.1186/s13068-021-01939-5 (2021).
- 7 Solarte-Toro, J. C. & Cardona Alzate, C. A. Biorefineries as the base for accomplishing the sustainable development goals (SDGs) and the transition to bioeconomy: Technical aspects, challenges and perspectives. *Bioresour Technol* **340**, 125626, doi:10.1016/j.biortech.2021.125626 (2021).
- 8 Amer, B. & Baidoo, E. E. K. Omics-Driven Biotechnology for Industrial Applications. *Front Bioeng Biotechnol* **9**, 613307, doi:10.3389/fbioe.2021.613307 (2021).
- 9 Lieven, C. *et al.* MEMOTE for standardized genome-scale metabolic model testing. *Nat Biotechnol* **38**, 272-276, doi:10.1038/s41587-020-0446-y (2020).
- 10 Saa, P. A. & Nielsen, L. K. Formulation, construction and analysis of kinetic models of metabolism: A review of modelling frameworks. *Biotechnol Adv* **35**, 981-1003, doi:10.1016/j.biotechadv.2017.09.005 (2017).
- 11 Cardoso, J. G., Andersen, M. R., Herrgard, M. J. & Sonnenschein, N. Analysis of genetic variation and potential applications in genome-scale metabolic modeling. *Front Bioeng Biotechnol* **3**, 13, doi:10.3389/fbioe.2015.00013 (2015).

- 12 Holowko, M. B., Frow, E. K., Reid, J. C., Rourke, M. & Vickers, C. E. Building a biofoundry. *Synth Biol (Oxf)* **6**, ysaa026, doi:10.1093/synbio/ysaa026 (2021).
- 13 Sandberg, T. E., Salazar, M. J., Weng, L. L., Palsson, B. O. & Feist, A. M. The emergence of adaptive laboratory evolution as an efficient tool for biological discovery and industrial biotechnology. *Metabolic Engineering* **56**, 1-16, doi:10.1016/j.ymben.2019.08.004 (2019).
- 14 Keasling, J. D. Manufacturing molecules through metabolic engineering. *Science* **330**, 1355-1358, doi:10.1126/science.1193990 (2010).
- 15 Stephanopoulos, G. Synthetic biology and metabolic engineering. *ACS Synth Biol* **1**, 514-525, doi:10.1021/sb300094q (2012).
- 16 Shaw, A. J. *et al.* Metabolic engineering of microbial competitive advantage for industrial fermentation processes. *Science* **353**, 583-586, doi:10.1126/science.aaf6159 (2016).
- 17 Hayes, M., Ross, R. P., Fitzgerald, G. F. & Stanton, C. Putting microbes to work: dairy fermentation, cell factories and bioactive peptides. Part I: overview. *Biotechnol J* **2**, 426-434, doi:10.1002/biot.200600246 (2007).
- 18 Calero, P. & Nikel, P. I. Chasing bacterial chassis for metabolic engineering: a perspective review from classical to non-traditional microorganisms. *Microb Biotechnol* **12**, 98-124, doi:10.1111/1751-7915.13292 (2019).
- 19 Nikel, P. I., Chavarria, M., Danchin, A. & de Lorenzo, V. From dirt to industrial applications: *Pseudomonas putida* as a Synthetic Biology chassis for hosting harsh biochemical reactions. *Curr Opin Chem Biol* **34**, 20-29, doi:10.1016/j.cbpa.2016.05.011 (2016).
- 20 Bagdasarian, M. *et al.* Specific-purpose plasmid cloning vectors. II. Broad host range, high copy number, RSF1010-derived vectors, and a host-vector system for gene cloning in *Pseudomonas*. *Gene* **16**, 237-247, doi:10.1016/0378-1119(81)90080-9 (1981).
- 21 Franklin, F. C., Bagdasarian, M., Bagdasarian, M. M. & Timmis, K. N. Molecular and functional analysis of the TOL plasmid pWWO from *Pseudomonas putida* and cloning of genes for the entire regulated aromatic ring meta cleavage pathway. *Proc Natl Acad Sci U S A* **78**, 7458-7462, doi:10.1073/pnas.78.12.7458 (1981).
- 22 Nelson, K. E. *et al.* Complete genome sequence and comparative analysis of the metabolically versatile *Pseudomonas putida* KT2440. *Environ Microbiol* **4**, 799-808, doi:10.1046/j.1462-2920.2002.00366.x (2002).

- 23 Belda, E. *et al.* The revisited genome of *Pseudomonas putida* KT2440 enlightens its value as a robust metabolic chassis. *Environ Microbiol* **18**, 3403-3424, doi:10.1111/1462-2920.13230 (2016).
- 24 Nikel, P. I., Martinez-Garcia, E. & de Lorenzo, V. Biotechnological domestication of pseudomonads using synthetic biology. *Nat Rev Microbiol* **12**, 368-379, doi:10.1038/nrmicro3253 (2014).
- 25 Nikel, P. I. & de Lorenzo, V. *Pseudomonas putida* as a functional chassis for industrial biocatalysis: From native biochemistry to trans-metabolism. *Metab Eng* **50**, 142-155, doi:10.1016/j.ymben.2018.05.005 (2018).
- 26 Kampers, L. F. C., Volkers, R. J. M. & Martins Dos Santos, V. A. P. *Pseudomonas putida* KT2440 is HV1 certified, not GRAS. *Microb Biotechnol* **12**, 845-848, doi:10.1111/1751-7915.13443 (2019).
- 27 Martinez-Garcia, E., Nikel, P. I., Aparicio, T. & de Lorenzo, V. *Pseudomonas* 2.0: genetic upgrading of *P. putida* KT2440 as an enhanced host for heterologous gene expression. *Microb Cell Fact* **13**, 159, doi:10.1186/s12934-014-0159-3 (2014).
- 28 Bitzenhofer, N. L. *et al.* Towards robust *Pseudomonas* cell factories to harbour novel biosynthetic pathways. *Essays Biochem* **65**, 319-336, doi:10.1042/EBC20200173 (2021).
- 29 Dvorak, P., Nikel, P. I., Damborsky, J. & de Lorenzo, V. Bioremediation 3.0: Engineering pollutant-removing bacteria in the times of systemic biology. *Biotechnol Adv* **35**, 845-866, doi:10.1016/j.biotechadv.2017.08.001 (2017).
- 30 Nikel, P. I. & de Lorenzo, V. Assessing Carbon Source-Dependent Phenotypic Variability in *Pseudomonas putida*. *Methods Mol Biol* **1745**, 287-301, doi:10.1007/978-1-4939-7680-5_16 (2018).
- 31 Nikel, P. I. & de Lorenzo, V. Robustness of *Pseudomonas putida* KT2440 as a host for ethanol biosynthesis. *N Biotechnol* **31**, 562-571, doi:10.1016/j.nbt.2014.02.006 (2014).
- 32 Chavarria, M., Nikel, P. I., Perez-Pantoja, D. & de Lorenzo, V. The Entner-Doudoroff pathway empowers *Pseudomonas putida* KT2440 with a high tolerance to oxidative stress. *Environ Microbiol* **15**, 1772-1785, doi:10.1111/1462-2920.12069 (2013).
- 33 Blank, L. M., Ionidis, G., Ebert, B. E., Buhler, B. & Schmid, A. Metabolic response of *Pseudomonas putida* during redox biocatalysis in the presence of a second octanol phase. *FEBS J* **275**, 5173-5190, doi:10.1111/j.1742-4658.2008.06648.x (2008).
- 34 Ankenbauer, A. *et al.* Micro-aerobic production of isobutanol with engineered *Pseudomonas putida*. *Eng Life Sci* **21**, 475-488, doi:10.1002/elsc.202000116 (2021).

- 35 Calero, P. *et al.* A fluoride-responsive genetic circuit enables in vivo biofluorination in engineered *Pseudomonas putida*. *Nat Commun* **11**, 5045, doi:10.1038/s41467-020-18813-x (2020).
- 36 Winsor, G. L. *et al.* Enhanced annotations and features for comparing thousands of *Pseudomonas* genomes in the *Pseudomonas* genome database. *Nucleic Acids Res* **44**, D646-653, doi:10.1093/nar/gkv1227 (2016).
- 37 Park, S. J. *et al.* PutidaNET: interactome database service and network analysis of *Pseudomonas putida* KT2440. *BMC Genomics* **10 Suppl 3**, S18, doi:10.1186/1471-2164-10-S3-S18 (2009).
- 38 Sohn, S. B., Kim, T. Y., Park, J. M. & Lee, S. Y. In silico genome-scale metabolic analysis of *Pseudomonas putida* KT2440 for polyhydroxyalkanoate synthesis, degradation of aromatics and anaerobic survival. *Biotechnol J* **5**, 739-750, doi:10.1002/biot.201000124 (2010).
- 39 Nogales, J., Palsson, B. O. & Thiele, I. A genome-scale metabolic reconstruction of *Pseudomonas putida* KT2440: iJN746 as a cell factory. *BMC Syst Biol* **2**, 79, doi:10.1186/1752-0509-2-79 (2008).
- 40 Puchalka, J. *et al.* Genome-scale reconstruction and analysis of the *Pseudomonas putida* KT2440 metabolic network facilitates applications in biotechnology. *PLoS Comput Biol* **4**, e1000210, doi:10.1371/journal.pcbi.1000210 (2008).
- 41 Nogales, J. *et al.* High-quality genome-scale metabolic modelling of *Pseudomonas putida* highlights its broad metabolic capabilities. *Environ Microbiol* **22**, 255-269, doi:10.1111/1462-2920.14843 (2020).
- 42 Tokic, M., Hatzimanikatis, V. & Miskovic, L. Large-scale kinetic metabolic models of *Pseudomonas putida* KT2440 for consistent design of metabolic engineering strategies. *Biotechnol Biofuels* **13**, 33, doi:10.1186/s13068-020-1665-7 (2020).
- 43 Silva-Rocha, R. *et al.* The Standard European Vector Architecture (SEVA): a coherent platform for the analysis and deployment of complex prokaryotic phenotypes. *Nucleic Acids Res* **41**, D666-675, doi:10.1093/nar/gks1119 (2013).
- 44 Martinez-Garcia, E., Aparicio, T., Goni-Moreno, A., Fraile, S. & de Lorenzo, V. SEVA 2.0: an update of the Standard European Vector Architecture for de-/re-construction of bacterial functionalities. *Nucleic Acids Res* **43**, D1183-1189, doi:10.1093/nar/gku1114 (2015).
- 45 Kim, S. H., Cavaleiro, A. M., Rennig, M. & Norholm, M. H. SEVA Linkers: A Versatile and Automatable DNA Backbone Exchange Standard for Synthetic Biology. *ACS Synth Biol* **5**, 1177-1181, doi:10.1021/acssynbio.5b00257 (2016).

- 46 Martinez-Garcia, E. *et al.* SEVA 3.0: an update of the Standard European Vector Architecture for enabling portability of genetic constructs among diverse bacterial hosts. *Nucleic Acids Res* **48**, D1164-D1170, doi:10.1093/nar/gkz1024 (2020).
- 47 Calero, P., Jensen, S. I. & Nielsen, A. T. Broad-Host-Range ProUSER Vectors Enable Fast Characterization of Inducible Promoters and Optimization of p-Coumaric Acid Production in *Pseudomonas putida* KT2440. *ACS Synth Biol* **5**, 741-753, doi:10.1021/acssynbio.6b00081 (2016).
- 48 Zobel, S. *et al.* Tn7-Based Device for Calibrated Heterologous Gene Expression in *Pseudomonas putida*. *ACS Synth Biol* **4**, 1341-1351, doi:10.1021/acssynbio.5b00058 (2015).
- 49 Martinez-Garcia, E., Aparicio, T., de Lorenzo, V. & Nikel, P. I. Engineering Gram-Negative Microbial Cell Factories Using Transposon Vectors. *Methods Mol Biol* **1498**, 273-293, doi:10.1007/978-1-4939-6472-7_18 (2017).
- 50 Martinez-Garcia, E., Aparicio, T., de Lorenzo, V. & Nikel, P. I. New transposon tools tailored for metabolic engineering of gram-negative microbial cell factories. *Front Bioeng Biotechnol* **2**, 46, doi:10.3389/fbioe.2014.00046 (2014).
- 51 Weimer, A., Kohlstedt, M., Volke, D. C., Nikel, P. I. & Wittmann, C. Industrial biotechnology of *Pseudomonas putida*: advances and prospects. *Appl Microbiol Biotechnol* **104**, 7745-7766, doi:10.1007/s00253-020-10811-9 (2020).
- 52 Cook, T. B. *et al.* Genetic tools for reliable gene expression and recombineering in *Pseudomonas putida*. *J Ind Microbiol Biotechnol* **45**, 517-527, doi:10.1007/s10295-017-2001-5 (2018).
- 53 Martin-Pascual, M. *et al.* A navigation guide of synthetic biology tools for *Pseudomonas putida*. *Biotechnol Adv* **49**, 107732, doi:10.1016/j.biotechadv.2021.107732 (2021).
- 54 Martinez-Garcia, E. & de Lorenzo, V. Molecular tools and emerging strategies for deep genetic/genomic refactoring of *Pseudomonas*. *Curr Opin Biotechnol* **47**, 120-132, doi:10.1016/j.copbio.2017.06.013 (2017).
- 55 Martinez-Garcia, E. & de Lorenzo, V. Engineering multiple genomic deletions in Gram-negative bacteria: analysis of the multi-resistant antibiotic profile of *Pseudomonas putida* KT2440. *Environ Microbiol* **13**, 2702-2716, doi:10.1111/j.1462-2920.2011.02538.x (2011).
- 56 Stephanopoulos, G. & Vallino, J. J. Network rigidity and metabolic engineering in metabolite overproduction. *Science* **252**, 1675-1681, doi:10.1126/science.1904627 (1991).

- 57 Conrado, R. J., Varner, J. D. & DeLisa, M. P. Engineering the spatial organization of metabolic enzymes: mimicking nature's synergy. *Curr Opin Biotechnol* **19**, 492-499, doi:10.1016/j.copbio.2008.07.006 (2008).
- 58 Lee, H., DeLoache, W. C. & Dueber, J. E. Spatial organization of enzymes for metabolic engineering. *Metab Eng* **14**, 242-251, doi:10.1016/j.ymben.2011.09.003 (2012).
- 59 Vital-Lopez, F. G., Armaou, A., Nikolaev, E. V. & Maranas, C. D. A computational procedure for optimal engineering interventions using kinetic models of metabolism. *Biotechnol Prog* **22**, 1507-1517, doi:10.1021/bp060156o (2006).
- 60 Fernandez-Cabezón, L., Cros, A. & Nikel, P. I. Evolutionary Approaches for Engineering Industrially Relevant Phenotypes in Bacterial Cell Factories. *Biotechnol J* **14**, e1800439, doi:10.1002/biot.201800439 (2019).
- 61 Nielsen, J. It is all about metabolic fluxes. *J Bacteriol* **185**, 7031-7035, doi:10.1128/JB.185.24.7031-7035.2003 (2003).
- 62 Nielsen, J. & Keasling, J. D. Engineering Cellular Metabolism. *Cell* **164**, 1185-1197, doi:10.1016/j.cell.2016.02.004 (2016).
- 63 Petzold, C. J., Chan, L. J., Nhan, M. & Adams, P. D. Analytics for Metabolic Engineering. *Front Bioeng Biotechnol* **3**, 135, doi:10.3389/fbioe.2015.00135 (2015).
- 64 Kanehisa, M. & Goto, S. KEGG: kyoto encyclopedia of genes and genomes. *Nucleic Acids Res* **28**, 27-30, doi:10.1093/nar/28.1.27 (2000).
- 65 Karp, P. D. *et al.* Computational Metabolomics Operations at BioCyc.org. *Metabolites* **5**, 291-310, doi:10.3390/metabo5020291 (2015).
- 66 Caspi, R. *et al.* The MetaCyc database of metabolic pathways and enzymes and the BioCyc collection of pathway/genome databases. *Nucleic Acids Res* **40**, D742-753, doi:10.1093/nar/gkr1014 (2012).
- 67 Schomburg, I. *et al.* BRENDA, the enzyme database: updates and major new developments. *Nucleic Acids Res* **32**, D431-433, doi:10.1093/nar/gkh081 (2004).
- 68 Maia, P., Rocha, M. & Rocha, I. In Silico Constraint-Based Strain Optimization Methods: the Quest for Optimal Cell Factories. *Microbiol Mol Biol Rev* **80**, 45-67, doi:10.1128/MMBR.00014-15 (2016).
- 69 Volkova, S., Matos, M. R. A., Mattanovich, M. & Marin de Mas, I. Metabolic Modelling as a Framework for Metabolomics Data Integration and Analysis. *Metabolites* **10**, doi:10.3390/metabo10080303 (2020).

- 70 Lloyd, C. J. *et al.* COBRAME: A computational framework for genome-scale models of metabolism and gene expression. *PLoS Comput Biol* **14**, e1006302, doi:10.1371/journal.pcbi.1006302 (2018).
- 71 Sarathy, C. *et al.* Comparison of metabolic states using genome-scale metabolic models. *PLoS Comput Biol* **17**, e1009522, doi:10.1371/journal.pcbi.1009522 (2021).
- 72 Saa, P. & Nielsen, L. K. A general framework for thermodynamically consistent parameterization and efficient sampling of enzymatic reactions. *PLoS Comput Biol* **11**, e1004195, doi:10.1371/journal.pcbi.1004195 (2015).
- 73 Faulon, J. L. & Faure, L. In silico, in vitro, and in vivo machine learning in synthetic biology and metabolic engineering. *Curr Opin Chem Biol* **65**, 85-92, doi:10.1016/j.cbpa.2021.06.002 (2021).
- 74 Lawson, C. E. *et al.* Machine learning for metabolic engineering: A review. *Metab Eng* **63**, 34-60, doi:10.1016/j.ymben.2020.10.005 (2021).
- 75 Jumper, J. *et al.* Highly accurate protein structure prediction with AlphaFold. *Nature* **596**, 583-589, doi:10.1038/s41586-021-03819-2 (2021).
- 76 Gibson, D. G. *et al.* Creation of a bacterial cell controlled by a chemically synthesized genome. *Science* **329**, 52-56, doi:10.1126/science.1190719 (2010).
- 77 Meng, F. & Ellis, T. The second decade of synthetic biology: 2010-2020. *Nat Commun* **11**, 5174, doi:10.1038/s41467-020-19092-2 (2020).
- 78 . (!!! INVALID CITATION !!! {}).
- 79 Zeng, W., Guo, L., Xu, S., Chen, J. & Zhou, J. High-Throughput Screening Technology in Industrial Biotechnology. *Trends Biotechnol* **38**, 888-906, doi:10.1016/j.tibtech.2020.01.001 (2020).
- 80 Beuter, D. *et al.* Selective Enrichment of Slow-Growing Bacteria in a Metabolism-Wide CRISPRi Library with a TIMER Protein. *ACS Synth Biol* **7**, 2775-2782, doi:10.1021/acssynbio.8b00379 (2018).
- 81 Wiedenheft, B. *et al.* RNA-guided complex from a bacterial immune system enhances target recognition through seed sequence interactions. *Proc Natl Acad Sci U S A* **108**, 10092-10097, doi:10.1073/pnas.1102716108 (2011).
- 82 Jinek, M. *et al.* A programmable dual-RNA-guided DNA endonuclease in adaptive bacterial immunity. *Science* **337**, 816-821, doi:10.1126/science.1225829 (2012).
- 83 Nishida, K. & Kondo, A. CRISPR-derived genome editing technologies for metabolic engineering. *Metab Eng*, doi:10.1016/j.ymben.2020.12.002 (2020).

- 84 Anzalone, A. V., Koblan, L. W. & Liu, D. R. Genome editing with CRISPR-Cas nucleases, base editors, transposases and prime editors. *Nat Biotechnol* **38**, 824-844, doi:10.1038/s41587-020-0561-9 (2020).
- 85 Arnold, F. H. How proteins adapt: lessons from directed evolution. *Cold Spring Harb Symp Quant Biol* **74**, 41-46, doi:10.1101/sqb.2009.74.046 (2009).
- 86 Bloom, J. D. & Arnold, F. H. In the light of directed evolution: pathways of adaptive protein evolution. *Proc Natl Acad Sci U S A* **106 Suppl 1**, 9995-10000, doi:10.1073/pnas.0901522106 (2009).
- 87 Mavrommati, M., Daskalaki, A., Papanikolaou, S. & Aggelis, G. Adaptive laboratory evolution principles and applications in industrial biotechnology. *Biotechnol Adv*, 107795, doi:10.1016/j.biotechadv.2021.107795 (2021).
- 88 Sarnaik, A., Liu, A., Nielsen, D. & Varman, A. M. High-throughput screening for efficient microbial biotechnology. *Curr Opin Biotechnol* **64**, 141-150, doi:10.1016/j.copbio.2020.02.019 (2020).
- 89 Goni-Moreno, A. & Nikel, P. I. High-Performance Biocomputing in Synthetic Biology-Integrated Transcriptional and Metabolic Circuits. *Front Bioeng Biotechnol* **7**, 40, doi:10.3389/fbioe.2019.00040 (2019).
- 90 Malyshev, D. A. *et al.* A semi-synthetic organism with an expanded genetic alphabet. *Nature* **509**, 385-388, doi:10.1038/nature13314 (2014).
- 91 Hirao, I. *et al.* An unnatural base pair for incorporating amino acid analogs into proteins. *Nat Biotechnol* **20**, 177-182, doi:10.1038/nbt0202-177 (2002).
- 92 Shen, Y. *et al.* Deep functional analysis of synII, a 770-kilobase synthetic yeast chromosome. *Science* **355**, doi:10.1126/science.aaf4791 (2017).
- 93 van der Sloot, A. & Tyers, M. Synthetic Genomics: Rewriting the Genome Chromosome by Chromosome. *Mol Cell* **66**, 441-443, doi:10.1016/j.molcel.2017.05.007 (2017).
- 94 Hutchison, C. A., 3rd *et al.* Design and synthesis of a minimal bacterial genome. *Science* **351**, aad6253, doi:10.1126/science.aad6253 (2016).
- 95 Martinez-Garcia, E. & de Lorenzo, V. The quest for the minimal bacterial genome. *Curr Opin Biotechnol* **42**, 216-224, doi:10.1016/j.copbio.2016.09.001 (2016).
- 96 Antczak, M., Michaelis, M. & Wass, M. N. Environmental conditions shape the nature of a minimal bacterial genome. *Nat Commun* **10**, 3100, doi:10.1038/s41467-019-10837-2 (2019).
- 97 Vickers, C. E. The minimal genome comes of age. *Nat Biotechnol* **34**, 623-624, doi:10.1038/nbt.3593 (2016).

- 98 Fredens, J. *et al.* Total synthesis of *Escherichia coli* with a recoded genome. *Nature* **569**, 514-518, doi:10.1038/s41586-019-1192-5 (2019).
- 99 Fan, C. *et al.* Chromosome-free bacterial cells are safe and programmable platforms for synthetic biology. *Proc Natl Acad Sci U S A* **117**, 6752-6761, doi:10.1073/pnas.1918859117 (2020).
- 100 Burkhardt, R. W., Jr. Lamarck, evolution, and the inheritance of acquired characters. *Genetics* **194**, 793-805, doi:10.1534/genetics.113.151852 (2013).
- 101 Grissa, I., Vergnaud, G. & Pourcel, C. The CRISPRdb database and tools to display CRISPRs and to generate dictionaries of spacers and repeats. *BMC Bioinformatics* **8**, 172, doi:10.1186/1471-2105-8-172 (2007).
- 102 Ishino, Y., Shinagawa, H., Makino, K., Amemura, M. & Nakata, A. Nucleotide sequence of the *iap* gene, responsible for alkaline phosphatase isozyme conversion in *Escherichia coli*, and identification of the gene product. *J Bacteriol* **169**, 5429-5433, doi:10.1128/jb.169.12.5429-5433.1987 (1987).
- 103 Jansen, R., van Embden, J. D. A., Gaastra, W. & Schouls, L. M. Identification of genes that are associated with DNA repeats in prokaryotes. *Mol Microbiol* **43**, 1565-1575, doi:DOI 10.1046/j.1365-2958.2002.02839.x (2002).
- 104 Gasiunas, G., Barrangou, R., Horvath, P. & Siksnys, V. Cas9-crRNA ribonucleoprotein complex mediates specific DNA cleavage for adaptive immunity in bacteria. *Proc Natl Acad Sci U S A* **109**, E2579-2586, doi:10.1073/pnas.1208507109 (2012).
- 105 Gao, C. *et al.* Programmable biomolecular switches for rewiring flux in *Escherichia coli*. *Nat Commun* **10**, 3751, doi:10.1038/s41467-019-11793-7 (2019).
- 106 Kim, S. G. CRISPR innovations in plant breeding. *Plant Cell Rep* **40**, 913-914, doi:10.1007/s00299-021-02703-7 (2021).
- 107 Ishino, Y., Krupovic, M. & Forterre, P. History of CRISPR-Cas from Encounter with a Mysterious Repeated Sequence to Genome Editing Technology. *J Bacteriol* **200**, doi:10.1128/JB.00580-17 (2018).
- 108 Jansen, R., Embden, J. D., Gaastra, W. & Schouls, L. M. Identification of genes that are associated with DNA repeats in prokaryotes. *Mol Microbiol* **43**, 1565-1575, doi:10.1046/j.1365-2958.2002.02839.x (2002).
- 109 Makarova, K. S., Grishin, N. V., Shabalina, S. A., Wolf, Y. I. & Koonin, E. V. A putative RNA-interference-based immune system in prokaryotes: computational analysis of the predicted enzymatic

- machinery, functional analogies with eukaryotic RNAi, and hypothetical mechanisms of action. *Biol Direct* **1**, 7, doi:10.1186/1745-6150-1-7 (2006).
- 110 Barrangou, R. *et al.* CRISPR provides acquired resistance against viruses in prokaryotes. *Science* **315**, 1709-1712, doi:10.1126/science.1138140 (2007).
- 111 Brouns, S. J. *et al.* Small CRISPR RNAs guide antiviral defense in prokaryotes. *Science* **321**, 960-964, doi:10.1126/science.1159689 (2008).
- 112 Garneau, J. E. *et al.* The CRISPR/Cas bacterial immune system cleaves bacteriophage and plasmid DNA. *Nature* **468**, 67-71, doi:10.1038/nature09523 (2010).
- 113 Deveau, H. *et al.* Phage response to CRISPR-encoded resistance in *Streptococcus thermophilus*. *J Bacteriol* **190**, 1390-1400, doi:10.1128/JB.01412-07 (2008).
- 114 Deltcheva, E. *et al.* CRISPR RNA maturation by trans-encoded small RNA and host factor RNase III. *Nature* **471**, 602-607, doi:10.1038/nature09886 (2011).
- 115 Sapranaukas, R. *et al.* The *Streptococcus thermophilus* CRISPR/Cas system provides immunity in *Escherichia coli*. *Nucleic Acids Res* **39**, 9275-9282, doi:10.1093/nar/gkr606 (2011).
- 116 Adli, M. The CRISPR tool kit for genome editing and beyond. *Nat Commun* **9**, 1911, doi:10.1038/s41467-018-04252-2 (2018).
- 117 Walton, R. T., Christie, K. A., Whittaker, M. N. & Kleinstiver, B. P. Unconstrained genome targeting with near-PAMless engineered CRISPR-Cas9 variants. *Science* **368**, 290-296, doi:10.1126/science.aba8853 (2020).
- 118 Larson, M. H. *et al.* CRISPR interference (CRISPRi) for sequence-specific control of gene expression. *Nat Protoc* **8**, 2180-2196, doi:10.1038/nprot.2013.132 (2013).
- 119 Gilbert, L. A. *et al.* CRISPR-Mediated Modular RNA-Guided Regulation of Transcription in Eukaryotes. *Cell* **154**, 442-451, doi:10.1016/j.cell.2013.06.044 (2013).
- 120 Lian, J., Hamedirad, M., Hu, S. & Zhao, H. Combinatorial metabolic engineering using an orthogonal tri-functional CRISPR system. *Nat Commun* **8**, 1688, doi:10.1038/s41467-017-01695-x (2017).
- 121 Abdullah *et al.* CRISPR base editing and prime editing: DSB and template-free editing systems for bacteria and plants. *Synth Syst Biotechnol* **5**, 277-292, doi:10.1016/j.synbio.2020.08.003 (2020).
- 122 Komor, A. C. *et al.* Improved base excision repair inhibition and bacteriophage Mu Gam protein yields C:G-to-T:A base editors with

- higher efficiency and product purity. *Sci Adv* **3**, eaao4774, doi:10.1126/sciadv.aao4774 (2017).
- 123 Gaudelli, N. M. *et al.* Programmable base editing of A*T to G*C in genomic DNA without DNA cleavage. *Nature* **551**, 464-471, doi:10.1038/nature24644 (2017).
- 124 Komor, A. C., Kim, Y. B., Packer, M. S., Zuris, J. A. & Liu, D. R. Programmable editing of a target base in genomic DNA without double-stranded DNA cleavage. *Nature* **533**, 420-424, doi:10.1038/nature17946 (2016).
- 125 Halperin, S. O. *et al.* CRISPR-guided DNA polymerases enable diversification of all nucleotides in a tunable window. *Nature* **560**, 248-252, doi:10.1038/s41586-018-0384-8 (2018).

Chapter 2

ACCELERATED GENOME ENGINEERING OF *PSEUDOMONAS PUTIDA* BY I-SCEI- MEDIATED RECOMBINATION AND CRISPR- CAS9 COUNTERSELECTION

Nicolas T. Wirth¹, Ekaterina Kozaeva¹, and Pablo I. Nikel^{1*}.

Microbial Biotechnology (2020) 13(1): 233-249.

1. The Novo Nordisk Foundation Center for Biosustainability, Technical University of Denmark, 2800 Kgs. Lyngby, Denmark

* Correspondence to:

Pablo I. Nikel

(pabnik@biosustain.dtu.dk)

The Novo Nordisk Foundation Center for
Biosustainability

Technical University of Denmark

Kgs Lyngby 2800, Denmark

Tel: (+45) 93 51 19 18

INTRODUCTION

Supported by the advances in synthetic biology and metabolic engineering made in the last few years, several microbes have emerged from a rather shadowy existence to become suitable biotechnological platforms¹. Several members of the genus *Pseudomonas*, for instance, are being adopted by a steadily increasing number of laboratories worldwide as *chassis* for both fundamental and applied studies²⁻⁵. *Pseudomonas* species, usually found in natural environments, distinguish themselves from other microorganisms by an unrivalled wealth of biochemical functions that are embedded in robust and flexible metabolisms⁶ – allowing bacteria to adapt to a diverse range of stressful conditions⁷.

A rich set of synthetic biology tools has been developed to untap the metabolic potential of key representatives of the genus, e.g. *P. putida*, *P. taiwanensis* and *P. fluorescens*⁸⁻¹¹. A breakthrough in the standardization of a toolbox of reliable molecular tools for Gram-negative bacteria has been the creation of the *Standard European Vector Architecture* (SEVA) platform^{12,13}, including a variety of genetic parts (e.g. promoters, origins of replication and antibiotic-resistance determinants) that are functional in a number of *Pseudomonas* species. More recently, synthetic libraries of constitutive promoters have facilitated the predictable expression of a gene of interest with a desired strength¹⁴, particularly when the promoter of choice is to be combined with standardized translational couplers¹⁵.

Considerable efforts in the scientific *Pseudomonas* community have led to the development of tools for the construction of clean deletion mutants. Counterselection strategies adapted to *Pseudomonas* include a *pyrF*-based dual-selection system¹⁶, *sacB* as counterselectable marker¹⁷ and the *upp* gene (uracil phosphoribosyltransferase) in an *upp*-deficient mutant¹⁸. The λ *Red* system, widely used in *Escherichia coli* for recombineering¹⁹, has been combined with Cre/*loxP* site-specific recombination to enable genomic modifications with linear DNA fragments²⁰. Cook *et al.*¹⁰ introduced a recombineering method based on the λ *Red* system together with CRISPR-Cas9 counterselection. Such recombinase-based genome-editing approaches

have recently been complemented by the design of a RecET system for *P. putida*^{21,22}, and Aparicio *et al.*²³ further honed the CRISPR-Cas9 counterselection strategy, combining it with Ssr-based recombination for genome engineering.

Among all these efforts, the standardized genome engineering method developed by Martínez-García and de Lorenzo²⁴, based on the chromosomal integration of a suicide plasmid followed by the action of the homing nuclease I-SceI from *Saccharomyces cerevisiae*, excels for its efficiency and robustness to mediate any kind of genetic modification (e.g. large deletions, point mutations and allelic exchanges) – and is thus amongst the most intensively used by the scientific *Pseudomonas* community. The system relies on vector pEMG; this vector contains the conditional origin of replication *R6K*, which requires the cognate Rep protein π encoded by *pir* for replication. In bacterial strains that lack *pir*, vector pEMG behaves as a suicide plasmid. The vector contains a polylinker region (multiple cloning site) flanked by two I-SceI recognition sites cloned into the *lacZ* α fragment, thus allowing for blue–white screening in *E. coli* cells carrying the *lacZ* Δ *M15* mutation. A set of auxiliary SEVA plasmids harbors the gene encoding I-SceI under the control of the 3-methylbenzoate (3-*mBz*)-inducible XylS/*Pm* expression system from strain mt-2²⁴.

In this study, we present a smooth and quick workflow for genome editing of *P. putida* based on the action of I-SceI or CRISPR/Cas9 as a counterselection strategy. The integration of genes encoding fluorescent proteins (and antibiotic-resistance determinants) into the target locus circumvents experimental steps that would be needed to ensure the presence of the suicide vector.

Table 2.1. Plasmids used in this work

Name^a	Relevant features^b	Source or reference
pEMG	Suicide vector used for deletions in Gram-negative bacteria; <i>oriT</i> , <i>traJ</i> , <i>lacZα</i> , <i>oriV(R6K)</i> ; Km ^R	Martínez-García and de Lorenzo (2011)
pRK600	Helper plasmid used for conjugation; <i>oriV(ColE1)</i> , <i>mob(RK2)</i> , <i>tra(RK2)</i> ; Cm ^R	Kessler <i>et al.</i> (1992)
pGNW2	Derivative of vector pEMG carrying <i>P_{14g}→msfGFP</i>	This work
pGNW4	Derivative of vector pGNW2; Sm ^R	This work
pGNW6	Derivative of vector pGNW2; Gm ^R	This work
pGNW2 Δ <i>nicX</i>	Derivative of vector pGNW2 carrying HRs to delete <i>nicX</i> (<i>PP_3945</i>) in <i>P. putida</i> KT2440	This work
pGNW4 Δ <i>nicX</i>	Derivative of vector pGNW4 carrying HRs to delete <i>nicX</i> (<i>PP_3945</i>) in <i>P. putida</i> KT2440	This work
pGNW6 Δ <i>nicX</i>	Derivative of vector pGNW6 carrying HRs to delete <i>nicX</i> (<i>PP_3945</i>) in <i>P. putida</i> KT2440	This work
pGNW2 Δ <i>aceEF</i>	Derivative of vector pGNW2 carrying HRs to delete <i>aceEF</i> (<i>PP_0338-PP_0339</i>) in <i>P. putida</i> KT2440	This work
pSEVA2313	Expression vector; <i>oriV(pBBR1)</i> , <i>P_{EM7}</i> ; Km ^R	This work
pS2313 R	Derivative of vector pSEVA2313 carrying <i>P_{EM7}→mRFPI</i> (Campbell <i>et al.</i> , 2002); Km ^R	This work

Name ^a	Relevant features ^b	Source or reference
pS2313 B	Derivative of vector pSEVA2313 carrying $P_{EM7} \rightarrow mBFP2$ (Subach <i>et al.</i> , 2011); Km ^R	This work
pS2313 O	Derivative of vector pSEVA2313 carrying $P_{EM7} \rightarrow mOrange2$ (Shaner <i>et al.</i> , 2008); Km ^R	This work
pS2313 T	Derivative of vector pSEVA2313 carrying $P_{EM7} \rightarrow mTurquoise2$ (Goedhart <i>et al.</i> , 2012); Km ^R	This work
pGNW2 LP:: P_{EM7} -mRFP	Derivative of vector pGNW2 carrying $P_{EM7} \rightarrow mRFP1$	This work
pGNW2 LPR	Derivative of vector pGNW2 carrying HRs to insert $P_{14g}(BCD2) \rightarrow mRFP1$ into a landing pad in the chromosome of <i>P. putida</i> KT2440	This work
pGNW2 LPG	Derivative of vector pGNW2 carrying HRs to insert $P_{14g}(BCD2) \rightarrow msfGFP$ into a landing pad in the chromosome of <i>P. putida</i> KT2440	This work
pGNW2 LPB	Derivative of vector pGNW2 carrying HRs to insert $P_{14g}(BCD2) \rightarrow mBFP2$ into a landing pad in the chromosome of <i>P. putida</i> KT2440	This work
pGNW4 LPO	Derivative of vector pGNW4 carrying HRs to insert $P_{14g}(BCD2) \rightarrow mOrange2$ into a landing pad in the chromosome of <i>P. putida</i> KT2440	This work
pGNW6 LPT	Derivative of vector pGNW6 carrying HRs to insert $P_{14g}(BCD2) \rightarrow mTurquoise2$ into a landing pad in the chromosome of <i>P. putida</i> KT2440	This work
pSEVA128S	Helper plasmid; $oriV(RK2)$, $xylS$, $P_m \rightarrow I-SceI$; Amp ^R	Aparicio <i>et al.</i> (2015)

Name ^a	Relevant features ^b	Source or reference
pSEVA228S	Helper plasmid; <i>oriV(RK2)</i> , <i>xylS</i> , <i>Pm</i> → <i>I-SceI</i> ; Km ^R	Aparicio <i>et al.</i> (2015)
pSEVA428S	Helper plasmid; <i>oriV(RK2)</i> , <i>xylS</i> , <i>Pm</i> → <i>I-SceI</i> ; Sm ^R	Aparicio <i>et al.</i> (2015)
pSEVA628S	Helper plasmid; <i>oriV(RK2)</i> , <i>xylS</i> , <i>Pm</i> → <i>I-SceI</i> ; Gm ^R	Aparicio <i>et al.</i> (2015)
pSEVA1213S	Helper plasmid; <i>oriV(RK2)</i> , <i>P_{EM7}</i> → <i>I-SceI</i> ; Amp ^R	This work
pSEVA6213S	Helper plasmid; <i>oriV(RK2)</i> , <i>P_{EM7}</i> → <i>I-SceI</i> ; Gm ^R	This work
pSEVA448	Expression vector; <i>oriV(pRO1600/ColE1)</i> , <i>xylS</i> , <i>Pm</i> ; Sm ^R	Silva-Rocha <i>et al.</i> (2013)
pSEVA421.Cas9tr	Cloning vector; <i>oriV(RK2)</i> , <i>cas9</i> , <i>tracrRNA</i> ; Sm ^R	Aparicio <i>et al.</i> (2018)
pS448 CsR	Derivative of vector pSEVA448 used for CRISPR-Cas9 counterselection; <i>xylS</i> (cured of <i>BsaI</i> restriction sites), <i>Pm</i> → <i>cas9</i> , <i>P_{EM7}</i> → <i>sgRNA</i> ; Sm ^R	This work
pS448 CsR_aceEF	Derivative of vector pS448 CsR carrying <i>P_{EM7}</i> → <i>aceF</i> -targeting <i>sgRNA</i> ; Sm ^R	This work

a. Plasmids can be obtained from Addgene (www.addgene.org) with the following deposit numbers: pGNW2 (122086), pGNW4 (122088), pGNW6 (122093), pSEVA1213S (122095), pSEVA6213S (122094) and pS448 CsR (122096).

b. Antibiotic markers: *Amp*, ampicillin; *Cm*, chloramphenicol; *Km*, kanamycin; *Sm*, streptomycin; and *Gm*, gentamicin. HRs, homology regions.

Furthermore, we propose the adoption of the *USER* assembly method²⁵⁻²⁸ to enable the quick and highly accurate assembling of homology regions (HRs) required for the genome engineering protocol. Helper plasmids for the constitutive expression of the gene encoding the homing I-*SceI* endonuclease from yeast were also designed to avoid the addition of chemical inducers during the process. The resulting streamlined protocol enables the introduction of virtually any genomic modification in *P. putida* within 5 days (for a single genetic manipulation including the construction of all necessary plasmids) down to 3 days (time required for each mutagenesis round once the relevant plasmids have been constructed), followed by plasmid curing. We demonstrate the potential of the technique by deleting both non-essential and difficult-to-knock-out metabolic genes in the platform strain KT2440. We furthermore show the integration of genes encoding different fluorescent proteins into a suitable landing pad in the *P. putida* chromosome and discuss their application as insertional reporters.

Technical implementation

The overall genome-editing procedure begins with the construction of donor DNA that is cloned into the suicide vector pGNW and derivatives thereof (**Figure 2.1**) Such donor DNA, containing suitable HRs, serves as template for the endogenous homologous DNA recombination machinery. The procedure also includes the cloning of a target-specific synthetic guide RNA (sgRNA) into a dedicated CRISPR-Cas9 plasmid (when applicable), the integration of the donor DNA into the *Pseudomonas* chromosome, and the specific cleavage of chromosomal DNA by endonucleases (i.e. I-*SceI* or Cas9) for the resolution of co-integrates. The specific steps of the procedure are detailed in the sections below.

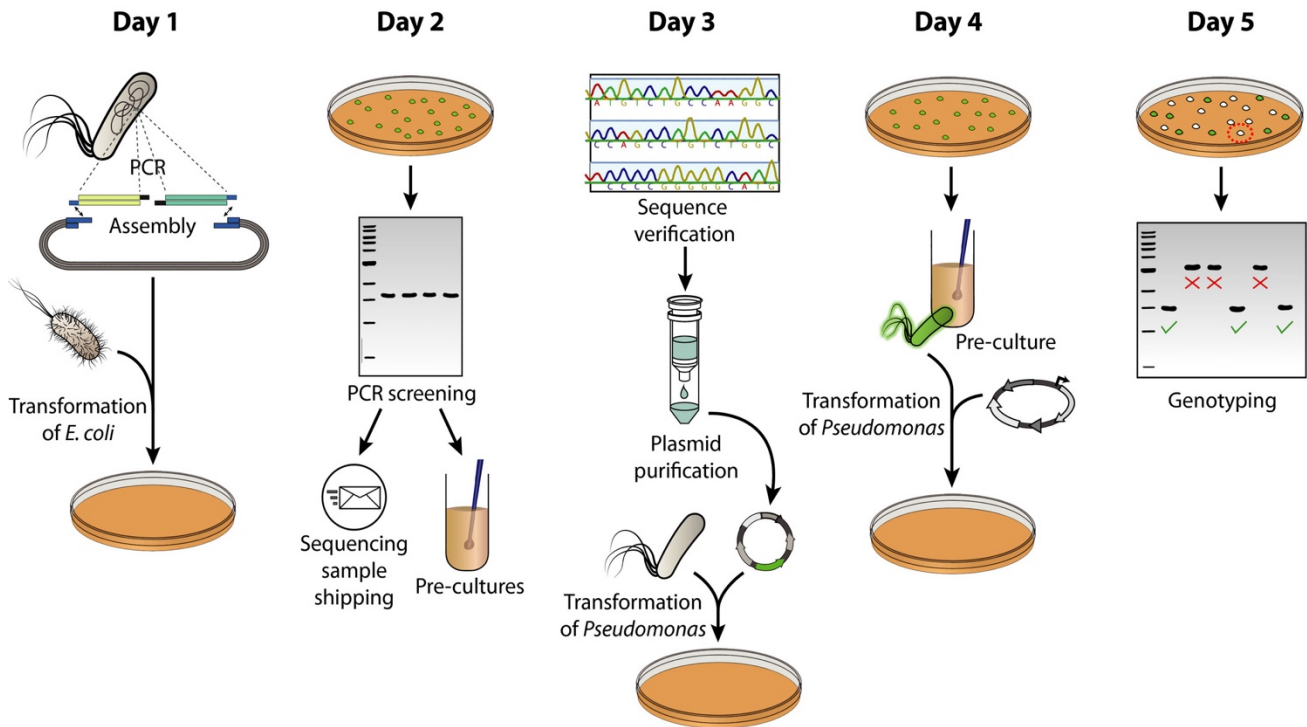


Figure 2.1. Overview diagram of the genome engineering procedure in *Pseudomonas putida*. On the delivery date of the designed oligonucleotides, homologous regions are amplified from the *Pseudomonas* genome and assembled into a suitable pGNW vector. The resulting plasmid is then delivered into *E. coli* λ pir cells via chemical transformation. Furthermore (if applicable), a synthetic spacer, completing a specific synthetic guide RNA (sgRNA), is separately prepared and cloned into the CRISPR-Cas9—vector pS448·CsR. On day 2, *E. coli* transformants are screened for the correct pGNW insert size (and spacer insertion in vector pS448·CsR, if applicable) via colony PCR, the resulting amplicons are sent out for sequencing, and the corresponding clones are used to inoculate liquid cultures. Day 3 includes the verification of sequence integrity of the insert in the pGNW vector, the purification of individual plasmids, and their delivery into *Pseudomonas* either via electroporation or tri-parental mating. The resulting co-integrants are enriched in liquid LB cultures during the course of day 4 and transformed with either an I-SceI—bearing plasmid or plasmid pS448·CsR carrying an appropriate sgRNA. Finally, *Pseudomonas* colonies without fluorescence are tested on day 5 for their genotype via colony PCR.

Design and construction of plasmids

Construction of the suicide vector pGNW and derivatives

We first equipped plasmid pEMG with the gene encoding the monomeric superfolder GFP (*msfGFP*)¹⁵ in the vector backbone while screening different combinations of promoters and translation initiation regions (*TIR*) that would give a high fluorescence output when the plasmid is integrated into the target chromosome. The fusion of the strong constitutive *P*_{14g} promoter and a variation of the *TIR* sequence preceding *msfGFP*¹⁵ allowed for the direct visualization of *Pseudomonas* colonies harboring a single (chromosomal) copy of the novel vector pGNW2 (**Table 2.1.**) by inspecting the plates on a blue-light transilluminator. A set of pGNW vectors was constructed by swapping the kanamycin resistance (*Km*^R) determinant present in vector pGNW2 by the corresponding, SEVA-based genes conferring streptomycin (*Sm*^R) or gentamicin (*Gm*^R) resistance, giving rise to vectors pGNW4 and pGNW6, respectively (**Table 2.1.**).

A pGNW plasmid ready for genome engineering in *Pseudomonas* (**Figure 2.2.**) is composed of the vector backbone with an antibiotic-resistance gene, the R6K origin of replication [*oriV(R6K)*], the *traJ* gene and a relaxation region (*oriT*) required for bacterial conjugation, and a site-specific DNA insert that (i) is homologous to the target locus (i.e. HRs upstream and downstream to the region of interest) within the *Pseudomonas* genome and (ii) contains a desired modification. Such modification can be as short as a single base for a point mutation or arbitrarily long for the insertion of whole gene clusters. The insert and the vector backbone are assembled employing standard protocols, e.g. traditional cloning by restriction digest and ligation²⁹, Gibson assembly³⁰ or *USER* assembly²⁸ that is recommended and further described here.

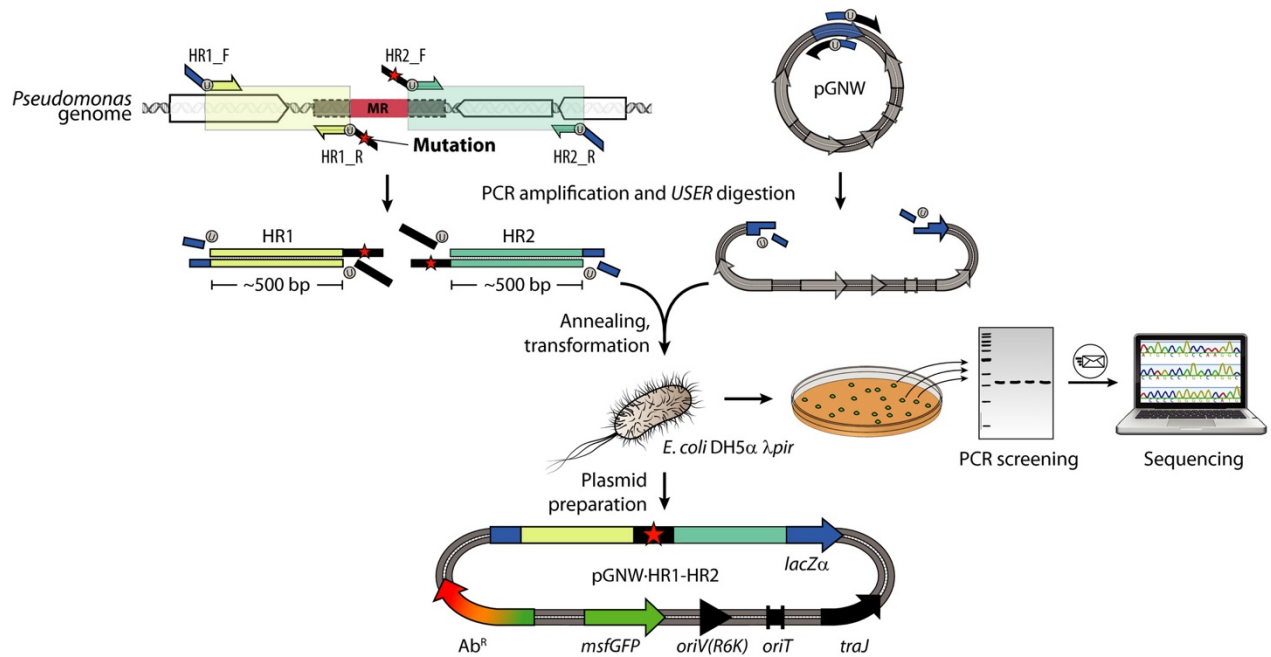


Figure 2.2. Workflow for the construction of derivatives of pGNW vectors for genome engineering. Two homology regions (HR1 and HR2), each one spanning about 500 bp and located upstream and downstream of the mutagenesis region (MR), are amplified from genomic DNA of *Pseudomonas* via PCR. Modifications (i.e. insertions or substitutions) are introduced between the HRs as overhangs in the oligonucleotides (indicated in the diagram with a red star) or as additional DNA fragments (not shown). For gene deletions, the sequences of the HRs are designed so that they frame the genome sequence to be deleted. HR1 and HR2 are fused and integrated into one of the pGNW vectors via USER assembly (shown here) or alternative molecular cloning techniques. The thereby assembled pGNW plasmid is then introduced into *E. coli* DH5α λpir. Individual *E. coli* clones obtained after transformation are examined for green fluorescence on a blue-light transilluminator and checked for the correct pGNW insert size via colony PCR, and the purified amplicon is sent for sequencing. After the sequence integrity is confirmed, pGNW plasmids are purified from the respective *E. coli* strain and saved for the next step.

Oligonucleotide design

One primer pair is required to amplify each fragment that constitutes the pGNW derivative *via* PCR. Depending on the type of modification (see description below), this means that a minimum of three oligonucleotide pairs are required for cloning. A first pair of oligonucleotides (pGNW-*USER_F* and pGNW-*USER_R*, **Table S2.1**) is used to reverse-amplify the pGNW backbone, and the resulting linear fragment can be used in a standardized way for every cloning procedure. Two further pairs of primers are required to amplify the homologous regions HR1 and HR2 from the *Pseudomonas* genome, flanking the mutagenesis region (MR) targeted. The sequences of the primers HR1_F and HR2_R (**Figure 2.2.**) are determined by the MR to be modified (or deleted), and by the type of modification (i.e. deletion, insertion or substitution).

- i. Identify the ends of the MR sequence. The binding part of HR1_R starts upstream of the MR and extends into HR1, while the binding part of HR2_F starts downstream of the 3'-end of the MR and extends into HR2 (**Figure 2.2.**). Extend the sequence of both oligonucleotides so that they fulfil general primer design requirements satisfactorily (i.e. 18–25 nt length, 40–60% GC content and GC-clamp).
 - a. For deletions of chromosomal sequences, use the last ~ 100 bp of HR1 and the first ~ 100 bp of HR2 as input sequences for the *AMUSER* tool³¹, available online at <http://www.cbs.dtu.dk/services/AMUSER/>, to identify suitable *USER* overhangs for the two primers. Add the required bases to the 5'-end of both oligonucleotides. For gene deletions to have minimum polar effects and to avoid the potential creation of toxic, truncated polypeptides, we recommend leaving the *START* and *STOP* codons of the target gene intact and deleting the interjacent sequence. Upon deletion, this approach will leave e.g. 5'-ATG TGA-3' in lieu of the coding sequence, where ATG and TGA are the *START* and the *STOP* codons, respectively.
 - b. For substitutions and small insertions, the mutation can be introduced within the primer overhangs. Add the desired

sequence including the modification to the 5'-end of HR2 and use the first ~ 100 bp of this extended HR2, as well as the last ~ 100 bp of HR1, as input sequences for the *AMUSER* online tool. Add any additional bases including the *USER* overhangs to the 5'-end of both primers.

- c. For larger insertions (exceeding 2× the annealing region of the primers), additional DNA fragments should be amplified separately and assembled with HR1 and HR2 to form the insert to be cloned in the pGNW vector of choice. The *AMUSER* tool can be used to design primers with suitable overhangs for their assembly.
- ii. Design HR1_F at a distance of ~ 500 bp upstream of HR1_R with a similar melting temperature. Design HR2_R at ~ 500 bp downstream of HR2_F (**Figure 2.2.**). Add the motif 5'-AGA TCC U-3' as the primer overhang to HR1_F, and 5'-AGG TCG ACU-3' as overhang to HR2_R. These two overhangs match the ones that have been used in the primers to reverse-amplify vector pGNW.
- iii. Design one pair of 'g-check' primers to test for the genotype of individual colonies after the genome engineering procedure. For deletions and insertions larger than 30 bp, the primers bind upstream and downstream of the MR, respectively, and amplify a product that can be distinguished from the wild-type sequence with agarose gel electrophoresis according to its size (a size difference of > 10% is recommended). For substitutions of identical size, one primer should be able to bind only within the MR. The wild-type sequence should thus give no amplification. For substitutions of only a few base pairs, the mutation-containing region must be amplified and the genotype confirmed by restriction analysis (if applicable) or sequencing.

Amplification and assembly of DNA fragments

- i. Amplify vector pGNW using 5 ng of plasmid as template and primers pGNW-*USER*_F and pGNW-*USER*_R (**Table S2.1**) using *Phusion*TM U Hot Start DNA polymerase. Use standard reaction conditions as recommended by the manufacturer, with an elongation time of 3 min as well as an annealing temperature 'touchdown' from 65 to 59°C,

with a decrement of -1°C per cycle and a final annealing temperature of 58°C for 30 further cycles. We recommend to perform gel purification on the amplified pGNW fragment and to use the purified product as template for further PCRs. In this way, digestion with *DpnI* to remove circular plasmids (i.e. template) can be omitted. We further recommend generating a large amount of linearized pGNW vector in several parallel PCRs for repeated use in *USER* assembly.

- ii. Perform separate amplification reactions on purified genomic *Pseudomonas* DNA with the adequate primer pairs (HR1_F/HR1_R and HR2_F/HR2_R) to generate the HR1 and HR2 fragments. Perform, if needed, additional PCRs to generate the DNA fragments required for insertions. We generally recommend the use of a touchdown PCR protocol to reduce the formation of unspecific by-products.
- iii. Analyse a 3- to 5- μl aliquot of each PCR by agarose gel electrophoresis to verify the correct amplification of the products. The concentrations of the fragments can be roughly estimated from the intensities of their bands. If agarose gel electrophoresis reveals the presence of non-specific by-products, the desired bands have to be purified from a gel prior to cloning. If the product appears clean, the PCR reaction can be used directly in the assembly reaction.
- iv. In a PCR tube, combine equimolar amounts of insert fragments in a volume of 7 μl with 3 μl of the linearized pGNW vector. Add 1 μl of 1 $\text{U } \mu\text{l}^{-1}$ *USER* enzyme (New England BioLabs, Ipswich, MA, USA). Set up a thermocycler and run a reaction programme as follows: *deoxyuracil excision*, 30 min at 37°C ; *annealing 1*, decrement from 28°C to 20°C , -2°C per step, 3 min step duration; and *annealing 2*, ≥ 10 min at 10°C . If a plasmid was used as template for the amplification of one of the fragments that contains the same antibiotic resistance as the employed pGNW vector, add 0.5 μl of *FastDigest DpnI* (Thermo Fisher Scientific, Waltham, MA, USA) to the reaction mix prior to incubation at 37°C .
- v. Transform 50 μl of chemically-competent *E. coli* DH5 α λpir cells with 5 μl of the assembly reaction from the previous step. Plate the cells on LB medium agar supplemented with the respective antibiotic for the pGNW vector used. If a circular plasmid was used as template in the PCR for pGNW linearization, and if the reaction was directly

employed for the assembly reaction (rather than using a gel-purified plasmid), spread the transformed *E. coli* DH5 α λ *pir* cells on plates containing 5-bromo-4-chloro-3-indolyl- β -D-galactopyranoside (Xgal) at 40 $\mu\text{g ml}^{-1}$.

Verification of clones

- i. Use primers Seq-pGNW_F and Seq-pGNW_R (**Table S2.1**) in a colony PCR (20 μl reaction volume for each PCR) to amplify the HR insert in pGNW of eight individual *E. coli* transformants that show green fluorescence under blue-light exposure (and are white under white light if Xgal was added to the plate).
- ii. Analyse a 3- to 5- μl aliquot of each PCR by agarose gel electrophoresis to verify the correct insert size. Purify the remaining volume of the PCRs with the correct insert size and send the samples for sequencing to verify sequence integrity.
- iii. Inoculate 3–5 ml LB cultures (add the corresponding antibiotic) with six individual clones that were tested for a correct insert size. Incubate the culture at 37°C for 12–18 h in a shaking incubator at 180–250 rpm (depending on the type of incubator). In order to continue with the genome engineering procedure in *Pseudomonas* on the subsequent day (section ‘Genome editing in *Pseudomonas putida*’), launch a pre-culture of strain KT2440 as well, and incubate with shaking (180–250 rpm) at 30°C.
- iv. Purify plasmid DNA from the *E. coli* cultures that tested positive by colony PCR and send the purified plasmid DNA for sequencing in addition to (or instead of) step 2.

Cloning of sgRNAs into vector pS448-CsR for counterselection of mutants

To adopt CRISPR-Cas9 as a counterselection tool, vector pS448-CsR was constructed by *USER* assembly from vector pSEVA448 (**Table 2.1.**) *via* reverse amplification with primers pS448_F and pS448_R (**Table S2.1**) and assembled with (i) *cas9*, amplified from plasmid pSEVA421.Cas9tr with primers Cas9_F and Cas9_R and (ii) a *P_{EM7}*→sgRNA module (synthesized by Integrated DNA Technologies, Leuven, Belgium; and amplified with primers sgRNA_F and sgRNA_R). This module contains a single guide

RNA construct fused to a *trans*-activating CRISPR RNA (*tracr*RNA)-part and two *Bsa*I recognition sites for the easy insertion of a spacer. The two *Bsa*I recognition sites are placed in inverse orientation immediately upstream of the *tracr*RNA part to enable the creation of incompatible, single-stranded overhangs during linearization by *Bsa*I. This step allows for the insertion of a double-stranded DNA (dsDNA) fragment with suitable overhangs. If CRISPR-Cas9 is to be used as counterselection tool, vector pS448·CsR must be equipped with an adequate spacer³², which targets the original sequence that becomes modified, as disclosed below.

Spacer design

For the use of CRISPR-Cas9 as counterselection tool, a spacer is inserted into vector pS448·CsR to target the original sequence that becomes modified after genome engineering. The spacer represents the CRISPR RNA (crRNA)-part of the sgRNA and is defined by the 20-nt sequence upstream of a spacer adjacent motif (PAM, 5'-NGG-3') on either of both DNA strands within a target DNA region. Strand specificity is not relevant when CRISPR-Cas9 is employed for counterselection, and the most important parameter is the sgRNA specificity for its target. To choose a suitable spacer sequence for counterselection, we recommend the use of the online tool *CRISPy-web*³³ as indicated below.

- i. Upload a GenBank file with the complete genomic sequence of your *Pseudomonas* species into CRISPy-web, available at <https://crispy.secondarymetabolites.org/>.
- ii. Specify either the gene that is to be deleted/substituted or the range of the MR.
- iii. Pick a suitable 20-nt spacer candidate sequence from the top entries in the list provided by the CRISPy-web application.
- iv. Design and order two oligonucleotides that are complementary to each other. The first oligonucleotide represents the 20 nt of the spacer sequence obtained in the previous step. The second oligonucleotide is the reverse complement of the first oligonucleotide. Add a 5'-AAAC-3' overhang to the 5'-end of the second oligonucleotide and a single C residue to its 3'-end. Add a 5'-GCGCG-3' overhang to the 5'-end of the first oligonucleotide. For example, if *aceF* (*PP_0338*) is to be

targeted, the sequences would be oligonucleotide 1 (*aceEF_F*), 5'-GCGCG CTC ATT CGC GTA CCT GAC AT C-3'; and oligonucleotide 2 (*aceEF_R*), 5'-AAAC ATG TCA GGT ACG CGA ATG AG C-3' **Table S2.1** in the Supporting Information; additions are indicated in boldface). For ligation, the oligonucleotides need to be phosphorylated at the 5'-OH terminus. The oligonucleotides can either be purchased with terminal phosphorylation or phosphorylated *in situ* using T4 polynucleotide kinase (PNK, see below).

DNA preparation and construction of derivatives of vector pS448·CsR

- i. Digest vector pS448·CsR with *BsaI* or *Eco31I* (Thermo Fisher Scientific) according to the manufacturer's recommendations. Use agarose gel electrophoresis and gel purification to isolate the linearized plasmid (9.9 kb) from the non-restricted fraction.
- ii. Dissolve the two-spacer oligonucleotides at 100 μ M. Phosphorylate and anneal the oligonucleotides in a thermocycler^{34,35}. This can be performed in a single 10- μ l reaction containing 6 μ l of water, 1 μ l of each oligonucleotide, 1 μ l of T4 ligase buffer and 1 μ l of T4 PNK (New England BioLabs). Use the following temperature protocol: 30 min at 37°C, 4 min at 95°C, followed by 70 cycles consisting of 12 s each, starting at 95°C and decreasing the temperature by 1°C in each cycle.
- iii. Dilute the annealed and phosphorylated oligonucleotides 1:200 with water, i.e. to a final concentration of dsDNA of 50 nM.
- iv. Ligate the dsDNA encoding the sgRNA-spacer into the linearized pS448·CsR vector in a 10- μ l reaction containing 3 μ l of diluted insert from the previous step, 10–30 ng of *BsaI*-digested pS448·CsR vector, 1 μ l of T4 ligase buffer, 1 μ l of T4 DNA ligase (New England BioLabs) and water, if needed, to reach the final volume.
- v. Ligate 30 min at room temperature and transform a 50- μ l aliquot of chemically competent *E. coli* DH5 α cells with 5 μ l of the ligation mixture. Plate on LB medium agar supplemented with streptomycin.
- vi. Purify plasmid DNA from three individual *E. coli* transformants and verify the sequence integrity by sequencing with primer SEVA-T0_F (**Table S2.1**).

Test efficiency of the sgRNA for counterselection

This step is optional and is meant to provide an estimation of the efficiency of the sgRNA in targeting the locus targeted during the procedure (thus providing an estimate of the success rate of the whole counterselection procedure).

- i. Inoculate 10 ml of LB medium with *P. putida* KT2440 and grow the cells overnight at 30°C with agitation.
- ii. Wash the cells four times with 1 ml of 300 mM sucrose (filter-sterilized) and finally resuspend in 400 µl of 300 mM sucrose.
- iii. Individually electroporate 100 ng of the empty pS448 ·CsR vector and 100 ng of plasmid pS448 ·CsR carrying the sgRNA of choice into 100-µl cell suspension aliquots with a voltage of 2.5 kV, 25 µF capacitance and 200 Ω resistance (e.g. in a Gene Pulser Xcell™ Electroporation System; Bio-Rad Laboratories, Hercules, CA, USA).
- iv. Let the cells recover for 2 h at 30°C and plate them onto the LB medium agar supplemented with streptomycin (100 µg ml⁻¹). Incubate the plates for overnight at 30°C.
- v. The plate with cells harbouring vector pS448 ·CsR with a functional sgRNA should have considerably less colonies (if any at all). We typically see a number of CRISPR-Cas9 escapers in the low double-digit range (i.e. 10–20 colonies) while *Pseudomonas* transformed with an empty pS448 ·CsR vector will form several hundred colonies within 16 h.

Genome editing in *Pseudomonas putida*

In order to introduce mutations into the *Pseudomonas* genome, the suicide plasmid pGNW (constructed in the previous section) is integrated into the chromosome at the target location employing the native homologous recombination mechanism (**Figure 2.3.**). After selection of positive co-integration events, the meganuclease I-SceI or the CRISPR-Cas9 system, respectively, is delivered into the cells on a replicative plasmid.

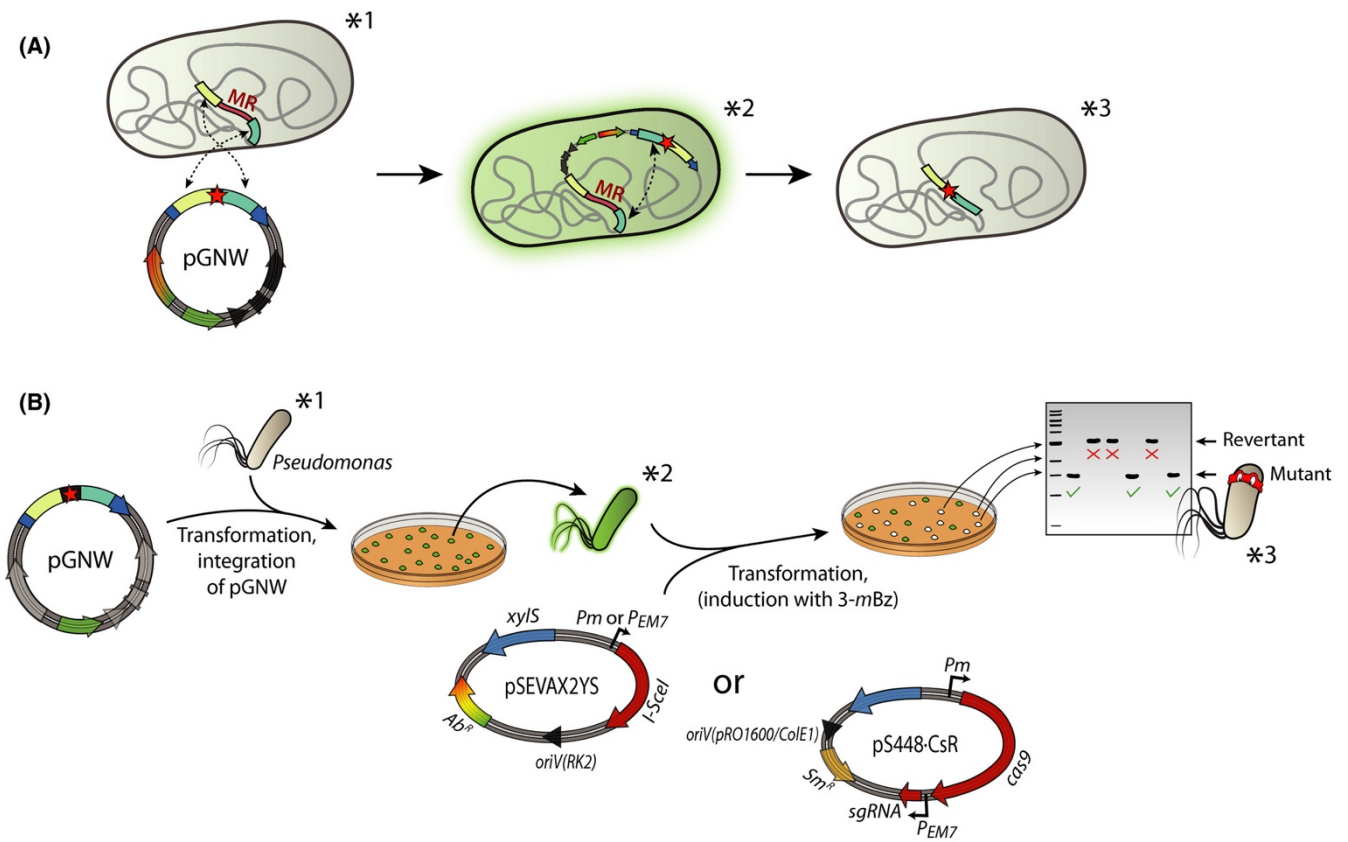


Figure 2.3. Workflow for targeted genomic manipulations in *Pseudomonas*. *Pseudomonas* cells are transformed with pGNW *via* electroporation or tri-parental mating. One to five individual green fluorescent colonies are combined and enriched in liquid LB medium cultures and transformed either with plasmid pSEVAX2YS or with a derivative of vector pS448-CsR carrying an appropriate sgRNA. Note that the antibiotic resistance could be different depending on the vector chosen for the deletion. Expression of the gene encoding the I-SceI meganuclease mediates the excision of the pGNW sequence from the chromosome, leading to non-fluorescent colonies under blue-light exposure. These clones are tested *via* colony PCR and sequencing for a revertant (i.e. wild-type) or mutant genotype. Asterisks indicate the relevant genotypes as well as the molecular events happening in the *Pseudomonas* chromosome (A) during the corresponding steps of the (B) genome engineering protocol.

The expression of the DNA modifying enzymes – and thus restriction of pGNW within the chromosome – enforces a second homologous recombination that can yield either the mutant genotype or a revertant genotype (i.e. wild-type sequence).

Integration of pGNW derivatives into the chromosome

The suicide vector pGNW carrying the corresponding HRs to the MR has to be delivered into the cells to enable its chromosomal integration *via* homologous recombination. This step can be achieved either by electroporation or by tri-parental mating. The latter procedure is recommended if multiple manipulations are conducted within the same strain. Thereby, the plasmid bearing I-*SceI* (e.g. pSEVAX28S, where X indicates any antibiotic resistance; see **Table 2.1.**) can be maintained within the cells by addition of the respective antibiotic during all cultivation steps. A leaky expression of the gene encoding I-*SceI*, however, interferes with the integration of pGNW – significantly decreasing the transformation efficiency. This issue can be countered by a much more efficient plasmid delivery achieved by tri-parental mating.

Plasmid delivery by electroporation

- i. Grow an overnight culture of *P. putida* KT2440 in 5–10 ml of LB medium. The *Pseudomonas* culture can be started at the same time that the overnight cultures of *E. coli* DH5 α λ *pir* with pGNW (Section ‘Verification of clones’, step 3).
- ii. For the electroporation of cells, we adopted the procedure by Choi *et al.* (2006). In brief, the cell suspension is distributed into four microcentrifuge tubes and pellet the cells in a microcentrifuge at 11 000 *g* for 1 min. Wash the cells twice with 1 ml of 300 mM sucrose for each pellet and finally resuspend and combine them in a total of 100 μ l of 300 mM sucrose in a single tube. Add 500 ng of pGNW vector to the suspension and transfer the mixture into an electroporation cuvette with 2 mm gap width. Apply an electric field pulse (2.5 kV voltage, 25 μ F capacitance, and 200 Ω resistance) and quickly add 1 ml of LB medium. All steps of the electroporation protocol can be performed at room temperature.
- iii. Transfer the cell suspension into a sterile test or centrifuge tube (5–50 ml) and recover the cells with shaking at 30°C for 2 h.
- iv. Harvest the cells by centrifugation (11 000 *g*; 1 min) at room temperature and plate the whole suspension onto LB medium agar supplemented with the respective antibiotic for the pGNW vector used

- (either 50 $\mu\text{g ml}^{-1}$ Km, 10 $\mu\text{g ml}^{-1}$ Gm or 100 $\mu\text{g ml}^{-1}$ Sm). Incubate the cells overnight at 30°C.
- v. Inspect the plate on a blue-light transilluminator. Transformants should show green fluorescence (usually all colonies).

Plasmid delivery by tri-parental mating

- i. Grow overnight cultures of *Pseudomonas*, *E. coli* DH5 α λ *pir*/pGNW and *E. coli* HB101/pRK600 in at least 1 ml of LB medium each. Incubate at 30°C for *Pseudomonas* or 37°C for *E. coli* respectively.
- ii. Dry an LB medium agar plate without added antibiotics in a clean bench for 1 h.
- iii. Combine 100 μl of each pre-culture into a reaction tube and pellet the cells in a microcentrifuge at 10 000 g for 1 min at room temperature. Wash the cells with 1 ml of fresh LB medium and finally resuspend them in 20–30 μl of LB medium. Pipette the whole suspension onto the pre-dried LB medium agar plate. In order for bacterial conjugation to work, the cells have to be brought into close proximity within a non-planktonic state. A dried agar plate will absorb a small volume of media, allowing the bacterial cells to form a biofilm-like structure on the agar surface.
- iv. Incubate the cells at 30°C for 3–5 h.
- v. Use an inoculation loop to take the biomass up from the agar surface and resuspend it in 1 ml of LB medium. Spread 100 μl of this suspension directly onto a ceftrimide agar plate supplemented with the antibiotic to select for the pGNW vector used, as well as 50 $\mu\text{g ml}^{-1}$ ampicillin, and the antibiotic for the I-*Sce*I plasmid (if already delivered at this step, see below). Concentrate the remaining cells to about 100 μl by centrifugation and resuspend and spread them onto a second plate. The chosen concentration of Amp was found to not affect the growth of *P. putida* KT2440 that is naturally resistant to β -lactam antibiotics while completely suppressing the growth of most *E. coli* strains, which may show some residual growth even in the presence of ceftrimide.
- vi. Incubate the plates at 30°C for 16–24 h until clear colonies have formed that show green fluorescence under blue-light exposure.

Introduction of endonucleases

- i. Combine 1–5 individual colonies of *Pseudomonas* with a co-integrated pGNW vector into 5–10 ml of LB medium in a test or centrifuge tube (5–50 ml) and incubate with shaking at 30°C for at least 5 h (see next step). Using several individual colonies increases the chances of having cells with both the two possible genetic configurations after pGNW co-integration (**Figure 2.5.**) and reduces the impact of unspecific insertion of the suicide plasmid at untargeted chromosomal sites. Furthermore, the more biomass is used to inoculate the LB medium culture, the quicker the cell density required for the next step is reached so that the protocol can be continued on the same day. If the cells still contain an inducible I-*SceI*—plasmid (i.e. pSEVAX28S) from prior mutagenesis procedures, continue directly with Step 3 below.
- ii. After the cells have reached an optical density at 600 nm ($OD_{600\text{ nm}}$) of at least 0.3, use 20–100 ng of an I-*SceI* plasmid (i.e. pSEVAX2YS, where the expression of I-*SceI* could be either constitutive or inducible; see **Table 2.1.**) or 100–200 ng of plasmid pS448·CsR to transform *Pseudomonas* co-integrants by electroporation as described in the previous section (Section ‘Plasmid delivery by electroporation’). Transfer the cell suspension into a sterile test or centrifuge tube and recover the cells shaking at 30°C for 1 h. If a plasmid containing the XylS/*Pm* expression system (i.e. pSEVAX28S or pS448·CsR) is used, add 3-*mBz* to a final concentration of 3 mM to the LB medium used for cell recovery.
- iii. Plate 70 μl of cell suspension on LB medium agar supplemented with the respective antibiotic for pSEVAX2YS (i.e. 500 $\mu\text{g ml}^{-1}$ Amp, 50 $\mu\text{g ml}^{-1}$ Km, 10 $\mu\text{g ml}^{-1}$ Gm or 100 $\mu\text{g ml}^{-1}$ Sm), or Sm for pS448·CsR selection. Incubate the cells overnight at 30°C. If a plasmid containing the XylS/*Pm* expression system (i.e. pSEVAX28S or pS448·CsR) is used, add 3-*mBz* to a final concentration of 3 mM to the LB medium plates to ensure proper induction of the system.
- iv. Inspect the plate on a blue-light table. *Pseudomonas* clones that have lost vector pGNW through a second homologous recombination event will show no green fluorescence.

- v. Test ≥ 8 individual non-fluorescent colonies *via* colony PCR using the *g*-check primers adequate for their genotype. If CRISPR-Cas9 counterselection was employed, all non-fluorescent clones are expected to harbour the mutation. The fraction of cells that have maintained fluorescence after counterselection is expected to be significantly higher when using CRISPR-Cas9 as compared to I-*Sce*I, due to a higher probability of escaping restriction by mutating the sgRNA recognition sequence.

Plasmid curing

The last step in the procedure, once the mutation has been confirmed, is to cure the mutant cells from the plasmid(s) used during genome editing (**Figure 2.4**).

- i. Use a single colony of mutant *Pseudomonas* to inoculate 3–10 ml of LB medium in a test or centrifuge tube.
- ii. Culture the cells shaking at 30°C. Every 4–12 h, transfer 1 μ l of the culture into 3–10 ml of fresh LB medium. Continue the culturing process for 2–3 days, and pass the cells into fresh medium even if you cannot see the formation of biomass in the tubes. This procedure ensures that the cells are kept in a state of maximum division rate. If your mutant cells have severe growth deficiencies due to the deletion of important genes or the introduction of DNA that could impair growth, the curing of a plasmid can require continuous cultivation for an extended period.
- iii. Dilution-streak the culture on an LB medium agar plate without added antibiotics.
- iv. Test individual colonies for the loss of the plasmid by re-streaking on LB medium agar with the respective antibiotic.

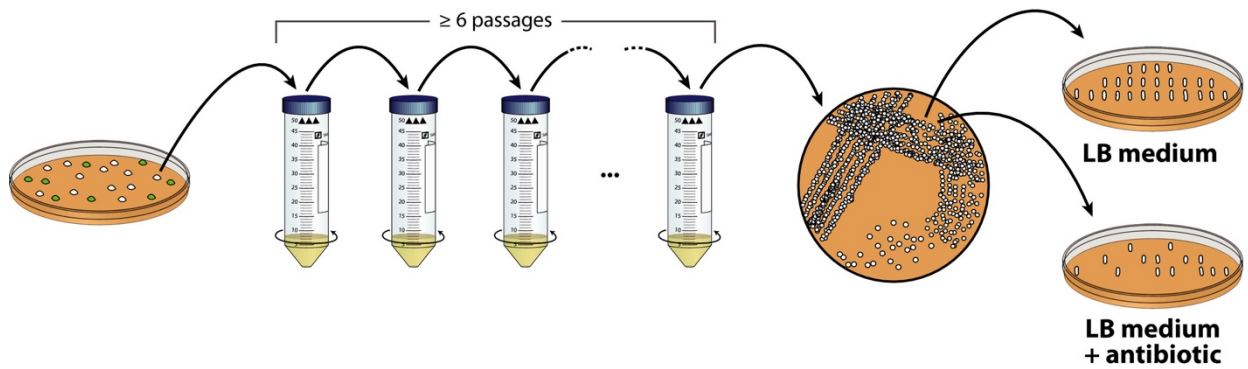


Figure 2.4. Plasmid curing after successful genome engineering of *Pseudomonas*. The biomass from a single mutant *Pseudomonas* colony is used to inoculate 5–10 ml of LB medium and the suspension is incubated at 30°C with shaking. Two to three times per day, a small volume of this culture is transferred into fresh LB medium. After 2–3 days (i.e. at least six passages), the cells are isolated on LB medium agar plates and tested for the loss of plasmids based on their antibiotic-resistance profile.

Application examples

Deletion of *nicX* in *Pseudomonas putida* KT2440 mediated by I-SceI activity

Pseudomonas putida KT2440 is able to grow on nicotinic acid as a sole carbon source³⁶. The degradation pathway, encoded in the *nic* gene cluster, involves the hydroxylation of nicotinate to 6-hydroxynicotinate, its further reduction to 2,5-dihydroxypyridine (**Figure 2.5, A**) and the deoxygenation to *N*-formylmaleamic acid, which can be further converted into fumarate (Jiménez *et al.*, 2008). An interruption of the metabolic route at the level of 2,5-dihydroxypyridine *via* the deletion of *nicX* (encoding a 2,5-dihydroxypyridine 5,6-dioxygenase) leads to the accumulation of a dark green colored compound with green fluorescence within and outside of the cells³⁷, which forms brown polymers upon autoxidation. A deletion of *nicX* in strain KT2440 was thus chosen to optimize the genome engineering protocol since it allows for the direct identification of mutant clones after addition of nicotinic acid to the culture medium.

The primer pairs *nicX*_HR1_F/*nicX*_HR1_R (**Table S2.1**) and *nicX*_HR2_F/*nicX*_HR2_R (**Table S2.1**) were used to amplify the two homology regions that flank *nicX*, and the products were assembled and cloned into vectors pGNW2, pGNW4 and pGNW6 *via* *USER* assembly, yielding pGNW2· Δ *nicX*, pGNW4· Δ *nicX* and pGNW6· Δ *nicX* respectively (**Figure 2.5, B** and **Table 5.1**). After their purification from *E. coli* DH5 α λ pir, the insertional plasmids were integrated into the chromosome of strain KT2440 by electroporation. Then, the successful co-integrant clones were transformed with either plasmid pSEVA6213S (in clones where either vector pGNW2· Δ *nicX* or pGNW4· Δ *nicX* was used for the integration) or plasmid pSEVA1213S (in clones where vector pGNW6· Δ *nicX* was used for the integration step). Cells were plated on LB medium agar containing Gm or Amp respectively. **Figure 2.5, C** shows a photograph of an LB medium agar plate supplemented with Gm and 5 mM nicotinic acid, taken 1 day after transforming *P. putida* KT2440/pGNW2· Δ *nicX* with plasmid pSEVA6213S.

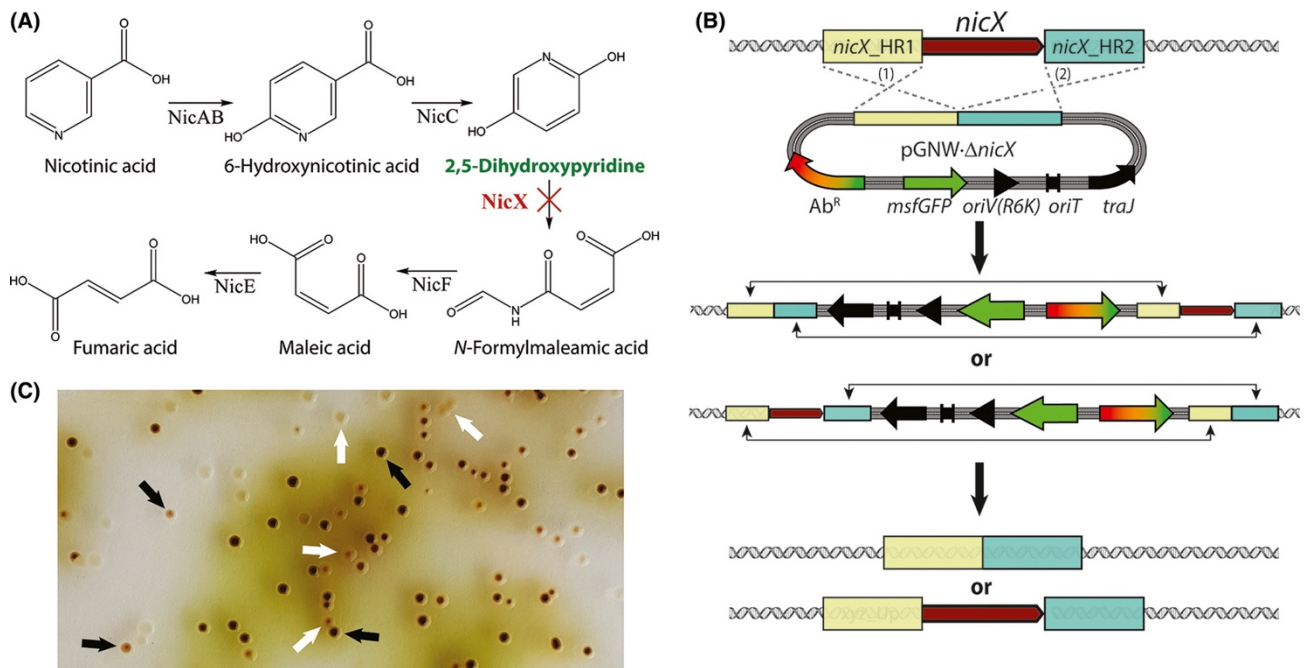


Figure 2.5. Deletion of *nicX* in *Pseudomonas putida* KT2440.

A. Proposed degradation pathway of nicotinic acid in *P. putida* based on the information available in the literature³⁷. The key metabolic intermediate accumulating upon elimination of *nicX* (encoding 2,5-dihydroxypyridine-5,6-dioxygenase) is highlighted in green. The targeted, in-frame deletion of *nicX* is indicated by a red cross.

B. Schematic representation of the molecular mechanism for the integration of the suicide plasmid pGNW- Δ *nicX* in the chromosome of strain KT2440 as well as the second recombination leading to either a revertant or a mutant genotype. Note that the antibiotic resistance could be different depending on the vector chosen for the deletion.

C. Representative picture of a section of an LB medium agar plate (containing $10 \mu\text{g ml}^{-1}$ Gm and 5 mM nicotinic acid) seeded with an isolate of strain KT2440 that was previously co-integrated with the suicide plasmid pGNW2- Δ *nicX* and transformed with the helper plasmid pSEVA6213S. The accumulation of 2,5-dihydroxypyridine (green-to-brown pigmented colonies) can be easily detected by visual inspection of the plates. The picture was taken after incubation for 16 h at 30°C followed by 24 h at 4°C. The black arrows indicate colonies formed by *P. putida* Δ *nicX* cells; the white arrows identify colonies displaying a revertant (i.e. wild-type) genotype.

Thirty randomly picked colonies from the plates obtained after each deletion procedure were tested for their genotype *via* colony PCR using primers *nicX_g-check_F/nicX-g-check_R* (**Table S2.1**). The different colorations of mutant and revertant colonies allowed for their direct identification. With all three plasmid combinations, the fraction of mutant colonies was always close to 50% (53%, 46% and 48% respectively).

Deletion of *aceEF* in *Pseudomonas putida* KT2440 using CRISPR-Cas9 counterselection

As an obligate aerobic bacterium, *P. putida* strongly relies on an active tricarboxylic acid cycle for the generation of reducing equivalents that are used, *inter alia*, to generate ATP through oxidative phosphorylation³⁸. The pyruvate dehydrogenase complex (PDHc), which catalyzes the entry reaction to the tricarboxylic acid cycle, plays a central role in the central carbon metabolism of *Pseudomonas*^{39,40}. The PDHc is a multimeric system composed of three different proteins, AceE, AceF and Lpd⁴¹. In *P. putida* KT2440, the genes encoding AceE (*PP_0339*) and AceF (*PP_0338*) form an operon³⁶. Considering its central role in sugar catabolism, genes encoding PDHc are considered a difficult knock-out to achieve if relying on an untargeted selection strategy, and the resulting mutant would become bradytroph for C2 units as the reaction converting pyruvate into acetyl-coenzyme A is blocked. Because of this reason, CRISPR-Cas9 was adopted for counterselection of the correct mutants in this study. The homology regions to delete *aceE* and *aceF* were amplified from chromosomal DNA of *P. putida* KT2440 using the primer pairs *aceEF_HR1_F/aceEF_HR1_R* and *aceEF_HR2_F/aceEF_HR2_R* (Table S1) and cloned into vector pGNW2. *Pseudomonas* co-integrants were then transformed with 200 ng of plasmid pS448-CsR_aceF (Table 1) and selected on LB medium agar supplemented with Sm, 3-*mBz* and 5 mM acetate to enhance the growth of bradytrophic mutant cells. After 2 days, 10 out of 39 colonies of normal size and a majority (29 out of 39) of very small colonies could be identified on the plate (**Figure S2.2**). Inspection under blue-light exposure revealed that all larger colonies had kept green fluorescence and thus had escaped CRISPR-

Cas9-mediated restriction. All smaller colonies were tested by colony PCR with primers *aceEF*_g-check_F/*aceEF*_g-check_R (Table S1) and were found to have *aceEF* deleted. In a separate experiment, co-integrant cells were transformed with both pSEVA628S and pS448·CsR_*aceF* (500 ng of each plasmid). Selection on LB medium agar plates containing Sm, 3-*mBz*, and acetate (as a direct source of acetyl-coenzyme A) led to the formation of only three colonies, all of which had *aceEF* deleted.

Integration of fluorescent protein-encoding genes into a landing pad in *Pseudomonas putida* KT2440

To evaluate the suitability of the system for the insertion of DNA at a defined position, a landing pad was chosen within the intergenic region between *PP_0013* (*gyrB*) and *PP_5421*, close to the chromosomal origin of replication of *P. putida* KT2440^{36,42,43}. First, plasmid pGNW2·LPR was assembled from four fragments in a *USER* assembly reaction. To this end, vector pGNW2 was amplified with pGNW-*USER*_F and pGNW-*USER*_R. The two HRs framing the landing pad were amplified from genomic DNA with the primer pairs LP_HR1_F/LP_HR1_R and LP_HR2_F/LP_HR2_R (**Table S2.1**). A fourth fragment containing the gene encoding the monomeric red fluorescent protein mRFP1⁴⁴ and the *rrnB*-T1 terminator element was amplified with RFP4LP_F and RFP4LP_R (**Table S2.1**) from vector pS2313·R. The primers RFP4LP_F and LP_HR1_R furthermore contained extended overhangs to introduce the constitutive *P_{EM7}* promoter upstream of the *mRFP1* coding sequence. Since this promoter was found to give a too low expression (data not shown), its sequence was exchanged with the strong *P_{14g}* promoter¹⁵ and the translational coupler *BCD2*⁴⁵ by amplifying pGNW2·LP::*P_{EM7}*-mRFP with oligonucleotides *P14 g-BCD2*_F/*P14 g-BCD2*_R and a *BCD2*-fragment from a gBlock containing this regulatory element (purchased from Integrated DNA Technologies) with *BCD2-P14g*_F/*BCD2-P14g*_R. The resulting plasmid was termed pGNW2·LPR (**Table 2.1**).

To exchange *mRFP1* in the landing pad with different fluorescent proteins and to transfer the landing pad to vectors pGNW4 or pGNW6, two- or four-fragment *USER* assembly reactions were performed with interchangeable modules. These modules were amplified and assembled as indicated in

Table S2.1. The *msfGFP* gene was amplified from vector pGNW4. The genes encoding the other fluorescent proteins were amplified from the plasmids pS2313·B, pS2313·O and pS2313·T that had been constructed as follows: The sequences of the genes *mBFP2*, *mOrange2* and *mTurquoise2* were extracted from their original publications (**Table 2.1**), cured from protein tags and restriction sites to make them SEVA-compatible and ordered as custom genes (Integrated DNA Technologies). The synthetic DNA fragments were then cloned into the expression vector pSEVA2313 *via USER* assembly using the primer pairs pS2313_F/pS2313_R (for pSEVA2313), pS_BFP2_F/pS_BFP2_R (for *mBFP2*) and pS_Ora_Tq_F/pS_Ora_Tq_F (for *mOrange2* and *mTurquoise2*; **Table S2.1**), yielding plasmids pS2313·B, pS2313·O and pS2313·T respectively.

The resulting plasmids pGNW2·LPR, pGNW2·LPG, pGNW2·LPB, pGNW4·LPO and pGNW6·LPT (**Table 2.1**) were individually integrated into the chromosome of *P. putida* KT2440 as indicated above. The backbones were removed from the co-integrants by the delivery and induction of plasmid pSEVA128S (for pGNW2·LPR), pSEVA628S (for pGNW2·LPG and pGNW2·LPB), pSEVA228S (for pGNW4·LPO) and pSEVA428S (for pGNW6·LPT) respectively (**Figure 2.6, A**). On the following day, the plates with the resulting strains (*P. putida* KT·LPR, KT·LPG, KT·LPB and KT·LPO; **Table 2.2**) were placed at 4°C to let the fluorescent proteins mature, since none of them showed any visible coloration under blue-light exposure. After 7 days, photographs of the plates were taken on a blue-light transilluminator (**Figure 2.6, B**).

Pseudomonas colonies with integrated *mBFP2* (strain KT·LPB) showed not visible fluorescence even after further prolonged incubation (data not shown). To determine the kinetics of the fluorescent proteins in *P. putida* KT2440, at least three biological replicates of the mutant strains (verified by colony PCR with primers Seq-LP_F and Seq-LP_R, **Table S2.1**) and the wild-type strain were grown at 30°C in 96-well plates (Greiner CELLSTAR™; Sigma-Aldrich, St. Louis, MO, USA; polystyrene, round bottom) with 200 µl of de Bont minimal medium⁴⁶ per well, supplemented with 30 mM citrate, and covered with a sealing membrane (Diversified Biotech Breathe-Easy™; VWR, Radnor, PA, USA).

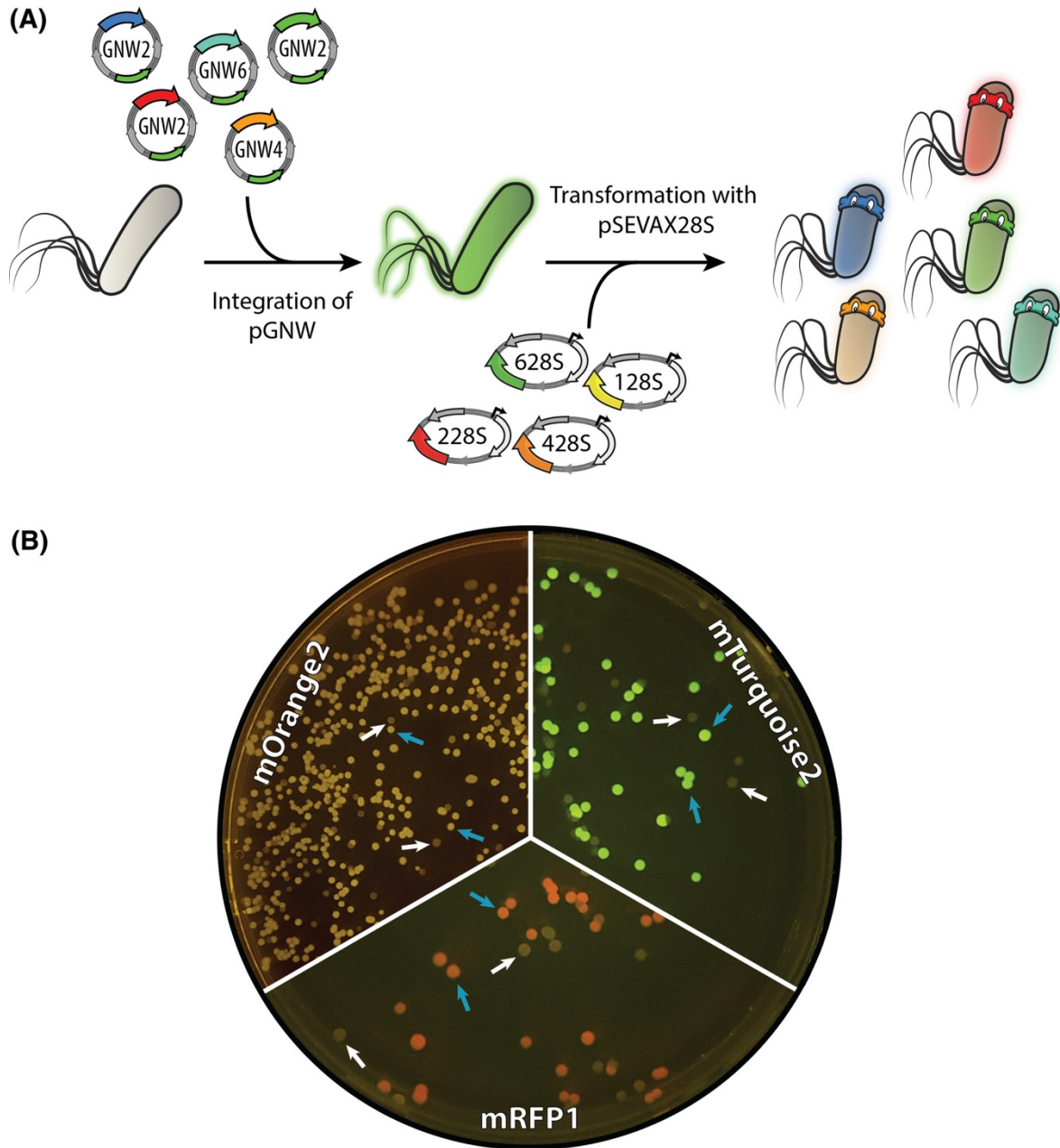


Figure 2.6. Integration of different fluorescent proteins into a landing pad in the chromosome of *Pseudomonas putida* KT2440.

A. Genes encoding the fluorescent proteins mRFP1, mOrange2, mTurquoise2, msfGFP, and mBFP2 [placed under transcriptional control of a $P_{14g}(BCD2)$ regulatory element], were integrated into a chosen landing site in the chromosome of *P. putida* KT2440 using the insertional vectors pGNW2, pGNW4, or pGNW6. After selection of co-integrants, the second homologous recombination was mediated by the inducible expression of the gene encoding the I-SceI meganuclease from pSEVAX28S vectors.

B. Images of the plates were taken after incubation for 16 h at 30°C followed by 7 days at 4°C to allow for proper fluorescent protein maturation. *mBFP2*-integrated colonies showed no visible fluorescence under blue-light exposure (not shown). The blue arrows indicate colonies of mutated strains displaying different integrated fluorescent proteins; white arrows identify colonies of cells displaying a revertant genotype (i.e. wild-type) without fluorescence.

The kinetics of bacterial growth and fluorescence were acquired by measuring the OD₆₃₀ as well as the excitation/emission values of mRFP1 at 582 nm/609 nm, mBFP2 at 385 nm/450 nm, mOrange2 at 541 nm/567 nm and mTurquoise2 at 451 nm/477 nm (**Figure S2.1**). Although under the transcriptional control of the same regulatory elements, the five fluorescent proteins differed in both the intensity of their signal as well as their expression pattern. The fluorescence intensity of only msfGFP increased steadily for the whole cultivation time of 50 h; the signal of the remaining four reporter proteins reached stagnation after 15 h (mOrange2), 8 h (mRFP1 and mBFP2) and 25 h (mTurquoise2). Since all cultured strains continue to grow until the end of the experiment, the biomass-specific fluorescence decreased continuously (**Figure S2.1**).

Table 2.2. Bacterial strains used in this study

Strain	Relevant characteristics	Reference or source
<i>Escherichia coli</i>		
DH5 α	Cloning host; F ⁻ λ^- <i>endA1 glnX44(AS) thiE1 recA1 relA1 spoT1 gyrA96(Nal^R) rfbC1 deoR nupG Φ80(<i>lacZ</i>ΔM15) Δ(<i>argF-lac</i>)U169 <i>hsdR17</i>(<i>rK</i>⁻ <i>mK</i>⁺)</i>	Hanahan and Meselson (1983)
DH5 α λ <i>pir</i>	Cloning host; same as DH5 α but λ <i>pir</i> lysogen	Platt <i>et al.</i> (2000)
HB101	Helper strain used for tri-parental mating; F ⁻ <i>thi-1 hsdS20</i> (<i>rB</i> ⁻ <i>mB</i> ⁻) <i>supE44 recA13 ara-14 leuB6 proA2 lacY1 galK2 rpsL20</i> (Sm ^R) <i>xyl-5 mtl-1</i>	Boyer and Roulland-Dussoix (1969)
<i>Pseudomonas putida</i>		
KT2440	Wild-type strain, derived from <i>P. putida</i> mt-2 (Worsey and Williams, 1975) cured of the TOL plasmid pWW0	Bagdasarian <i>et al.</i> (1981)
KT2440 Δ <i>aceEF</i>	Same as KT2440, but with an in-frame deletion of the <i>aceEF</i> genes (<i>PP_0038-PP_0339</i>)	This work
KT2440 Δ <i>nicX</i>	Same as KT2440, but with an in-frame deletion of the <i>nicX</i> gene (<i>PP_0395</i>)	This work
KT-LPR	Same as KT2440, but carrying a <i>P</i> _{14g} (<i>BCD2</i>) \rightarrow <i>mRFP1</i> element integrated between <i>PP_0013</i> (<i>gyrB</i>) and <i>PP_5421</i>	This work

Strain	Relevant characteristics	Reference or source
KT-LPG	Same as KT2440, but carrying a $P_{14g}(BCD2) \rightarrow msfGFP$ element integrated between PP_0013 (<i>gyrB</i>) and PP_5421	This work
KT-LPB	Same as KT2440, but carrying a $P_{14g}(BCD2) \rightarrow mBFP2$ element integrated between PP_0013 (<i>gyrB</i>) and PP_5421	This work
KT-LPO	Same as KT2440, but carrying a $P_{14g}(BCD2) \rightarrow mOrange2$ element integrated between PP_0013 (<i>gyrB</i>) and PP_5421	This work
KT-LPT	Same as KT2440, but carrying a $P_{14g}(BCD2) \rightarrow mTurquoise2$ element integrated between PP_0013 (<i>gyrB</i>) and PP_5421	This work

Discussion

The present genome engineering protocol reduces the hands-on work of the original procedure by Martínez-García and de Lorenzo (2011). We further streamlined the protocol with (i) the adoption of the *USER* assembly method that enables a standardized workflow²⁸, (ii) a reporter function (i.e. fluorescence) for the donor plasmid that allows for its direct visualization within host cells⁴⁷, (iii) additional antibiotic resistances to broaden the host spectrum and (iv) an efficient CRISPR-Cas9 counterselection, particularly relevant for the construction of difficult knock-outs.

The protocol described herein yields reliable results for targeted mutagenesis in *Pseudomonas* species within a standard workweek. We have illustrated the flexibility of the system by combining different molecular elements of the toolbox to delete genomic regions in *P. putida* KT2440 and demonstrated the functionality of four new fluorescent proteins (mRFP1, mOrange2, mTurquoise2 and, to some extent, mBFP2) in this host *via* their targeted integration into a landing site in the chromosome. While we optimized the critical steps of the protocol that yield the desired mutation, the subsequent curing of replicating plasmids still adds up time required to generate the final, plasmid-free strain. One possible solution could be to implement conditional origins of replication in the current plasmid system, e.g. temperature-sensitive derivatives of *oriV(RK2)*⁴⁸ that has been shown to function in *P. putida*²². This will be of particularly value for the curing of plasmid DNA from cells that are severely impaired in growth and are thus less prone to lose plasmids during proliferation. A reliable plasmid curing after each cycle of mutagenesis could also solve issues encountered with the non-induced, basal expression of the XylS/*Pm* expression system that can be observed particularly with increased copy numbers of the *xylS* gene⁴⁹ or would allow to rely exclusively on the constitutive system. Furthermore, if combined with the first pre-culturing step of *Pseudomonas* in this protocol, plasmid curing would not affect its time requirements. While the synthetic biology toolbox for *Pseudomonas* is subjected to continuous improvement, the protocol discussed herein represents the fastest extant procedure for genome editing of *P. putida* and related species.

Acknowledgements

We are indebted to Prof. Víctor de Lorenzo and Dr. Esteban Martínez-García (CNB-CSIC, Madrid, Spain) for sharing materials and fruitful discussions. We thank Francesco Romaniello (Università Cattolica del Sacro Cuore, Milan, Italy) for his help with the construction of the pGNW4 and pGNW6 vectors. The financial support from The Novo Nordisk Foundation (grants NNF10CC1016517 and *LiFe*, NNF18OC0034818), the Danish Council for Independent Research (*SWEET*, DFF-Research Project 8021-00039B), and the European Union's Horizon 2020 Research and Innovation Programme under grant agreement No. 814418 (*SinFonia*) to P.I.N. is gratefully acknowledged. E.K. is the recipient of a fellowship from the Novo Nordisk Foundation (grant NNF17CC0026768) as part of the Copenhagen Bioscience Ph.D. Programme. The responsibility of this article lies with the authors. The funding bodies are not responsible for any use that may be made of the information contained therein.

References

- 1 Calero, P. & Nikel, P. I. Chasing bacterial chassis for metabolic engineering: a perspective review from classical to non-traditional microorganisms. *Microb Biotechnol* **12**, 98-124, doi:10.1111/1751-7915.13292 (2019).
- 2 Loeschcke, A. & Thies, S. *Pseudomonas putida*-a versatile host for the production of natural products. *Appl Microbiol Biot* **99**, 6197-6214, doi:10.1007/s00253-015-6745-4 (2015).
- 3 Benedetti, I., de Lorenzo, V. & Nikel, P. I. Genetic programming of catalytic *Pseudomonas putida* biofilms for boosting biodegradation of haloalkanes. *Metab Eng* **33**, 109-118, doi:10.1016/j.ymben.2015.11.004 (2016).
- 4 Dvorak, P., Nikel, P. I., Damborsky, J. & de Lorenzo, V. Bioremediation 3.0: Engineering pollutant-removing bacteria in the times of systemic biology. *Biotechnol Adv* **35**, 845-866, doi:10.1016/j.biotechadv.2017.08.001 (2017).
- 5 Nikel, P. I. & de Lorenzo, V. *Pseudomonas putida* as a functional chassis for industrial biocatalysis: From native biochemistry to trans-metabolism. *Metab Eng* **50**, 142-155, doi:10.1016/j.ymben.2018.05.005 (2018).
- 6 Poblete-Castro, I., Becker, J., Dohnt, K., dos Santos, V. M. & Wittmann, C. Industrial biotechnology of *Pseudomonas putida* and related species. *Appl Microbiol Biotechnol* **93**, 2279-2290, doi:10.1007/s00253-012-3928-0 (2012).
- 7 Nikel, P. I., Chavarria, M., Danchin, A. & de Lorenzo, V. From dirt to industrial applications: *Pseudomonas putida* as a Synthetic Biology chassis for hosting harsh biochemical reactions. *Curr Opin Chem Biol* **34**, 20-29, doi:10.1016/j.cbpa.2016.05.011 (2016).
- 8 Domrose, A. *et al.* Rapid generation of recombinant *Pseudomonas putida* secondary metabolite producers using yTREX. *Synth Syst Biotechnol* **2**, 310-319, doi:10.1016/j.synbio.2017.11.001 (2017).

- 9 Martinez-Garcia, E. & de Lorenzo, V. Molecular tools and emerging strategies for deep genetic/genomic refactoring of *Pseudomonas*. *Curr Opin Biotechnol* **47**, 120-132, doi:10.1016/j.copbio.2017.06.013 (2017).
- 10 Cook, T. B. *et al.* Genetic tools for reliable gene expression and recombineering in *Pseudomonas putida*. *J Ind Microbiol Biotechnol* **45**, 517-527, doi:10.1007/s10295-017-2001-5 (2018).
- 11 Wynands, B. *et al.* Metabolic engineering of *Pseudomonas taiwanensis* VLB120 with minimal genomic modifications for high-yield phenol production. *Metab Eng* **47**, 121-133, doi:10.1016/j.ymben.2018.03.011 (2018).
- 12 Silva-Rocha, R. *et al.* The Standard European Vector Architecture (SEVA): a coherent platform for the analysis and deployment of complex prokaryotic phenotypes. *Nucleic Acids Res* **41**, D666-675, doi:10.1093/nar/gks1119 (2013).
- 13 Martinez-Garcia, E., Aparicio, T., Goni-Moreno, A., Fraile, S. & de Lorenzo, V. SEVA 2.0: an update of the Standard European Vector Architecture for de-/re-construction of bacterial functionalities. *Nucleic Acids Res* **43**, D1183-1189, doi:10.1093/nar/gku1114 (2015).
- 14 Elmore, J. R., Furches, A., Wolff, G. N., Gorday, K. & Guss, A. M. Development of a high efficiency integration system and promoter library for rapid modification of *Pseudomonas putida* KT2440. *Metab Eng Commun* **5**, 1-8, doi:10.1016/j.meteno.2017.04.001 (2017).
- 15 Zobel, S. *et al.* Tn7-Based Device for Calibrated Heterologous Gene Expression in *Pseudomonas putida*. *ACS Synth Biol* **4**, 1341-1351, doi:10.1021/acssynbio.5b00058 (2015).
- 16 Galvao, T. C. & de Lorenzo, V. Adaptation of the yeast URA3 selection system to gram-negative bacteria and generation of a Δ CDE *Pseudomonas putida* strain. *Appl Environ Microbiol* **71**, 883-892, doi:10.1128/AEM.71.2.883-892.2005 (2005).
- 17 Gay, P., Le Coq, D., Steinmetz, M., Berkelman, T. & Kado, C. I. Positive selection procedure for entrapment of insertion sequence elements in gram-negative bacteria. *J Bacteriol* **164**, 918-921, doi:10.1128/jb.164.2.918-921.1985 (1985).
- 18 Graf, N. & Altenbuchner, J. Development of a method for markerless gene deletion in *Pseudomonas putida*. *Appl Environ Microbiol* **77**, 5549-5552, doi:10.1128/AEM.05055-11 (2011).

- 19 Murphy, K. C. lambda Recombination and Recombineering. *EcoSal Plus* **7**, doi:10.1128/ecosalplus.ESP-0011-2015 (2016).
- 20 Luo, X. *et al.* Pseudomonas putida KT2440 markerless gene deletion using a combination of lambda Red recombineering and Cre/loxP site-specific recombination. *Fems Microbiology Letters* **363**, doi:ARTN fnw01410.1093/femsle/fnw014 (2016).
- 21 Choi, K. R. & Lee, S. Y. Protocols for RecET-based markerless gene knockout and integration to express heterologous biosynthetic gene clusters in Pseudomonas putida. *Microb Biotechnol* **13**, 199-209, doi:10.1111/1751-7915.13374 (2020).
- 22 Choi, K. R., Cho, J. S., Cho, I. J., Park, D. & Lee, S. Y. Markerless gene knockout and integration to express heterologous biosynthetic gene clusters in Pseudomonas putida. *Metab Eng* **47**, 463-474, doi:10.1016/j.ymben.2018.05.003 (2018).
- 23 Aparicio, T., de Lorenzo, V. & Martinez-Garcia, E. CRISPR/Cas9-Based Counterselection Boosts Recombineering Efficiency in Pseudomonas putida. *Biotechnol J* **13**, e1700161, doi:10.1002/biot.201700161 (2018).
- 24 Martinez-Garcia, E. & de Lorenzo, V. Engineering multiple genomic deletions in Gram-negative bacteria: analysis of the multi-resistant antibiotic profile of Pseudomonas putida KT2440. *Environ Microbiol* **13**, 2702-2716, doi:10.1111/j.1462-2920.2011.02538.x (2011).
- 25 Smith, C., Day, P. J. & Walker, M. R. Generation of cohesive ends on PCR products by UDG-mediated excision of dU, and application for cloning into restriction digest-linearized vectors. *PCR Methods Appl* **2**, 328-332, doi:10.1101/gr.2.4.328 (1993).
- 26 Bitinaite, J. & Nichols, N. M. DNA cloning and engineering by uracil excision. *Curr Protoc Mol Biol* **Chapter 3**, Unit 3 21, doi:10.1002/0471142727.mb0321s86 (2009).
- 27 Nour-Eldin, H. H., Geu-Flores, F. & Halkier, B. A. USER cloning and USER fusion: the ideal cloning techniques for small and big laboratories. *Methods Mol Biol* **643**, 185-200, doi:10.1007/978-1-60761-723-5_13 (2010).
- 28 Cavaleiro, A. M., Kim, S. H., Seppala, S., Nielsen, M. T. & Norholm, M. H. Accurate DNA Assembly and Genome Engineering with

- Optimized Uracil Excision Cloning. *ACS Synth Biol* **4**, 1042-1046, doi:10.1021/acssynbio.5b00113 (2015).
- 29 Armstrong, K. A. Molecular-Cloning - a Laboratory Manual - Maniatis, T, Fritsch, E, Sambrook, J. *Q Rev Biol* **58**, 234-234, doi:10.1086/413230 (1983).
- 30 Gibson, D. G. *et al.* Enzymatic assembly of DNA molecules up to several hundred kilobases. *Nat Methods* **6**, 343-341, doi:10.1038/Nmeth.1318 (2009).
- 31 Genee, H. J. *et al.* Software-supported USER cloning strategies for site-directed mutagenesis and DNA assembly. *ACS Synth Biol* **4**, 342-349, doi:10.1021/sb500194z (2015).
- 32 Bhaya, D., Davison, M. & Barrangou, R. CRISPR-Cas systems in bacteria and archaea: versatile small RNAs for adaptive defense and regulation. *Annu Rev Genet* **45**, 273-297, doi:10.1146/annurev-genet-110410-132430 (2011).
- 33 Blin, K., Pedersen, L. E., Weber, T. & Lee, S. Y. CRISPy-web: An online resource to design sgRNAs for CRISPR applications. *Synth Syst Biotechnol* **1**, 118-121, doi:10.1016/j.synbio.2016.01.003 (2016).
- 34 Ruiz, J. A., Fernandez, R. O., Nikel, P. I., Mendez, B. S. & Pettinari, M. J. dye (arc) Mutants: insights into an unexplained phenotype and its suppression by the synthesis of poly (3-hydroxybutyrate) in *Escherichia coli* recombinants. *FEMS Microbiol Lett* **258**, 55-60, doi:10.1111/j.1574-6968.2006.00196.x (2006).
- 35 Jiang, W. Y., Bikard, D., Cox, D., Zhang, F. & Marraffini, L. A. RNA-guided editing of bacterial genomes using CRISPR-Cas systems. *Nature Biotechnology* **31**, 233-239, doi:10.1038/nbt.2508 (2013).
- 36 Belda, E. *et al.* The revisited genome of *Pseudomonas putida* KT2440 enlightens its value as a robust metabolic chassis. *Environ Microbiol* **18**, 3403-3424, doi:10.1111/1462-2920.13230 (2016).
- 37 Jimenez, J. I. *et al.* Deciphering the genetic determinants for aerobic nicotinic acid degradation: The nic cluster from *Pseudomonas putida* KT2440. *P Natl Acad Sci USA* **105**, 11329-11334, doi:10.1073/pnas.0802273105 (2008).
- 38 Nikel, P. I., Silva-Rocha, R., Benedetti, I. & de Lorenzo, V. The private life of environmental bacteria: pollutant biodegradation at the

- single cell level. *Environ Microbiol* **16**, 628-642, doi:10.1111/1462-2920.12360 (2014).
- 39 Sudarsan, S., Dethlefsen, S., Blank, L. M., Siemann-Herzberg, M. & Schmid, A. The functional structure of central carbon metabolism in *Pseudomonas putida* KT2440. *Appl Environ Microbiol* **80**, 5292-5303, doi:10.1128/AEM.01643-14 (2014).
- 40 Nickel, P. I., Chavarria, M., Fuhrer, T., Sauer, U. & de Lorenzo, V. *Pseudomonas putida* KT2440 Strain Metabolizes Glucose through a Cycle Formed by Enzymes of the Entner-Doudoroff, Embden-Meyerhof-Parnas, and Pentose Phosphate Pathways. *J Biol Chem* **290**, 25920-25932, doi:10.1074/jbc.M115.687749 (2015).
- 41 Angelides, K. J., Akiyama, S. K. & Hammes, G. G. Subunit stoichiometry and molecular weight of the pyruvate dehydrogenase multienzyme complex from *Escherichia coli*. *Proc Natl Acad Sci U S A* **76**, 3279-3283, doi:10.1073/pnas.76.7.3279 (1979).
- 42 Nelson, K. E. *et al.* Complete genome sequence and comparative analysis of the metabolically versatile *Pseudomonas putida* KT2440. *Environ Microbiol* **4**, 799-808, doi:10.1046/j.1462-2920.2002.00366.x (2002).
- 43 Reynolds, T. S. & Gill, R. T. Quantifying Impact of Chromosome Copy Number on Recombination in *Escherichia coli*. *Acs Synthetic Biology* **4**, 776-780, doi:10.1021/sb500338g (2015).
- 44 Campbell, R. E. *et al.* A monomeric red fluorescent protein. *Proc Natl Acad Sci U S A* **99**, 7877-7882, doi:10.1073/pnas.082243699 (2002).
- 45 Mutalik, V. K. *et al.* Precise and reliable gene expression via standard transcription and translation initiation elements. *Nat Methods* **10**, 354-360, doi:10.1038/nmeth.2404 (2013).
- 46 Hartmans, S., Smits, J. P., Vanderwerf, M. J., Volkering, F. & Debont, J. A. M. Metabolism of Styrene Oxide and 2-Phenylethanol in the Styrene-Degrading *Xanthobacter* Strain 124x. *Appl Environ Microb* **55**, 2850-2855, doi:Doi 10.1128/Aem.55.11.2850-2855.1989 (1989).
- 47 Calero, P., Jensen, S. I. & Nielsen, A. T. Broad-Host-Range ProUSER Vectors Enable Fast Characterization of Inducible Promoters and Optimization of p-Coumaric Acid Production in *Pseudomonas putida* KT2440. *ACS Synth Biol* **5**, 741-753, doi:10.1021/acssynbio.6b00081 (2016).

- 48 Valla, S., Haugan, K., Durland, R. & Helinski, D. R. Isolation and properties of temperature-sensitive mutants of the *trfA* gene of the broad host range plasmid RK2. *Plasmid* **25**, 131-136, doi:10.1016/0147-619x(91)90025-r (1991).
- 49 Gawin, A., Valla, S. & Brautaset, T. The XylS/Pm regulator/promoter system and its use in fundamental studies of bacterial gene expression, recombinant protein production and metabolic engineering. *Microbial Biotechnology* **10**, 702-718, doi:10.1111/1751-7915.12701 (2017).

Supporting Information

Table S2.1 · Oligonucleotides used in this work.

Name	Sequence (5' → 3')	T _m (°C)
pGNW-USER_F	AGTCGACCUGCAGGCATGCAAGCTTCT	71.8
pGNW-USER_R	AGGATCUAGAGGATCCCCGGGTACCG	66.1
Seq-pGNW_F	TGTAAAACGACGGCCAGT	54.2
Seq-pGNW_R	ATGACCATGATTACGCCGG	55.2
SEVA-T0_F	GAACGCTCGGTTGCCGCC	64.4
nicX_HR1_F	AGATCCUCATGCGGCGGAAGATTTTC	59.1
nicX_HR1_R	ACCCCTACAUCGGGGTTCTCCTGGG	62.7
nicX_HR2_F	ATGTAGGGGUTATACTGGCCGG	59.9
nicX_HR2_R	AGGTGACUGCAGCAGGTACAAAATGGC	59.1
nicX_g-check_F	GCCTGACGATTTAGAGCG	53.7
nicX_g-check_R	AAGAAGCAGGCCAGAGATG	54.9
LP_HR1_F	AGATCCUTCATCGAAAGTAACGCGC	58.9
LP_HR1_R	ATGCCGAUATACTATGCCGATGATTAATTGTCA ACAGAT CAGGTCTGAAGCTCTCG	58.9
LP_HR2_F	ACCAAUTGCTCCAGCGATCAC	59.1
LP_HR2_R	AGGTGACUGAACACGTTCCCTCACTGGG	59.6
pS448_F	AGTCGGUGCAATTCGAGCTCGGTACCCG	57.4
pS448_R	ATATGTUTTTTCCTCCTAACCGCGGC	58.3
Cas9_F	AACATAUGGATAAGAAATACTCAATAGGCT	52.2
Cas9_R	AGATCAGUCACCTCCTAGCTGACTCA	55.1
sgRNA_F	ACTGATCUAGAGTCGACCTGCAGGCA	57.7
sgRNA_R	ACCGACUCGGTGCCACTTTTTCAAGTTG	57.3
pS2313_F	ACTAGTCTUGGACTCCTGTTGATAGAT	56.0
pS2313_R	ATGTTTUTCCTCCTAAGCTTGCATG	55.8
pS_BFP2_F	ACATATGGUGTCTAAGGGCGAAGAGCTGAT	58.3
pS_BFP2_R	AGTTTAAUTAAGTTTGTGCCCCAGTTTGCT	59.0
pS_Ora_Tq_F	AAAACAUATGGTGAGCAAGGGCGA	57.8
pS_Ora_Tq_R	AAGACTAGUTTACTTGTACAGCTCGTCCAT	58.9
RFP4LP_F	ATCGGCAUAGTATAATACGACAAGGTGAGGAAC TAAACC ACTGAGCACTACTAGAGAAAG	55.6
RFP4LP_R	ATTTGGUAGAGAGCGTTCACCGAC	59.5

P14g-BCD2_F	AATGGCTUCCTCCGAAGACG	61.2
P14g-BCD2_R	AGAGCCUTGTCAATGGGCGATCAGGTCTGAAG CTCTCG	58.9
BCD2_R	AGAAAACCUCCTTAGCATGATTAAG	58.4
pGNW_LP_F	AAGTAAUAACGCTGATAGTGCTAGTG	57.8
BFP2_F	AGGTTTTCUAATGGTGTCTAAGGGCGAAGAG	61.1
BFP2_R	ATTACTUAATTAAGTTTGTGCCCCAGTTTGC	62.3
GFP_F	AGGTTTTCUAATGCGTAAAGGTGAAGAACTGTT C	60.9
GFP_R	ATTACTUATTTGTAGAGTTCATCCATGCCG	64.0
Ora_Tq_F	AGGTTTTCUAATGGTGAGCAAGGGCGAG	61.7
Ora_Tq_R	ATTACTUGTACAGCTCGTCCATGC	62.1
aceEF_HR1_F	AGATCCUCGAAGACTCGCTTGAAGAGG	59.7
aceEF_HR1_R	AGCCATGUAAGCCAGCACACTGC	55.9
aceEF_HR2_F	ACATGGCUTGCTCCAGGG	58.3
aceEF_HR2_R	AGGTGACUCGATGAACTGCTGGTTGCG	59.6
Seq-LP_F	ACCAACTTTTCCGCTTTGCAC	57.2
Seq-LP_R	CGAAAGACTGGGCCTTTTCGT	58.4
aceEF_g-check_F	GTTTGGCTGGAGATTTTGGG	54.8
aceEF_g-check_R	CCTTGATCGGCGTGAAATAG	53.8

The melting temperatures (T_m) were calculated using the online T_m calculator by Thermo Fisher Scientific (only the annealing parts of the primers were included in the analysis). For primers used in PCR amplifications with Phusion U polymerase, ‘Phusion DNA polymerase’ was chosen as the setting, with a primer concentration of 0.5 μ M. For primers used for colony PCR, ‘Taq-based DNA polymerase’ was chosen as the setting, with a primer concentration of 0.2 μ M. N.A., not applicable.

Table S2.2 · Assembly of pGNW plasmids with genes encoding fluorescent proteins within a chromosomal landing pad.

Fluorescent protein	Plasmid backbone (oligonucleotide)	Primers for HR1	Primers for gene insert	Primers for HR2
msfGFP	pGNW2 (pGNW_LP_F/ BCD2_R)	–	GFP_F/ GFP_R	–
mBFP2	pGNW2 (pGNW_LP_F/ BCD2_R)	–	BFP2_F/ BFP2_R	–
mOrange2	pGNW4 (pGNW-USER_F/ pGNW-USER_R)	LP_HR1_F / BCD2_R	Ora_Tq_F/ Ora_Tq_R	pGNW_L P_F/ LP_HR2 _R
mTurquoise2	pGNW6 (pGNW-USER_F/ pGNW-USER_R)	LP_HR1_F / BCD2_R	Ora_Tq_F/ Ora_Tq_R	pGNW_L P_F/ LP_HR2 _R

Listed are the respective plasmid backbones used for each fluorescent protein, as well as the primers that were used to amplify these plasmids and the additional fragments to assemble the corresponding DNA fragments. The sequences of the primers are presented in Table S2.1.

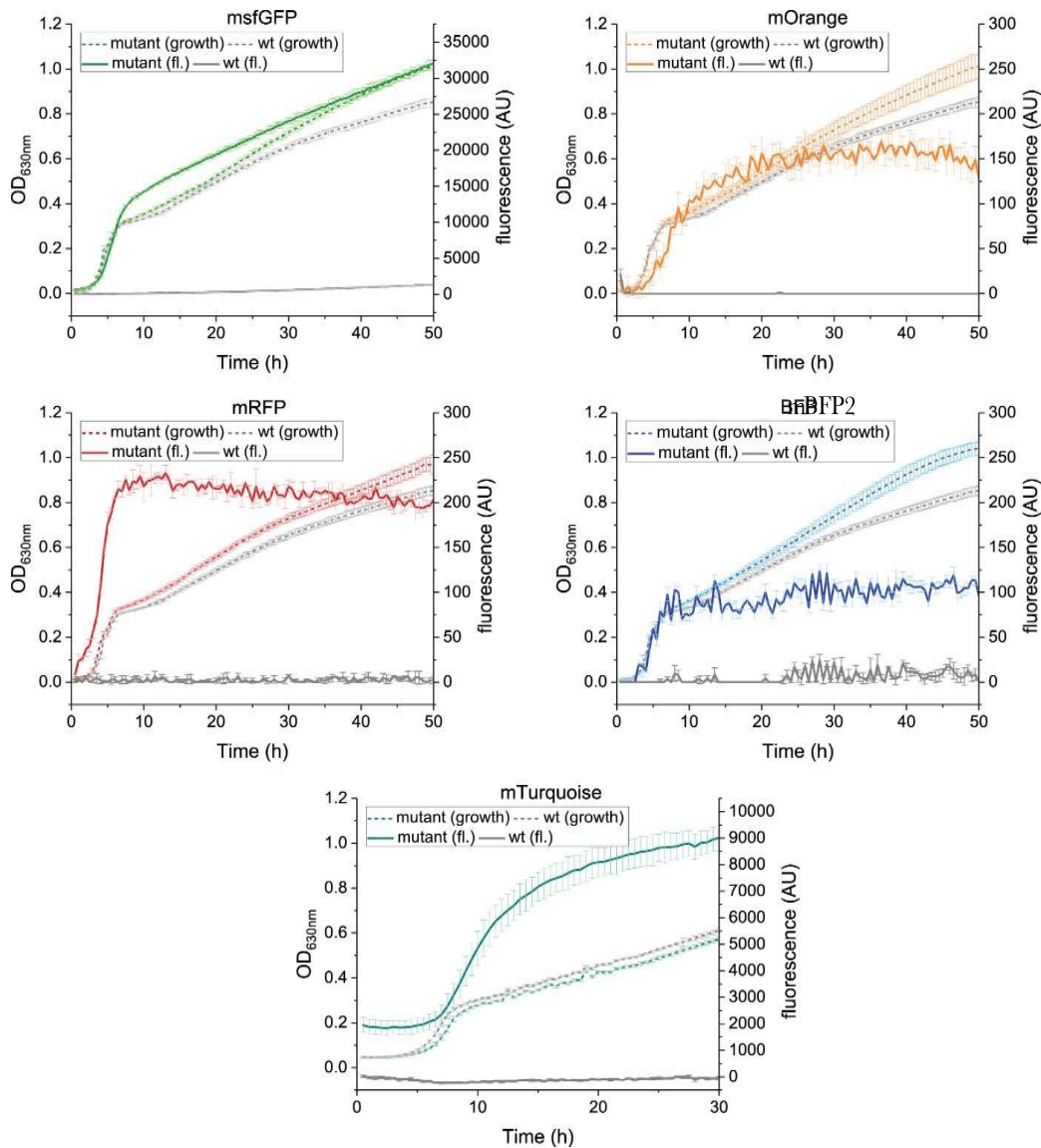


Figure S2.1 · Kinetics of the accumulation of selected fluorescent proteins measured in *P. putida* KT2440. Mutant and wild-type cells were grown in 96-well plates with de Bont medium supplemented with 30 mM citrate as the sole carbon source. Growth and fluorescence kinetics were acquired by measuring the culture optical density at 630 nm (OD_{630 nm}) as well as the excitation/emission values of fluorescent proteins as follows: msfGFP at 485 nm/528 nm, mRFP1 at 582 nm/609 nm, mBFP2 at 385 nm/450 nm, mOrange2 at 541 nm/567 nm, and mTurquoise2 at 451 nm/477 nm. Error bars indicate standard deviations from at least three biological replicates.

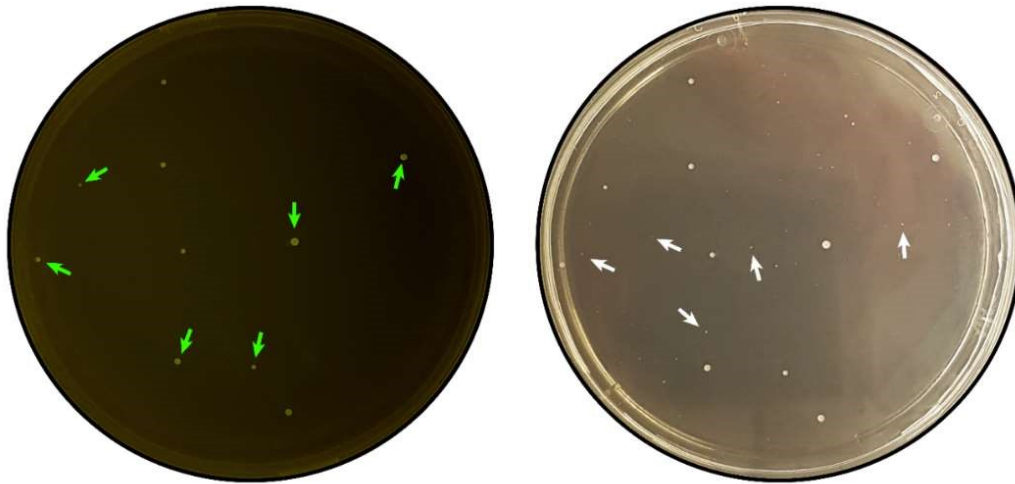


Figure S2.2 · Deletion of *aceEF* in *P. putida* *KT2440* using a synthetic CRISPR-Cas9 device for counterselection. Green arrows in the left plate indicate fluorescent colonies that escaped restriction by Cas9; white arrows in the right plate identify colonies arising from *P. putida* $\Delta aceEF$ cells.

Chapter 3

AN EXPANDED CRISPR_i TOOLBOX FOR TUNABLE GENE EXPRESSION IN *PSEUDOMONAS PUTIDA*

Ekaterina Kozaeva^{§1}, Christos Batiannis^{§2}, Stamatios G. Dalamas^{§2}, Maria M. Pascual², Daniel C. Volke¹, Pablo I. Nickel^{1*}, and Vitor A. P. Martins dos Santos^{2*}.

Microbial Biotechnology (2020) 13(2): 368-385.

1. Laboratory of Systems and Synthetic Biology, Wageningen & Research University, Stippeneng 4, 6708 WE, Wageningen, The Netherlands
2. The Novo Nordisk Foundation Center for Biosustainability, Technical University of Denmark, 2800 Kgs. Lyngby, Denmark

§ These authors made equal contributions and should be considered joint first authors.

* Correspondence to:

Vitor A. P. Martins dos Santos

(vitor.martinsdosantos@wur.nl)

Wageningen University and Research

6708 Wageningen, The Netherlands

Tel: (+31 31) 748 28 65

Pablo I. Nickel

(pabnik@biosustain.dtu.dk)

The Novo Nordisk Foundation Center for
Biosustainability

Technical University of Denmark

Kgs Lyngby 2800, Denmark

Tel: (+45) 93 51 19 18

INTRODUCTION

Pseudomonas putida KT2440 is Gram-negative soil bacterium and the microbial cell factory of choice for many applications in biotechnology due to a number of unique qualities. It is endowed with considerable metabolic versatility, a remarkable tolerance to various stress conditions as well as rapid growth with simple nutrient requirements¹⁻⁶. Moreover, this bacterium is equipped with a unique glycolysis, the *EDEMP cycle*, resulting in catabolic NAD(P)H overproduction that can be used as reducing power for biocatalysis or to counteract oxidative stress⁷. All these traits render this bacterium a robust platform for a range of industrial and environmental applications. In connection to this, the available toolbox for manipulating its genome and metabolism is still under extensive development to further enhance the applicability of *P. putida* as a cell platform⁸⁻¹⁰.

In an effort to broaden the existing toolbox, many groups have focused on clustered regularly interspaced short palindromic repeats (CRISPR)/CRISPR-associated protein (Cas9)-based methods for knocking-out or knocking-down target genes in *P. putida*. Recently, type II CRISPR/Cas systems have been utilized in combination with the λ -Red system, SSR recombinases or the I-*SceI* meganuclease for precise gene deletion¹¹⁻¹⁶. Engineered catalytically inactive variants of the Cas9 protein (dead Cas9, dCas9) have been shown to act as a transcription repressor in *Pseudomonas* strains, including *P. putida* KT2440. Tan *et al.*¹⁷, for instance, used a two-plasmid CRISPR interference (CRISPRi) system, based on the type II dCas9 homologue of *Streptococcus pasteurianus*. In this example, dCas9 from *S. pasteurianus* could be harnessed for efficient CRISPRi-mediated downregulation of genes, requiring specific protospacer adjacent motif (PAM) sequences (5'-NNGTGA-3' or 5'-NNGCGA-3', where N represents any nucleotide). These PAM sequences, however, are significantly less abundant in the genome of *P. putida* KT2440 in comparison with the simpler PAM motif 5'-NGG-3', associated with the most commonly used Cas9 from *Streptococcus pyogenes* (*Sp*Cas9).

Recently, two alternative $\mathcal{S}p$ dCas9-based CRISPRi systems were developed and explored in *Pseudomonas* species^{13,17}. Both systems were demonstrated to be functional for repression of genes encoding fluorescent proteins, and Kim *et al.*¹⁸ also employed CRISPRi for metabolic engineering *via* gene repression by depleting the GlpR regulator to enhance the glycerol-dependent synthesis of mevalonate. Other examples on the development of CRISPRi systems have been reported for *P. aeruginosa*^{19,20} and *P. fluorescens*²¹. While the CRISPRi toolbox for *Pseudomonas* species offers alternatives depending on the intended application (ranging from fundamental studies to simple metabolic engineering manipulations), the techniques applied so far are afflicted by either leaky expression of the components or limited ability to titrate repression levels – thus restricting the applicability of the tool in complex engineering approaches. Moreover, the possibility of performing multiple, simultaneous knock-downs in gene expression with minimal cloning efforts is still largely missing.

Here, we present an expanded CRISPRi toolbox allowing for the tunable regulation of one or multiple target genes in *Pseudomonas* species. Specifically, we have developed a set of modular, composable vectors encoding CRISPRi systems using either (i) non-coding *trans*-activating CRISPR RNA (tracrRNA) and the CRISPR locus needed for CRISPR RNA (crRNA) generation, present in the native type II CRISPR/Cas9 system of *S. pyogenes*²², or (ii) a single gRNA (sgRNA) in short fusion form of tracrRNA and crRNA²³. The immense majority of the already developed tools have utilized sgRNAs due to simplicity of working with a single RNA molecule²⁴⁻²⁶. In general, the efficiency of using just sgRNA or both tracrRNA and crRNA was observed to be comparable – although the architecture of crRNA allows for a rapid and simple cloning strategy when generating multiplex crRNA arrays. Therefore, in this study we tested and employed both sgRNA- and crRNA-based CRISPRi systems in *P. putida* KT2440, and we describe alternative protocols for efficient downregulation of the expression of single or multiple target genes. Furthermore, we compared the efficiency of three different inducible expression systems to control the expression levels of the $\mathcal{S}p$ dCas9 gene and showed that the XylS/ P_m expression system was able to accurately modulate repression levels by adjusting the amount of inducer (3-methylbenzoate, 3-*mBz*) – thus

resulting in a tunable, titrable CRISPRi system. Additionally, we demonstrate that CRISPRi-mediated downregulation of gene expression is more efficient in a *P. putida* strain lacking the main component of the homologous recombination machinery, RecA. Our study expands the currently available CRISPRi toolbox, enabling to gain insights on transcriptional repression in non-model bacteria, and allowing for depletion of one or several proteins of interest to support rational metabolic engineering of *P. putida*.

Overview of the workflow

The overall gene downregulation procedure begins with the construction of the target-specific vector pCRi (**Table 3.1** and extended explanation below), followed by plasmid transformation in the strain of interest and induction of the system for targeted repression (**Figure 3.1**). The whole procedure typically takes around 6 days. All bacterial strains used in this study are listed in **Table S3.1** in the Supporting Information, and the specific steps of the protocol are detailed below.

Table 3.1. Plasmids used in this work.

Name	Relevant features	Source or reference
pSEVA448	Cloning vector; <i>oriV</i> (pRO1600/ColE1); <i>XylS</i> , P_m ; Sm^R/Sp^R	Silva-Rocha <i>et al.</i> (2013)
pSEVA421-Cas9tr	pSEVA421 derivative bearing the <i>SpCas9</i> gene and a tracrRNA module; <i>oriV</i> (RK2); Sm^R/Sp^R	Aparicio <i>et al.</i> (2018)
pSEVA231-CRISPR	pSEVA231 derivative bearing the CRISPR array; <i>oriV</i> (pBBR1); Km^R	Aparicio <i>et al.</i> (2018)
pSEVA441	Cloning vector; <i>oriV</i> (pRO1600/ColE1); Sm^R/Sp^R	Silva-Rocha <i>et al.</i> (2013)
pMCRi	Plasmid for CRISPRi; <i>oriV</i> (pRO1600/ColE1), <i>xylS</i> (cured of <i>BsaI</i> -sites), $P_m \rightarrow SpdCas9, P_{EM7} \rightarrow sgRNA$; Sm^R/Sp^R	This work
pMCRi_ <i>gfp</i>	Plasmid for CRISPRi; <i>oriV</i> (pRO1600/ColE1), <i>xylS</i> (cured of <i>BsaI</i> -sites), $P_m \rightarrow SpdCas9, P_{EM7} \rightarrow msf:gfp$ -specific sgRNA; Sm^R/Sp^R	This work
pMCRi_ <i>pyrF</i>	Plasmid for CRISPRi; <i>oriV</i> (pRO1600/ColE1), <i>xylS</i> (cured of <i>BsaI</i> -sites), $P_m \rightarrow SpdCas9, P_{EM7} \rightarrow pyrF$ -specific sgRNA; Sm^R/Sp^R	This work

Name	Relevant features	Source or reference
pMCRi_ftsZ	Plasmid for CRISPRi; <i>oriV</i> (pRO1600/ColE1), <i>xyIS</i> (cured of <i>BsaI</i> -sites), $P_m \rightarrow SpdCas9$, $P_{EM7} \rightarrow ftsZ$ -specific sgRNA; Sm ^R /Sp ^R	This work
pMCRi_yfp	Plasmid for CRISPRi; <i>oriV</i> (pRO1600/ColE1), <i>xyIS</i> (cured of <i>BsaI</i> -sites), $P_m \rightarrow SpdCas9$, $P_{EM7} \rightarrow yfp$ -specific sgRNA; Sm ^R /Sp ^R	This work
pCCRi	Plasmid for CRISPRi; <i>oriV</i> (pRO1600/ColE1), <i>chnR</i> , $P_{chnB} \rightarrow SpdCas9$, $P_{EM7} \rightarrow sgRNA$; Sm ^R /Sp ^R	This work
pCCRi_gfp	Plasmid for CRISPRi; <i>oriV</i> (pRO1600/ColE1), <i>chnR</i> , $P_{chnB} \rightarrow SpdCas9$, $P_{EM7} \rightarrow sgRNA$; $P_{EM7} \rightarrow msf$ <i>gfp</i> -specific sgRNA; Sm ^R /Sp ^R	This work
pDCRi	Plasmid for CRISPRi; <i>oriV</i> (pRO1600/ColE1), <i>cprK1</i> , $P_{DB3} \rightarrow SpdCas9$, $P_{EM7} \rightarrow sgRNA$; Sm ^R /Sp ^R	This work
pDCRi_gfp	Plasmid for CRISPRi; <i>oriV</i> (pRO1600/ColE1), <i>cprK1</i> , $P_{DB3} \rightarrow SpdCas9$, $P_{EM7} \rightarrow sgRNA$; $P_{EM7} \rightarrow msf$ <i>gfp</i> -specific sgRNA; Sm ^R /Sp ^R	This work
pGCRi-R	Plasmid for CRISPRi; <i>oriV</i> (pRO1600/ColE1), <i>xyIS</i> (cured of <i>BsaI</i> -sites), $P_m \rightarrow GCSpdCas9$, crRNA cassette with <i>eforRed</i> ; Sm ^R /Sp ^R	This work

Name	Relevant features	Source or reference
pGCRi_ <i>yfp</i>	Plasmid for CRISPRi; <i>oriV</i> (pRO1600/ColE1), <i>xylS</i> (cured of <i>BsaI</i> -sites), $P_m \rightarrow GCSpdCas9$, <i>yfp</i> -specific crRNA; Sm ^R /Sp ^R	This work
pGCRi_ <i>ftsZ</i>	Plasmid for CRISPRi; <i>oriV</i> (pRO1600/ColE1), <i>xylS</i> (cured of <i>BsaI</i> -sites), $P_m \rightarrow GCSpdCas9$, <i>ftsZ</i> -specific crRNA; Sm ^R /Sp ^R	This work
pGCRi_ <i>pyrF</i>	Plasmid for CRISPRi; <i>oriV</i> (pRO1600/ColE1), <i>xylS</i> (cured of <i>BsaI</i> -sites), $P_m \rightarrow GCSpdCas9$, <i>ftsZ</i> -specific crRNA; Sm ^R /Sp ^R	This work
pCRiMs	Plasmid for mCRISPRi; <i>oriV</i> (pRO1600/ColE1), <i>xylS</i> (cured of <i>BsaI</i> -sites), $P_m \rightarrow SpdCas9$, $P_{EM7} \rightarrow ftsZ$ -specific sgRNA, $P_{EM7} \rightarrow yfp$ -specific sgRNA, $P_{EM7} \rightarrow mCherry$ -specific sgRNA; Sm ^R /Sp ^R	This work
pCRiMc	Plasmid for mCRISPRi; <i>oriV</i> (pRO1600/ColE1), <i>xylS</i> (cured of <i>BsaI</i> -sites), $P_m \rightarrow GCSpdCas9$, tracrRNA module, <i>ftsZ</i> -specific crRNA, <i>yfp</i> -specific crRNA, <i>mCherry</i> -specific crRNA; Sm ^R /Sp ^R	This work

Antibiotic markers and abbreviations: Ap, ampicillin; Km, kanamycin; Gm, gentamicin; Sm, streptomycin; and Sp, spectinomycin; Ts, temperature-sensitive replicon; mCRISPRi, multiplex CRISPR interference.

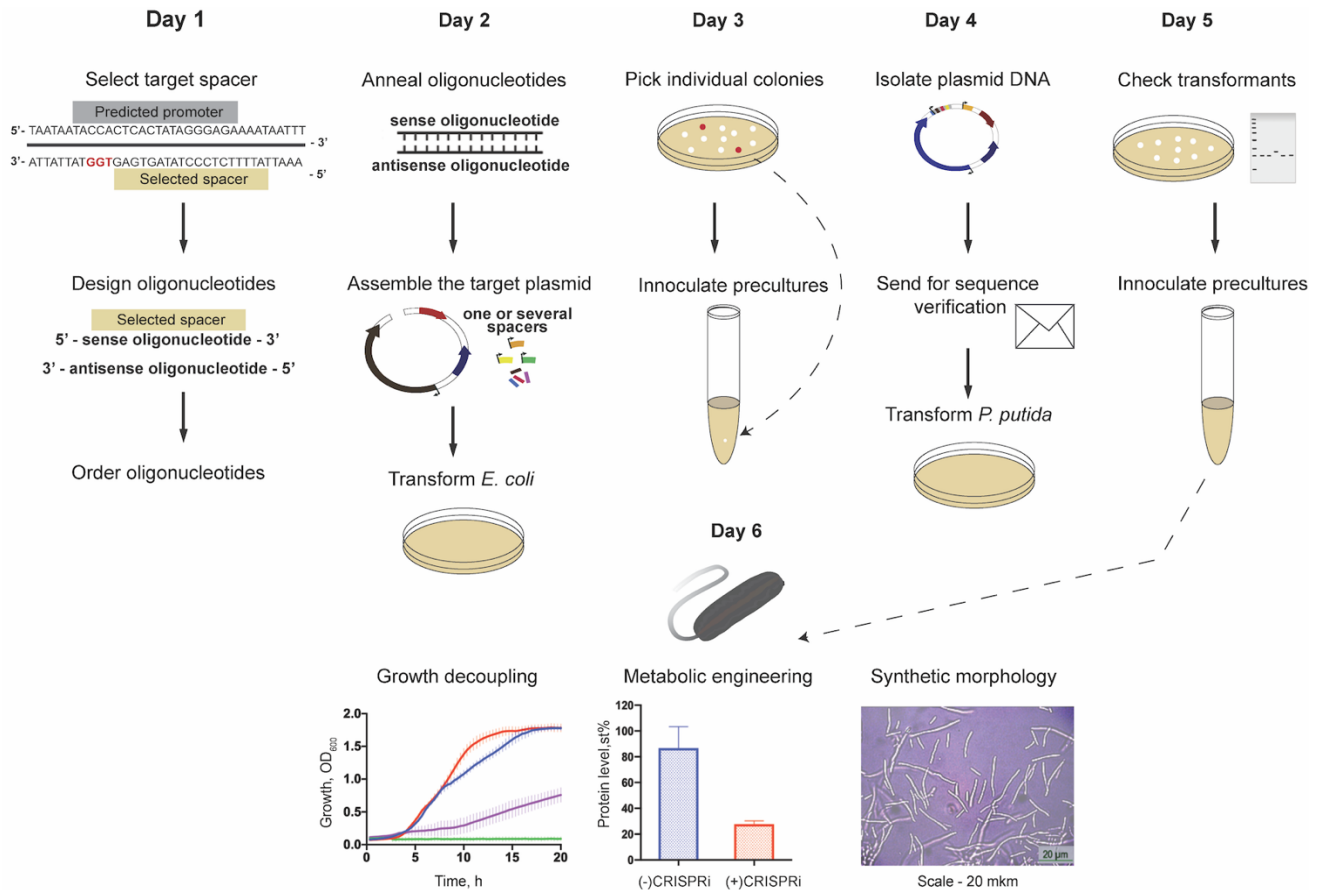


Figure 3.1. Overview of the workflow for CRISPRi-mediated gene knock-down in *Pseudomonas putida*.

Day 1: Choose a PAM sequence (5'-NGG-3', where N represents any nucleotide) within the non-template DNA strand sequence of the target gene. For efficient gene repression, we recommend choosing a PAM within the promoter sequence, or, if the promoter is not clearly defined or if it overlaps with a coding sequence, choose the PAM closest to the start *ATG* codon. Design and order two oligonucleotides for cloning of the spacer (upstream the PAM, following the format 5'-*spacer*-NGG-3')

Day 2: Anneal single-strand DNA oligonucleotides by reverse cooling to form a double-stranded DNA spacer-insert array and clone it into the respective derivative of vector pCRi. Transform a suitable cloning *E. coli* strain and incubate the plates overnight (under streptomycin selection).

Day 3: Inoculate three transformants in liquid cultures and grow the cultures overnight.

Day 4: Purify three independent plasmids and send them out for sequence verification by DNA sequencing. Transform the target *Pseudomonas* strain with isolated and sequence-verified plasmids and incubate the plates under streptomycin selection.

Day 5: Inoculate a fresh culture in the appropriate medium with verified *Pseudomonas* colonies and the additives needed and incubate the cultures overnight.

Day 6: Perform CRISPRi-mediated gene downregulation in the presence of 1 mM 3-methylbenzoate (or other inducer concentrations as needed) to activate the system

Overview and construction of derivatives of the pCRi vector

To expand the CRISPRi toolbox, we constructed a set of vectors that harbour *SpdCas9*, along with either the native gRNAs (crRNA and tracrRNA) or its short fusion form (sgRNA). The *SpdCas9* gene and the corresponding gRNAs were expressed from a single vector using the backbone pSEVA441. This approach enabled to construct composable plasmids, the modules of which can be swapped at the user's will^{27,28}. Both gRNAs were placed under constitutive expression of either the native Sp promoter (crRNA) or the synthetic, constitutive P_{EM7} promoter²⁹ ($P_{EM7} \rightarrow$ sgRNA), while the transcription of *SpdCas9* was driven by inducible expression systems. The level of constitutive expression brought about by the P_{EM7} promoter was shown to be appropriate for expression of the sgRNAs tested in this work, and other versions of the same promoter (displaying different strengths) can be implemented if needed³⁰. In this context, the inducible expression of *SpdCas9* would enable tunable repression levels – allowing, in turn, for the interference of essential genes expression as well as controlling the repression timing. First, we created a set of sgRNA-based vectors by using different modules for inducible expression of *SpdCas9*: XylS/ P_m , ChnR/ P_{cmB} or CprK1/ P_{DB3} ^{27,28,31,32} which resulted in vectors pMCRi, pCCRi and pDCRi respectively (**Figure 3.2**).

We have selected these three inducible expression systems as they are known to be active in *P. putida*, and they are titrable (i.e. promoter output varies as a consequence of increasing concentrations of the inducer) to different extents²⁸. The well-characterized XylS/P_m expression system was observed to be the most effective mediating the repression of target genes, and we proceeded further in constructing the crRNA-based vector pGCRi by adopting this system. Vector pGCRi consists of three main functional elements: (i) a GC-rich, dead *SpCas9* version (a codon-optimized *SpdCas9* for *Streptomyces* species, termed *GC^{SpdCas9}*)³³ under the control of the XylS/P_m expression system, (ii) the tracrRNA under the control of the native, constitutive Sp promoter and (iii) the leader-crRNA.

Streptococcus species have a relatively low average genomic GC-content (~41.2%), while *Pseudomonas* and *Streptomyces* display high average genomic GC-content (~60%). We thus reasoned that the *GC^{SpdCas9}* gene (displaying a GC-content ~62%) could be suitable for CRISPRi in *P. putida* as compared to the wild-type version of *SpdCas9* (having a GC-content ~45%). Additionally, to enable one-step assembly of single or multiple spacers into vector pGCRi *via* Golden Gate cloning and to simplify the selection process, we engineered the crRNA cassette by incorporating an eforRed chromoprotein construct (BBa_K592012; endowed with a constitutive promoter and a ribosome binding site, RBS) flanked by two *BsaI* recognition sites between the two direct repeats (DRs) (**Figure 3.2, B**).

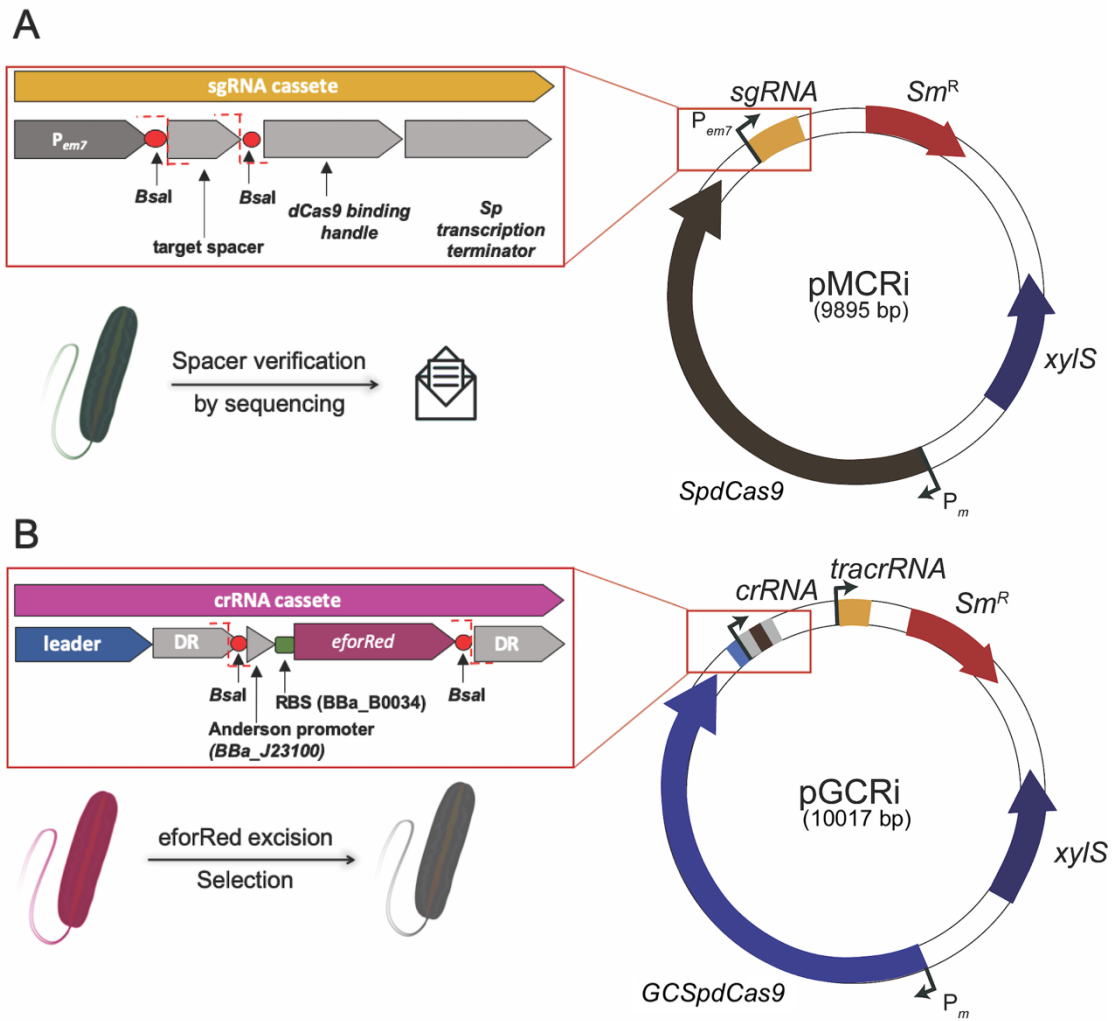


Figure 3.2. Overview of key expression vectors constructed for CRISPRi-mediated knock-down of gene expression in *Pseudomonas putida*.

A. Vector pMCRi contains *SpdCas9* under the control of the XylS/ P_m expression system and a constitutively expressed sgRNA cassette. The sgRNA cassette is composed by the synthetic, constitutive P_{EM7} promoter followed by the sgRNA chimera, spanning three domains: a 20-nt region for target-specific binding, a 42-nt hairpin for dCas9 binding (dCas9 handle) and a 40-nt transcription terminator (Sp Terminator) derived from *S. pyogenes*. To clone the target spacer, two *BsaI* recognition sites have been incorporated between the P_{EM7} promoter and the sgRNA cassette.

B. The crRNA-based CRISPRi vector pGCRI-R. This vector contains a GC-rich *SpdCas9* gene (the expression of which is placed under control of the XylS/ P_m expression system), a constitutively expressed crRNA cassette and the constitutively expressed *tracrRNA*. The crRNA cassette is formed by an AT-rich sequence (leader) that contains a promoter driving the transcription of the crRNA³⁴ and the two direct repeats (DRs) with an intervening gene encoding the

eforRed chromoprotein from *Echinopora forskaliana* (expressed from the constitutive BBa_J23100 Anderson promoter and equipped with the BBa_B0034 ribosome binding site). The crRNA cassette is flanked by two *BsaI* recognition sites to facilitate cloning the target spacer sequence. If the target spacer is successfully assembled by Golden Gate cloning into vector pGCRi, the *eforRed* reporter gene is split (and inactivated), and the resulting *E. coli* transformants will appear white instead of reddish when isolated on solid culture medium plates.

When accumulated in cells containing this construct, the eforRed chromoprotein from the coral *Echinopora forskaliana*³⁵ confers a pink or reddish coloration to the colonies. In this way, when ligation of a spacer is successful, the reporter is split and the *E. coli* transformants containing the intended constructs appear white instead of reddish. These operations do not affect the overall efficiency of transformation while they greatly facilitate the screening. The construction of the sgRNA-based vectors was done essentially according to Wirth *et al.*¹⁴ A detailed description of the pGCRi vector construction, including the list of oligonucleotides used for cloning functional modules into both vectors (**Table S3.2**), is given in the Supporting Information.

Protocol for CRISPRi-mediated downregulation of one or multiple targets

Spacer design and selecting a suitable target sequence

The CRISPRi system requires a specific spacer sequence in the gRNA, which determines the binding site of S_{pd} Cas9. This sequence has to be selected specifically for each target as a 20-nt spacer for the sgRNA or a 30-nt spacer for the crRNA array^{23,36}. In both cases, it must be immediately followed by a PAM (5'-NGG-3'). DNA strand specificity is relevant for CRISPRi, and targeting the non-template strand is crucial for efficient repression – whereas targeting the template DNA strand of the coding sequence is less effective or not effective at all³⁷. It has also been shown that the downregulation effect is the most efficient when dCas9 binds to the promoter sequence^{17,38}. Bacterial promoters can be predicted using freely available *in silico* tools (such as online tool BPRM from Softberry.com). In case that there is no available PAM in the promoter sequence or if the promoter is poorly defined or overlaps with other coding sequences or promoters, the spacer sequence should be chosen on the non-template strand, closest to the beginning of the start *ATG* codon of the target gene. To avoid off-target effects, the spacer sequence should be unique. To ensure that this is the case, a simple BLAST analysis³⁹ against the complete genomic DNA sequence of the target *Pseudomonas* strain⁴⁰ should reveal no sequence similarities.

Assembly of a target-specific CRISPRi vector in *E. coli*

The vectors described herein contain two *BsaI* (a type IIS restriction enzyme targeting the sequence 5'-GGTCTC(N₁)/(N₅)-3', where N represents any nucleotide) recognition sites that are placed upstream of the sgRNA fusion construct. These recognition targets are placed in either an inverted orientation (to insert a 20-nt spacer) or a forward orientation between the DRs of the crRNA cassette (to insert a 30-nt spacer). Further linearization of the vector by treatment with *BsaI* allows for the incorporation of a spacer-

insert with unique overhangs, resulting in a target-specific vector that expresses *SpCas9*. Below we present two cloning strategies for addition of specific spacers into the corresponding RNAs.

sgRNA design and construction of the pCRi_target vector

Design and order two oligonucleotides that are complementary to each other. The first oligonucleotide contains the 20-nt spacer sequence from non-template strand of target gene and flanked at the 5'-end with 5'-GCGCG-3'. The second oligonucleotide contains a reverse complement 20-nt spacer sequence as mentioned above, with the addition of a 5'-AAAC-3' motif to its 5'-end and a C nucleotide to its 3'-end.

For example, if the *pyrF* gene (*PP_1815*, encoding orotidine 5'-phosphate decarboxylase, an essential activity for growth of *P. putida* in minimal media) is to be targeted, the resulting sequences are as follows: *oligonucleotide 1 (EK.pyrF-F)*, 5'-GCG CGG GAA ATC CAG GGC GAC GAT C-3'; and *oligonucleotide 2 (EK.pyrF-R)*, 5'-AAA CGA TCG TCG CCC TGG ATT TCC C-3' (**Table S3.2** in the Supporting Information). In these oligonucleotides, the nucleotides in bold represent *BsaI*-compatible overhangs for efficient ligation of the spacer. To perform a ligation reaction with the linearized pCRi vector, oligonucleotides have to be phosphorylated at the 5'-end, which could be done either by *in situ* phosphorylation using T4 polynucleotide kinase (PNK) or by chemical modification during oligonucleotide synthesis.

Step-by-step procedure (cloning of a construct to target a single gene)

- i. Digest vector pCRi with *BsaI* (or its *Eco31I* isoschizomer; New England Biolabs Inc., Ipswich, MA, USA) according to the manufacturer's recommendations. In order to purify the linearized plasmid after digestion, perform electrophoresis of the digestion mixture followed by gel purification of the isolated fragment. We recommend purifying the amplified pCRi vector fragment (9800 bp) from a gel and to use it as template for further applications.
- ii. Dissolve the two spacer oligonucleotides in water at a final concentration of 100 μ M. Phosphorylate and anneal the oligonucleotides in a thermocycler. This can be performed in a single 10 μ l reaction containing 6 μ l of water, 1 μ l of each oligonucleotide

- solution, 1 μ l of T4 ligase buffer and 1 μ l of T4 PNK (New England Biolabs Inc.). Use the following temperature protocol: 30 min at 37°C, 4 min at 95°C, followed by 70 cycles consisting of 12 s each, starting at 95°C and decreasing the temperature by 1°C in each cycle.
- iii. Dilute the annealed and phosphorylated oligonucleotides 1:200 with water, that is to a final concentration of double-stranded DNA (dsDNA) of 50 nM. Ligate the dsDNA encoding the spacer for sgRNA into the linearized pCRi vector in a 10 μ l reaction containing 1 μ l of diluted insert from the previous step, 10 ng of *Bsa*I-digested and purified pCRi vector or its derivative, 1 μ l of T4 ligase buffer, 1 μ l of T4 DNA ligase (New England Biolabs Inc.) and water, if needed, to reach the final volume. Other ligases, such as the QuickLigase™ DNA ligase (New England Biolabs Inc.) can be used as needed.
 - iv. Ligate 30 min at room temperature and transform a 100- μ l aliquot of chemically competent *E. coli* DH5 α cells with the total ligation mixture. Plate the bacterial suspension on LB agar plates supplemented with streptomycin. Purify plasmid DNA from three individual *E. coli* transformants, and verify the sequence integrity by sequencing with primer EK.SEVA_T0-F (**Table S3.2** in the Supporting Information).

In order to repress multiple targets, several sgRNAs should be cloned into the vector, each of them placed under its own promoter. Individual P_{EM7} \rightarrow sgRNA modules are synthesized as ultramers (Integrated DNA Technologies, Leuven, Belgium). Multiple sgRNA ultramers (i.e. containing promoter, target spacer, sgRNA fusion construct and unique overhangs) have to be amplified with the corresponding set of primers (depending on the sequence) and assembled together into the selected pCRiMs vector (**Figure 3.3**), for example with *USER* cloning⁴¹. The *AMUSER** tool⁴² can be used to design primers with suitable overhangs for the assembly.

* (Available online at <http://www.cbs.dtu.dk/services/AMUSER/>).

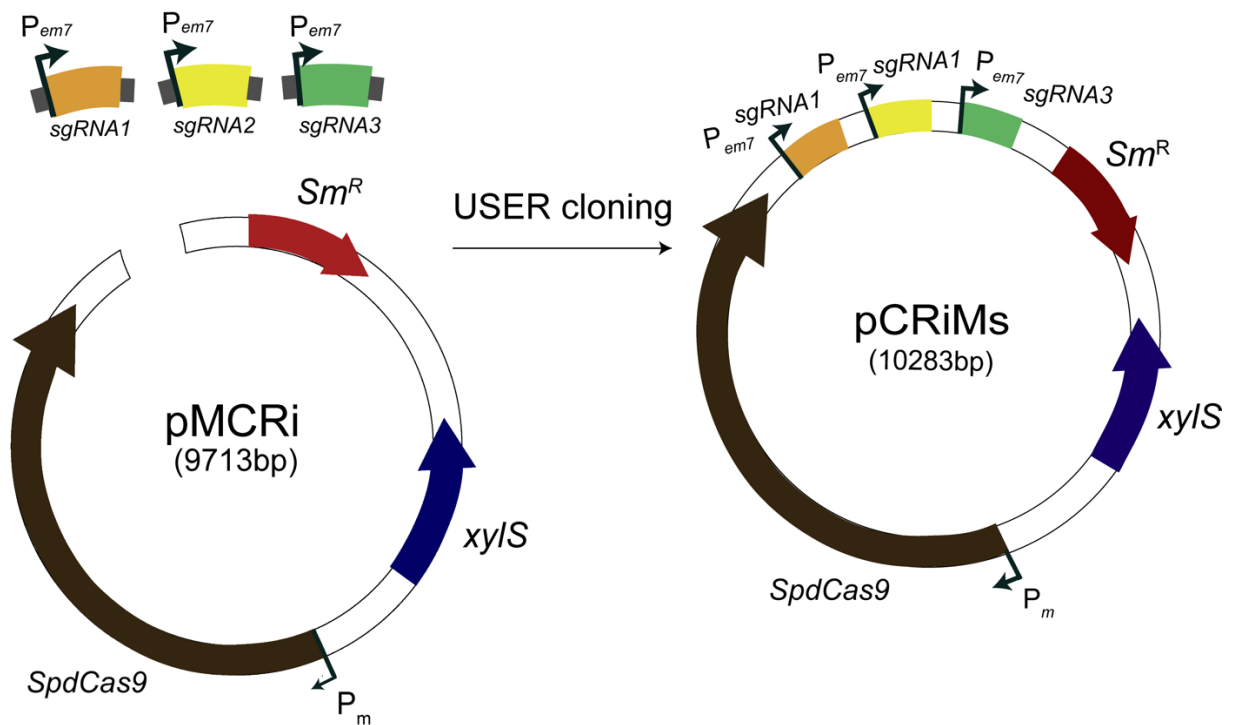


Figure 3.3. Assembly of pCRiMs vectors. Double-stranded sgRNA ultramers with unique target spacers are combined with a PCR-amplified pMCRi vector for *USER* cloning reactions, resulting in a suite of vectors tailored for downregulation of several targets (i.e. pCRiMs plasmids)

Step-by-step procedure (cloning of a construct to target multiple genes)

- i. Amplify vector pCRi using 1–5 ng of plasmid as template and primers EK.pCRi-U-F and EK.pCRi-U-R (**Table S3.2** in the Supporting Information) using *Phusion*TM U Hot Start DNA polymerase according to the manufacturer's recommendations (Thermo Fisher Scientific, Waltham, MA, USA), 3 min elongation time, and employing an annealing temperature of 60°C for 30 cycles.
- ii. Amplify double-stranded sgRNAs using synthesized ultramer as a template and respective primers (EK.sgRNA-F and EK.sgRNA-R; **Table S2** in the Supporting Information) using *Phusion*TM U Hot Start DNA polymerase (according to the manufacturer's recommendations), 20 s elongation time, and annealing temperature of 60°C for 30 cycles.
- iii. Combine equimolar amounts of sgRNAs and 100-150 ng of pCRi derivative with 1 µl of 1 U µl⁻¹ *USER* enzyme (New England BioLabs Inc.) in a final volume of 10 µl. Incubate 30 min at 37°C or 20 min at room temperature. Transform 50 µl of chemically competent *E. coli* DH5α cells with 10 µl of the resulting mixture. Plate the cells on LB medium agar supplemented with streptomycin.

Quickly verify correct constructs *via* PCR of 6-10 colonies with primers EK.SEVA_T0-F and EK.sgRNA-R (**Table S3.2** in the Supporting Information). The size of the band for the negative control (i.e. an empty pCRi vector) is 210 bp; each spacer insert will yield a 195-bp longer amplicon. Purify DNA from the remaining volume of the PCR tubes that had the correct insert size and send the samples for DNA sequencing for final verification. Inoculate cultures of two individual *E. coli* clones (having the correct band size and sequence) in LB medium with streptomycin and incubate the cultures overnight at 37°C with shaking for further isolation of the plasmids.

Plasmid delivery in *Pseudomonas* by electroporation

- i. Inoculate 10 ml of LB medium with the *P. putida* strain to be transformed and grow the cells overnight at 30°C with agitation (170-200 rpm).
- ii. Wash the cells three times with 1 ml of 300 mM sucrose (filter-sterilized) and resuspend them in 400 µl of 300 mM sucrose.
- iii. Individually electroporate 100 ng of empty pCRi vector and 100 ng of pCRi vector with the target-specific gRNA into 100-µl cell suspension aliquots with a voltage of 2.5 kV, 25 µF capacitance, and 200 Ω resistance (e.g. in a Gene Pulser Xcell™ Electroporation System, Bio-Rad Laboratories Inc., Hercules, CA, USA).
- iv. Let the cells recover in LB medium for 2 h at 30°C with agitation and plate them onto LB agar supplemented with streptomycin (100 µg ml⁻¹). Incubate the plates overnight at 30°C.

Downregulation of the target gene(s) with CRISPRi

The plate with *P. putida* cells harboring a pCRi plasmid with a functional gRNA should have a repressed gene of interest within 2 h after induction with 3-*mBz* (for the maximal downregulation we recommend using the inducer at 1 mM). Inoculate the culture medium of interest with *P. putida* harbouring the derivative of pCRi plasmid with target-specific gRNA(s) and grow the cells overnight at 30°C with agitation as indicated above. We recommend supplementing the culture medium with streptomycin (100 µg ml⁻¹) to select for the pCRi vector derivative.

APPLICATION EXAMPLES

CRISPRi-mediated repression efficiency with different inducible expression systems

We first examined the efficiency of the target gene repression with CRISPRi using different expression systems: XylS/ P_m on the pMCRi plasmid, ChnR/ P_{chnB} on the pCCRi plasmid and CprK1/ P_{DB3} on the pDCRi plasmid, which all drive *SpdCas9* expression (**Figure 3.4, A**). To determine the capability of the newly established CRISPRi system for regulation of heterologous gene expression, we used *P. putida* strain KT·BG42, harbouring a *msf::gfp* gene (encoding the monomeric super-folder green fluorescent protein, msfGFP) and a gentamicin resistance marker in the unique Tn7 locus of the bacterial chromosome^{30,43} (see **Table S3.2** in the Supporting Information).

Each pCRi vector was transformed into strain KT·BG42, and cells were grown at 30°C on LB medium plates, containing both 100 µg ml⁻¹ streptomycin (to select for the plasmid) and 20 µg ml⁻¹ gentamicin (to select for the Tn7 insertion). Three single colonies were then individually inoculated to set overnight pre-cultures into 3 ml of M9 minimal medium (6 g l⁻¹ Na₂HPO₄, 3 g l⁻¹ KH₂PO₄, 1.4 g l⁻¹(NH₄)₂SO₄, 0.5 g l⁻¹ NaCl, 0.2 g l⁻¹ MgSO₄, 2.5 ml l⁻¹ of a trace elements solution)^{44,45} containing 100 µg ml⁻¹ streptomycin and 20 µg ml⁻¹ gentamicin. Cultures were incubated for 15 h at 30°C with agitation. Then, 5 µl of the preculture was inoculated into 195 µl of M9 minimal medium containing 100 µg ml⁻¹ streptomycin, 20 µg ml⁻¹ gentamicin and 1 mM of the corresponding inducer depending on the expression system (XylS/ P_m , induced by 3-*m*Bz; ChnR/ P_{chnB} , induced by cyclohexanone; and CprK1/ P_{DB3} , induced by 3-chloro-4-hydroxyphenylacetic acid). All inducers were directly added to the liquid culture medium from stock, concentrated solutions.

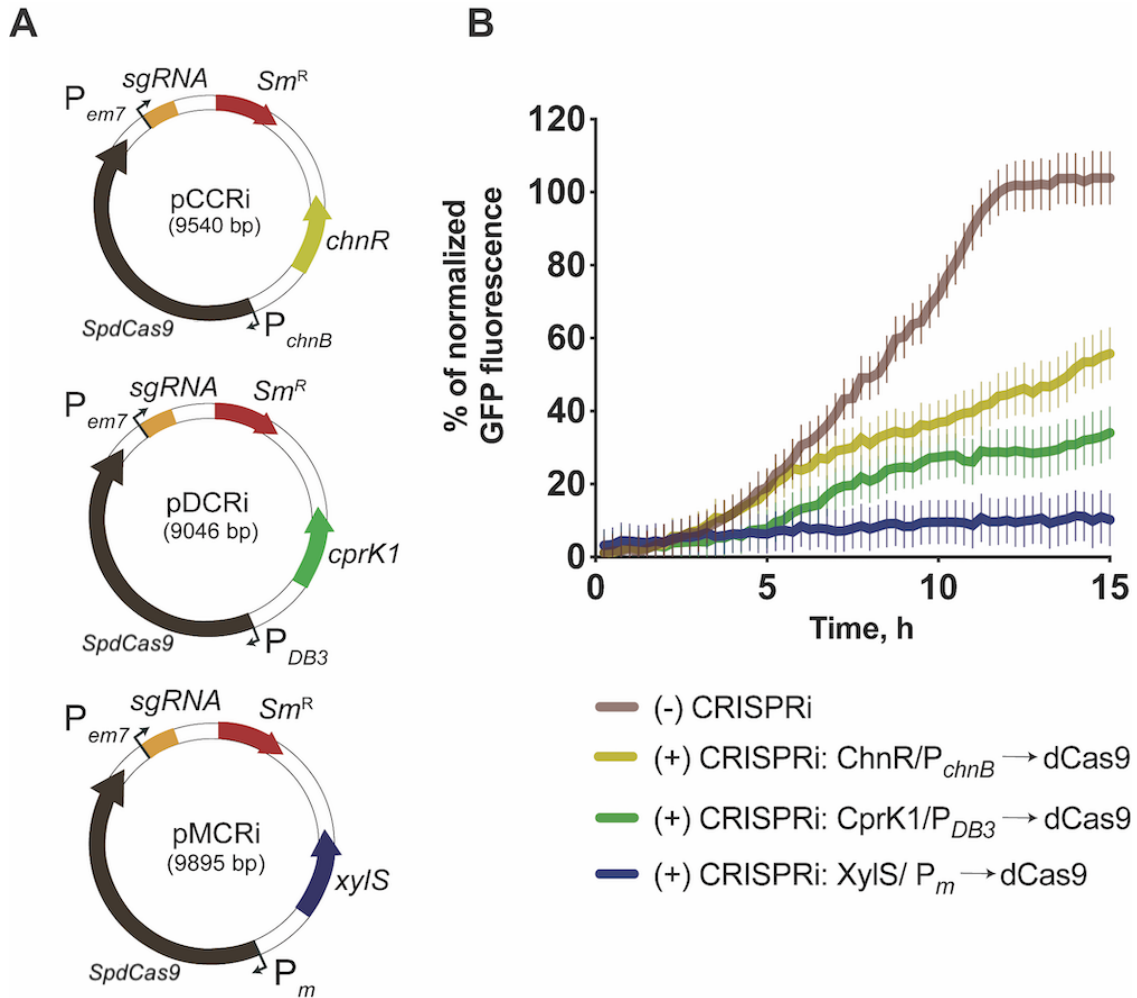


Figure 3.4.

Titratable downregulation of *msf::gfp* expression with CRISPRi using inducible expression systems to drive *SpdCas9* expression

A. Schematic representation of derivatives of plasmid pCRI_{*gfp*} (plasmids pCCRi, pDCRi and pMCRi). All plasmids were separately introduced into *P. putida* KT·BG42, and three different expression systems were adopted: XylS/ P_m (induced by addition of 3-methylbenzoate), ChnR/ P_{chnB} (induced by addition of cyclohexanone) and CprK1/ P_{DB3} (induced by addition of 3-chloro-4-hydroxyphenylacetic acid).

B. CRISPRi experiment on fluorescent proteins. *P. putida* KT·BG42 was used as a control [indicated in the figure as (-) CRISPRi], and grown on M9 minimal medium supplemented with 0.2% (w/v) glucose and 20 $\mu\text{g ml}^{-1}$ gentamicin. *P. putida* KT·BG42 transformants, harbouring the different CRISPRi vectors indicated, were re-grown on M9 minimal

medium supplemented with 0.2% (w/v) glucose, 100 $\mu\text{g ml}^{-1}$ streptomycin, 20 $\mu\text{g ml}^{-1}$ gentamicin and 1 mM of the corresponding inducer [indicated in the figure as (+) CRISPRi]. Bacterial growth and msfGFP fluorescence ($\lambda_{\text{excitation}}/\lambda_{\text{emission}} = 485 \text{ nm}/516 \text{ nm}$) were continuously measured during 15 h in a Synergy HI plate reader (BioTek Instruments, Inc., Winooski, VT, USA) using microtiter 96-well plates incubated at 30°C. Fluorescence readings were normalized to the bacterial growth (estimated as the optical density measured at 600 nm). Each data point represents the mean value of the percentage of normalized fluorescence \pm standard deviation from at least three biological replicates.

The CRISPRi-mediated decrease of msfGFP fluorescence in *P. putida* KT·BG42 transformed with different plasmids varied across conditions depending on the expression system. After 12 h of induction, the msfGFP fluorescence in *P. putida* KT·BG42/pMCRi_*gfp*, (where *SpdCas9* expression is placed under control of XylS/ P_m) decreased by up to 90% compared with control *P. putida* KT·BG42 cells carrying an empty vector. When the ChnR/ P_{chnB} or CprK1/ P_{DB3} expression systems were used under the same culture and induction conditions, the msfGFP fluorescence decreased by 65% and 80% respectively (**Figure 3.4, B**).

In view of the results above, we concluded that the XylS/ P_m system outperformed the other expression systems for msfGFP depletion – thus we adopted this system for gene downregulation in further experiments. To analyse its tunability upon induction, we followed the msfGFP fluorescence levels of *P. putida* KT·BG42 cells carrying the corresponding CRISPRi vector in the presence of different concentrations of 3-*mBz*, ranging from 0 to 1 mM. Expectedly, the level of repression of *msf:gfp* expression increased as a function of the inducer concentration (hence resulting in a graded decrease in the fluorescence levels in the cells; **Figure 3.5, A**). In particular, by using various concentrations of 3-*mBz* (i.e. 0, 0.01, 0.1, 0.5 and 1 mM) we managed to decrease msfGFP fluorescence intensities up to 15%, 55%, 63%, 66% and 88%, respectively, after 15 h of incubation.

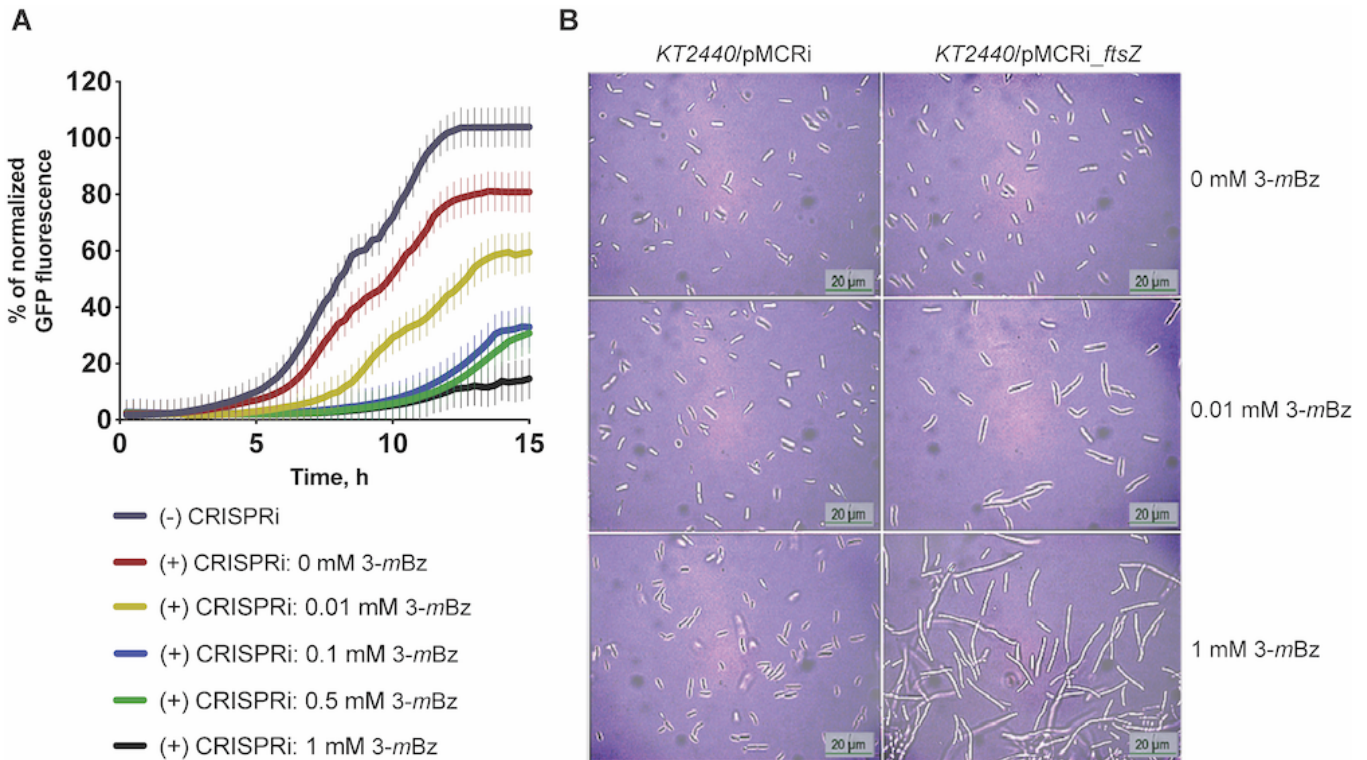


Figure 3.5. Tunable effect of the CRISPRi system in *P. putida* KT-BG42 cells harbouring plasmid pMCRi with different inducer concentrations.

A. Strain KT-BG42 cells transformed with plasmid pMCRi_{gfp}, harbouring the *msf::gfp*-specific spacer [indicated in the figure as (+) CRISPRi] or with vector pMCRi_{non-target} [harbouring a non-target-specific unique spacer, and indicated in the figure as (-) CRISPRi], were grown on M9 minimal medium with 0.2% (w/v) glucose, 100 $\mu\text{g ml}^{-1}$ streptomycin, 20 $\mu\text{g ml}^{-1}$ gentamicin and different concentrations of 3-methylbenzoate (3-mBz) in the 0 to 1 mM range. Bacterial growth and *msf*GFP fluorescence ($\lambda_{\text{excitation}}/\lambda_{\text{emission}} = 485 \text{ nm}/516 \text{ nm}$) were continuously measured during 15 h in a Synergy HI plate reader (BioTek Instruments, Inc., Winooski, VT, USA) using microtiter 96-well plates incubated at 30°C. Fluorescence readings were normalized to the bacterial growth (estimated as the optical density measured at 600 nm). Each data point represents the mean value of the percentage of normalized fluorescence \pm standard deviation from at least three biological replicates.

B. Microscope pictures showing tunable, inducer-dependent morphology changes of cells during CRISPRi-mediated downregulation of *ftsZ* in wild-type strain KT2440. Pictures were taken after 15 h with a Leica 2000 LED microscopy system (Leica Microsystems GmbH, Germany) at 100 \times resolution (F1 type emission oil)

In order to demonstrate how the system can be used to modify a physiological property of the cells, we also performed CRISPRi-mediated inhibition of the expression of *ftsZ* (*PP_1342*). This gene encodes the FtsZ protein that plays a key role in septum formation during bacterial cell division^{46,47}. Efficient repression of *ftsZ* leads to a filamentous cell phenotype^{17,48}. In this case, we showed that, contrary to other reported CRISPRi systems, the very low leakiness of the CRISPRi modules constructed in this study does not result in any visible repression effect in the absence of the inducer. Moreover, we found that gene repression strictly depends on the amount of the inducer (i.e. 3-*mBz*) added to the culture medium (**Figure 3.5, B**). Thus, the present approach is suitable for homogenous and tunable gene repression by adjusting the amounts of ^{Sp}dCas9 in the cell.

CRISPRi-mediated downregulation of multiple targets (mCRISPRi) in *P. putida*

The CRISPRi systems described above afford flexibility and modularity features that can be adapted depending on the intended application. We wanted to further extend the range of targets that can be suppressed following the same design principle (mCRISPRi, multiplex CRISPRi). To this end, and in order to express more than one gRNA from a single plasmid, we constructed and adopted two approaches: (i) a CRISPRi system equipped with several sgRNAs under control of individual P_{EM7} promoters, or (ii) a system harbouring the native crRNA cassette with multiple spacers (**Figure 3.6, A**). The detailed structure of the constructs was described in the previous sections.

To perform mCRISPRi, we first constructed *P. putida* KT-YFP-mCherry, harbouring constitutively expressed *yfp* and *mCherry* genes – encoding yellow fluorescent protein (YFP) and red fluorescent protein (mCherry), respectively – and a kanamycin resistance marker integrated into the Tn7 locus of the chromosome (**Table S3.1** in the Supporting Information).

The design and construction of the strain *P. putida* KT ·YFP mCherry was done essentially according to Wirth *et al.*¹⁴

P. putida KT ·YFP mCherry is a derivative of wild-type strain KT2440 carrying a $P_{100} \rightarrow mCherry$ and $P_{tet} \rightarrow yfp$ cassette integrated in the Tn7 locus *via* a synthetic mini-Tn7 transposon. As such, this strain displays constitutive expression of the two fluorescent protein genes driven by the P_{100} and P_{tet} promoters. We first assessed repression of either *yfp* or *mCherry* expression.

P. putida KT2440 ·YFP mCherry harbouring the empty pGCRi vector was used as a control was grown on M9 minimal medium supplemented with 0.2% (w/v) glucose and streptomycin ($100 \mu\text{g ml}^{-1}$). *P. putida* KT2440 ·YFP mCherry harbouring pGCRi_*yfp* or pMCRi_*mCherry* was grown under the same conditions. The cultures were supplemented with 1 mM 3-mBz to induce the XylS/ P_m expression system. In this case, downregulation of single-gene targets (*yfp*, *mCherry*) resulted in repression up to 65-68 % (**Figure S3.1, A** in the Supporting Information).

Furthermore, and in order to simultaneously downregulate the expression of *yfp*, *mCherry* and *ftsZ* (which, as indicated above, affects cell division and thereby results in a filamentous phenotype), *P. putida* KT ·YFP mCherry cells were first transformed with constructs harbouring multiple target-specific spacers (i.e. plasmids pCRiMs and pCRiMc, **Figure 3.6, A**). Both systems exhibited similar efficiency in repressing the chosen targets (an expected result, considering that the spacer sequences in plasmids pCRiMs_*yfp/mCherry/ftsZ* and pCRiMc_*yfp/mCherry/ftsZ* were the same; **Table S3.2** in the Supporting Information). Specifically, after 15 h of cultivation, the relative fluorescence was reduced by 55%–65% for mCherry and by 55%–60% for YFP (**Figure 3.6, B**).

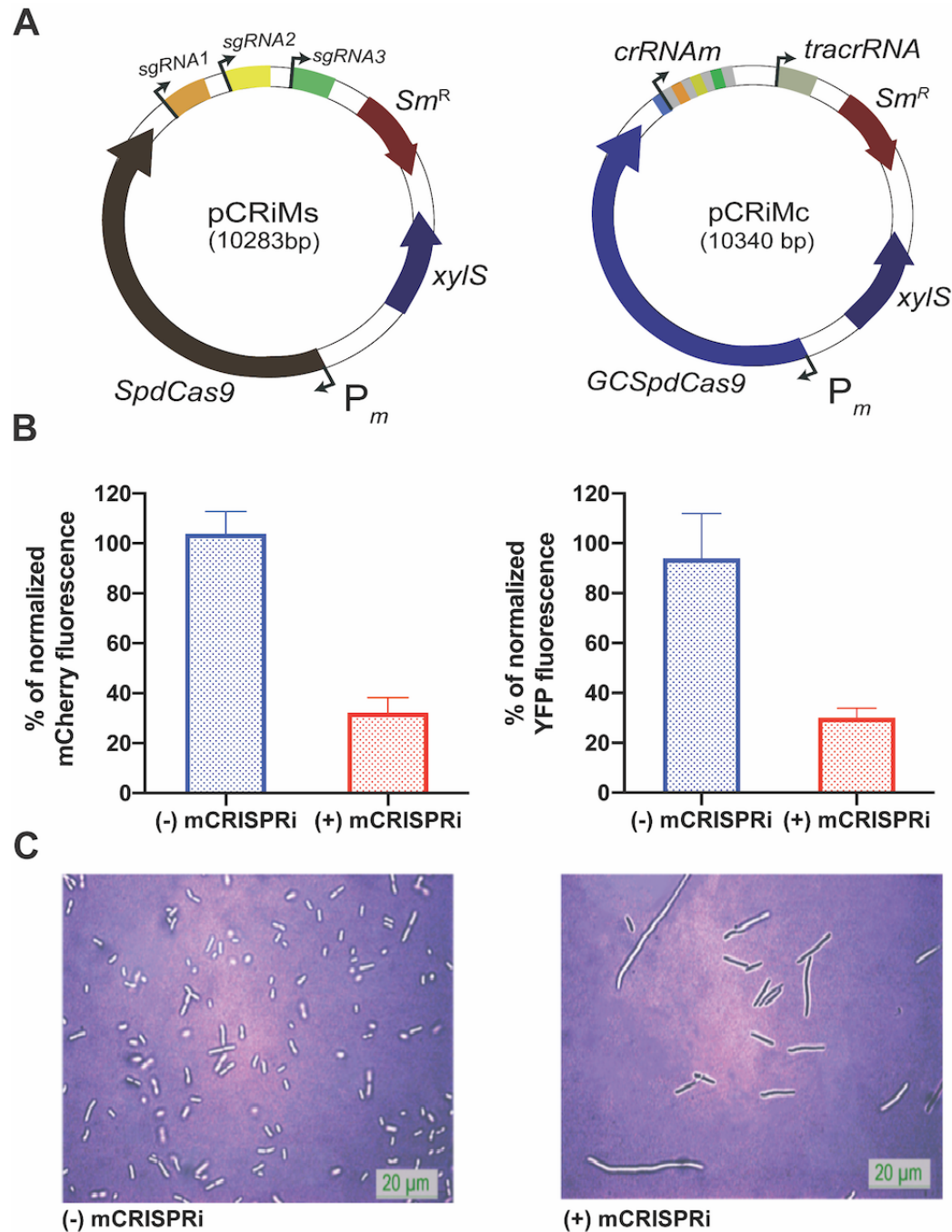


Figure 3.6. CRISPRi-mediated downregulation of multiple gene targets (mCRISPRi) in *P. putida* KT-YFP-mCherry. For simultaneous repression of the expression of *mCherry*, *yfp* and *ftsZ*, cells containing the corresponding CRISPRi vector were grown in M9 minimal medium with 0.2% (w/v) glucose, supplemented with 100 $\mu\text{g ml}^{-1}$ streptomycin, 50 $\mu\text{g ml}^{-1}$ kanamycin and induced with 3-methylbenzoate at 1 mM. In the figure, (-) mCRISPRi represents cells harbouring a non-target-specific pMCRi vector, and (+) mCRISPRi represents cells containing pCRiMs vector.

A. Schematic representation of vectors pCRiMs and pCRiMc, harbouring multiple target-specific spacers.

B. Bacterial growth, Cherry fluorescence ($\lambda_{\text{excitation}}/\lambda_{\text{emission}} = 567 \text{ nm}/610 \text{ nm}$) and YFP fluorescence ($\lambda_{\text{excitation}}/\lambda_{\text{emission}} = 495 \text{ nm}/527 \text{ nm}$) were measured at 15 h in a Synergy HI plate reader (BioTek Instruments, Inc., Winooski, VT, USA) using microtiter 96-well plates incubated at 30°C. Fluorescence readings were normalized to the bacterial growth (estimated as the optical density measured at 600 nm). Basal levels of fluorescence detected in *P. putida* KT2440 were also subtracted from the reading. Each bar represents the mean value of the percentage of normalized fluorescence \pm standard deviation from at least three biological replicates.

C. Microscope pictures showing morphology changes of cells during mCRISPRi-mediated downregulation of *ftsZ* in wild-type strain KT2440 after 15 h. Pictures were taken with a Leica 2000 LED microscopy system (Leica Microsystems GmbH, Germany) at 100 \times resolution (F1 type emission oil)

Note that, according to the measurement of fluorescence levels, the repression of the target gene in the absence of the specific spacer was fairly comparable for the two CRISPRi systems. Targeting of *ftsZ* with mCRISPRi resulted in cell morphology changes (detectable under light microscopy), with a significant shift in the cell size from ca. 5 μm rods to filament-like shaped cells with a length up to 60 μm (**Figure 3.6, C**). Importantly, repression levels remained within the same range (i.e. around 60%) during multiple or single-gene targeting with CRISPRi (pCRiMc_*yfp*/mCherry/*ftsZ* or pGCRi_*yfp*, respectively; see **Figure S1, B** in the Supporting Information). Thus, the single-plasmid mCRISPRi system developed here allows for regulatable downregulation of several genes of interest, which was demonstrated by simultaneous repression of three genes in *P. putida*.

Characterization of the RecA-dependent genetic stability of the system using CRISPRi-mediated downregulation of *pyrF*

Several teams have employed CRISPRi-based technologies to arrest cell growth by targeting essential chromosomal loci. In particular, CRISPRi has been successfully deployed in engineered bacteria to redirect carbon fluxes from cell growth to production⁴⁹⁻⁵², thereby enhancing yields and titres of target compounds. CRISPRi approaches have also been implemented for high-throughput functional characterization of putative essential genes in bacterial platforms such as *Bacillus subtilis*⁵³, *Streptococcus pneumoniae*⁵⁴ and *Vibrio natriegens*⁵⁵. However, it has been shown that long-term repression of essential loci often results in accumulation of deleterious mutations in *dCas9* and/or the gRNAs (or regulatory elements thereof), eventually resulting in their inactivation⁵⁶.

In order to characterize the stability and long-term efficiency of gene repression mediated by our CRISPRi system in *P. putida*, we downregulated the expression of *pyrF* (*PP_1815*), encoding the key orotidine 5'-phosphate decarboxylase reaction within the pyrimidine biosynthetic pathway. Following the protocol described above, we implemented the *pyrF*-specific CRISPRi vectors pGCRi_*pyrF* and pMCRi_*pyrF* (**Table 3.2**). As expected, downregulation of *pyrF* led to significantly low growth rates when the cells were grown in M9 minimal medium with glucose as the only carbon source (**Table 3.2**). In particular, and during the first 10 h of cultivation, the growth of *P. putida* KT2440 cells harbouring target-specific pCRi_*pyrF* vectors was repressed up to 90% (**Figure 3.7**). After 10 h, however, bacterial growth resumed, a phenomenon which could be accounted for by the accumulation of mutations in key elements of the CRISPRi system – probably including homologous recombination between the two DRs of the crRNA module and further overgrowth of escapers cells in which the expression of *pyrF* is no longer repressed.

Table 3.2. Growth characterization of wild-type *P. putida* KT2440 and the streamlined strain EM383 upon CRISPRi-mediated downregulation of *pyrF* expression

<i>P. putida</i> strain	Growth parameter	
	Specific growth rate ^a (h ⁻¹)	Final optical density ^b
KT2440	0.27 ± 0.08	1.78 ± 0.09
EM383	0.33 ± 0.05	1.78 ± 0.08
KT2440/pGCRi_no target	0.19 ± 0.02	2.59 ± 0.03
EM383/pGCRi_no target	0.12 ± 0.01	2.32 ± 0.18
KT2440/pGCRi_ <i>pyrF</i>	N.D.	1.05 ± 0.27
EM383/pGCRi_ <i>pyrF</i>	N.D.	0.42 ± 0.05
KT2440/pMCRi_no target	0.24 ± 0.02	1.75 ± 0.09
EM383/pMCRi_no target	0.28 ± 0.07	1.73 ± 0.09
KT2440/pMCRi_ <i>pyrF</i>	N.D.	0.71 ± 0.07
EM383/pMCRi_ <i>pyrF</i>	N.D.	0.15 ± 0.09

^a The specific growth rate for each strain was calculated during exponential growth. Cultures were carried out in 96-well microtiter plates, and the optical density at 600 nm was measured every 15 min during 20 h using a Synergy HI Biotek microplate reader (BioTek Instruments, Inc., Winooski, VT, USA). Glucose was added as a carbon source to M9 minimal medium at 0.2% (w/v). Results represent the mean and standard deviation of two independent experiments. N.D., not detected.

^b The final optical density at 600 nm is reported for each strain after 20 h of incubation.

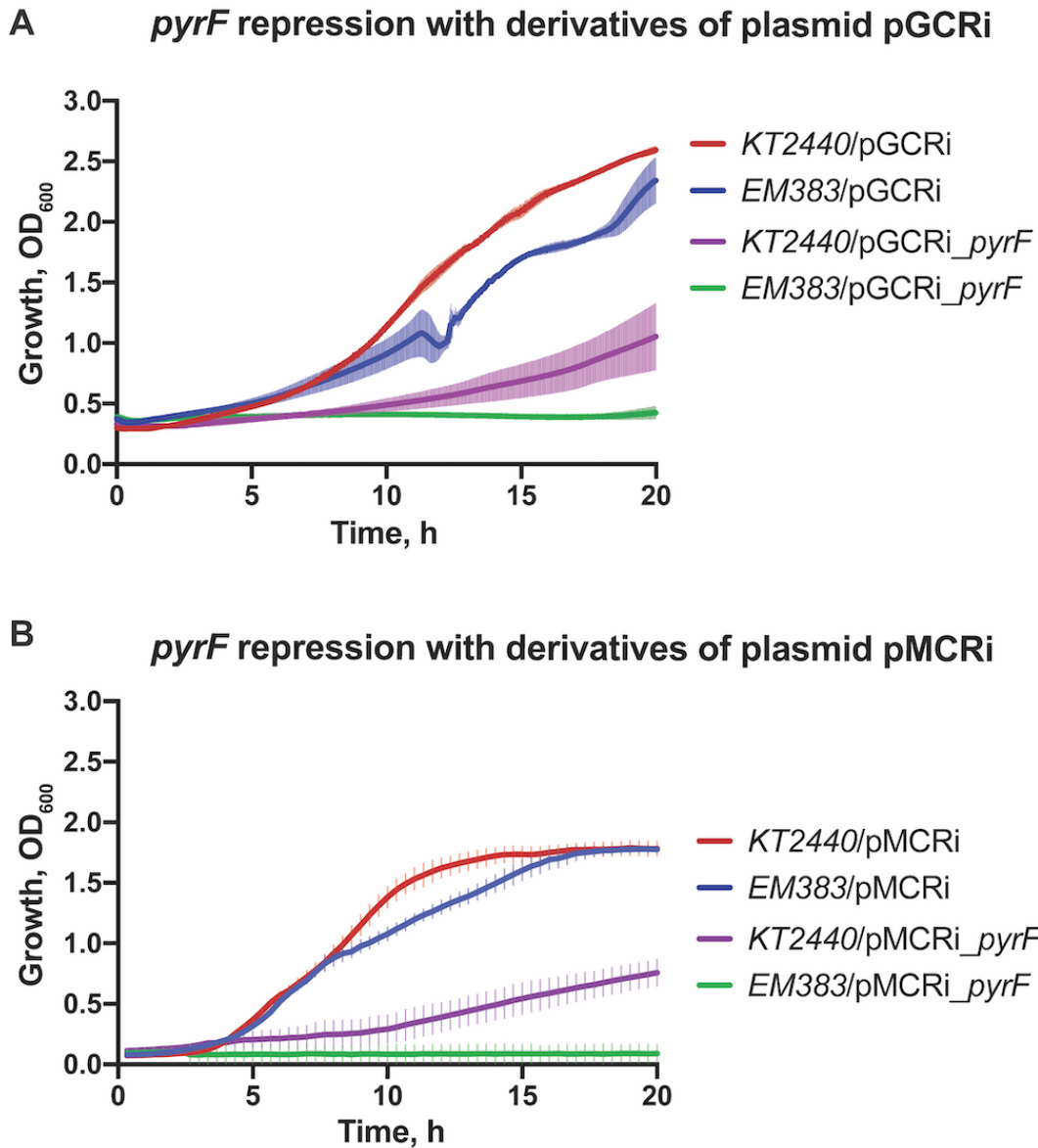


Figure 3.7. CRISPRi-based, targeted downregulation of *pyrF* expression in *P. putida*. Wild-type KT2440 and the streamlined *P. putida* strain EM383 were transformed with either non-target-specific vectors pGCRi or pMCRi, or the corresponding target-specific vectors (indicated with the suffix *pyrF*). The resulting strains were grown in 96-well plates in M9 minimal medium supplemented with 0.2% (w/v) glucose, 100 $\mu\text{g ml}^{-1}$ streptomycin and 1 mM 3-methylbenzoate. Bacterial growth was monitored in a Synergy HI plate reader (BioTek Instruments, Inc., Winooski, VT, USA) for 20 h at 30°C with shaking by periodically measuring the optical density at 600 nm (OD_{600}). Gene repression experiments are indicated for cells transformed with

A. plasmid pGCRi (no target and *pyrF*-specific) and **B.** plasmid pMCRi (no target and *pyrF*-specific). Each data point represents the mean value of OD_{600} readings \pm standard deviation of at least three biological replicates.

We further analyzed the sequence of the constructs in the *pyrF*-downregulated strains harvested at the end of the growth-inhibition experiments, and the results indicated that multiple modifications were accumulated in the constructs, including (i) recombination events between the two DRs of the crRNA cassette that led to the loss of the target spacer (which could be even noticed by PCR amplification of the cassette and separating the amplicons by gel electrophoresis, see **Figure S3.2** in the Supporting Information) and (ii) point mutations in the promoter sequence and/or the coding sequence of *GC^{Sp}Cas9* itself (data not shown).

To suppress these deleterious effects, and to further characterize the genetic stability of the target-specific CRISPRi system, we repeated the growth-inhibition experiment using *P. putida* strain EM383, a streamlined, reduced-genome strain derivative of KT2440 lacking several non-adjacent genomic deletions, including the whole flagellar machinery, four prophages, two transposons and three key components of DNA restriction-modification systems^{57,58}. This reduced-genome strain also lacks the gene encoding the main component of the homologous recombination machinery, *recA*, preventing any further recombination^{59,60}.

We reasoned that such strain would give rise to a limited fraction of escapers upon CRISPRi-mediated downregulation of essential genes. Indeed, the growth arrest in strain EM383, mediated by targeting the essential *pyrF* gene with CRISPRi, was extended from 10 to 20 h (**Figure 3.7, Table 3.2**). Moreover, wild-type strain KT2440, expressing either the crRNA or sgRNA module targeting *pyrF*, reached a 59% and 56% lower optical density after 20 h compared with the control experiments respectively. At the same time, strain EM383 harboring the same CRISPRi plasmids showed almost no growth after 20 h in contrast to the corresponding controls. These results indicate a clear role for RecA on the genetic stability of CRISPRi systems in *P. putida*, which can be circumvented by using strains in which the recombination machinery has been eliminated.

DISCUSSION

CRISPRi technologies have been widely applied for metabolic engineering and synthetic biology approaches in a range of eukaryotic and prokaryotic organisms. CRISPRi systems have been successfully optimized for a range of bacterial *chassis* including *E. coli*, *Bacillus subtilis* and *Corynebacterium glutamicum* 61-64.

In the present work, we aimed at improving the existing CRISPRi-based genome engineering toolbox for *P. putida*, implementing modularity, robustness and tunability towards the development of this bacterium as an effective, efficient, and controllable *chassis* for biotechnological applications. These features are separately discussed in the sections below.

Tunable gene regulation and multiplexing

Two variants of a single-plasmid CRISPRi system (either sgRNA-based or crRNA-based) were developed for the transcriptional control of gene expression in *P. putida*. Tight and tunable downregulation of gene expression was achieved through controlling the expression of *SpdCas9* with the XylS/ P_m system. Furthermore, the system displayed low leakiness – up to 15% (when downregulating the expression of *msf:gfp*, *mCherry* or *yfp*) or non-detectable (in the case of targeting *ftsZ*) under non-induced conditions. A linear response of downregulation levels of a chromosomally expressed *msf:gfp* was observed as a function of the inducer (3-*mBz*) concentration. This feature represents a substantial improvement to previously CRISPRi-based approaches, which did not allow for titratable gene downregulation¹⁸, sometimes exhibiting high leakiness (> 50%) in the absence of the corresponding inducers¹⁷. Importantly, we also demonstrated the ability to simultaneously downregulate three genes in *P. putida* with this system.

Inducible downregulation through CRISPRi enables conditional control of essential gene expression. Such an approach would be effective for controlling growth (e.g. to establish growth-decoupling switches for

bioproduction)⁶⁵ or for the assessment of fundamental questions in metabolism (e.g. related to gene essentiality)⁶⁶. As an example, we applied the versatile CRISPRi system described in this study to control the expression of the conditionally essential gene *pyrF*. The growth of *P. putida* strains harbouring either the sgRNA- or crRNA-based CRISPRi vectors was totally suppressed during the first 10 h in a minimal culture medium supplemented with glucose as sole carbon source. Additionally, we demonstrated a significant increase in the stability of the CRISPRi repression when essential genes are targeted in a strain devoid of the RecA machinery, which points to the importance of RecA-dependent mechanisms for stability of genetic constructs in *P. putida*⁶⁷. Therefore, the expanded, single-plasmid CRISPRi toolbox combines all the essential features desired for precise transcriptional control of single and multiple genes in *P. putida*.

Cloning, standardization, and modularity of CRISPRi components and portability

In addition to the examples illustrating the applicability of the tool, we also focused on improving cloning procedures and implementing standardization and modularity in the intervening components of the CRISPRi system. Two detailed protocols are provided for the construction of multiplex sgRNA and crRNA arrays. In general, the efficiency of using just sgRNA or both tracrRNA and crRNA was observed to be fairly comparable. The architecture of crRNA allows for a rapid and simple cloning strategy when generating multiplex crRNA arrays. In particular, the construction of multiplex gRNA arrays has been shown to be a laborious and time-consuming process, where often additional PCR or ligation steps are required. The genetic architecture of the sgRNA (promoter^{–SpCas9} handle^{–terminator}) limits the applicability of several assembly methods that rely on the ligation of homologous sequences – but it is particularly useful and straightforward when targeting a single or dual target(s) for downregulation. To tackle this problem, we constructed the crRNA-based CRISPRi vector (pGCRi), which enables the construction of the array with multiple spacers in a modular and directional single step with all elements in the array regulated by a master promoter. In addition, the pGCRi vector is equipped with the gene encoding an eforRed chromoprotein that gets inactivated if the

spacers are correctly integrated into the vector, simplifying, and accelerating the selection process. Therefore, vector pGCRi (and derivatives) is suitable for combinatorial, high-throughput genetic screenings where hundreds or thousands of CRISPRi plasmids need to be built⁶⁸. In terms of overall impact of the different CRISPRi systems presented herein on the cell physiology, we would recommend using plasmids containing *SpdCas9* due to limited effects on bacterial growth parameters as compared with *GC^{SpdCas9}*-bearing vectors.

In conclusion, the present study describes suitable strategies based on CRISPRi to efficiently control transcription levels in *P. putida* KT2440 while implementing modularity, standardization, and robustness. Along the line, low leakiness levels and tunable repression of single and multiple genes has been achieved, and detailed protocols for the construction of both sgRNA- and crRNA-based CRISPRi vectors are provided (which can be adapted at the user's will, depending on the intended application and its specific needs). Considering that all the components of the CRISPRi toolbox presented in this study follow the modular and standard formatting brought about by the SEVA platform, the vectors presented in this work can be transferred to other *Pseudomonas* species – and, essentially, to any other Gram-negative bacterium where an appropriate combination of antibiotic resistance markers and origin of replications from the SEVA collection can be used. Preliminary tests in *P. aeruginosa* PAO1 indicate that *SpdCas9*-based CRISPRi on genes encoding fluorescent proteins yield similar levels of repression as those reported herein (data not shown), which sheds a positive light on the system portability across species. As such, our study considerably expands the CRISPRi toolbox of *Pseudomonads* and opens new avenues for functional characterization of genes and advanced metabolic engineering.

Acknowledgements

We thank Prof. Víctor de Lorenzo and Dr. Esteban Martínez-García (CNB-CSIC, Madrid, Spain) for sharing research materials and for fruitful discussions. Funding was provided by European Union's *Horizon2020* Research and Innovation Programme under grant agreement Nos. 635536 (*EmPowerPutida*) and 730976 (*IBISBA*) to V.A.P.M.d.S. The financial support from The Novo Nordisk Foundation (NNF10CC1016517) and the European Union's *Horizon2020* Research and Innovation Programme under grant agreement No. 814418 (*SinFonia*) to P.I.N. is also gratefully acknowledged. E.K. is the recipient of a fellowship from the Novo Nordisk Foundation as part of the Copenhagen Bioscience Ph.D. Programme, supported through grant NNF17CC0026768.

References

- 1 Nelson, K. E. *et al.* Complete genome sequence and comparative analysis of the metabolically versatile *Pseudomonas putida* KT2440. *Environ Microbiol* **4**, 799-808, doi:10.1046/j.1462-2920.2002.00366.x (2002).
- 2 Poblete-Castro, I., Wittmann, C. & Nikel, P. I. Biochemistry, genetics and biotechnology of glycerol utilization in *Pseudomonas* species. *Microb Biotechnol* **13**, 32-53, doi:10.1111/1751-7915.13400 (2020).
- 3 Poblete-Castro, I., Becker, J., Dohnt, K., dos Santos, V. M. & Wittmann, C. Industrial biotechnology of *Pseudomonas putida* and related species. *Appl Microbiol Biotechnol* **93**, 2279-2290, doi:10.1007/s00253-012-3928-0 (2012).
- 4 Nikel, P. I., Martinez-Garcia, E. & de Lorenzo, V. Biotechnological domestication of pseudomonads using synthetic biology. *Nat Rev Microbiol* **12**, 368-379, doi:10.1038/nrmicro3253 (2014).
- 5 Nikel, P. I., Chavarria, M., Danchin, A. & de Lorenzo, V. From dirt to industrial applications: *Pseudomonas putida* as a Synthetic Biology chassis for hosting harsh biochemical reactions. *Curr Opin Chem Biol* **34**, 20-29, doi:10.1016/j.cbpa.2016.05.011 (2016).
- 6 Belda, E. *et al.* The revisited genome of *Pseudomonas putida* KT2440 enlightens its value as a robust metabolic chassis. *Environ Microbiol* **18**, 3403-3424, doi:10.1111/1462-2920.13230 (2016).
- 7 Nikel, P. I., Chavarria, M., Fuhrer, T., Sauer, U. & de Lorenzo, V. *Pseudomonas putida* KT2440 Strain Metabolizes Glucose through a Cycle Formed by Enzymes of the Entner-Doudoroff, Embden-Meyerhof-Parnas, and Pentose Phosphate Pathways. *J Biol Chem* **290**, 25920-25932, doi:10.1074/jbc.M115.687749 (2015).
- 8 Martinez-Garcia, E. & de Lorenzo, V. *Pseudomonas putida* in the quest of programmable chemistry. *Curr Opin Biotech* **59**, 111-121, doi:10.1016/j.copbio.2019.03.012 (2019).
- 9 Calero, P. & Nikel, P. I. Chasing bacterial chassis for metabolic engineering: a perspective review from classical to non-traditional microorganisms. *Microb Biotechnol* **12**, 98-124, doi:10.1111/1751-7915.13292 (2019).
- 10 Leprince, A., de Lorenzo, V., Voller, P., van Passel, M. W. & Martins dos Santos, V. A. Random and cyclical deletion of large DNA segments in the genome of *Pseudomonas putida*. *Environ Microbiol* **14**, 1444-1453, doi:10.1111/j.1462-2920.2012.02730.x (2012).

- 11 Martinez-Garcia, E. & de Lorenzo, V. Engineering multiple genomic deletions in Gram-negative bacteria: analysis of the multi-resistant antibiotic profile of *Pseudomonas putida* KT2440. *Environ Microbiol* **13**, 2702-2716, doi:10.1111/j.1462-2920.2011.02538.x (2011).
- 12 Mougiakos, I. *et al.* Characterizing a thermostable Cas9 for bacterial genome editing and silencing. *Nat Commun* **8**, 1647, doi:10.1038/s41467-017-01591-4 (2017).
- 13 Sun, J. *et al.* Genome editing and transcriptional repression in *Pseudomonas putida* KT2440 via the type II CRISPR system. *Microb Cell Fact* **17**, 41, doi:10.1186/s12934-018-0887-x (2018).
- 14 Wirth, N. T., Kozaeva, E. & Nikel, P. I. Accelerated genome engineering of *Pseudomonas putida* by I-SceI-mediated recombination and CRISPR-Cas9 counterselection. *Microb Biotechnol* **13**, 233-249, doi:10.1111/1751-7915.13396 (2020).
- 15 Aparicio, T., de Lorenzo, V. & Martinez-Garcia, E. CRISPR/Cas9-Based Counterselection Boosts Recombineering Efficiency in *Pseudomonas putida*. *Biotechnol J* **13**, e1700161, doi:10.1002/biot.201700161 (2018).
- 16 Aparicio, T., de Lorenzo, V. & Martinez-Garcia, E. CRISPR/Cas9-enhanced ssDNA recombineering for *Pseudomonas putida*. *Microb Biotechnol* **12**, 1076-1089, doi:10.1111/1751-7915.13453 (2019).
- 17 Tan, S. Z., Reisch, C. R. & Prather, K. L. J. A Robust CRISPR Interference Gene Repression System in *Pseudomonas*. *Journal of Bacteriology* **200**, doi:ARTN e00575-1710.1128/JB.00575-17 (2018).
- 18 Kim, S. K. *et al.* CRISPR interference-mediated gene regulation in *Pseudomonas putida* KT2440. *Microb Biotechnol* **13**, 210-221, doi:10.1111/1751-7915.13382 (2020).
- 19 Qu, J. *et al.* Modulating Pathogenesis with Mobile-CRISPRi. *J Bacteriol* **201**, doi:10.1128/JB.00304-19 (2019).
- 20 Peters, J. M. *et al.* Enabling genetic analysis of diverse bacteria with Mobile-CRISPRi. *Nat Microbiol* **4**, 244-250, doi:10.1038/s41564-018-0327-z (2019).
- 21 Noirot-Gros, M. F., Forrester, S., Malato, G., Larsen, P. E. & Noirot, P. CRISPR interference to interrogate genes that control biofilm formation in *Pseudomonas fluorescens*. *Sci Rep-Uk* **9**, doi:ARTN 1595410.1038/s41598-019-52400-5 (2019).
- 22 Cong, L. *et al.* Multiplex genome engineering using CRISPR/Cas systems. *Science* **339**, 819-823, doi:10.1126/science.1231143 (2013).
- 23 Jinek, M. *et al.* A programmable dual-RNA-guided DNA endonuclease in adaptive bacterial immunity. *Science* **337**, 816-821, doi:10.1126/science.1225829 (2012).

- 24 Zalatan, J. G. *et al.* Engineering complex synthetic transcriptional programs with CRISPR RNA scaffolds. *Cell* **160**, 339-350, doi:10.1016/j.cell.2014.11.052 (2015).
- 25 Deaner, M. & Alper, H. S. Systematic testing of enzyme perturbation sensitivities via graded dCas9 modulation in *Saccharomyces cerevisiae*. *Metabolic Engineering* **40**, 14-22, doi:10.1016/j.ymben.2017.01.012 (2017).
- 26 Rousset, F. *et al.* Genome-wide CRISPR-dCas9 screens in *E. coli* identify essential genes and phage host factors. *Plos Genetics* **14**, doi:ARTN e100774910.1371/journal.pgen.1007749 (2018).
- 27 Silva-Rocha, R. *et al.* The Standard European Vector Architecture (SEVA): a coherent platform for the analysis and deployment of complex prokaryotic phenotypes. *Nucleic Acids Res* **41**, D666-675, doi:10.1093/nar/gks1119 (2013).
- 28 Martinez-Garcia, E. *et al.* SEVA 3.0: an update of the Standard European Vector Architecture for enabling portability of genetic constructs among diverse bacterial hosts. *Nucleic Acids Res* **48**, D1164-D1170, doi:10.1093/nar/gkz1024 (2020).
- 29 Nikel, P. I., Perez-Pantoja, D. & de Lorenzo, V. Why are chlorinated pollutants so difficult to degrade aerobically? Redox stress limits 1,3-dichloroprop-1-ene metabolism by *Pseudomonas pavonaceae*. *Philos Trans R Soc Lond B Biol Sci* **368**, 20120377, doi:10.1098/rstb.2012.0377 (2013).
- 30 Zobel, S. *et al.* Tn7-Based Device for Calibrated Heterologous Gene Expression in *Pseudomonas putida*. *ACS Synth Biol* **4**, 1341-1351, doi:10.1021/acssynbio.5b00058 (2015).
- 31 Kemp, L. R., Dunstan, M. S., Fisher, K., Warwicker, J. & Leys, D. The transcriptional regulator CprK detects chlorination by combining direct and indirect readout mechanisms. *Philos T R Soc B* **368**, doi:ARTN 2012032310.1098/rstb.2012.0323 (2013).
- 32 Benedetti, I., Nikel, P. I. & de Lorenzo, V. Data on the standardization of a cyclohexanone-responsive expression system for Gram-negative bacteria. *Data Brief* **6**, 738-744, doi:10.1016/j.dib.2016.01.022 (2016).
- 33 Cobb, R. E., Wang, Y. & Zhao, H. High-efficiency multiplex genome editing of *Streptomyces* species using an engineered CRISPR/Cas system. *ACS Synth Biol* **4**, 723-728, doi:10.1021/sb500351f (2015).
- 34 Pul, U. *et al.* Identification and characterization of *E. coli* CRISPR-cas promoters and their silencing by H-NS. *Mol Microbiol* **75**, 1495-1512, doi:10.1111/j.1365-2958.2010.07073.x (2010).

- 35 Alieva, N. O. *et al.* Diversity and evolution of coral fluorescent proteins. *PLoS One* **3**, e2680, doi:10.1371/journal.pone.0002680 (2008).
- 36 Cong, L. *et al.* Multiplex Genome Engineering Using CRISPR/Cas Systems. *Science* **339**, 819-823, doi:10.1126/science.1231143 (2013).
- 37 Larson, M. H. *et al.* CRISPR interference (CRISPRi) for sequence-specific control of gene expression. *Nat Protoc* **8**, 2180-2196, doi:10.1038/nprot.2013.132 (2013).
- 38 Qi, L. S. *et al.* Repurposing CRISPR as an RNA-Guided Platform for Sequence-Specific Control of Gene Expression. *Cell* **152**, 1173-1183, doi:10.1016/j.cell.2013.02.022 (2013).
- 39 Ladunga, I. Finding Similar Nucleotide Sequences Using Network BLAST Searches. *Curr Protoc Bioinformatics* **58**, 3 3 1-3 3 25, doi:10.1002/cpbi.29 (2017).
- 40 Winsor, G. L. *et al.* Enhanced annotations and features for comparing thousands of *Pseudomonas* genomes in the *Pseudomonas* genome database. *Nucleic Acids Res* **44**, D646-653, doi:10.1093/nar/gkv1227 (2016).
- 41 Cavaleiro, A. M., Kim, S. H., Seppala, S., Nielsen, M. T. & Norholm, M. H. Accurate DNA Assembly and Genome Engineering with Optimized Uracil Excision Cloning. *ACS Synth Biol* **4**, 1042-1046, doi:10.1021/acssynbio.5b00113 (2015).
- 42 Genee, H. J. *et al.* Software-supported USER cloning strategies for site-directed mutagenesis and DNA assembly. *ACS Synth Biol* **4**, 342-349, doi:10.1021/sb500194z (2015).
- 43 Volke, D. C., Turlin, J., Mol, V. & Nikel, P. I. Physical decoupling of XylS/Pm regulatory elements and conditional proteolysis enable precise control of gene expression in *Pseudomonas putida*. *Microb Biotechnol* **13**, 222-232, doi:10.1111/1751-7915.13383 (2020).
- 44 Nikel, P. I. & de Lorenzo, V. Engineering an anaerobic metabolic regime in *Pseudomonas putida* KT2440 for the anoxic biodegradation of 1,3-dichloroprop-1-ene. *Metab Eng* **15**, 98-112, doi:10.1016/j.ymben.2012.09.006 (2013).
- 45 Nikel, P. I. & de Lorenzo, V. Robustness of *Pseudomonas putida* KT2440 as a host for ethanol biosynthesis. *N Biotechnol* **31**, 562-571, doi:10.1016/j.nbt.2014.02.006 (2014).
- 46 Rowlett, V. W. & Margolin, W. The Min system and other nucleoid-independent regulators of Z ring positioning. *Front Microbiol* **6**, 478, doi:10.3389/fmicb.2015.00478 (2015).
- 47 Stricker, J. & Erickson, H. P. In vivo characterization of *Escherichia coli* ftsZ mutants: Effects on Z-ring structure and function. *Journal of*

- Bacteriology* **185**, 4796-4805, doi:10.1128/Jb.185.16.4796-4805.2003 (2003).
- 48 Elhadi, D., Lv, L., Jiang, X. R., Wu, H. & Chen, G. Q. CRISPRi engineering E-coli for morphology diversification. *Metabolic Engineering* **38**, 358-369, doi:10.1016/j.ymben.2016.09.001 (2016).
- 49 Li, S. Y. *et al.* Enhanced protein and biochemical production using CRISPRi-based growth switches. *Metabolic Engineering* **38**, 274-284, doi:10.1016/j.ymben.2016.09.003 (2016).
- 50 Shabestary, K. *et al.* Targeted Repression of Essential Genes To Arrest Growth and Increase Carbon Partitioning and Biofuel Titrers in Cyanobacteria. *ACS Synth Biol* **7**, 1669-1675, doi:10.1021/acssynbio.8b00056 (2018).
- 51 Kent, R. & Dixon, N. Contemporary Tools for Regulating Gene Expression in Bacteria. *Trends in Biotechnology* **38**, 316-333, doi:10.1016/j.tibtech.2019.09.007 (2020).
- 52 Tian, T., Kang, J. W., Kang, A. & Lee, T. S. Redirecting Metabolic Flux via Combinatorial Multiplex CRISPRi-Mediated Repression for Isopentenol Production in Escherichia coli. *ACS Synth Biol* **8**, 391-402, doi:10.1021/acssynbio.8b00429 (2019).
- 53 Peters, J. M. *et al.* A Comprehensive, CRISPR-based Functional Analysis of Essential Genes in Bacteria. *Cell* **165**, 1493-1506, doi:10.1016/j.cell.2016.05.003 (2016).
- 54 Liu, X. *et al.* High-throughput CRISPRi phenotyping identifies new essential genes in Streptococcus pneumoniae. *Mol Syst Biol* **13**, doi:ARTN 93110.15252/msb.20167449 (2017).
- 55 Lee, H. H. *et al.* Functional genomics of the rapidly replicating bacterium *Vibrio natriegens* by CRISPRi. *Nat Microbiol* **4**, 1105-1113, doi:10.1038/s41564-019-0423-8 (2019).
- 56 Zhao, H. *et al.* Depletion of Undecaprenyl Pyrophosphate Phosphatases Disrupts Cell Envelope Biogenesis in *Bacillus subtilis*. *J Bacteriol* **198**, 2925-2935, doi:10.1128/JB.00507-16 (2016).
- 57 Martinez-Garcia, E., Aparicio, T., de Lorenzo, V. & Nikel, P. I. New transposon tools tailored for metabolic engineering of gram-negative microbial cell factories. *Front Bioeng Biotechnol* **2**, 46, doi:10.3389/fbioe.2014.00046 (2014).
- 58 Martinez-Garcia, E., Nikel, P. I., Chavarria, M. & de Lorenzo, V. The metabolic cost of flagellar motion in *Pseudomonas putida* KT2440. *Environ Microbiol* **16**, 291-303, doi:10.1111/1462-2920.12309 (2014).
- 59 Abella, M., Campoy, S., Erill, I., Rojo, F. & Barbe, J. Cohabitation of two different *lexA* regulons in *Pseudomonas putida*. *J Bacteriol* **189**, 8855-8862, doi:10.1128/JB.01213-07 (2007).

- 60 Akkaya, O., Nikel, P. I., Perez-Pantoja, D. & de Lorenzo, V. Evolving metabolism of 2,4-dinitrotoluene triggers SOS-independent diversification of host cells. *Environ Microbiol* **21**, 314-326, doi:10.1111/1462-2920.14459 (2019).
- 61 Jakociunas, T., Jensen, M. K. & Keasling, J. D. System-level perturbations of cell metabolism using CRISPR/Cas9. *Curr Opin Biotech* **46**, 134-140, doi:10.1016/j.copbio.2017.03.014 (2017).
- 62 Adli, M. The CRISPR tool kit for genome editing and beyond. *Nat Commun* **9**, 1911, doi:10.1038/s41467-018-04252-2 (2018).
- 63 Cho, S., Shin, J. & Cho, B. K. Applications of CRISPR/Cas System to Bacterial Metabolic Engineering. *Int J Mol Sci* **19**, doi:10.3390/ijms19041089 (2018).
- 64 Donohoue, P. D., Barrangou, R. & May, A. P. Advances in Industrial Biotechnology Using CRISPR-Cas Systems. *Trends in Biotechnology* **36**, 134-146, doi:10.1016/j.tibtech.2017.07.007 (2018).
- 65 Durante-Rodriguez, G., de Lorenzo, V. & Nikel, P. I. A Post-translational Metabolic Switch Enables Complete Decoupling of Bacterial Growth from Biopolymer Production in Engineered *Escherichia coli*. *ACS Synth Biol* **7**, 2686-2697, doi:10.1021/acssynbio.8b00345 (2018).
- 66 Poulsen, B. E. *et al.* Defining the core essential genome of *Pseudomonas aeruginosa*. *Proc Natl Acad Sci U S A* **116**, 10072-10080, doi:10.1073/pnas.1900570116 (2019).
- 67 Aparicio, T., de Lorenzo, V. & Martinez-Garcia, E. A Broad Host Range Plasmid-Based Roadmap for ssDNA-Based Recombineering in Gram-Negative Bacteria. *Methods Mol Biol* **2075**, 383-398, doi:10.1007/978-1-4939-9877-7_27 (2020).
- 68 Reis, A. C. *et al.* Simultaneous repression of multiple bacterial genes using nonrepetitive extra-long sgRNA arrays. *Nature Biotechnology* **37**, 1294-+, doi:10.1038/s41587-019-0286-9 (2019).

Supporting Information

Table S3.1. Bacterial strains used in this work.

Strain	Relevant characteristics ^a	Source or reference
<i>Escherichia coli</i>		
DH5 α	Cloning host; <i>fhuA2 lac(Δ)UI169 phoA glnV44 Φ80' lacZ(Δ)M15 gyrA96 recA1 relA1 endA1 thi-1 hsdR17</i>	Taylor <i>et al.</i> (1993)
DH5 α λ pir	Cloning host; F ⁻ λ ⁻ <i>endA1 glnX44(AS) thiE1 recA1 relA1 spoT1 gyrA96(Nal^R) rfbC1 deoR nupG F80(lacZΔM15) Δ(argF-lac)UI169 hsdR17(<i>rK⁻ mK⁺</i>), λpir lysogen</i>	Hanahan <i>et al.</i> (1983)
<i>Pseudomonas putida</i>		
KT2440	Wild-type strain, derived from <i>P. putida</i> mt-2 (Worsey and Williams, 1975) cured of the TOL plasmid pWW0	Regenhardt <i>et al.</i> (2002)
KT-BG42	Derivative of strain KT2440 carrying a <i>P_{14g}(BCD2)→msfGFP</i> cassette integrated in the Tn7 locus, Gm ^R	Zobel <i>et al.</i> (2015)
KT-YFP mCherry	Derivative of strain KT2440 carrying a <i>P₁₀₀→mCherry</i> and <i>P_{tet}→yfp</i> cassette integrated in the Tn7 locus, Km ^R	This work
EM383	Reduced-genome derivative of strain KT2440 («cell factory»), Δ <i>recA</i>	Martínez-García <i>et al.</i> (2014)

^a Antibiotic markers: Nal, nalidixic acid; Km, kanamycin; and Gm, gentamicin.

Table S3.2. Oligonucleotides used in this work.

Name	Sequence (5'→3')	Description and use
<i>Oligonucleotides used for construction of the CRISPRi vectors</i>		
GC-dCas9-D10-F	agg tct cat gga caa gaa gta cag cat cgg cct ggc cat c	D10 point mutation of GC-rich <i>Cas9</i> and assembly with tracrRNA by Golden Gate cloning
GC-dCas9-H840A-R	ggt ctc agt cgt agt cgc tca gcc ggt tg	H840A point mutation of GC-rich <i>Cas9</i> by Golden Gate cloning
GC-dCas9-H840A-F	ggt ctc acg acg tcg acg cca tcg tgc cgc agt c	
GC-dCas9-R	ttg ggt ctc cgg act gca gcg gcc gct act agt att att agt cgc cgc cga gct g	Insertion of GC-rich <i>dCas9</i> into vector pSEVA621 by Golden Gate cloning
trRNA_Cas9pr-F	agg tct cag aat tcg cgg ccg ctt cta gag tca tcc tgt gga gct tag	Amplification of tracrRNA and the <i>SpCas9</i> native promoter to clone into vector pSEVA621
trRNA_Cas9pr-R	agg tct cac cat ttt tgc ctc cta aaa taa aaa g	
crRNA-F	agg tct cag aat tcg cgg ccg ctt cta gag aag att att tct taa taa cta aaa ata tg	Amplification of the crRNA cassette to clone into vector pSEVA231
crRNA-R	agg tct cag gac tgc agc ggc cgc tac tag taa act caa caa gtc tca g	
Xp-F	gga tga tttc tgg aat tcg cgg ccg gtc tct act aga	Amplification of the tracrRNA-GC-rich <i>SpdCas9</i> cassette for Golden Gate cloning
Pp-R	acc ttg ccc ttt ttt gcc ggt ctc gac tgc agc g	
Ep-F	agc ttt cgc taa gga tga ttt ctg gtc tcg gaa ttc gcg	Amplification of the crRNA cassette and eForRed transcription unit for Golden Gate cloning
Sp-R	ccc ttt ttt gcc gga ctg cag cgg ccg cta ggt ctc cta gta	
Pa-R	acc ttg ccc ttt ttt gcc ggt ctc aaa aag gtc tcg act gca gcg	Amplification of eForRed transcription unit for Golden Gate cloning

SEVA.GG-F	agg tct cgc agt ccg gca aaa aag ggc aag gtc ttg gac tcc tgt tga tag	Amplification of SEVA backbones for Golden Gate cloning
SEVA.GG-R	ggt ctc att cca gaa atc atc ctt agc gaa agc tct taa tta aag gca tca aat aaa acg	
pCRi.Cas9-F	tac tag aga aag agg aga aat act aga tgg aca aga agt aca gca tcg	Amplification of GC-rich <i>SpdCas9</i> for Gibson assembly
pCRi.Cas9-R	cca tat ttt tag tta tta aga aat aac aga aaa gcc cgc ctt tcg gcg ggc ttt gtt att agt cgc cgc cga gc	
pCRi.crRNA-F	tat ttc tta ata act aaa aat atg gta taa tac tc	Amplification of crRNA for Gibson assembly
pCRi.crRNA-R	cgg act gca gcg gcc gct act agt act ttt aaa aag tag ttt att ttg tta tc	
pCRi. <i>Pm</i> / <i>XylS</i> -F	ccg ctt cta gag tca agc cac ttcc tttt tgc att gac gc	Amplification of the <i>XylS/P_m</i> module for Gibson assembly
pCRi. <i>Pm</i> / <i>XylS</i> -R	cta gta ttt ctc ctc ttt ctc tag taa tta ttg ttt ctg ttg cat aaa gc	
pCRi.SEVA44-F	tac tag tag cgg ccg ctg	Amplification of the pSEVA441 vector backbone for Gibson assembly
pCRi.SEVA44-R	gga agt ggc ttg act cta gaa gcg gcc gcg	
U-sgRNA-F	aat taa utg ttg aca att aat cat cgg ca	Amplification of a <i>P_{EM7}→sgRNA</i> module with USER cloning for assembly of vector pMCRi (pCCRi, pDCRi)
U-sgRNA-R	aat tat ugg gat ccc cgg gta ccg a	
U-SpdCas9-F	agg ccg cgg uta gga gga aaa aca tat gga taa	Amplification of <i>SpdCas9</i> with USER cloning for assembly of vector pMCRi (pCCRi, pDCRi)
U- SpdCas9-R	att aat uaa agg gac ccc tgg att ctc	
U-448(11,12)-F	aat aat uac gat tta cgt att taa atg aac c	Template amplification for pSEVA448 (pSEVA4411, pSEVA4412) with USER cloning for assembly of vector pMCRi (pCCRi, pDCRi)
U-448-R	acc gcg gcc uag gca tgg tca tga ctc c	
U-4411(12)-R	acc gcg gcc uag gat tag aca tgt ga	
sgRNA	gag acc cga gac tgg tct cag ttt tag agc tag aaa tag caa gtt aaa ata agg cta gtc	sgRNA sequence (20-nt spacer, 42-nt dCas9 handle, 40-nt Sp terminator)

cgt tat caa ctt gaa aaa gtg gca ccg agt
cgg tgc

Name	Sequence (5'→3')	Description and use
<i>Oligonucleotides used for spacer cloning</i>		
CB. <i>yfp</i> -F	agg tct caa aac tag tag tgc tca gta tct cta tca ctg ata gtt ttt gag acc a	Construction of plasmid pGCRi_ <i>yfp</i>
CB. <i>yfp</i> -R	tgg tct caa aaa cta tca gtg ata gag ata ctg agc act act agt ttt gag acc t	
CB. <i>pyrF</i> -F	agg tct caa aac tca cgg gta ggg aaa tcc agg gcg acg atc gtt ttt gag acc a	Construction of plasmid pGCRi_ <i>pyrF</i>
CB. <i>pyrF</i> -R	tgg tct caa aaa cga tcg tcg ccc tgg att tcc cta ccc gtg agt ttt gag acc t	
CB.Triple. <i>yfp</i> -F	agg tct caa aac tag tag tgc tca gta tct cta tca ctg ata gtt tta aga gac ca	Construction of plasmid(s) pCRiMc
CB.Triple. <i>yfp</i> -R	tgg tct ctt aaa act atc agtg ata gag ata ctg agc act act agt ttt gag acc t	
CB.Triple.DR2-F	agg tct cgt tta gag cta tgc tgt ttt gaa tgg tcc caa acg aga cca	
CB.Triple.DR2-R	tgg tct cgt ttg gga cca ttc aaa aca gca tag ctc taa acg aga cct	
CB.Triple.mCh-F	agg tct cac aaa acc ctc ttt ctc tag tag cta gca ctg tac ctg ttt tag tga gac ca	
CB.Triple.mCh-R	tgg tct cac taa aac agg tac agt gct agc tac tag aga aag agg gtt ttg tga gac ct	
CB.Triple.DR3-F	agg tct cg tta gag cta tgc tgt ttt gaa tgg tcc caa cga gac ca	
CB.Triple.DR3-R	tgg tct cgt tgg gac cat tca aaa cag cat agc tct aac gag acc t	
CB.Triple. <i>ftsZ</i> -F	agg tct cac caa aac tag gcg caa caa cta gag aac tgt aag gag gtt ttt gag acc a	
CB.Triple. <i>ftsZ</i> -R	tgg tct caa aaa cct cct tac agt tct cta gtt gtt gcg cct agt ttt ggt gag acc t	

CB.non_target-F	agg tct caa aac tga gac cag tct cgg aag ctc aaa ggt ctc ggt ttt tga gac ca	Construction of plasmid pGCRi
CB.non_target-R	tgg tct caa aaa ccg aga cct ttg agc ttc cga gac tgg tct cag ttt tga gac ct	
EK.yfp-F	gcg cgg acc agg atg ggc acc acc c	Construction of plasmid(s) pMCRi_yfp, pCRiMs
EK.yfp-R	aaa cgg gtg gtg ccc atc ctg gtc c	
EK.pyrF-F	gcg cgg gaa atc cag ggc gac gat c	Construction of plasmid pMCRi_pyrF
EK.pyrF-R	aaa cga tcg tcg ccc tgg att tcc c	
EK.ftsZ-F	gcg cgc ttt aat gac cgg act ttg c	Construction of plasmid(s) pMCRi_ftsZ, pCRiMs
EK.ftsZ-R	aaa cgc aaa gtc cgg tca tta aag c	
EK.gfp-F	gcg cga acc agg atc gga aca aca	Construction of plasmid(s) pM(C,D)CRi_gfp
EK.gfp-R	aaa cgt gtt gtt ccg atc ctg gtt	
EK.non_target-F	gcg cgg aga ccc gag act ggt ctc a	Construction of plasmid(s) pM(C,D)CRi
EK.non_target-R	aaa ctg aga cca gtc tcg ggt ctc c	
EK.SEVA_T0-F	act agt ctt gga ctc ctg ttg a	Sequencing of constructs for spacer verification
EK.pCRi-U-F	atg caa caa uaa tta cga ttt acg tat tta aat g	pCRi-template amplification for pCRiMs assembly
EK.pCRi-U-R	agc tcg aau tgg gac ccc tgg att ctc a	
EK.sgRNA-F	att cga gcu cgg tat tgt tga caa tta atc atc	sgRNA amplification for pCRiMs assembly
EK.sgRNA-R	att gtt gca ugc ctg cac cga ctc ggt g	

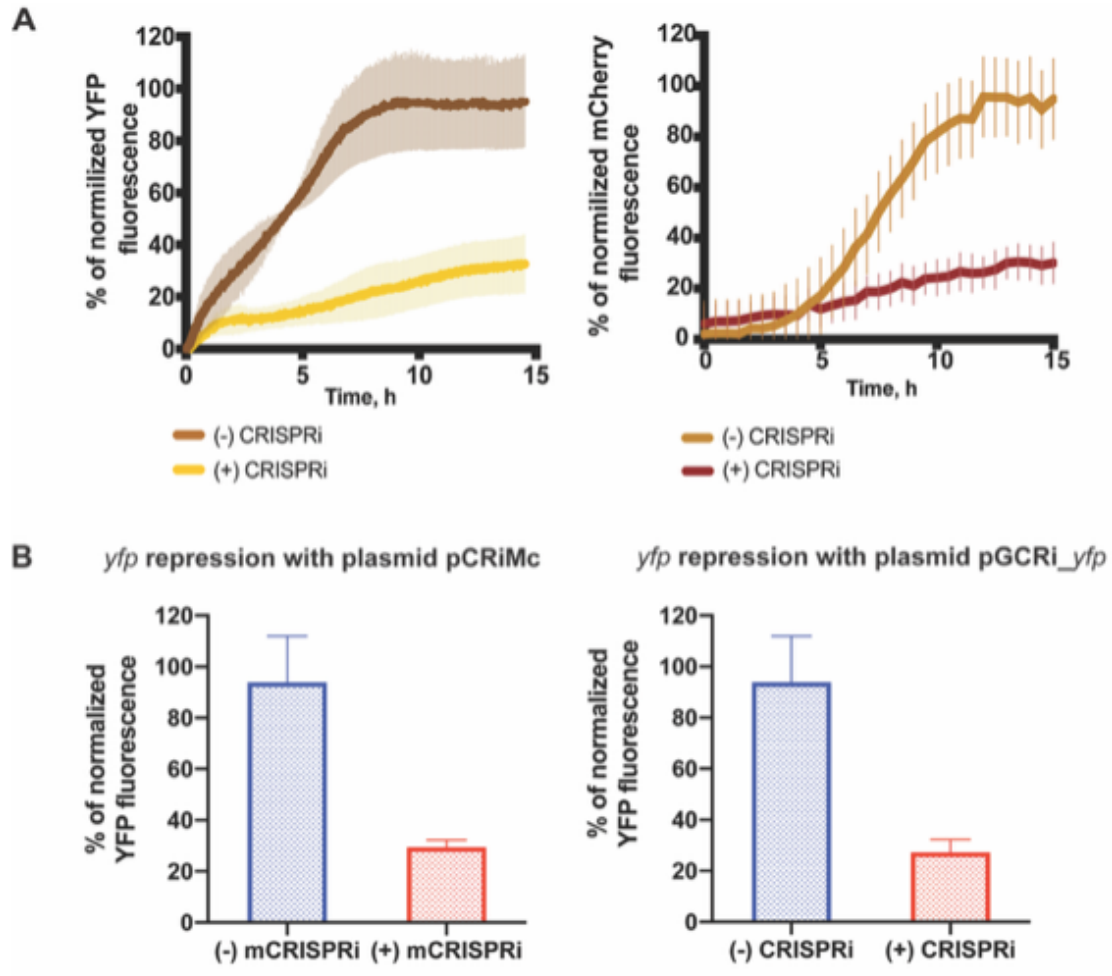


Figure S3.1. A. Down-regulation of the single target (*yfp*) and (*mcherry*) with CRISPRi, using vector pGCRi_yfp. *P. putida* KT2440-YFP-mCherry harbouring empty pGCRi vector was used as a control [indicated as (-) CRISPRi], and grown on M9 minimal medium supplemented with 2% (w/v) glucose and streptomycin (100 $\mu\text{g ml}^{-1}$). The *P. putida* KT2440-YFP-mCherry, harbouring pGCRi_yfp, was grown on M9 minimal medium supplemented with 2% (w/v) glucose, streptomycin (100 $\mu\text{g ml}^{-1}$) and 1 mM of the 3-MBz [indicated as (+) CRISPRi]. The YFP fluorescence ($\lambda_{\text{excitation}}/\lambda_{\text{emission}} = 490 \text{ nm}/510 \text{ nm}$) was measured with a Synergy H1 plate reader using microtiter 96-well plate in a continuous manner during 15 h at 30°C with shaking. **B.** Comparison in repression efficiency using several (pCRiMc) or one (pGCRi_yfp) gRNAs. The percentage of YFP fluorescence, normalized to the basal fluorescence of the control *P. putida* KT2440 strain. Each bar represents the mean value of normalized fluorescence \pm standard deviation of at least 3 biological replicates.

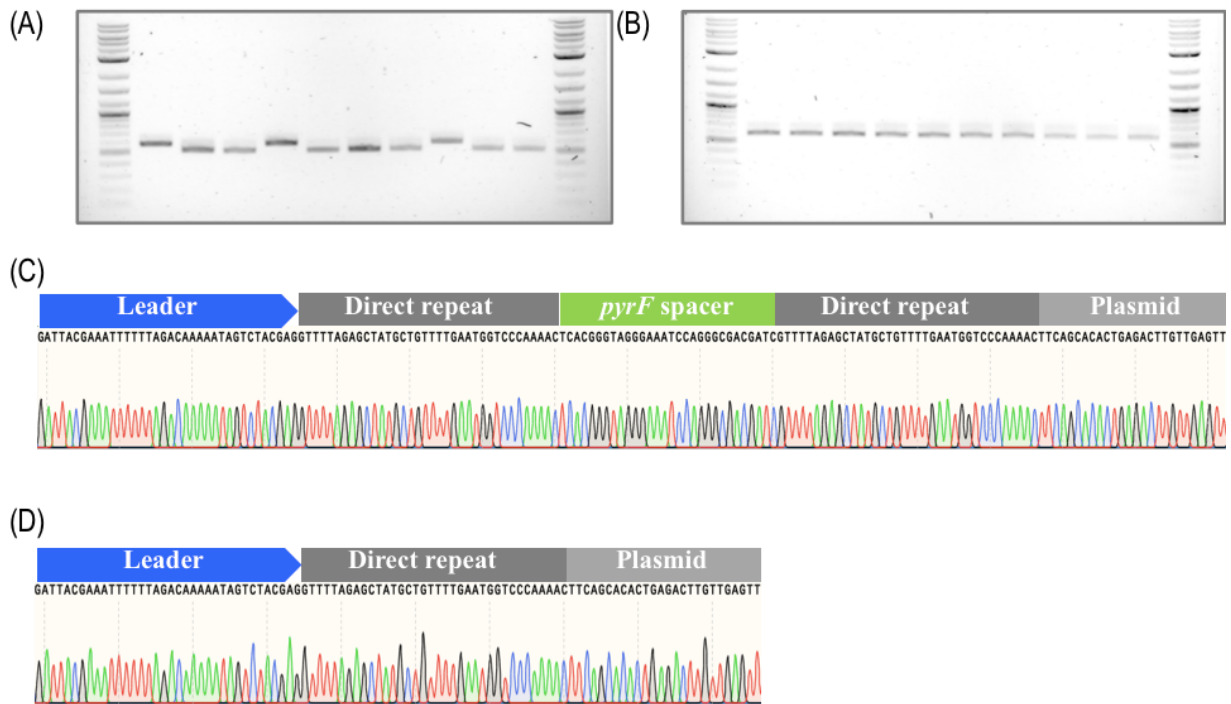


Figure S3.2. Recombination event between the two direct repeats of crRNA that led to the loss of the target spacer.

- A.** Colony PCR on strain KT2440 after repression of *pyrF* gene for 20 h.
- B.** Colony PCR on strain EM383 after repression of *pyrF* gene for 20h.
- C.** Extracted plasmid from strain EM383 harboring *pyrF* spacer.
- D.** Extracted plasmid from strain KT2440 with *pyrF* spacer.

Chapter 4

THE pABLO·pCASSO SELF-CURING VECTOR TOOLSET FOR UNCONSTRAINED CRISPR-SpRY CYTIDINE AND ADENINE BASE-EDITING IN NON-TRADITIONAL BACTERIAL HOSTS

Ekaterina Kozaeva¹, Zacharias S. Nielsen¹ and Pablo I. Nikel^{1*}.

1. The Novo Nordisk Foundation Center for Biosustainability, Technical University of Denmark, 2800 Kgs. Lyngby, Denmark

* Correspondence to:

Pablo I. Nikel
(pabnik@biosustain.dtu.dk)
The Novo Nordisk Foundation
Center for Biosustainability
Technical University of Denmark
Kgs Lyngby 2800, Denmark
Tel: (+45) 93 51 19 18

INTRODUCTION

Genome editing has revolutionized life sciences. Recently, a lot of attention has been focused on base editing assisted with Clustered Regularly Interspaced Short Palindromic Repeats and associated proteins (CRISPR-Cas), which allow introduction of target genomic sites without relying on homologous recombination ¹. Such DNA engineering relies on synthetic editing modules, and the common ones represent cytidine base editor (CBE) resulting in a cytidine C → thymidine T (or guanine G → adenine A) substitution and adenine base editor (ABE) enabling A → G (or T → C) base editing ². CBE typically carries a cytidine deaminase fused to Cas nickase and uracil glycosylase inhibitor ³, and ABE consists from an evolved adenine deaminase, capable of recognizing ssDNA and a Cas nickase ⁴. For the base editing to be possible the presence of a protospacer adjacent motif (PAM) is required for binding of the nCas9 domain to the target sequence. Naturally occurring CRISPR enzymes recognize their targets with the help of guide RNAs, and this target recognition is constrained by a PAM sequence.

For example, the well-known *Streptococcus pyogenes* Cas9 (^{Sp}Cas9) requires target recognition of the NGG motif, where N can be A, C, G, or T. In the context of genome editing, the requirement to recognize PAM reduces CRISPR targeting resolution and leaves some genome sites inaccessible to editing. This results in limitation of target accessibility during strain engineering of the poor for GC genomic regions. To tackle this, DNA-binding CRISPR proteins were optimized for more flexible PAM availability and have a great potential for improved genome editing by making more DNA sites accessible. Fusing these proteins with base editors provides the opportunity of changing almost any base of choice.

This strategy is especially relevant for strain development, allowing cheap and fast genome engineering. For example, it allows integration of premature stop codons into the cognate reading frame, in such a way that CAG/CAA/CGA codons should be converted into TAG/TAA/TGA triplets, thereby inactivating the target protein function—and reversed to restore the original (coding) sequence.

In this work, we developed novel constructs for base-editing of the non-pathogenic soil bacterium *Pseudomonas putida*, a robust alternative host for bioproduction. We characterized different types of editors (CBE and ABE) using both canonical nCas9 and near PAM-less SpRY, observing editing efficiencies up to 95% for both types of editors. We have also created and optimized a set of induction-dependent, self-curing vectors showing conditional replication in the presence of inducer. Developed genome editing methods combined with efficient curing would greatly simplify the genetic manipulation in *Pseudomonas* species and accelerate a wide variety of investigations.

Materials and Methods

Bacterial strains, plasmids, and culture conditions

All bacterial strains and plasmids used in this study are listed in **Table 4.1**. *E. coli* and *P. putida* cultures were grown in lysogeny broth (LB) medium (10 g L⁻¹ tryptone, 5 g L⁻¹ yeast extract and 10 g L⁻¹ NaCl; solid culture media additionally contained 15 g L⁻¹ agar) at 37°C and 30°C, respectively. Streptomycin (Str) was added whenever needed at 100 µg mL⁻¹. Cultures were agitated at 200 rpm (MaxQ™ 8000 incubator; ThermoFisher Scientific, Waltham, MA, USA). The optical density measured at 600 nm (OD₆₀₀) was recorded in a Genesys 20 spectrophotometer (Thermo Fisher Scientific) to estimate bacterial growth. For preculture preparation, four colonies were picked from an LB plate and used to inoculate wells of a 96-deep well plate filled with 1 mL of LB supplemented with antibiotic(s). During the experiment, bacterial growth, mCherry fluorescence ($\lambda_{\text{excitation}}/\lambda_{\text{emission}} = 567 \text{ nm}/610 \text{ nm}$) and msfGFP fluorescence ($\lambda_{\text{excitation}}/\lambda_{\text{emission}} = 475 \text{ nm}/510 \text{ nm}$) were measured in a Synergy HI plate reader (BioTek Instruments, Inc., Winooski, VT, USA). All cultivations were performed in 96-well microtiter plates with F-bottom and a lid. Basal levels of fluorescence detected in *P. putida* KT2440 were subtracted from the reading. Growth kinetics were followed at OD₆₀₀ with light path correction

for physiological characterization of engineered strains and performed in a ELx808 plate reader (Buch and Holm A/S), constant shaking.

General cloning procedures and construction of plasmids

Oligonucleotides used in this work are listed in **Table S4.1** in the Supplementary Information. Unless stated otherwise, uracil-excision (*USER*) cloning ⁵ was used for the construction of all plasmids. The *AMUSER* tool was employed for designing oligonucleotides ⁶. Phusion™ *U* high-fidelity DNA polymerase (ThermoFisher Scientific) was used according to the manufacturer's specifications in amplifications intended for *USER* cloning. For colony PCR, the commercial *OneTaq*™ master mix (New England BioLabs, Ipswich, MA, USA) was used according to the supplier's instructions. *E. coli* DH5α λ *pir* (**Table 4.1.**) was employed as a host for general cloning purposes. Chemically-competent *E. coli* cells were prepared and transformed with plasmids using the *Mix and Go*™ commercial kit (Zymo Research, Irvin, CA, USA) according to the manufacturer's indications. Electrocompetent *P. putida* cells were prepared by washing the biomass from LB medium cultures with 300 mM sucrose, followed by transformation with plasmids by electroporation. The sequence of all used plasmids was verified by Mix2Seq sequencing (Eurofins Genomics, Ebersberg, Germany).

Editing events confirmation by Sanger sequencing

Eight to 24 primarily identified positive clones of each strain were picked, and inoculated into 5 mL LB broth with proper antibiotics. After overnight (~16 h) cultivation, cultures were subjected to plasmid isolation using the NucleoSpin® Plasmid EasyPure Kit (Macherey-Nagel, Germany) or colony PCR using Q5® High-Fidelity 2× Master Mix (New England Biolabs, USA) if a chromosomal region was targeted. The isolated plasmids and the cleaned PCR products were Sanger sequenced using the Mix2Seq kit (Eurofins Scientific, Luxembourg) with proper primers. The obtained sequence traces were analyzed and visualized using SnapGene (GSL Biotech, USA).

Table 4.1. Bacterial strains and plasmids used in this study.

Bacterial strain	Relevant characteristics^a	Reference or source
<i>Escherichia coli</i>		
DH5 α λ pir	Cloning host; F ⁻ λ^- <i>endA1 glnX44(AS) thiE1 recA1 relA1 spoT1 gyrA96(Nal^R) rfbC1 deoR nupG Φ80(lacZΔM15) Δ(argF-lac)U169 <i>hsdR17</i>(rK⁻ mK⁺), λpir lysogen</i>	7
<i>Pseudomonas putida</i>		
KT2440	Wild-type strain, derived from <i>P. putida</i> mt-2 ⁸ cured of the catabolic TOL plasmid pWW0	9
EM42	Reduced-genome derivative of strain KT2440; Δ prophage1 Δ prophage4 Δ prophage3 Δ prophage2 Δ Tn7 Δ endA-1 Δ endA-2 Δ hsdRMS Δ flagellum Δ Tn4652	10
SEM1.3	Derivative of strain EM42; Δ phaC1ZC2DFI (Δ PP_5003-PP_5008) Δ benABCD (Δ PP_3161-PP_3164)	11
Plasmid	Relevant characteristics^a	Reference or source
pMCRi	Plasmid for CRISPRi; <i>oriV</i> (pRO1600/ColE1), <i>xylS</i> (cured of <i>BsaI</i> -sites), <i>Pm</i> \rightarrow <i>dCas9^{Sp}</i> , <i>P_{EM7}</i> \rightarrow sgRNA; Sm ^R /Sp ^R	12
pEditA	Plasmid for adenine base editing; <i>oriV</i> (pRO1600/ColE1), <i>xylS</i> (cured of <i>BsaI</i> -sites), <i>Pm</i> \rightarrow <i>nCas9^{Sp}</i> , <i>P_{EM7}</i> \rightarrow non-specific sgRNA; Sm ^R /Sp ^R	This work

pEditA-RY	Plasmid for adenine base editing; <i>oriV</i> (pRO1600/ColE1), <i>xylS</i> (cured of <i>BsaI</i> -sites), <i>Pm</i> → <i>SpRY</i> , <i>P_{EM7}</i> →non-specific sgRNA; Sm ^R /Sp ^R	This work
pEditC	Plasmid for cytidine base editing; <i>oriV</i> (pRO1600/ColE1), <i>xylS</i> (cured of <i>BsaI</i> -sites), <i>Pm</i> → <i>nCas9^{Sp}</i> , <i>P_{EM7}</i> →non-specific sgRNA; Sm ^R /Sp ^R	This work
pEditC-RY	Plasmid for cytidine base editing; <i>oriV</i> (pRO1600/ColE1), <i>xylS</i> (cured of <i>BsaI</i> -sites), <i>Pm</i> → <i>SpRY</i> , <i>P_{EM7}</i> →non-specific sgRNA; Sm ^R /Sp ^R	This work
pEditC_Q47	Plasmid for cytidine editing of mCherry Q47 codon; <i>oriV</i> (pRO1600/ColE1), <i>xylS</i> (cured of <i>BsaI</i> -sites), <i>Pm</i> → <i>nCas9^{Sp}</i> , <i>P_{EM7}</i> → <i>mCherry</i> -specific sgRNA; Sm ^R /Sp ^R	This work
pEditC_W64	Plasmid for cytidine editing of codon encoding W63 in mCherry; <i>oriV</i> (pRO1600/ColE1), <i>xylS</i> (cured of <i>BsaI</i> -sites), <i>Pm</i> → <i>nCas9^{Sp}</i> , <i>P_{EM7}</i> → <i>mCherry</i> -specific sgRNA; Sm ^R /Sp ^R	This work
pEditC-RY_Q47	Plasmid for cytidine editing of codon encoding Q47 in mCherry; <i>oriV</i> (pRO1600/ColE1), <i>xylS</i> (cured of <i>BsaI</i> -sites), <i>Pm</i> → <i>SpRY</i> , <i>P_{EM7}</i> → <i>mCherry</i> -specific sgRNA; Sm ^R /Sp ^R	This work
pEditC-RY_W64	Plasmid for cytidine editing of codon encoding W63 in mCherry; <i>oriV</i> (pRO1600/ColE1), <i>xylS</i> (cured of <i>BsaI</i> -sites), <i>Pm</i> → <i>SpRY</i> , <i>P_{EM7}</i> → <i>mCherry</i> -specific sgRNA; Sm ^R /Sp ^R	This work

pEditA_M1-1	Plasmid for adenine base editing of codon encoding M1 in mCherry, PAM1; <i>oriV</i> (pRO1600/ColE1), <i>xylS</i> (cured of <i>BsaI</i> -sites), <i>Pm</i> → <i>nCas9^{Sp}</i> , <i>P_{EM7}</i> → <i>mCherry</i> -specific sgRNA; Sm ^R /Sp ^R	This work
pEditA_M1-2	Plasmid for adenine base editing of codon encoding M1 in mCherry, PAM2; <i>oriV</i> (pRO1600/ColE1), <i>xylS</i> (cured of <i>BsaI</i> -sites), <i>Pm</i> → <i>nCas9^{Sp}</i> , <i>P_{EM7}</i> → <i>mCherry</i> -specific sgRNA; Sm ^R /Sp ^R	This work
pEditA_M1-3	Plasmid for adenine base editing of codon encoding M1 in mCherry, PAM3; <i>oriV</i> (pRO1600/ColE1), <i>xylS</i> (cured of <i>BsaI</i> -sites), <i>Pm</i> → <i>nCas9^{Sp}</i> , <i>P_{EM7}</i> → <i>mCherry</i> -specific sgRNA; Sm ^R /Sp ^R	This work
pEditA-RY_M1-1	Plasmid for adenine base editing of codon encoding M1 in mCherry, PAM1; <i>oriV</i> (pRO1600/ColE1), <i>xylS</i> (cured of <i>BsaI</i> -sites), <i>Pm</i> → <i>SpRY</i> , <i>P_{EM7}</i> → <i>mCherry</i> -specific sgRNA; Sm ^R /Sp ^R	This work
pEditA-RY_M1-2	Plasmid for adenine base editing of codon encoding M1 in mCherry, PAM2; <i>oriV</i> (pRO1600/ColE1), <i>xylS</i> (cured of <i>BsaI</i> -sites), <i>Pm</i> → <i>SpRY</i> , <i>P_{EM7}</i> → <i>mCherry</i> -specific sgRNA; Sm ^R /Sp ^R	This work
pEditA-RY_M1-3	Plasmid for adenine base editing of codon encoding M1 in mCherry, PAM3; <i>oriV</i> (pRO1600/ColE1), <i>xylS</i> (cured of <i>BsaI</i> -sites), <i>Pm</i> → <i>SpRY</i> , <i>P_{EM7}</i> → <i>mCherry</i> -specific sgRNA; Sm ^R /Sp ^R	This work
pSEVA448	Expression vector; <i>oriV</i> (pRO1600/ColE1), <i>xylS</i> , <i>Pm</i> ; Sm ^R /Sp ^R	13

pS44i8HG	Conditionally-replicating derivative of vector pSEVA448, high-copy-number; <i>oriV</i> (pRO1600/ColE1), <i>xyIS</i> (cured of <i>BsaI</i> -sites), <i>Pm</i> → <i>repA</i> , <i>P_{14d}</i> → <i>msfGFP</i> ; Sm ^R /Sp ^R	This work
pS44i8MG	Conditionally-replicating derivative of vector pSEVA448, medium-copy-number; <i>oriV</i> (pRO1600/ColE1), <i>xyIS</i> (cured of <i>BsaI</i> -sites), <i>Pm</i> → <i>repA</i> , <i>P_{14d}</i> → <i>msfGFP</i> ; Sm ^R /Sp ^R	This work
pAblo	Conditionally-replicating plasmid for adenine base editing; <i>oriV</i> (pRO1600/ColE1), <i>xyIS</i> (cured of <i>BsaI</i> -sites), <i>Pm</i> → <i>SpRY</i> , <i>P_{EM7}</i> → <i>non-specific</i> sgRNA; Sm ^R /Sp ^R	This work
pCasso	Conditionally-replicating plasmid for cytidine base editing; <i>oriV</i> (pRO1600/ColE1), <i>xyIS</i> (cured of <i>BsaI</i> -sites), <i>Pm</i> → <i>SpRY</i> , <i>P_{EM7}</i> → <i>non-specific</i> sgRNA; Sm ^R /Sp ^R	This work
pAblo_Q47	Conditionally-replicating plasmid for adenine editing of mCherry Q47 codon; <i>oriV</i> (pRO1600/ColE1), <i>xyIS</i> (cured of <i>BsaI</i> -sites), <i>Pm</i> → <i>SpRY</i> , <i>P_{EM7}</i> → <i>mCherry-specific</i> sgRNA; Sm ^R /Sp ^R	This work
pCasso_Q47	Conditionally-replicating plasmid for cytidine editing of mCherry Q47 codon; <i>oriV</i> (pRO1600/ColE1), <i>xyIS</i> (cured of <i>BsaI</i> -sites), <i>Pm</i> → <i>SpRY</i> , <i>P_{EM7}</i> → <i>mCherry-specific</i> sgRNA; Sm ^R /Sp ^R	This work

^a Antibiotic markers: Sm, streptomycin; and Sp, spectinomycin.

Curing efficiency evaluation using a fluorescence-based counting assay

50 μL of the edited culture normalized to the same optical density (OD 0.5) for each strain was plated onto LB agar plates supplemented with 100 $\mu\text{g mL}^{-1}$ of Str antibiotic and 1 mM of inducer 3-mBz. All plates were covered by aluminium foil and incubated at 30 °C for 24 h. After cultivation, total colonies were counted by a Doc-It imaging station (Fisher Scientific, USA) with a trisection protocol. Non-fluorescent colonies in each zone of all three zones were further counted with and without a Blue-Light Transilluminator (Safe Imager 2.0, Thermo Fisher Scientific, USA). The editing efficiency was calculated as: the number of non-fluorescent colonies in each zone divided for the total number of visible colonies in the same zone.

Gene copy number analysis by qPCR

Copy number analysis was performed by qPCR on QuantStudio 5 Real-Time PCR System (Applied Biosystems). Expression levels of *aadA* gene, encoding adenylyltransferase and providing streptomycin resistance were defined and converted to the copy number of plasmids, carrying the indicated gene. Reference plasmid pSEVA448 was purified using NucleoSpin® Plasmid EasyPure Kit (Macherey-Nagel, Germany) according to manufacturer's instructions and diluted to 1-10 ng μL^{-1} to build calibration curve. *P. putida* cells were grown for 10h in 96-well plates upon reaching mid-exponential phase, afterwards samples were collected from each well, diluted with PBS buffer to contain 10^3 cells per sample and stored at -20°C. qPCR amplification was performed under the following conditions: 50°C for 2 min, 95°C for 10 min; 40 cycles: 95°C for 15 s, 60°C for 1 min, 72°C for 30 s. Each experiment included no template control (mixture of primers with water and mixture of primers with the reaction mix without plasmid), three technical replicates for each sample. Results were analysed in QuantStudio Design and Analysis software. A comparative Ct method was applied to calculate gene copy number by comparing $\Delta\Delta\text{Ct}$ values of analysed clones to $\Delta\Delta\text{Ct}$ values of calibration.

Flow cytometry analysis

Flow cytometry analysis was performed on the Miltenyi MACSQuant VYB, using medium mixing and fast running mode. 5000 - 10000 events were recorded for each well analyzed. Cells were gated for singlets in exponential phase, and events within the singlet gate were recorded for each well analyzed. Median fluorescence values of each triplicate (consisting of min. 5000 events) were calculated. FlowLogic software (Mentone VIC, Australia) was used for the analysis and data interpretation.

Data and statistical analysis

Study visualization and figures were created using Adobe Illustrator (San Jose, CA, USA). The graphs are generated by Prism 9 GraphPad software (San Diego, CA, USA). All the experiments reported were independently repeated at least three times with individual biological replicates (as indicated in the corresponding figure or table legend), and the mean value of the corresponding parameter \pm standard deviation is presented. Data analysis of the qPCR and flow cytometry data was assisted by R programming using RStudio, and customized flowCore R scripts¹⁴. Mean and standard deviation were exported to GraphPadPrism. When relevant, the level of significance of differences when comparing results was evaluated by ANOVA (Barlett's test, Prism 9, GraphPad software, San Diego, CA, USA) with a P value = 0.01.

Results and discussion

Cytidine and Adenine base-editors for nucleotide substitution in *P. putida*

The use of Cas9 variant without PAM restrictions had remained elusive until very recently: an evolved Cas9 nickase variant (SpRY) conferred nearly PAM-less genome editing in human cells¹⁵, plants¹⁶, and yeast¹⁷. To our knowledge, this variant was not tested so far in bacterial cells thus far. In this work, we implemented SpRY-based toolbox to push the PAM restriction boundaries in bacterial genome engineering. Compared to wild-type Cas9, SpRY contains 11 amino acid changes¹⁵ (**Figure S4.1**). As reported, SpRY remain similarly efficient with canonical NGG PAM, and additionally allows other PAMs with preference to edit NR (R = A, G) PAM sites over than NY (Y = C, T) sites¹⁵, making it an attractive template for base-editing tool-box.

We adapted two types of molecular machines for DNA engineering: cytidine base editor (CBE), which allows cytidine (C•G) to thymine (T•A) substitutions (**Figure 4.1, A**), and adenine base editor (ABE), which converts adenine (A•T) to guanine (G•C), (**Figure 4.1, B**). CBE typically has three components²: a cytidine deaminase (APOBEC1), fused to catalytically impaired Cas nickase and two copies of uracil glycosylase inhibitor (2UGI), which efficiently inhibit counterproductive DNA repair processes³. ABE is comprised of two components: an evolved adenine deaminase, *Escherichia coli* tRNA^{ARG}-modifying enzyme, TadA, capable of recognizing single-stranded DNA (ssDNA) and a Cas nickase⁴. To avoid ABEs limitations of the narrow editing window and general lower efficiencies, we chose ABE8.20-m, a recently evolved adenine base editor of the ABE_{max}8 generation (ABE_{max}, **Figure 4.1, B**). This ABE was demonstrated to display increased activity, improved Cas compatibility, broadened editing window and it is deemed suitable for therapeutic application¹⁸.

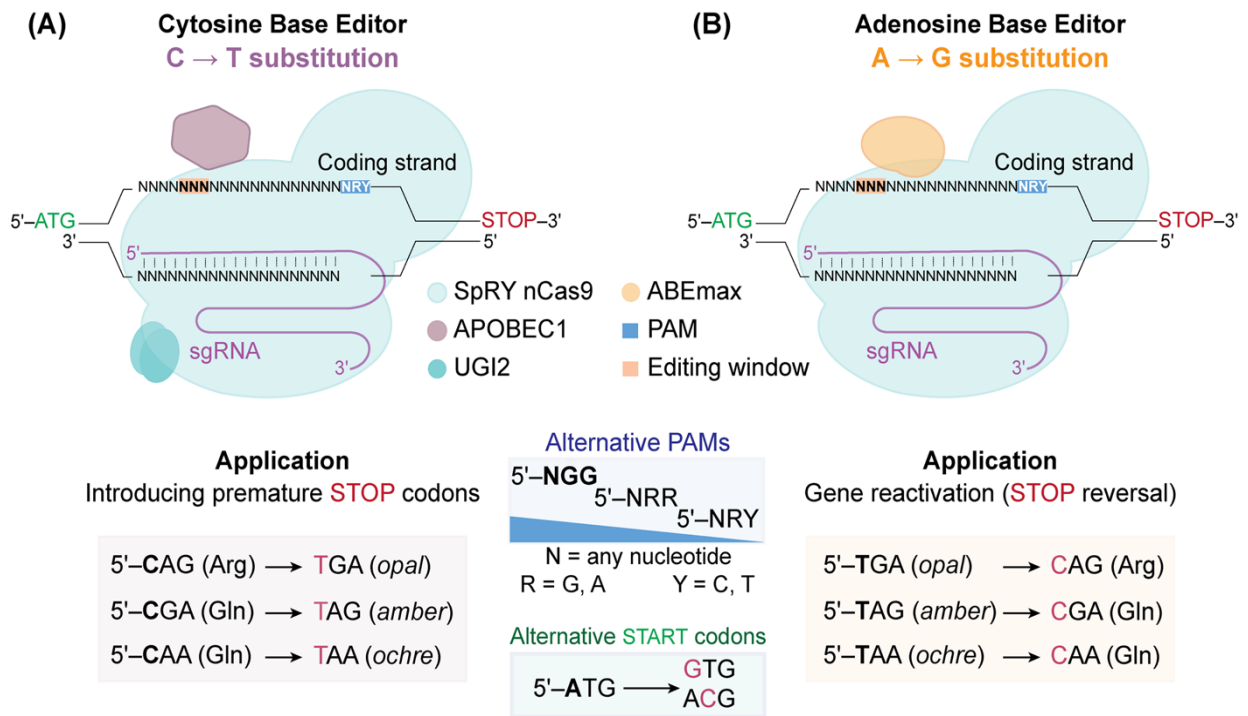


Figure 4.1. Mechanistic features of the two CRISPR/nCas9 base-editors and their applications for bacterial genome editing.

(A) cytidine base editor. A fusion of SpRY nCas9 to APOBEC1 (apolipoprotein B mRNA editing enzyme) and a duplex UGI2 (uracil DNA glycosylase inhibitor) allows for cytidine to thymine substitutions. Such editing tool can be useful for integrating premature *STOP* codon(s) into the reading frame of gene(s) of interest (*opal*, *amber* or *ochre* codons), thus resulting in a functional knock-out.

(B) Adenine base editor. In this case, the SpRY nCas9 protein is fused with an evolved variant of adenine deaminase (ABEmax) enables adenine to guanine substitutions. Application examples of the tool include restoring gene functionality by re-editing premature *STOP* codon(s) or introduction of alternative *START* codons. Both base editors have a relaxed specificity for the cognate PAM (protospacer adjacent motif) as indicated in the diagram.

We first repurposed all the elements of base editors applied in mammalian cells as described above for bacterial system. Synthesized DNA fragments of SpRY, APOBEC1, 2UGI and ABE_{max} were codon optimized and cured from restriction sites used in Standard European Vector Architecture (SEVA) framework¹³. The user-friendly SEVA platform facilitates standardization and is based on genetic modules swapping (e.g. promoters, replication origins and selection markers) to expand the options for genome engineering in Gram-negative bacteria (including *P. putida*). As a backbone we used the pMCRi vector previously developed in our team for CRISPRi in *P. putida*¹², and exchanged dCas9 with the respective editor module. The resulting SEVA-based vectors (**Table 4.1.**) are defined as follows: pEditC (CBE, based on canonical Sp nCas9) and pEditA (ABE, based on canonical Sp nCas9), as well as pEditC-RY (CBE, based on evolved SpRY) and pEditA-RY (ABE, based on evolved SpRY).

To compare the editing performance of designed CBE in *P. putida*, we first used spacers with canonical PAM sequences targeting nucleotide sequence of *mCherry* gene, encoding red fluorescent protein. Particularly, we targeted cytidines of codons Q47 (**Figure 4.2, A**) and W64, to create premature *STOP* codons and inactivate correct gene translation. We tested the editing for both types of editors in the strain KT-Tn7:mCherry, carrying integrated *mCherry* gene in the chromosome (positive control). To this end, pEditC and pEditC-RY vectors with spacers Q47 and W64 were transformed in the strain KT-Tn7:mCherry, and after 1 h recovery, 1 µl of the transformation mixture was inoculated in 10 mL of LB medium and grown at 30C for 24h. Resulting mixture was diluted with PBS buffer to have around 10³ cells per sample and analyzed by flow cytometry based on mCherry fluorescence, the efficiency of editing was calculated with FlowLogics software based on the population shifting fluorescence values to compare with positive control and varied from 75 to 95%. The variation was mostly spacer dependent (Q47 was edited in 85-95 % of cells, W64 was edited in 75-85% of cells), whereas nCas9 and SpRY showed similar editing performance (**Figure 4.2, B**).

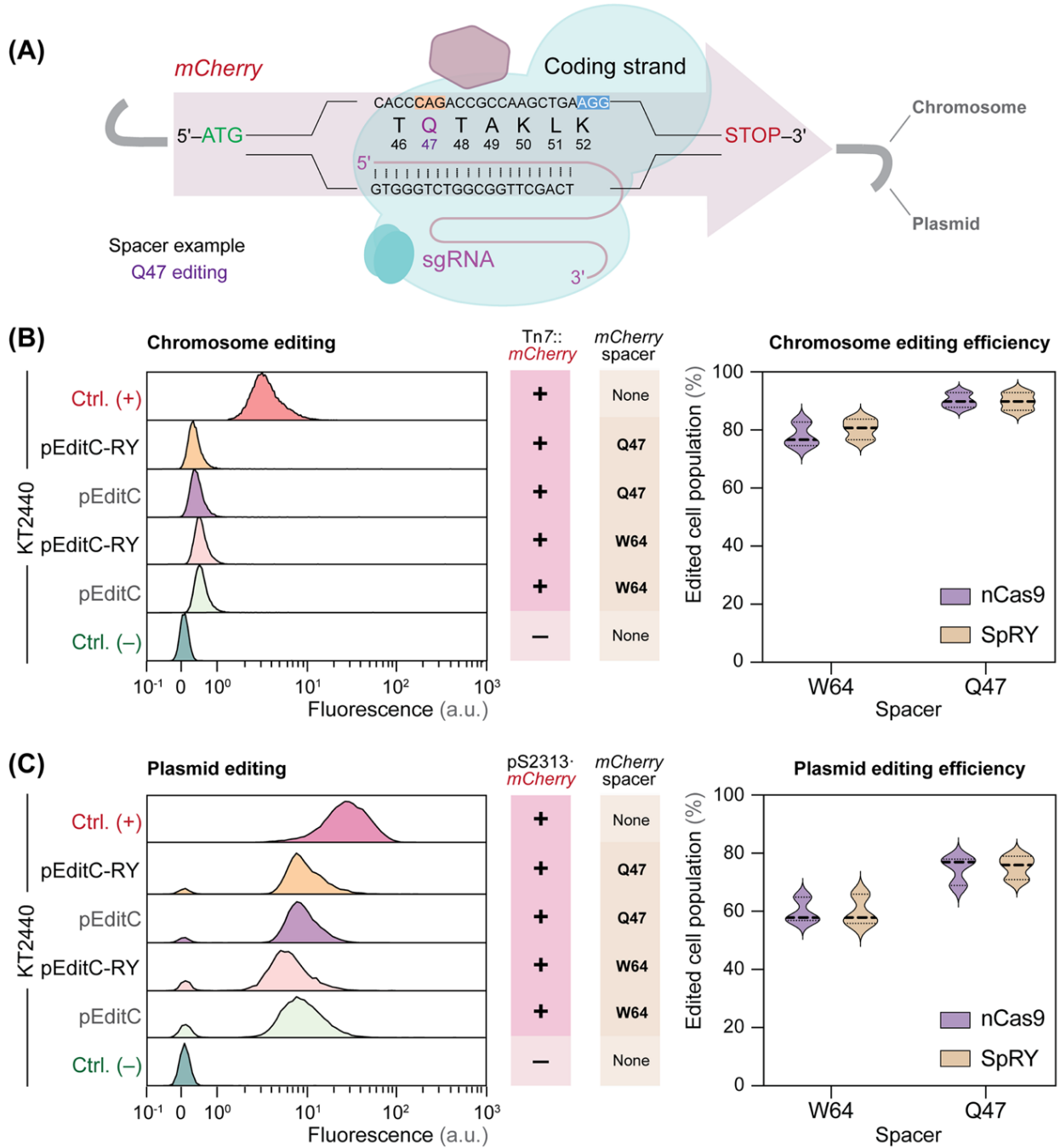


Figure 4.2. Cytidine base-editing of *P. putida*, targeting *mCherry* encoded on the plasmid pSEVA2313:*mCherry* or integrated into the chromosome. Comparison of editing performance for canonical nCas9 or evolved SpRY variant using spacers with classical NGG PAM.

(A) Schematic representation of the example spacer to edit the cytidine inside of the start Q47 codon, this substitution results in premature stop codon integration.

(B) Flow cytometry analysis showing population distribution after 24 h of editing.

Strain KT2440 transformed with plasmid pS2313 *mCherry* was used as a positive control. Strain KT2440 was used as a negative control. Different spacers targeting *mcherry* sequence (Q47, W64) were tested to compare editing performance of canonical nCas9 or evolved SpRY variant.

(C) Flow cytometry analysis showing population distribution after 24 h of editing. Strain KT-BG42 harboring *mCherry* integrated into Tn7 locus was used as a positive control. Strain KT2440 was used as a negative control. Different spacers were tested to compare editing performance of canonical nCas9 or evolved SpRY variant. Editing efficiency was calculated based on the population shift using Flowlogics software.

Additionally, we tested the editing for both types of editors in the KT2440 strain transformed with the pSEVA2313:mCherry plasmid (**Figure 4.2, C**), carrying 20-30 copies of gene per cell. We observed shifting of the fluorescence in all the edited strains, providing a small fraction of mCherry-free cells and additional population accumulating mCherry signal from partly edited less-producing cells. Even though overall editing efficiency for the multiple gene copies dropped by 20%, the nCas9 and SpRY remain comparable activity.

Next step was to test SpRY activity in *P. putida* using spacers with different PAMs, with the preference to NRR. Based on results described above, we compared both types of editors only in the strain KT-Tn7:mCherry, carrying integrated mCherry gene in the chromosome. For editing, we targeted the same start codon of mCherry, using 3 different spacers with varying PAM motifs: M1-1 (AGG), M1-2 (GAG), M1-3 (CGA) (**Figure 4.3, A**). Resulting base substitution allows integration of alternative start codon GTG¹⁹, which might effect on the protein expression and transcription strength²⁰, allowing study Shine-Dalgarno sequence dependence and transcription activity²¹.

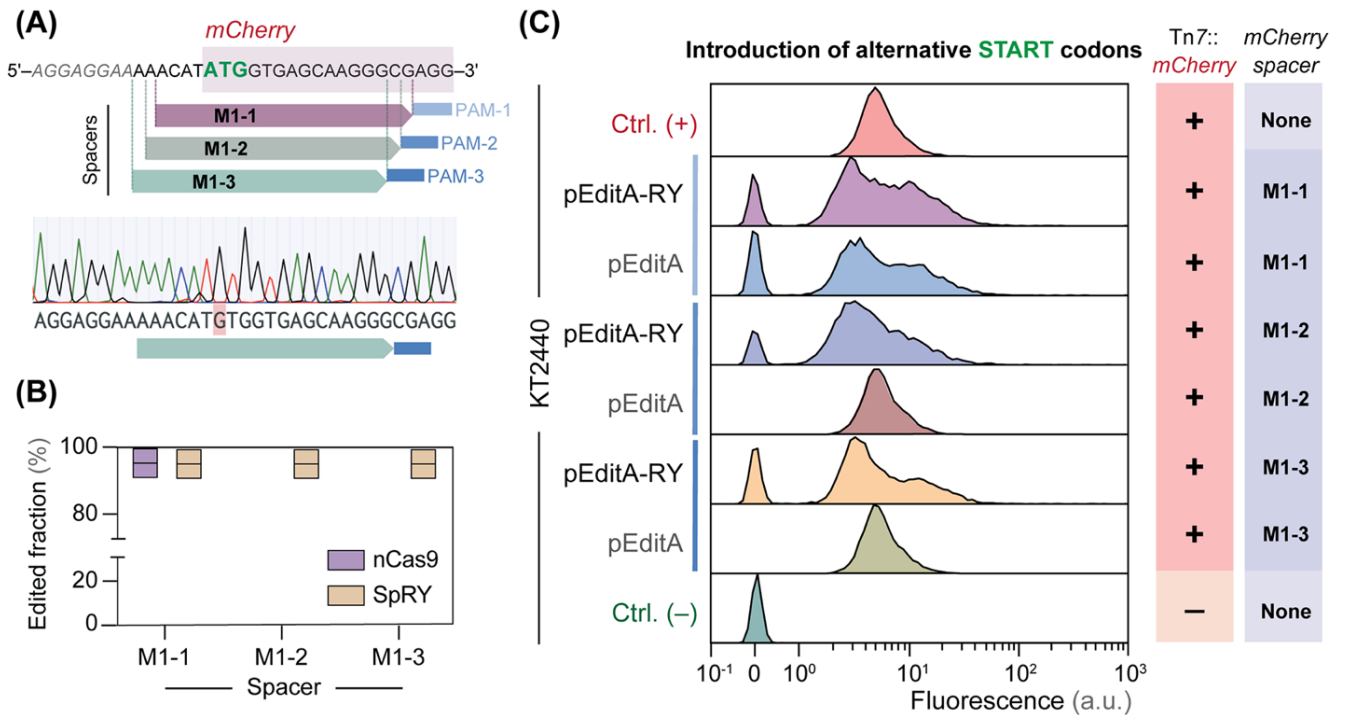


Figure 4.3. Adenine base-editing of *P. putida*, using canonical nCas9 or evolved SpRY variant and spacers with different PAM. **(A)** Flow cytometry analysis showing population distribution after 24 h of editing. Strain KT-BG42 harboring *mCherry* integrated into Tn7 locus was used as a positive control. Strain KT2440 was used as a negative control. Different spacers were tested to compare editing performance of canonical nCas9 or evolved SpRY variant. **(B)** Schematic representation of the tested spacers to edit the first adenine within the start ATG codon. The M1-1 spacer encodes the classical NGG PAM, whereas M1-2, and M1-3 display the alternative NRG and NGR PAMs, respectively. **(C)** Editing efficiency was calculated after 24 h of editing. Cells were plated and individual colonies were selected for PCR followed by sequencing of the amplified fragments. nCas9-base editing was efficient only with M1-1 PAM spacer, for SpRY editing with similar efficiency was observed with all spacers.

We tested the editing for both types of editors in the strain KT-Tn7:mCherry, transformed with vectors carrying adenine editors pEditA and pEditA-RY and 3 different spacers. 1 μ l of the transformation mixture was inoculated in 10 mL of LB medium and grown at 30C for 24h. Resulting edited mixture was plated on the LB agar plate *via* dilution streaking and single colonies were used for PCR analysis followed by sequencing (Eurofins, Germany). The editing efficiency for the M1-1 spacer with canonical NGG PAM was high for both nCas9 and SpRY (95%), as for M1-2 and M1-3 spacers with NRR PAM, only evolved SpRY showed activity, which was comparable to M1-1 spacer (95%), (**Figure 4.3, B**). In parallel, edited 24h mixture was diluted with PBS buffer as calculated to be approximately 10^3 cells per sample and analyzed by flow cytometry based on mCherry fluorescence.

As expected, the activity of nCas9 with spacers M1-2, and M1-2 was not observed, while cells edited with SpRY showed a clear phenotype with all spacers. Surprisingly, replacement of ATG with a weak GTG start codon resulted in diverse populations in all the edited strains, providing a fraction of cells not producing mCherry, and population accumulating different amounts of mCherry, in some cases even more than positive control. This can be explained by Shine-Dalgarno dynamics in relation to translation initiation which in some cases may improve protein expression and counteract mRNA secondary structures ¹⁹.

To our knowledge, the function of this evolved ABEmax variant is shown for the first time in bacteria, and very high efficiency rate combined with less PAM restricted SpRY variant secures a promising position in the toolbox for bacterial engineering, e.g., *P. putida*.

High-copy vectors with conditional plasmid replication allow efficient plasmid curing

With the established base-editors at hand, we then addressed curability of the vectors after editing process to further develop editing toolbox. It is important because plasmid-borne genome editing has a clear bottleneck: after obtaining the desired genotype the plasmid needs to be cured from the strain which is especially relevant for continuous editing events with different spacers or different types of editors. Generally, plasmid-curing is accomplished by repetitive dilution and passaging in the culture media with no selection pressure (i.e. antibiotic resistance), and further screening of the single colonies afterwards for antibiotic sensitivity ²⁰. Recently, an efficient vector curing approach was described to be used in *Pseudomonas* species, based on *in vivo* digestion of vectors by the I-SceI meganuclease and conditional control of *trfA* expression, facilitating inducer-dependent medium copy oriV(RK2) origin or replication ²¹.

In this work, we expanded the set of curable vectors for *Pseudomonas species*, based only on synthetic control of replication of high copy plasmids, especially relevant for boosting editing efficiency. As a template we used pSEVA448 vector, which was also used to construct various pEdit plasmids (**Table 4.1**). Such plasmids harbor a hybrid of two origins (pRO1600/ColE1): the narrow-host-range ColE1 for replication in *E. coli* and pRO1600 (from *P. aeruginosa* isolate) for replication in *P. putida* and closely related species ¹³. To this end, a set of plasmids pSEVA44i8 (where 4i is indicating inducibility of the origin of replication) was constructed containing engineered pRO1600 origin *via* integration of the synthetic module providing conditional replication (**Figure 4.4, A**). This design provides easy cloning and stable replication in *E. coli*, as it relies on the ColE1 origin, whereas it is rapidly lost in *Pseudomonas* without an addition of inducer to the medium. Developed plasmids additionally harboring a *msfgfp* gene, encoding monomeric super folding green fluorescent protein msfGFP, under the constitutive P_{14g} promoter without translational coupler ²² to ensure optimal screening conditions. Native bacterial promoter and regulation regions were be predicted using *in silico* tools (BPRM from Softberry.com) and replaced by the inducible by 3-mBz promoter P_m and synthetic RBS,

resulting in the pS44i8HG (high copy) and pS44i8MG (medium copy) plasmids (**Figure 4.4, A**).

We further analyzed how stable is the conditional vector replication in the engineered plasmids. For this purpose, *P. putida* cells were inoculated in the microtiter plate at the same starting optical density (OD 0.05) in the LB medium containing 100 $\mu\text{g mL}^{-1}$ of streptomycin and different concentrations of inducer (0.5 mM, 1 mM, 2 mM of 3-mBz). After 10h of growth cells reached mid-exponential phase, and samples were collected from each well, diluted with PBS buffer to contain 10^3 cells per sample and stored at -20C. Further analysis of the gene expression and relative copy number quantification was performed by quantitative polymerase chain reaction (qPCR). Copy number was calculated by normalizing of the *aadA* (Str^R) expression rates measured using qPCR and compared with the previously reported data for oriV(pRO1600/ColE1) we used for engineering^{23,24}. We observed stable replication of the plasmids remaining the same copy number using different tested concentrations of inducer (**Figure 4.4, B**).

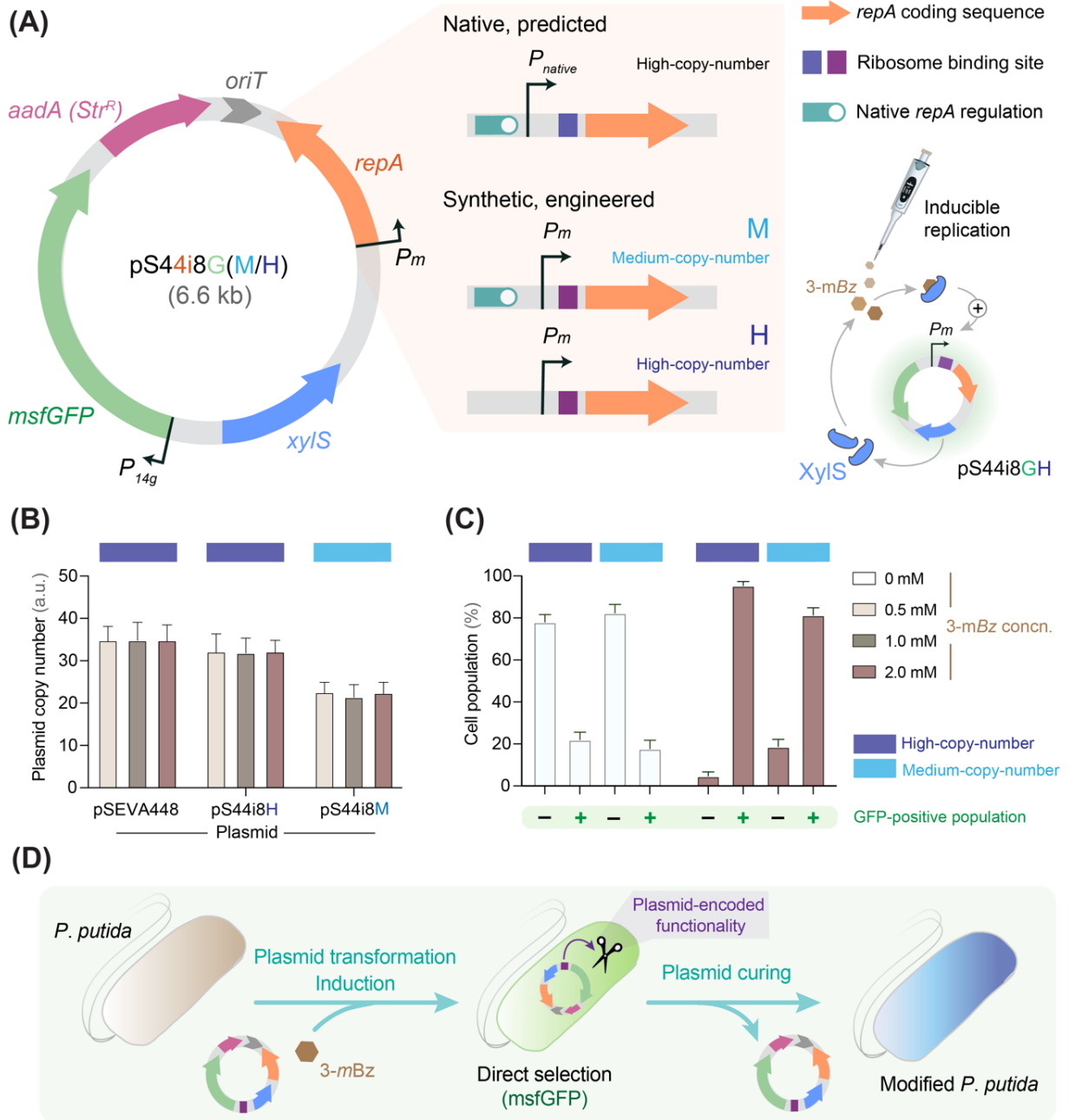


Figure 4.4. Engineering conditional plasmid replication for *P. putida* using a high-copy-number vector of the SEVA framework.

(A) Representation of the structure and functional modules in vector pS44i8G and derivatives. Integration of a synthetic RBS and a *XylS/P_m* module to replace the native transcription initiation regulation of *repA* in *oriV*(RO1600) results in high- and low-copy-number plasmid variants.

(B) Vector stability analysis by relative copy number quantification in *P. putida* cells after 10 h of growth (mid-exponential phase). Copy number was calculated by normalizing of the *aadA* (*Str^R*) expression rates measured using qPCR and compared with literature data.

(C) Curing efficiency for pS44i8GM and pS44i8GH vectors. Cells of *P. putida* were grown for 16 h in LB medium with (1 mM) and without 3-mBz.

The cell culture was diluted with PBS buffer as calculated to be adjust the density to 10^3 cells per sample and analyzed by flow cytometry based on msfGFP fluorescence.

(D) Schematic representation of the curing approach. The replication of *oriV* is supported by the presence of inducer 3-mBz. Note that conditional-replication plasmids carry essentially any potential functionality that may be required transiently for genome editing.

One of the engineered vectors pS44i8HG shown to have a high-copy number (~ 32 -38 copies per cell) which has similar values to the high copy number of the original pSEVA448 vector (~ 35 -42 copies per cell). Another vector pS44i8MG corresponded to the medium copy number plasmid (~ 20 -26 copies per cell). These variation in the replication efficiency has also resulted in the different msfGFP production rates, exhibiting ~ 5 -fold decrease in fluorescence for cells harboring pS44i8MG plasmids (data not shown). Such variation in the copy number may be caused by the efforts of removing the native potential regulatory sequence resulting in the less efficient transcription of *repA* (**Figure 4.4, A**).

As the presence of fluorescent marker in vectors allows to perform various screenings, we used fluorescence-activated cell sorting to analyze curing efficiency for the pS44i8HG and pS44i8MG vectors. To this end, bacterial cultures of *P. putida* were inoculated in the 10 mL of the LB medium at the same starting optical density (OD 0.05) with 1 mM 3-mBz or without and were grown for 16-20 h. Resulting mixture was diluted with PBS buffer as calculated to be approximately 10^3 cells per sample and analyzed by flow cytometry based on msfGFP fluorescence. As a result (**Figure 4.4, C**), we observed distribution of cells into the population positive for msfGFP fluorescent signal, and negative population, in which the plasmids were lost. When cells were cultivated in the absence of both antibiotic and inducer, the calculated efficiency of curing for the pS44i8HG (high-copy) and pS44i8MG (medium-copy) was 67%, and 84%, respectively. As expected, when cells were grown in the presence of 2 mM of 3-mBz, most of the population contained msfGFP, sustaining the plasmid (**Figure 4.4, C**). These results

support further application of robust plasmid curing and easy screening for the desired phenotype and can be reached when the inducer 3-mBz is not present in the medium (**Figure 4.4, D**). Constructed vectors described herein not only expand the set of curable vectors, but also provide an option of choice (high copy/ medium copy) depending on the cargo of interest.

Detailed navigation guide on pAblo pCasso construction and application as a novel toolbox for unconstrained base-editing

The CRISPR-editing system requires a specific spacer sequence in the gRNA, which determines the binding site of nCas9. This sequence has to be selected specifically for each target as a 20-nt spacer for the sgRNA followed by a PAM (Canonical 5'-NGG-3', where GG can be replaced with preferably any combination of GA, AG, AA, or other nucleotides, if alternative design is not possible), the detailed representation is shown in **Figure 4.5, A**. It is very important to choose unique spacer sequence compared to bacterial genome which is planned to be edited to avoid off-target effect. To ensure that this is the case, a BLAST analysis²⁵ against the complete genomic DNA sequence of the target strain should reveal no sequence similarities: absent homology in the seed sequence, comprised with 8-10 bases at the 3' end of the gRNA targeting *sequence, will refrain nCas9 binding*^{26,27}. It was also reported that the efficiency of editing also depends on the bases adjacent to the target nucleotide. The optimal preference for CBE activity is 5'-[TC ≥ CC ≥ AC > GC]-3' with the target C being in the second position, and for ABE activity 5'-[TA ≥ GA ≥ AA > CA]-3' with the target A being in the second position².

The vectors described herein (pEditA, pEditC, pEditA-SpRY, pEditC-SpRY, pAblo and pCasso) contain two *BsaI* (*Eco31I*) recognition sites that are placed upstream of the sgRNA fusion construct. Further linearization of the selected plasmid with *BsaI* allows integration of the unique target-specific spacer, which can be assembled as a duplex of two oligonucleotides that are complementary to each other and having *BsaI*-compatible overhangs for the ligation into the vector. One oligonucleotide contains the 20-nt spacer sequence from target gene and flanked at the 5'-end with 5'-GCGCG-3'. Another oligonucleotide is its reverse complement with the addition of a 5'-AAAC-3' sequence to 5'-end and a C' nucleotide at the 3'-end.

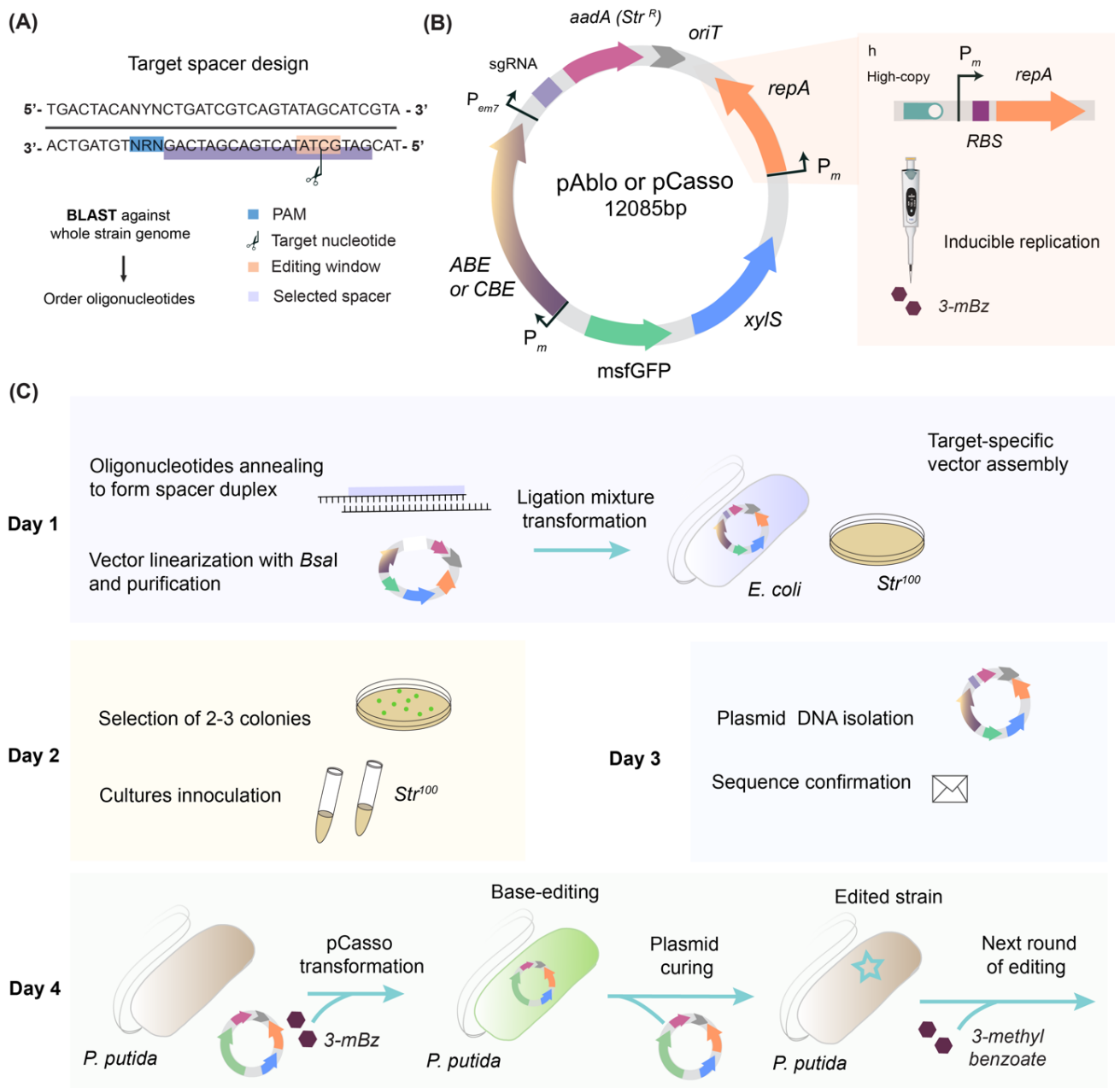


Figure 4.5. Base-editing platform pAblo pCasso consisting of vectors with conditional plasmid replication in *P. putida*.

(A) Target spacer design guidelines. A PAM sequence (5'-NGG-3', where N represents any nucleotide) is chosen within the DNA strand sequence of the target gene.

(B) Schematic representation of the constructed plasmids pAblo and pCasso, indicating their functional elements.

(C) Overview of the workflow for base-editing system in *Pseudomonas*.

Day 1: Anneal single-strand DNA oligonucleotides by reverse cooling to form a double-stranded DNA spacer-insert array and clone it into the respective vector

derivative. Transform a suitable cloning *E. coli* strain and incubate the plates overnight (with 100 µg ml⁻¹ of streptomycin for selection). **Day 2:** Inoculate two or three transformants in liquid cultures and grow the cultures overnight. **Day 3:** Purify independent plasmids and send them for sequence verification by DNA Sanger sequencing. **Day 4:** Transform the target *Pseudomonas* strain with isolated and sequence-verified plasmid and incubate the plates under streptomycin selection with addition of 2 mM of inducer 3-mBz to ensure plasmid replication and efficient editing. Verify edited sequence with sequencing analysis of the PCR fragment amplified from the target gene. Inoculate 10 mL fresh culture of the medium with a single edited *Pseudomonas* colony and incubate for curing. Resulting bacterial culture is streaked by dilution on the agar plate with non-selective medium. Next day the cured colonies can be peaked in the UV light (non-fluorescent) and inoculated for the next round of editing or further strain characterization.

For example, to edit the Q47 codon of *mCherry* (**Figure 4.2**) gene we used following oligonucleotides to create a duplex:

CBE_spacerQ47_for (5'-GCGCG-CACCCAGACCGCCAAGCTGA-3')
 CBE_spacer Q47_rev (5'-AAA-TCAGCTTGGCGGTCTGGGTG-C-3').

To boost ligation efficiency with the linearized vector, oligonucleotides can be phosphorylated using T4 polynucleotide kinase (PNK) or by chemical modification during oligonucleotide synthesis.

Gathering all the obtained findings together, we further constructed self-curing pAblo pCasso platform for base-editing of Adenine and Cytidine respectively. Plasmid pSEVA44i-h8G (high-copy) was selected for integration of the respective editor module to ensure high editing efficiency. The structure of resulting vectors is presented in **Figure 4.5, B**, while detailed structure of each editor is presented in **Figure 4.1**. Additionally, we have optimized cloning of the plasmids and base-editing procedure, as presented at the schematic workflow in **Figure 4.5, C**.

Example step-by-step procedure with target-specific pCasso cloning:

- i. Digesting of the vector pCasso with FastDigest *Eco31I* (or *BsaI*) according to the manufacturer's recommendations. Purify the linearized plasmid after digestion, by agarose gel purification of the digestion mixture *via* DNA electrophoresis. The fragment corresponding to the pCasso vector (12,000 bp) can be purified once in high quantity as a concentrated stock to be used for further applications.
- ii. Phosphorylation and annealing of the two 100 μ M spacer oligonucleotides in a thermocycler. The following mixture 10 μ l in total: 6 μ l of water, 1 μ l of each oligonucleotide, 1 μ l of T4 ligase buffer and 1 μ l of T4 polynucleotide kinase (10 U/ μ l, Thermo Scientific) incubate as indicated: 30 min at 37°C, 3 min at 95°C for phosphorylation and kinase deactivation, followed by cycles starting at 95°C and decreasing the temperature by 1°C in each cycle until 25°C for the annealing.
- iii. Ligation resulting spacer duplex into the linearized pCasso vector. Mixture of dsDNA oligonucleotides should be diluted 1:200 with water. Then, 10 μ l reaction of 5 μ l of the diluted duplex, 1 μ l (10 ng) of linearized pCasso, 1 μ l of T4 ligase buffer, 1 μ l of T4 DNA ligase (5 U/ μ l, Thermo Scientific) and 2 μ l of water to reach the final volume. Resulting mixture is incubated for 30 min at the room temperature.
- iv. Transformation of the 100- μ l aliquot of chemically competent *E. coli* DH5 α cells with the total ligation mixture. Bacterial suspension should be plated on LB agar plates supplemented with streptomycin (100 μ g ml⁻¹). Purified plasmid from two-three individual transformants is verified by sequencing with primer 153 (Table S1 in the Supplementary Information).

Once the target-specific vectors are constructed and verified, they can be transformed in *Pseudomonas* for the editing event. After transformation, the 10 μ l of bacterial culture is inoculated in 10 mL of the selective medium and grown overnight. To sustain the plasmid replication 2 mM of 3-mBz should

be added to the medium, because as soon as the inducer is removed the plasmid will be lost (**Figure 4.4, D**).

Editing of the target should be verified: 10 individual colonies should be peaked, and the target fragment amplified with PCR and sent for sequencing. Curing these novel plasmids, which contain a green fluorescent reporter gene, could be achieved in a single cultivation step within 8 h. For curing of the plasmid, the edited colony should be inoculated into 10 mL of non-selective medium without antibiotic and without inducer (optionally, it could have additional passaging into the fresh medium after 5h of growth to boost curing efficiency), and resulting bacterial culture is streaked by dilution on the agar plate with non-selective medium. Next day the cured colonies can be peaked in the UV light (non-fluorescent) and inoculated for the next round of editing or further strain characterization (**Figure 4.5, C**). This strategy thus eases complex strain engineering programs independently of homologous recombination and yields plasmid-free engineered cells.

Conclusion & Outlook

CRISPR-mediated nucleotide editing has only recently been established in bacteria but is already widely adapted for multiple purposes. While the PAM requirement of CRISPR systems enables bacteria to distinguish self from non-self, the necessity of PAM recognition constrains CRISPR-Cas9 systems for genome editing applications. The SpRY variant circumvent this limitation by relaxing the dependence of SpCas9 on a requisite PAM, extending targeting to sites with NGN and NAN PAMs, as well as other sites with reduced relative efficiency. In this work we implemented SpRY-based plasmid borne toolbox to break a PAM restriction barrier in bacterial genome engineering by enabling DNA editing of *P. putida* in a more target accessible fashion.

We used this nearly PAM-less Cas9 variant to adapt two kinds of base editors (ABE and CBE) to make substitution of any desirable nucleotide possible. Moreover, we suggest a fast and efficient approach for the plasmid curing,

based on the conditional replication of the parent vectors. Those vectors were equipped with base-editor of choice, resulting in pAblo/pCasso editing system, which could be used for the programmed nucleotide substitution, followed by the controlled plasmid elimination from the edited strain. Further experiments would be needed to analyze the potential off-target effect, characterize the system in depth and optimize the curing protocol. Building on this toolset, the next steps will include testing of the developed system performance, e.g., comparison of the editing efficiency using vectors pAblo/pCasso with a number of genomic targets (spacers with different types of PAM, as well as editing of the different genes), optimization of the final editing protocol for Pseudomonads and addressing its potential applications for industrial biotechnology.

Acknowledgements

We are thankful to Daria Sergeeva for the technical assistance with qPCR. The financial support from The Novo Nordisk Foundation through grants NNF20CC0035580, *LiFe* (NNF18OC0034818) and *TARGET* (NNF21OC0067996), the Danish Council for Independent Research (*SWEET*, DFF-Research Project 8021-00039B), and the European Union's Horizon 2020 Research and Innovation Programme under grant agreement No. 814418 (*SinFonia*) to P.I.N. is gratefully acknowledged. E.K. is supported by the Novo Nordisk Foundation (grant NNF17CC0026768) as part of the Copenhagen Bioscience Ph.D. Programme. The authors declare that there are no competing interests associated with the contents of this article.

References

- 1 Anzalone, A. V., Koblan, L. W. & Liu, D. R. Genome editing with CRISPR-Cas nucleases, base editors, transposases and prime editors. *Nat. Biotechnol.* **38**, 824-844, doi:10.1038/s41587-020-0561-9 (2020).
- 2 Komor, A. C., Kim, Y. B., Packer, M. S., Zuris, J. A. & Liu, D. R. Programmable editing of a target base in genomic DNA without double-stranded DNA cleavage. *Nature* **533**, 420-424, doi:10.1038/nature17946 (2016).
- 3 Komor, A. C. *et al.* Improved base excision repair inhibition and bacteriophage Mu Gam protein yields C:G-to-T:A base editors with higher efficiency and product purity. *Sci. Adv.* **3**, eaao4774, doi:10.1126/sciadv.aao4774 (2017).
- 4 Gaudelli, N. M. *et al.* Programmable base editing of A*T to G*C in genomic DNA without DNA cleavage. *Nature* **551**, 464-471, doi:10.1038/nature24644 (2017).
- 5 Cavaleiro, A. M., Kim, S. H., Seppälä, S., Nielsen, M. T. & Nørholm, M. H. Accurate DNA assembly and genome engineering with optimized uracil excision cloning. *ACS Synth. Biol.* **4**, 1042-1046, doi:10.1021/acssynbio.5b00113 (2015).
- 6 Genee, H. J. *et al.* Software-supported *USER* cloning strategies for site-directed mutagenesis and DNA assembly. *ACS Synth. Biol.* **4**, 342-349, doi:10.1021/sb500194z (2015).
- 7 Hanahan, D. & Meselson, M. Plasmid screening at high colony density. *Methods Enzymol.* **100**, 333-342 (1983).
- 8 Worsey, M. J. & Williams, P. A. Metabolism of toluene and xylenes by *Pseudomonas putida (arvilla)* mt-2: evidence for a new function of the TOL plasmid. *J. Bacteriol.* **124**, 7-13 (1975).
- 9 Bagdasarian, M. *et al.* Specific purpose plasmid cloning vectors. II. Broad host range, high copy number, RSF1010-derived vectors, and a host-vector system for gene cloning in *Pseudomonas*. *Gene* **16**, 237-247, doi:10.1016/0378-1119(81)90080-9 (1981).
- 10 Martínez-García, E., Nikel, P. I., Aparicio, T. & de Lorenzo, V. *Pseudomonas* 2.0: genetic upgrading of *P. putida* KT2440 as an enhanced

- host for heterologous gene expression. *Microb. Cell Fact.* **13**, 159, doi:10.1186/s12934-014-0159-3 (2014).
- 11 Kozaeva, E. *et al.* Model-guided dynamic control of essential metabolic nodes boosts acetyl-coenzyme A-dependent bioproduction in rewired *Pseudomonas putida*. *Metab. Eng.* **67**, 373-386 (2021).
 - 12 Batianis, C. *et al.* An expanded CRISPRi toolbox for tunable control of gene expression in *Pseudomonas putida*. *Microb. Biotechnol.* **13**, 368-385, doi:10.1111/1751-7915.13533 (2020).
 - 13 Silva-Rocha, R. *et al.* The Standard European Vector Architecture (SEVA): a coherent platform for the analysis and deployment of complex prokaryotic phenotypes. *Nucleic Acids Res.* **41**, D666-D675, doi:10.1093/nar/gks1119 (2013).
 - 14 Hahne, F. *et al.* flowCore: a Bioconductor package for high throughput flow cytometry. *BMC Bioinformatics* **10**, 106, doi:10.1186/1471-2105-10-106 (2009).
 - 15 Walton, R. T., Christie, K. A., Whittaker, M. N. & Kleinstiver, B. P. Unconstrained genome targeting with near-PAMless engineered CRISPR-Cas9 variants. *Science* **368**, 290-296, doi:10.1126/science.aba8853 (2020).
 - 16 Ren, Q. *et al.* PAM-less plant genome editing using a CRISPR-SpRY toolbox. *Nat. Plants* **7**, 25-33, doi:10.1038/s41477-020-00827-4 (2021).
 - 17 Evans, B. A. & Bernstein, D. A. SpRY Cas9 Can Utilize a Variety of Protospacer Adjacent Motif Site Sequences To Edit the *Candida albicans* Genome. *mSphere* **6**, doi:10.1128/mSphere.00303-21 (2021).
 - 18 Gaudelli, N. M. *et al.* Directed evolution of adenine base editors with increased activity and therapeutic application. *Nat. Biotechnol.* **38**, 892-900, doi:10.1038/s41587-020-0491-6 (2020).
 - 19 Cao, X. & Slavoff, S. A. Non-AUG start codons: Expanding and regulating the small and alternative ORFeome. *Exp. Cell Res.* **391**, 111973, doi:10.1016/j.yexcr.2020.111973 (2020).
 - 20 Martínez-García, E., Aparicio, T., de Lorenzo, V. & Nikel, P. I. Engineering Gram-negative microbial cell factories using transposon vectors. *Methods in molecular biology* **1498**, 273-293, doi:10.1007/978-1-4939-6472-7_18 (2017).
 - 21 Volke, D. C., Friis, L., Wirth, N. T., Turlin, J. & Nikel, P. I. Synthetic control of plasmid replication enables target- and self-curing of vectors

- and expedites genome engineering of *Pseudomonas putida*. *Metab. Eng. Commun.* **10**, e00126, doi:10.1016/j.mec.2020.e00126 (2020).
- 22 Zobel, S. *et al.* Tn7-Based device for calibrated heterologous gene expression in *Pseudomonas putida*. *ACS Synth. Biol.* **4**, 1341-1351, doi:10.1021/acssynbio.5b00058 (2015).
- 23 Jahn, M., Vorpahl, C., Hübschmann, T., Harms, H. & Müller, S. Copy number variability of expression plasmids determined by cell sorting and droplet digital PCR. *Microb. Cell Fact.* **15**, 211, doi:10.1186/s12934-016-0610-8 (2016).
- 24 Cook, T. B. *et al.* Genetic tools for reliable gene expression and recombineering in *Pseudomonas putida*. *J. Ind. Microbiol. Biotechnol.* **45**, 517-527, doi:10.1007/s10295-017-2001-5 (2018).
- 25 Ladunga, I. Finding similar nucleotide sequences using network BLAST Searches. *Curr. Protoc. Bioinformatics* **58**, 3.3.1-3.3.25, doi:10.1002/cpbi.29 (2017).
- 26 Kunne, T., Swarts, D. C. & Brouns, S. J. Planting the seed: target recognition of short guide RNAs. *Trends Microbiol.* **22**, 74-83, doi:10.1016/j.tim.2013.12.003 (2014).
- 27 Wiedenheft, B. *et al.* RNA-guided complex from a bacterial immune system enhances target recognition through seed sequence interactions. *Proc. Natl. Acad. Sci. USA* **108**, 10092-10097, doi:10.1073/pnas.1102716108 (2011).

Chapter 5

MODEL-GUIDED DYNAMIC CRISPRi CONTROL BOOSTS BIOPRODUCTION IN REWired *PSEUDOMONAS PUTIDA*

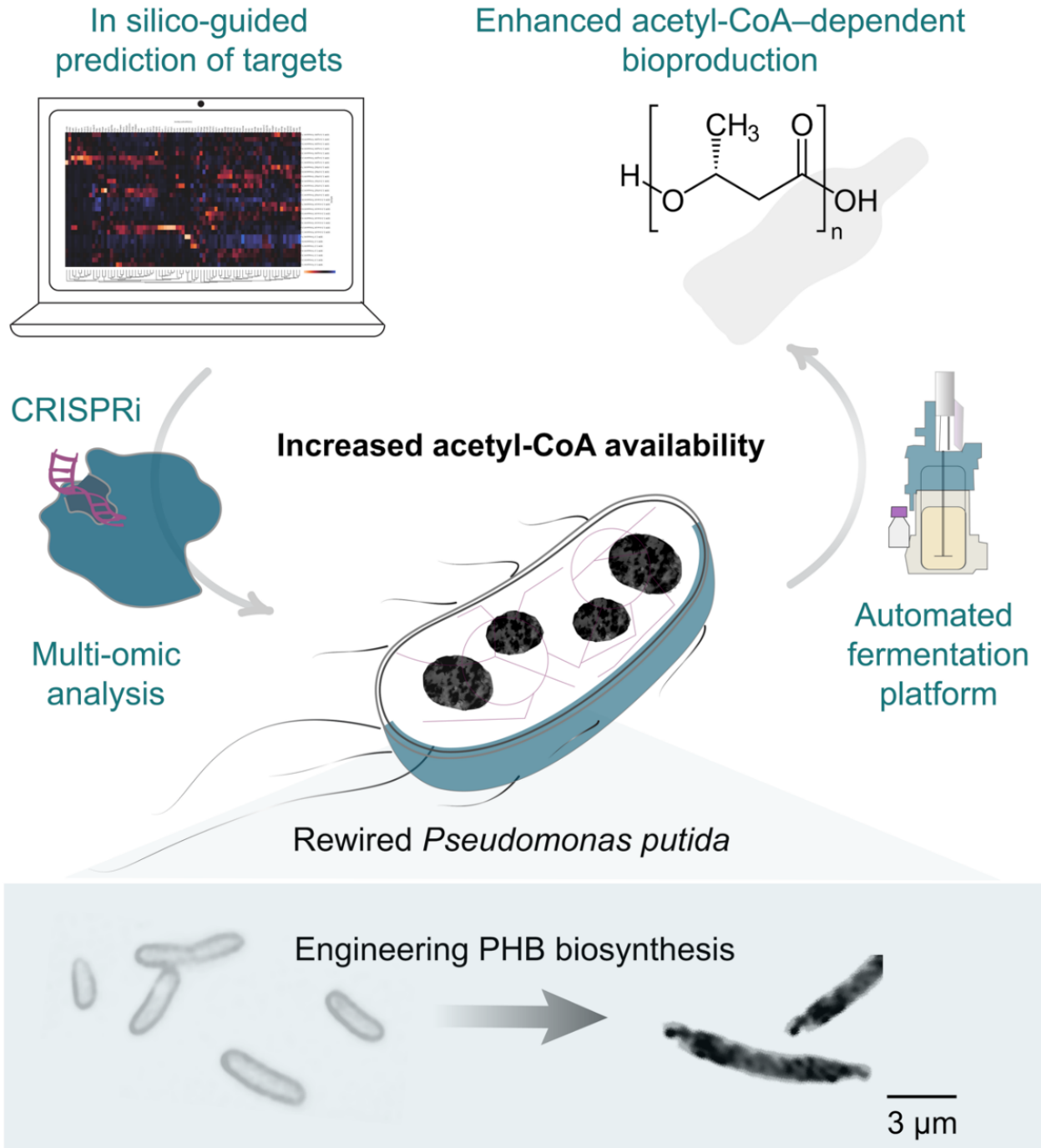
Ekaterina Kozaeva¹, Svetlana Volkova¹, Marta R. A. Matos¹,
Mariela P. Mezzina¹, Tune Wulff¹, Daniel C. Volke¹, Lars K. Nielsen^{1,2} and
Pablo I. Nikel^{1*}

Metabolic Engineering (2021) 67: 373-386.

- ¹ *The Novo Nordisk Foundation Center for Biosustainability, Technical University of Denmark, 2800 Kongens Lyngby, Denmark*
- ² *Australian Institute for Bioengineering and Nanotechnology (AIBN), The University of Queensland, Brisbane QLD 4072, Australia*

* Correspondence to:

Pablo I. Nikel
(pabnik@biosustain.dtu.dk)
The Novo Nordisk Foundation
Center for Biosustainability
Technical University of Denmark
Kgs Lyngby 2800, Denmark
Tel: (+45) 93 51 19 18



INTRODUCTION

After decades of continuous and intensive technological development, a broad range of bulk and fine chemicals, drugs and biofuels can be accessed by metabolic engineering of microorganisms¹⁻⁴. Multiple strategies have been deployed to this end, including the selection of suitable hosts for strain engineering^{5,6}, modelling control of biochemical networks designed *in silico*^{7,8} and elimination or fine-tuned balancing of competing pathways^{9,10}—an aspect supported by the ever expanding synthetic biology toolbox¹¹⁻¹³. In this sense, the inception of *Clustered Regularly Interspaced Short Palindromic Repeats* (CRISPR) and the *CRISPR-associated protein 9* (Cas9) of *Streptococcus pyogenes* played a central role in our ability to access and harness the metabolic potential of microbial species¹⁴⁻¹⁶, including non-traditional bacterial platforms¹⁷⁻²¹.

Among the applications of CRISPR strategies relevant for metabolic engineering, repressing genes encoding key enzymes is very often required to balance metabolic pathways to increase production titers, yields and productivities²². Hence, CRISPR elements have been repurposed for repressing gene expression (*CRISPR interference*, CRISPRi). This genetic tool only requires an endonuclease activity-deficient version of Cas9, termed *dead Cas9* (dCas9), and a chimeric single-guide RNA (sgRNA) to recognize a DNA target of interest and block transcription of the cognate sequence^{23,24}. CRISPRi is particularly useful for tuning metabolic or physiological traits encoded by essential genes, which precludes the implementation of gene deletions to eliminate the functions at stake²⁵⁻²⁷.

Pseudomonas species sparked interest for a variety of metabolic engineering applications that require high levels of stress resistance and a versatile, resourceful metabolism²⁸⁻³⁰. *P. putida* KT2440 has been used as a platform for production of bulk and fine chemicals^{18,21,31-34}, and this soil bacterium is also known as an efficient producer of biopolymers³⁵⁻³⁸—especially medium-chain-length polyhydroxyalkanoates (PHAs). The metabolic versatility of *P. putida*, characterized by multiple catabolic modules that enable the use of multiple carbon and nitrogen sources³⁹, comes at the price of a relatively low assimilation and biosynthetic efficiency^{40,41}. A caveat hampering the broad

adoption of *P. putida* as a bioproduction platform is a low acetyl-coenzyme A (CoA) availability^{42,43}, a key building block for added-value compounds, e.g. fatty acids, PHAs, isoprenoids, sterols and alcohols^{44,45}. The evolutionary adoption of the Entner-Doudoroff (ED) pathway as the main catabolic module for sugars, and part of the EDEMP cycle^{46,47}, is the main reason behind this occurrence. As recently demonstrated by Sánchez-Pascuala, et al.⁴⁸, the functional replacement of the native catabolism by a linear Embden-Meyerhof-Parnas glycolysis increased the acetyl-CoA pool—but the engineered *P. putida* strain grew slowly and only reached moderate cell densities. Hence, balancing the acetyl-CoA node, a metabolic hub where multiple reactions (several of which are essential) converge and branch out, requires a delicate fine-tuning of fluxes⁴⁹.

On the background exposed above, in this work we built and interrogated a kinetic model of *P. putida* KT2440 central carbon metabolism to identify key targets for manipulation towards increasing acetyl-CoA availability. Essential metabolic functions emerged as the main sink for the thioester, and we deployed a CRISPRi system for redirecting metabolic fluxes towards acetyl-CoA by depleting substrate-competing proteins. The effectiveness of this dynamic regulation approach was demonstrated by metabolomic and proteomic analyses in engineered strains where the fluxes around the acetyl-CoA node have been downregulated by direct interference of essential metabolic functions.

The utility of dynamic metabolic regulation was further illustrated by implementing two synthetic routes for poly(3-hydroxybutyrate) (PHB) accumulation, the most widespread short-chain-length PHA with applications in medicine, agriculture, and food industry applications⁵⁰. PHB biosynthesis exclusively relies on acetyl-CoA as the precursor⁵¹, and it can be used as a proxy of the intracellular availability of this coenzyme. The multi-level CRISPRi approach not only enabled a substantial redirection of fluxes towards product synthesis, but this strategy also improved PHB accumulation by manipulating the cell morphology in automated bioreactor cultures.

2. Materials and Methods

2.1. Bacterial strains, plasmids and culture conditions

Bacterial strains and plasmids used in this study are listed in **Table 1**. *Escherichia coli* and *P. putida* cultures were incubated at 37°C and 30°C, respectively. For cloning procedures and during genome engineering manipulations, cells were grown in lysogeny broth (LB) medium (10 g L⁻¹ tryptone, 5 g L⁻¹ yeast extract and 10 g L⁻¹ NaCl; solid culture media additionally contained 15 g L⁻¹ agar). All shaken-flask cultures were agitated at 200 rpm (MaxQ™ 8000 incubator; ThermoFisher Scientific, Waltham, MA, USA). Kanamycin (Km), gentamicin (Gm) and streptomycin (Str) were added whenever needed at 50 µg mL⁻¹, 10 µg mL⁻¹ and 100 µg mL⁻¹, respectively. Unless otherwise indicated, shaken-flask and bioreactor cultures were conducted in de Bont minimal medium [**Table S1** in the Supplementary Data, formulated according to Hartmans, et al. ⁵²] containing 1% (w/v) glucose as the carbon source. The optical density measured at 600 nm (OD₆₀₀) was recorded in a Genesys 20 spectrophotometer (Thermo Fisher Scientific) to estimate bacterial growth. During physiological characterization of engineered strains, growth kinetics were followed at OD₆₀₀ with light path correction in a Synergy™ MX microtiter plate reader (BioTek Instruments Inc., Winooski, VT, USA).

2.2. General cloning procedures and construction of plasmids and mutant strains

All plasmids and oligonucleotides used in this work are listed in **Table 1** and **Table S2** in the Supplementary Data, respectively. Unless stated otherwise, uracil-excision (*USER*) cloning ⁵³ was used for the construction of all plasmids. The *AMUSER* tool was employed for designing oligonucleotides ⁵⁴. Phusion™ *U* high-fidelity DNA polymerase (ThermoFisher Scientific) was used according to the manufacturer's specifications in amplifications intended for *USER* cloning. For colony PCR, the commercial *OneTaq*™ master mix (New England BioLabs, Ipswich, MA, USA) was used according to the supplier's instructions. *E. coli* DH5α λ*pir* (**Table 1**) was employed as a

host for general cloning purposes. Chemically-competent *E. coli* cells were prepared and transformed with plasmids using the *Mix and Go*TM commercial kit (Zymo Research, Irvin, CA, USA) according to the manufacturer's indications. Electrocompetent *P. putida* cells were prepared by washing the biomass from LB medium cultures with 300 mM sucrose, followed by transformation with plasmids by electroporation^{55,56}. Gene deletions were implemented by antibiotic-free allelic exchange assisted by curable plasmids^{57,58}. The sequence of all used plasmids and strains was verified by Mix2Seq sequencing (Eurofins Genomics, Ebersberg, Germany).

2.3. Ensemble model building

The General Reaction Assembly and Sampling Platform (*GRASP*) developed by Saa and Nielsen⁵⁹ was used to build and parametrize a thermodynamically consistent kinetic model of central carbon metabolism for *P. putida* KT2440. In this framework, each reaction is decomposed into elementary reactions according to its enzyme mechanism⁶⁰, which specifies the order of substrate binding and product release. Each elementary reaction was modeled using mass action kinetics. Following the ensemble modeling framework⁶¹, *GRASP* calculates the rate constant values as a function of (i) the change in the Gibbs free energy ($\Delta_r G'$) of the reaction, (ii) reference reaction fluxes and (iii) reference metabolite concentrations. We started by listing all the reactions in the biochemical network of *P. putida* KT2440 representing central carbon metabolism (**Table S3, S4** in the Supplementary Data). To parameterize the models within the *GRASP* framework, we resorted to: (i) a reference flux distribution from glucose-grown *P. putida* KT2440^{47,62}; (ii) steady-state metabolite concentrations in mol L⁻¹ and $\Delta_r G'^0$ values from *eQuilibrator*⁶³ to calculate $\Delta_r G'$ for each reaction; (iii) enzyme mechanisms, including order of binding and release of reactants, number of subunits for each enzyme, and (iv) information on enzyme regulation, i.e. any known allosteric effectors as well as inhibitors or activators (all this information is listed in **Tables S5-S9** in the Supplementary Data). In this way, an ensemble of kinetic models was built where each model reaches the reference state and is consistent with experimental data and additional information about the system. The

ensemble is composed by 10,000 independent models and was used to perform *metabolic control analysis* (MCA) ⁶⁴ in order to find which enzymes can affect the steady-state acetyl-CoA concentration. A detailed explanation on model building and validation is presented in Supplementary Methods **S1**.

2.4. LC-MS-assisted metabolomic analysis

At the indicated time-points, 1-mL culture aliquots were withdrawn, and the biomass was harvested by vacuum filtering (Durapore™ Membrane Filter, 0.45 µm). Upon filtration, cells were quenched with 3 mL of an acetonitrile-CH₃OH-water solution [40-40-20% (v/v)] and acidified with 0.1 M formic acid at -20°C ⁶⁴. Subsequently, cell debris were removed by centrifugation at 17,000×g for 10 min as described in Nickel, et al. ⁶². The supernatant was transferred to a new tube and solvents were removed by evaporation at 30°C for 90 min at reduced pressure (Concentrator Plus, Eppendorf, Hamburg, Germany). The samples were freeze dried and stored at -80°C. Prior to analysis, the sediment was reconstituted in 100 µL of deionized water and insoluble particles were removed by centrifugation at 17,000×g for 10 min. Metabolites were quantified using LC-MS/MS according to the method of McCloskey, et al. ⁶⁵, and the chromatograms were analyzed using the MultiQuant™ software (Sciex, CA, USA). The Prism 8 software (GraphPad Software Inc., San Diego, CA, USA) was used to plot results obtained for selected metabolites. The Matplotlib (NumPy based cross-platform) library was used in order to visualize data as heatmap ⁶⁶. The mean metabolite concentrations across replicates were taken and normalized to the mean value of the control condition for this analysis.

2.5. Genome-wide targeted proteomics analysis by LC-MS/MS

A genome-wide proteomics analysis was used to quantify relative levels of pathway proteins in samples from 50-mL shaken-flask cultures. At the time points indicated in the text, 1-mL aliquots from each culture were pelleted at 10,000×g for 10 min and flash-frozen with liquid nitrogen. Pellets were stored at -80°C until they were processed according to the procedure of Bongers, et al. ⁶⁷. Cells were lysed in 6 M guanidinium ·HCl, 5 mM *tris*(2-carboxyethyl)phosphine, 10 mM chloroacetamide and 100 mM Tris ·HCl

(pH = 8.5) while being disrupted in a Mixer Mill (MM 400 Retsch, Haan, Germany) set at 25 Hz for 5 min at room temperature, followed by 10 min in a thermomixer at 95°C at 2,000 rpm. A clarified supernatant was obtained by centrifugation at 15,000×g for 10 min. The protein concentration in the cell-free lysate was estimated by means of the bicinchoninic acid method, and 100 µg of proteins were tryptically digested for 8 h. After this digestion step, 10 µL of 10% (w/v) trifluoroacetic acid was added and samples were fractionated using a StageTip C18 (Empore, 3M, USA). Next, 1 µg of the purified peptides was injected into a Orbitrap Exploris 480 mass spectrometer (Thermo Scientific). The instrument was operated in data dependent acquisition mode, and the listed settings MS-level scans were performed with Orbitrap resolution set at 120,000; AGC target of 300%; maximum injection time set in auto; intensity threshold at 5.0×10^3 and dynamic exclusion of 20 sec. Data-dependent MS2 selection was performed in Top 20 Speed mode with HCD collision energy set to 40% (AGC target = 75, maximum injection time of 30 ms and isolation window of 1.3 m/z). The peptides were eluted over a gradient from 4% (v/v) acetonitrile in water to 76% (v/v) over a total of 60 min. The raw files were analyzed in the Proteome discoverer 2.4 software with the following settings: fixed modifications, carbamidomethyl and variable modifications, and oxidation of methionine residues. The first search was set to a mass tolerance of 20 ppm and a MS/MS tolerance of 20 ppm, trypsin as an enzyme and allowing one missed cleavage. The false discovery rate was set at 0.1%, and the match-between-runs window was defined as 0.7 min. Quantifications were performed including only unique peptides and normalization between samples was based on total peptide amounts. A protein database, consisting of the *P. putida* reference proteome (UP000000556) together with the amino acid sequence of the heterologous proteins (when relevant), was used for sequence identification. Bioinformatic analysis was performed in Python, and a principal component analysis (PCA) was firstly run for quality control purposes. PCA was done *via* `sklearn.decomposition.PCA` to perform dimensional reduction using standardized data. Two-sample Student's *t*-test was used to determine proteins that displayed significantly changed abundance between control and experimental groups with a false discovery rate of 0.01% corrected by the Benjamini-Hochberg method⁶⁸. For this purpose, `scipy.stats.ttest_ind`

was used to calculate *t*-test probabilities for the means of two independent samples. Enzymes involved in reactions within the central carbon metabolism of *P. putida* KT2440 were identified by the gene-protein-reaction rule by using the genome-scale metabolic model *j*JN1463⁶⁹. The same set of reactions of central carbon metabolism was chosen as per the kinetic model. Matplotlib library was used to visualize data as heatmap as explained above. The mean values across replicates were taken and normalized to the mean value of control conditions across experiments. In both metabolomics and proteomic analyses, the lowest value for the color scheme of a heatmap is 0.1 and the biggest is 2.5, which means that any value smaller than 0.1 or bigger than 2.5 is visualized with the same color as 0.1 or 2.5, respectively. Metabolic pathway enrichment analysis was performed in order to determine metabolic pathways with enriched proteins with altered abundance. Protein sets with significantly increased and decreased abundance in every comparison group were used to run the analysis. The Biocyc online resource⁷⁰ and the associated SmartTables facility (<https://biocyc.org/smarttables>) were chosen for this analysis. The pathways were selected for *P. putida* and a *P*-value of 0.05 was set as a threshold for significance. Gene ontology analysis was furthermore used to establish a hierarchy of pathways enriched in proteins that showed either increased or decreased abundance across experimental conditions. The full set of proteins in these classifications is listed in **Tables S10-S15** in the Supplementary Data, with a detailed graphical representation of this ontology analysis shown in **Figures S4-S6**.

2.6. Analysis of PHB by methanolysis and GC-FID detection of methyl esters

This method was adapted from the protocol originally reported by Braunegg, et al.⁷¹ and modified by Ruiz, et al.⁷². In order to optimize reaction conditions, samples (either pure PHB or wet cell biomass) were firstly dissolved in 2 mL of CH₃OH with four concentrations [1%, 3%, 5% or 15% (v/v)] of H₂SO₄ and 2 mL of CHCl₃ in a screw-capped, Teflon-stoppered test tube. The solution was then incubated at 100°C for 4-6 h. After cooling to room temperature, 1 mL of a 1 M NaCl solution or water was added to the tubes, and the samples were shaken for 10 min. The two phases were separated by leaving the tubes at room temperature for 6 h without shaking.

The organic phase was collected in a new test tube and dried over 15 mg of anhydrous Na_2SO_4 prior to GC analysis, and benzoate (0.5 mg mL^{-1}) was included as internal standard compound in separate measurements. In the case of samples from bioreactor fermentations, the biomass was pelleted *via* centrifugation ($17,000\times g$ for 10 min) and lyophilized in a freeze drier for 24 h. For methanolysis, 5-10 mg of the dried biomass was treated with 2 mL of CH_3OH containing 15% (v/v) of H_2SO_4 and 2 mL of CHCl_3 , with benzoate as internal standard. The suspension was incubated at 100°C for 4 h and, after cooling to room temperature, 1 mL of water was added to each sample, mixed and centrifuged at $4,000\times g$ for 15 min to accelerate phase separation. The aqueous phase was discarded, and samples were additionally washed with 1 mL of water to remove any H_2SO_4 traces. After drying over Na_2SO_4 , the organic phase was then used for gas chromatography–flame ionization detection (GC-FID) analysis. These optimized conditions for extraction and methanolysis were kept for further experiments as they yielded consistent results across standards and experimental samples. A GC column BPX-5 (BGB Analytik, Rheinfelden, Germany; $30 \text{ m}\times 0.3 \text{ mm}\times 0.1 \mu\text{m}$) was used to separate the esterified monomers at 275°C as indicated elsewhere^{73,74}. Absolute amounts of PHB were determined by means of both the internal and the PHB standard, and expressed either as a concentration or as a percentage referred to the cell dry weight (CDW). A detailed explanation on how these values were calculated is provided in the Supplementary Data. Direct visualization of intracellular PHB granules was carried out by fluorescence microscopy after staining the cells with a $0.5 \mu\text{g mL}^{-1}$ Nile Red solution in dimethyl sulfoxide⁷⁵. Procedures for light field and fluorescence microscopy were done as described by Badianis, et al.¹⁷, and pictures were taken with a filter for Nile Red detection (excitation wavelength = 549 nm and emission wavelength = 628 nm).

2.7. Cultivation of *P. putida* strains in automated multi-parallel bioreactors

Batch bioreactor experiments were carried out in a 12-way AmbrTM 250 bioreactor system equipped with single-use, disposable bioreactors (microbial vessel type) in a fully automated platform (Sartorius Lab Instruments GmbH & Co. KG, Goettingen, Germany). The vessels were filled with 150-mL de

Bont minimal media containing 1% (w/v) glucose as the carbon source. The temperature was maintained at 30°C throughout the fermentation process and the agitation was set constant to 1,300 rpm. Airflow was kept at 1 vessel volume min^{-1} during the entire run and the pH was maintained at 7.0 by automatic addition of 2 N NaOH. All bioreactors were inoculated manually with 5 mL of a shaken-flask pre-culture with the same medium composition. Pre-cultures were harvested in exponential phase, and the initial OD_{600} of each bioreactor culture was normalized. Whenever needed, bioreactor cultures were added with cyclohexanone and 3-methylbenzoate (3-*mBz*) at 1 mM as chemical inducers of the ChnR/*P_{chnB}* and XylS/*P_m* expression systems, respectively, at 5 h post-inoculation. Samples were taken at the times indicated in the text for analytical determinations. The built-in Ambr™ 250 RunTime software and a fully integrated liquid handler was used to execute all process steps.

2.8. Data and statistical analysis

All the experiments reported were independently repeated at least three times (as indicated in the corresponding figure or table legend), and the mean value of the corresponding parameter \pm standard deviation is presented. When relevant, the level of significance of differences when comparing results was evaluated by ANOVA (Barlett's test, Prism 8, GraphPad software, San Diego, CA, USA) with a *P* value = 0.01, as indicated in the figure legends. *GRASP* was encoded and implemented in MATLAB™; the analysis was performed in Matlab R2018a. To compute feasible ranges of Gibbs free energy, the Gurobi Optimizer version 9.0.3 (build v9.0.3rc0) was used with the following parameters: optimality tolerance = 1×10^{-6} ; feasibility tolerance = 1×10^{-6} ; and integer feasibility tolerance = 1×10^{-5} . Each model was checked for linear stability using a threshold of the Jacobian's eigenvalues of 1×10^{-5} . For MCA, a step size of 1×10^{-10} was used. All data and code used in omic data analysis and kinetic model construction is freely available in GitHub (https://github.com/svevol/accoa_project_data_analysis).

Table 1. Bacterial strains and plasmids used in this study.

Bacterial strain	Relevant characteristics^a	Reference or source
<i>Escherichia coli</i>		
DH5 α λ <i>pir</i>	Cloning host; F ⁻ λ^- <i>endA1 glnX44(AS) thiE1 recA1 relA1 spoT1 gyrA96(Nal^R) rfbC1 deoR nupG Φ80(lacZΔM15) Δ(argF-lac)U169 hsdR17(rK⁻ mK⁺), λ<i>pir</i> lysogen</i>	Hanahan and Meselson ¹¹³
<i>Pseudomonas putida</i>		
KT2440	Wild-type strain, derived from <i>P. putida</i> mt-2 ¹¹⁴ cured of the catabolic TOL plasmid pWW0	Bagdasarian, et al. ¹¹⁵
EM42	Reduced-genome derivative of strain KT2440; Δ prophage1 Δ prophage4 Δ prophage3 Δ prophage2 Δ Tn7 Δ endA-1 Δ endA-2 Δ hsdRMS Δ flagellum Δ Tn4652	Martínez-García, et al. ⁸²
SEM1.3	Reduced-genome derivative of strain EM42; Δ phaC1ZC2DFI (Δ PP_5003-PP_5008) Δ benABCD (Δ PP_3161-PP_3164)	This work
Plasmid	Relevant characteristics^a	Reference or source
pMCRi	Plasmid for CRISPRi; <i>oriV</i> (pRO1600/ColE1), <i>xylS</i> (cured of <i>Bsa</i> I-sites), <i>Pm</i> \rightarrow <i>dCas9^{Sp}</i> , <i>P_{EM7}</i> \rightarrow sgRNA; Sm ^R /Sp ^R	Batianis, et al. ¹⁷
pMCRi_ <i>gltA</i>	Plasmid for CRISPRi; <i>oriV</i> (pRO1600/ColE1), <i>xylS</i> (cured of <i>Bsa</i> I-sites), <i>Pm</i> \rightarrow <i>dCas9^{Sp}</i> , <i>P_{EM7}</i> \rightarrow <i>gltA</i> -specific sgRNA; Sm ^R /Sp ^R	This work
pMCRi_ <i>accA</i>	Plasmid for CRISPRi; <i>oriV</i> (pRO1600/ColE1), <i>xylS</i> (cured of <i>Bsa</i> I-sites), <i>Pm</i> \rightarrow <i>dCas9^{Sp}</i> , <i>P_{EM7}</i> \rightarrow <i>accA</i> -specific sgRNA; Sm ^R /Sp ^R	This work
pMCRi_ <i>accC</i>	Plasmid for CRISPRi; <i>oriV</i> (pRO1600/ColE1), <i>xylS</i> (cured of <i>Bsa</i> I-sites), <i>Pm</i> \rightarrow <i>dCas9^{Sp}</i> , <i>P_{EM7}</i> \rightarrow <i>accC</i> -specific sgRNA; Sm ^R /Sp ^R	This work

pMCRi_ftsZ	Plasmid for CRISPRi; <i>oriV</i> (pRO1600/ColE1), <i>xylS</i> (cured of <i>BsaI</i> -sites), <i>Pm</i> → <i>dCas9^{Sp}</i> , <i>P_{EM7}</i> → <i>ftsZ</i> -specific sgRNA; Sm ^R /Sp ^R	Batianis, et al. ¹⁷
pMCRi_gltA_accA	Plasmid for dual CRISPRi; <i>oriV</i> (pRO1600/ColE1), <i>xylS</i> (cured of <i>BsaI</i> -sites), <i>Pm</i> → <i>dCas9^{Sp}</i> , <i>P_{EM7}</i> → <i>gltA</i> - and <i>accA</i> -specific sgRNAs; Sm ^R /Sp ^R	This work
pMCRi_gltA_accA_ftsZ	Plasmid for triple CRISPRi; <i>oriV</i> (pRO1600/ColE1), <i>xylS</i> (cured of <i>BsaI</i> -sites), <i>Pm</i> → <i>dCas9^{Sp}</i> , <i>P_{EM7}</i> → <i>gltA</i> -, <i>accA</i> - and <i>ftsZ</i> -specific sgRNAs; Sm ^R /Sp ^R	This work
pGNW2	Suicide vector used for deletions in Gram-negative bacteria; <i>oriT</i> , <i>traJ</i> , <i>lacZα</i> , <i>ori</i> (R6K), <i>P_{EM7}</i> → <i>msfGFP</i> ; Km ^R	Wirth, et al. ⁵⁸
pGNW2·Δ <i>benA-D</i>	Derivative of vector pGNW2 carrying homology regions to delete <i>benABCD</i> (<i>PP_3161-PP_3164</i>); Km ^R	Volke, et al. ⁵⁷
pGNW2·Δ <i>phaC-I</i>	Derivative of vector pGNW2 carrying homology regions to delete <i>phaC1ZC2DFI</i> (<i>PP_5003-PP_5008</i>); Km ^R	This work
pSEVA2311	Expression vector; <i>oriV</i> (pBBR1), <i>chnR</i> , <i>P_{chnB}</i> (standardized, cyclohexanone-responsive expression system); Km ^R	Benedetti, et al. ⁹³ ; Silva-Rocha, et al. ¹¹⁶
pS2311·PHA	Derivative of vector pSEVA2311; canonical PHB biosynthesis route; <i>P_{chnB}</i> → <i>phaCAB</i> from <i>Cupriavidus necator</i> , including synthetic RBSs in front of each gene	This work
pS2311·PHAS	Derivative of vector pSEVA2311; alternative, NphT7-dependent PHB biosynthesis route; <i>P_{chnB}</i> → <i>nphT7 phaCB</i> ; <i>phaCB</i> from <i>C. necator</i> and <i>nphT7</i> from <i>Streptomyces</i> sp. strain CL190, including synthetic RBSs in front of each gene	This work

^a Antibiotic markers and abbreviations: Km, kanamycin; Nal, nalidixic acid; Sm, streptomycin; and Sp, spectinomycin.

3. Results and Discussion

3.1. Metabolic control analysis using an updated kinetic model of *P. putida* KT2440 reveals key targets for manipulation towards increasing acetyl-CoA availability

Acetyl-CoA, a key intermediate in central carbon metabolism and essential building block for the majority of industrially relevant compounds, is highly interconnected to other metabolic nodes. We first explored which interventions hold most potential to increase acetyl-CoA availability in *P. putida* KT2440. To this end, we used *GRASP*⁵⁹ to build an ensemble of kinetic models representing the biochemical network of *P. putida* KT2440. The model proposed herein is focused on the reactions of central carbon metabolism, including comprehensive kinetic mechanisms. Building on the latest genome-scale metabolic reconstructions for strain KT2440^{41,69}, our core kinetic model comprising a detailed description of the reactions involved in glucose uptake (and oxidized derivatives of the sugar), glycolysis (embodied by the EDMP cycle), pentose phosphate pathway and tricarboxylic acid (TCA) cycle (**Figure 5.1, A** and **Table S4** in the Supplementary Data).

In addition, the model includes (i) three key reactions for fatty acid biosynthesis, which directly consume acetyl-CoA as the precursor or use this coenzyme as acyl donor (coded as ACCOAC, MCOATA and KAS15), (ii) two lumped reactions for oxidative phosphorylation (either NADH- or quinone-dependent) and (iii) five reactions for cofactor regeneration that ensure that their intracellular concentrations are balanced under (pseudo) steady-state conditions. In particular, ACCOAC represents the reaction of acetyl-CoA carboxylase, which provides malonyl-CoA as the key starter of fatty acid synthesis. MCOATA and KAS15 are reactions catalyzed by FabB [malonyl-CoA–acyl carrier protein (ACP) transacylase] and the FabH condensing enzyme, respectively. These reactions initiate the cycles of fatty acid elongation by condensing acyl-CoA primers with malonyl-ACP^{35,76}.

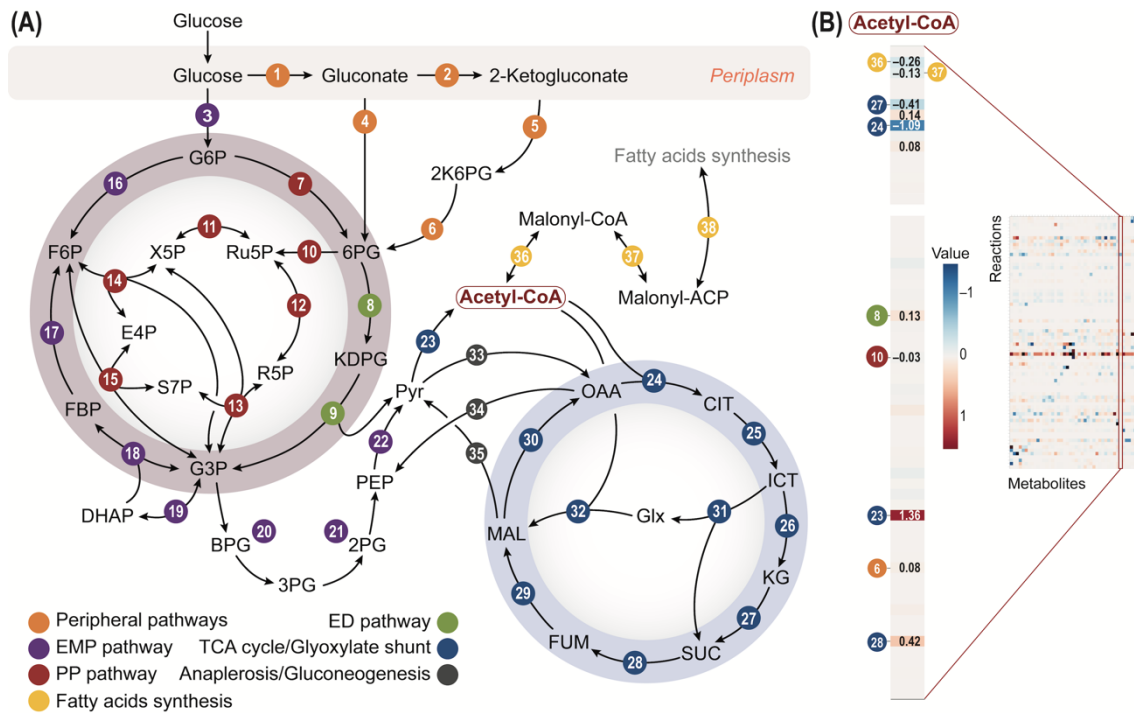


Figure 5.1. *In silico* analysis of metabolic nodes to increase acetyl-CoA availability in *P. putida*. (A) Biochemical network used to build the core kinetic model of *P. putida* towards exploring reactions that influence acetyl-CoA availability. The model includes the following modules: Embden-Meyerhof-Parnas (EMP) pathway, Entner-Doudoroff (ED) pathway, pentose phosphate (PP) pathway, tricarboxylic acids (TCA) cycle, as well as the glucose, gluconate and 2-ketogluconate uptake routes and gluconeogenesis^{47,62}. In addition, the kinetic reconstruction includes (i) fatty acid synthesis from malonyl-coenzyme A (CoA) (v_{37} and v_{38}), (ii) reactions involved in cofactor regeneration and (iii) two lumped reactions to model oxidative phosphorylation. The full list of reactions is provided in the Supplementary Data. Abbreviations for the metabolites in the network are as follows: G6P, glucose-6-P; F6P, fructose-6-P; FBP, fructose-1,6-P₂; DHAP, dihydroxyacetone-P; 6PG, 6-phosphogluconate; KDPG, 2-keto-3-deoxy-6-phosphogluconate; Ru5P, ribulose-5-P; R5P, ribose-5-P; X5P, xylulose-5-P; S7P, sedoheptulose-7-P; E4P, erythrose-4-P; G3P, glyceraldehyde-3-P; 3PG, glycerate-3-P; PEP, phosphoenolpyruvate; Pyr, pyruvate; Acetyl-CoA, acetyl-coenzyme A; Malonyl-CoA, malonyl-coenzyme A; OAA, oxaloacetate; CIT, citrate; ICT, isocitrate; KG, 2-ketoglutarate; SUC, succinate, FUM, fumarate; MAL, malate and Glx, glyoxylate. (B) Heatmap representing concentration control coefficient (CCC) values for acetyl-CoA for each reaction in the model, identified with the code number as in (A). In total, 78 reactions and 45 metabolites were accounted in the model. The detailed heatmap and the full list of all computed CCC values in the biochemical network is provided in **Figure S2** in the Supplementary Data.

Furthermore, and in order to increase the accuracy of the *in silico* predictions, the kinetic mechanism of 42 enzymes of central carbon metabolism in strain KT2440 was included in the reconstruction (**Table S4** and **S5** in the Supplementary Data). Moreover, the known regulatory patterns (e.g. allosteric inhibition or activation) for key enzymes [i.e., Zwf (glucose-6-P dehydrogenase), GntZ (6-phosphogluconate dehydrogenase), Edd (6-phosphogluconate dehydratase), Pyk (pyruvate kinase), the malic enzyme, isocitrate dehydrogenase and citrate synthase] were likewise added to the core model (**Table S6**). In order to find the steady-state distribution of the fluxes given the set of reactions included, the *i*JN1463 reconstruction⁶⁹ was analyzed by means of parsimonious enzyme usage flux balance analysis (pFBA)⁷⁷ with glucose as the carbon source. The model was constrained with the flux values obtained in glucose-grown *P. putida* KT2440⁴⁷. A consistency check was firstly implemented to validate the model (**Figure S1**) by evaluating *in silico* metabolic knock-outs (glucose transporter), knock-downs (Edd) and metabolic perturbations (ATP and NADPH deficiency). The results of these simulations showed a promising predictive power towards the specific metabolism of *P. putida* as reflected, for instance, in the time-resolved profile of normalized ATP, NADPH, acetyl-CoA and pyruvate concentrations (**Figure S1**), which followed previously reported experimental observations⁶². With this validated kinetic model at hand, we then ran metabolic control analysis (MCA) to identify reactions that affect acetyl-CoA availability (**Figure 5.1, B**, **Figure S2**) in the form of concentration control coefficients (CCC) for acetyl-CoA, thereby guiding the process of target evaluation.

Despite the high degree of interconnectivity of the acetyl-CoA node, only a few biochemical reactions were found to be responsible for significant changes of the steady-state concentration of the coenzyme. As indicated in (**Figure 5.1, B**), the reactions with the highest CCC absolute values were PDH (v_{23} , the pyruvate dehydrogenase complex, 1.36), AKGDH (v_{27} , α -ketoglutarate dehydrogenase, -0.41), CS (v_{24} , citrate synthase, -1.09), ACCOAC (v_{37} , acetyl-CoA carboxylase—one of the reactions explicitly added to the updated model, -0.26) and SUCDi (v_{28} , component of succinate dehydrogenase, 0.42). PDH is the only reaction in the model that produces acetyl-CoA, thus it had a high positive impact on the coenzyme concentration at steady-state; i.e., the higher the flux through PDH, the

higher the acetyl-CoA availability. Out of the several reactions that depleted acetyl-CoA, CS and ACCOAC had the most significant impact on the simulated coenzyme concentration. CS seemed to have a larger effect as compared to ACCOAC, which is likely due to the significantly higher flux through the former reaction over that of ACCOAC⁴⁷. Since malonyl-CoA is only needed at relatively low levels for lipid biosynthesis⁷⁸, the ACCOAC flux through is comparatively low. AKGDH, part of the TCA cycle, had a moderately negative impact on acetyl-CoA concentration as it consumes CoA, thus competing with PDH and impacting acetyl-CoA production. Interestingly, SUCDi showed a positive effect on the coenzyme availability, as a higher flux through SUCDi would redirect the carbon flow from the TCA cycle into gluconeogenesis (i.e., using the malic enzyme instead of malate dehydrogenase), which then leads to a higher flux through PDH by replenishing the pyruvate pool. Increasing the PDH flux by direct manipulation of the cognate genes, however, has proven very difficult due to the intricate regulatory patterns of this enzymatic complex⁴⁹, and we thus discarded this possibility. SUCDi, on the other hand, is a membrane complex, and overexpressing the cognate genes would be likewise tricky, potentially leading to protein aggregation. Therefore, the pFBA and CCC analyses herein pointed to two obvious metabolic targets for downregulation: CS (encoded by *gltA*, *PP_4194*) and ACCOAC (Acc, a complex with four subunits encoded by *accA*, *PP_1607*, *accB*, *PP_0559*, *accC*, *PP_0558* and *accD*, *PP_1996*). Both reactions are considered essential for cell survival in bacteria⁷⁹⁻⁸¹, and their elimination by gene knockouts is therefore not an option—which makes them attractive targets for CRISPRi-mediated transcriptional tuning of the cognate genes, as explained in the next section.

3.2. Single and dual CRISPRi-mediated knock-down balances acetyl-CoA levels in reduced-genome *P. putida* strains

We developed a series of 3-*mBz*-inducible CRISPRi plasmids (pMCRi) for tuning gene expression of single and multiple gene targets in *P. putida* (**Figure 5.2, A**). The direct cloning of spacers against different genes in vector pMCRi is facilitated by the introduction of *Bsa*I restriction sites, and the *dCas9* gene from *Streptococcus pyogenes* in this plasmid is placed under transcriptional control of the XylS/*Pm* expression system.

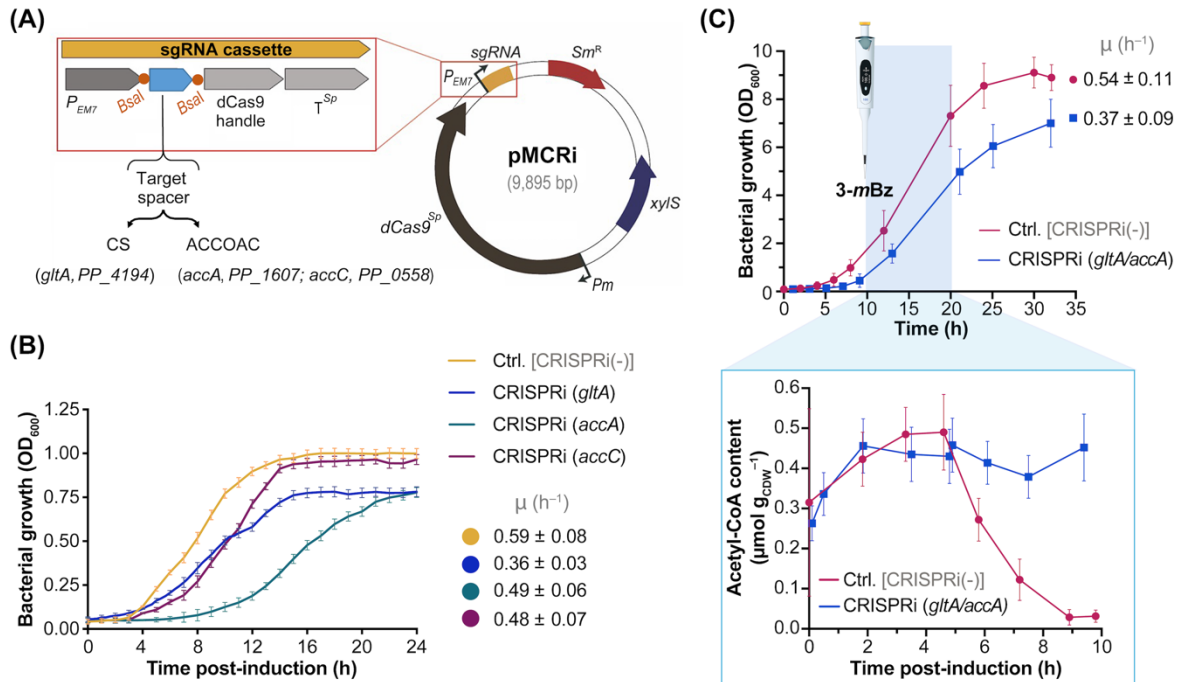


Figure 5.2. CRISPRi-mediated gene repression in *P. putida* for boosting acetyl-CoA availability.

(A) Schematic representation of vector pMCRi, used for single-guide RNA (sgRNA)-based, 3-methylbenzoate (3-*mBz*)-inducible CRISPRi. This streptomycin resistant (Sm^R)-vector contains $dCas9^{Sp}$ (dead Cas9 gene from *Streptococcus pyogenes*) under control of the XylIS/ P_m expression system and a constitutively-expressed sgRNA cassette. The sgRNA cassette is composed by the synthetic, constitutive P_{EM7} promoter followed by the sgRNA chimera, spanning three μ domains: a 20-nt region for target-specific binding, a 42-nt hairpin for dCas9 binding (dCas9 handle) and the native 40-nt transcription terminator (T^{Sp}) from *S. pyogenes*. Two *BsaI* recognition sites have been incorporated between the P_{EM7} promoter and the sgRNA cassette to facilitate cloning of target spacer. **(B)** *P. putida* SEM1.3 was transformed with the empty pMCRi vector [non-target spacer, indicated as CRISPRi(-) and used as a control (Ctrl.)] or with pMCRi plasmids carrying spacers against the *gltA*, *accA* and *accC* sequences (either in single- or multi-format, as indicated in the figure). The resulting strains were grown in microtiter plates in 200 μ L of de Bont minimal medium supplemented with 0.1% (w/v) glucose, 100 μ g mL⁻¹ Sm and 1 mM 3-*mBz* as inducer of the CRISPRi system. Specific growth rates (μ) were calculated during exponential growth based on the optical density at 600 nm (OD₆₀₀) profiles. **(C)** Growth and acetyl-CoA content in *P. putida* SEM1.3 with dual *accA* and *gltA* repression. Strains SEM 1.3/pMCRi and SEM 1.3/pMCRi_{*gltA**accA*} were grown in shaken-flask cultures in 50 mL of de Bont minimal medium supplemented with 1% (w/v) glucose, 100 μ g mL⁻¹ Sm and 1mM 3-*mBz* was added to the cultures at 10 h to induce CRISPRi-mediated transcriptional repression of *gltA* and *accA*. The acetyl-CoA content, normalized to the biomass (CDW, cell dry weight), was assessed by LC-MS/MS after rapid quenching of cells sampled from these cultures over 10 h after activation of the CRISPRi system.

In parallel, *P. putida* EM42, a reduced-genome derivative of strain KT2440⁸², was further refactored to facilitate the use of our CRISPRi toolbox towards establishing a platform strain for acetyl-CoA-dependent bioproduction. As *P. putida* metabolizes benzoates^{83,84}, resulting in the formation of brown-colored products [catechols and polymers thereof; Jiménez, et al.⁸⁵], the *benABCD* cluster was deleted in strain EM42 to abolish oxidation of 3-*mBz*. This operation rendered 3-*mBz* a gratuitous inducer of the XylS/*Pm* system and allowed for precise OD₆₀₀ measurements in the cultures without the interference typically caused by catechols and polymerization products. Additionally, since PHB biosynthesis was selected as a proxy of the intracellular acetyl-CoA availability, we removed the endogenous *pha* gene cluster, comprising *phaC1ZC2DFI*, to avoid any potential cross-talk between the synthetic PHB biosynthesis routes (described in the next section) and the native machinery for medium-chain-length PHAs formation, including regulatory and granule-associated proteins³⁵. This derivative of *P. putida* EM42, termed *P. putida* SEM1.3 (**Table 1**), was constructed by I-*SceI*—mediated recombination⁵⁸ and was used as a host in the experiments described below.

A set of pMCRi-derivative plasmids was constructed by cloning synthetic spacers against *gltA* (encodes CS), *accA* and *accC* (encoding the A and C subunits of the ACCOAC complex) or a combination of them (**Figure 5.2, A**). We focused on the first and the last reaction catalyzed by the ACCOAC complex, where AccA (carboxyltransferase) and AccC play a key role. The *accC* gene (encoding biotin carboxylase) forms an operon with *accB* (encoding a biotin carboxyl carrier protein), and blocking each gene individually would probably have a similar effect on the overall stoichiometry (hence, the activity) of the ACCOAC complex as shown in *E. coli*⁸⁶. The resulting plasmids were transferred to *P. putida* SEM1.3 (**Table 1**), and the growth profile of the recombinant strains was determined in de Bont minimal medium containing glucose as the carbon source in microtiter plate cultures (**Figure 5.2, B**). All strains harboring pMCRi plasmids with sgRNAs against *gltA*, *accA* or *accC* had a slower growth and achieved lower biomass densities by the end of the experiment than *P. putida* SEM1.3 transformed with the

control vector. The strongest effect on growth was seen for *P. putida* SEM1.3 with CRISPRi-mediated repression of *gltA* and *accA*. In these two cases, the specific growth rate (μ) was reduced by ca. 40% and 20%, respectively, with a final biomass density of ca. 80% of that in control cultures. Repressing *accC* expression, in contrast, had a negligible effect on the cell density—hence, this target was discarded in further CRISPRi experiments. The two most efficient sgRNAs were combined to build plasmid pMCRi_ *gltA_accA* for dual target repression (**Figure 5.2, C**). *P. putida* SEM1.3 carrying this plasmid had a reduction in μ values of ca. 30% in glucose cultures as compared to the control experiment, suggesting a synergistic (but not necessarily additive) effect of repressing the expression of *gltA* and *accA*. These *P. putida* strains, with a ‘rewired’ acetyl-CoA node by CRISPRi, were subjected to further analysis to unveil the metabolic determinants of the growth patterns observed. To this end, the metabolomic profile of rewired strains grown in shaken-flask cultures using glucose as the sole carbon source was monitored in a time-course LC-MS/MS experiment. The full metabolomic dataset, which includes 80 individual metabolites and cofactors within central carbon metabolism, is presented in **Figure S3** in the Supplementary Data.

We firstly focused on the intracellular acetyl-CoA levels of strain *P. putida* SEM1.3/pMCRi_ *gltA_accA*, with dual CRISPRi knock-down of the two metabolic targets that had the most significant effects on cell physiology (**Figure 5.2, C**). The growth profile of both the rewired strain and *P. putida* SEM1.3 transformed with the control vector mirrored the behavior observed in microtiter plate cultures. The control strain grew with $\mu = 0.54 \pm 0.11 \text{ h}^{-1}$, whereas the dually *gltA*- and *accA*-repressed strain had a $\mu = 0.37 \pm 0.09 \text{ h}^{-1}$, which was further accompanied with a reduction of ca. 25% in the final cell density. The acetyl-CoA levels in both strains followed a similar trend within the first 5 h after addition of 3-*mBz* to the cultures, reaching ca. 0.5 $\mu\text{mol gCDW}^{-1}$. After this point, however, the acetyl-CoA content trajectories diverged substantially. While *P. putida* SEM1.3/pMCRi_ *gltA_accA* exhibited coenzyme levels virtually constant over the whole time-course experiment (slightly fluctuating around 0.45 $\mu\text{mol gCDW}^{-1}$, and close to the maximal value indicated above), the acetyl-CoA content in the control strain decreased down to $< 0.05 \mu\text{mol gCDW}^{-1}$ at 10 h post-induction. Thus, the acetyl-CoA

content in the rewired strain remained at levels at least 8-fold higher than that in the control strain. This trend was accompanied by a similar behavior in the availability of some metabolites within the TCA cycle (downstream the acetyl-CoA node), especially α -ketoglutarate (**Figure S3** in the Supplementary Data). The isocitrate, malate and succinate content decreased as the cultivation progressed, as observed in rewired *P. putida* strains individually targeting *gltA* or *accA*. Oxaloacetate levels in the rewired strains increased upon activation of the CRISPRi system, as this metabolite is no longer condensed with acetyl-CoA to yield citrate, and then decreased at a later stage of the cultivation. In the upper metabolism, the 6-phosphogluconate content increased immediately after blocking *accA*; as did the glucose-6-P and fructose-6-P availability upon targeting either *gltA* or *accA*. These manipulations also affected the intracellular pool of some amino acids. CRISPRi-depletion of GltA, for instance, increased the pool of asparagine and (over time) methionine in a similar fashion as observed for oxaloacetate—the metabolite from which these amino acids derive. In addition to this phenomenon, the phenylalanine and tyrosine pools increased significantly (and stably) in rewired strains where *accA* was targeted. These examples show how the network-wide metabolome is fully reshaped upon activation of CRISPRi, providing clues for further manipulations towards bioproduction. Taken together, the quantitative physiology experiments and the metabolomic profiling indicate that the CRISPRi system against *gltA* and *accA* mediates an increase acetyl-CoA levels in *P. putida* SEM1.3. The next question was whether these manipulations elicited any significant changes in the proteome of the rewired strains.

3.3. Network-wide proteomic analysis reveals a substantial rewiring of central carbon metabolism upon transcriptional repression of *gltA* and *accA*

To study the potential changes in metabolism induced by dynamic transcriptional repression in *P. putida*, a comparative proteomic analysis was performed with strains with and without CRISPRi grown in glucose shaken-flask cultures. *P. putida* SEM1.3 carrying the pMCRi vector with a non-target sgRNA was used as a control, whereas strains with plasmids pMCRi_ *gltA*, pMCRi_ *accA* or pMCRi_ *accA_gltA*, mediating the repression of *gltA* and *accA* either individually or simultaneously, were the test groups. Based on the metabolomic analysis described in the previous section, samples were collected at 10 h after 3-*mBz* addition (i.e., 20 h after inoculation of the cultures). The protein abundance was compared in the different strains by taking the average values across biological replicates and normalizing the abundances to the control experimental group. **Figure 5.3** illustrates the normalized protein abundances plotted as heatmaps according to the topology of the biochemical network in **Figure 5.1, A**. A principal component analysis of all proteomic data (**Figure S54** in the Supplementary Data) indicated that the individual repression of *gltA* or *accA* resulted in significantly altered levels of 37 and 88 proteins, respectively, as compared with control experiments, with a tight false discovery rate < 0.01%. Interestingly, dual repression of both *gltA* and *accA* was accompanied by significant changes in the abundance of 332 proteins.

As expected, the proteins directly targeted by the CRISPRi system, GltA (CS) and AccA (the carboxyltransferase subunit of the ACCOAC complex), had a lower abundance in *P. putida* SEM1.3/pMCRi_ *gltA*, SEM1.3/pMCRi_ *accA* and SEM1.3/pMCRi_ *gltA_accA* as compared to the control experiment (**Figure 5.3**). In the dually-rewired strain, the abundance of both GltA and AccA was < 40% of that in the control *P. putida* strain. Other components of the ACCOAC complex, i.e., AccB (biotin-carboxyl carrier unit), AccC (biotin carboxylase subunit), and AccD (carboxyltransferase) had a relatively high abundance when the expression of *accA* was targeted by CRISPRi. This effect could be connected to a compensating phenomenon, similarly reported in *E. coli* when genes encoding the individual subunits of the ACCOAC complex are overexpressed⁸⁷.

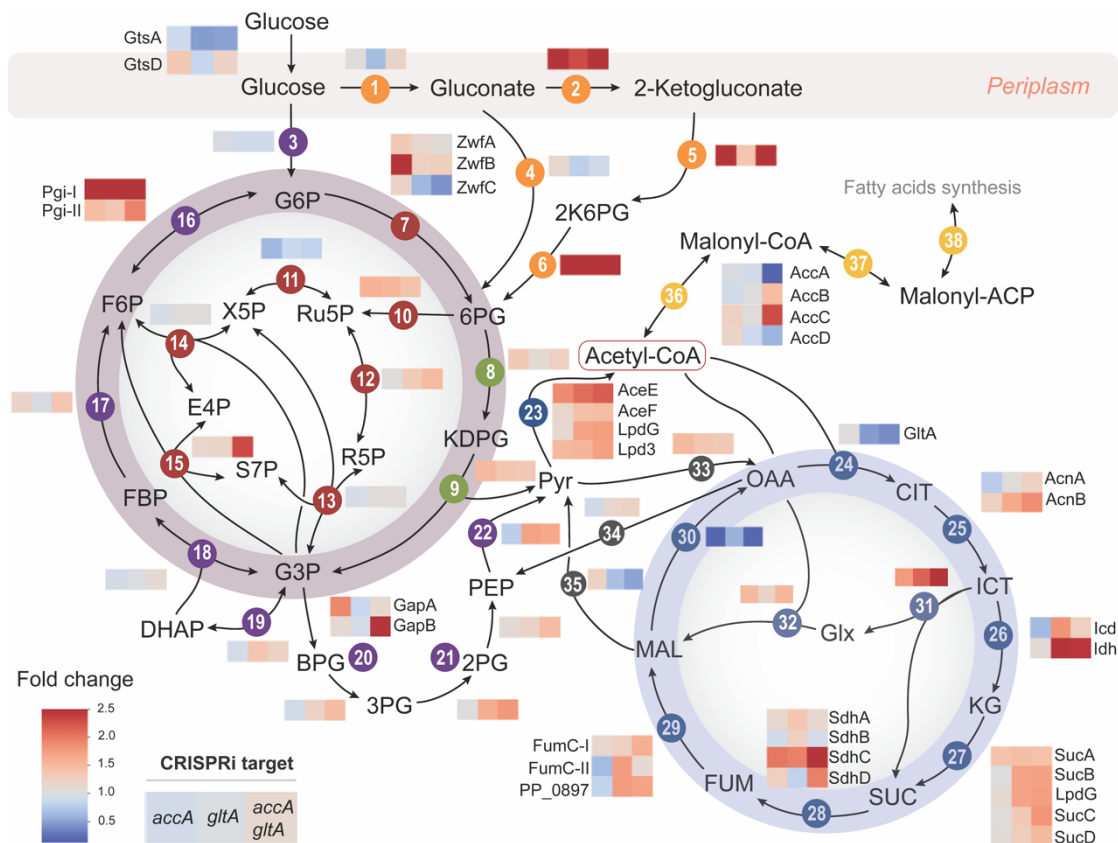


Figure 5.3. Comparative network-wide proteomic analysis of CRISPRi-rewired *P. putida* strains. Strain *P. putida* SEM1.3 carrying pMCRi plasmids targeting *accA*, *gltA* or both *accA* and *gltA*, were grown in de Bont minimal medium supplemented with 1% (w/v) glucose, 100 $\mu\text{g mL}^{-1}$ Sm and 1 mM 3-*m*Bz as inducer of the CRISPRi system. *P. putida* SEM1.3 transformed with the empty pMCRi vector (non-target spacer) was used as a control for normalization purposes. The relative protein abundance of enzymes within central carbon metabolism is shown in the plot according to their fold changes during exponential growth. Abundance values were averaged among three biological replicates and normalized to the control strain. When multiple isoforms exist for a given enzyme, they are represented separately, and the individual isozyme names are specified. The heatmap values are shaded to illustrate the effect of transcriptional *gltA* and/or *accA* repression on the respective protein abundance as grey, no impact; red, positive impact; and blue, negative impact.

Interestingly, the highest impact on the abundance of AccA was achieved when *gltA* and *accA* were targeted simultaneously. Such an additive effect was also observed in *P. denitrificans* engineered for 3-hydroxypropionic acid production⁸⁸. In this case, lowering the activities of the TCA cycle *via* cerulenin inhibition increased malonyl-CoA availability by modulating the flux through the ACCOAC complex. Beyond GltA and AccA themselves, we detected a general increase in the abundance of enzymes that could compensate for depletion of the two CRISPRi targets—especially when both of them were knocked-down simultaneously. Such was the case for components of the EDMP cycle [e.g., the gluconeogenic branch of the Embden-Meyerhof-Parnas (EMP) pathway, including fructose-1,6-P₂ bisphosphatase and glucose-6-P isomerase]. This proteomic pattern fits the observed increase in the steady-state glucose-6-P and fructose-6-P concentration, and also fructose-1,6-P₂ (**Figure S3** in the Supplementary Data). The peripheral glucose assimilation pathways through oxidation and phosphorylation, i.e., gluconate 2-dehydrogenase, 2-ketogluconate kinase and 2-ketogluconate-6-P reductase, which directly feeds the 6-phosphogluconate node⁸⁹, were likewise over-represented in rewired strains (which helps explaining the abundance of 6-phosphogluconate detected by metabolomics). The content of enzymes within both the glycolytic branch of the EMP pathway and the Entner-Doudoroff route were also increased (albeit slightly), which probably amplified the conversion of glucose (and their oxidized products) into pyruvate. Substrate availability could, in turn, result in an increase in the PDH complex components⁹⁰. Interestingly, overexpression of these genes was predicted to increase acetyl-CoA levels by the kinetic model of *P. putida* (**Figure 5.1, B**); hence, depleting GltA and AccA had an indirect effect on the PDH complex that further boosted acetyl-CoA availability in the rewired strains. The compensation effect was also detected in enzymes of the pyruvate shunt in the dually-repressed *P. putida* strain, which connects this metabolite and the TCA cycle in a GltA-independent fashion⁹¹—thus replenishing the lower catabolism to ensure ATP generation. The enzymes of the glyoxylate shunt were significantly affected by any these manipulations, probably reflecting a dearth of C2 units to feed the TCA cycle. Beyond

Taken together, the results of this network-wide proteomic analysis provide direct evidence of the tuning of protein abundance *via* CRISPRi, which results in diverted carbon fluxes towards enhanced levels of acetyl-CoA—and *P. putida* reacted to this perturbation by adjusting enzyme abundance (and likely, fluxes through them) in central carbon metabolism to counteract the depletion of GltA and AccA. Moreover, gene ontology enrichment analysis in this strain showed increased abundance of proteins in the metabolic routes involved in carbohydrate degradation and acetyl-CoA assimilation, such as purine and amino acid biosynthesis. The detailed gene ontology enrichment analysis is shown in the Supplementary Data (**Tables S10-S15** and **Figures S5-S7**). As an example, and consistently with previous observations at the level of metabolite profiling (**Figure S3** in the Supplementary Data), enzymes involved in aromatic amino acid biosynthesis had an increased abundance in strains depleted of AccA and GltA, either individually or combined. Enzymes involved in alginate accumulation were likewise over-produced in rewired *P. putida* strains, indicating re-routing of some intermediates (e.g. fructose-6-P, a precursor in the alginate biosynthesis pathway) into the formation of polymeric substances. Other pathway components, in contrast, were significantly downregulated upon interfering with GltA and AccA. A relevant example is the degradation of amino acids that yield acetyl-CoA and components of β -oxidation that would also result in the formation of C2 units for assimilation. In all, this state of affairs opens up the possibility of improving the synthesis of compounds derived from acetyl-CoA by introducing synthetic pathways that act as a sink for the coenzyme. For the next step of this study, we have chosen PHB accumulation as a model product to explore this hypothesis.

3.4. Design and construction of *P. putida* strains for PHB accumulation

Considering that PHB biosynthesis starts with acetyl-CoA as the precursor, we adopted this route as a proxy of the effects of rewiring metabolism *via* *gltA* and *accA* transcriptional repression. To this end, we designed two synthetic routes for PHB biosynthesis, based on either the canonical pathway of *Cupriavidus necator* or a malonyl-CoA shunt (**Figure 5.4, A**). The difference between the two synthetic pathways lies in the first step of the biochemical sequence: in the canonical pathway, two acetyl-CoA molecules are

condensed into acetoacetyl-CoA by PhaA, a 3-ketoacyl-CoA thiolase⁵¹. In the alternative route, this biochemical step is replaced by NphT7, an acetoacetyl-CoA synthase from *Streptomyces* sp. that irreversibly condenses acetyl-CoA and malonyl-CoA⁹². Hence, this topology enables a further layer of control on precursor availability around the acetyl-CoA and malonyl-CoA metabolic nodes. Using vector pSEVA2311 as the backbone [which bears the tightly regulated, cyclohexanone-inducible ChnR/*P_{chnB}* expression system⁹³], two plasmids were constructed for PHB synthesis (**Figure 5.4, B**). Plasmid pS2311-PHA contains the genes encoding the enzymes of the canonical PHB synthesis route (i.e., PhaC, PhaA and PhaB from *C. necator*), whereas the NphT7-dependent route is borne by plasmid pS2311-PHA, with *nphT7* replacing *phaA*. These plasmids confer PHB biosynthesis upon expression of the cognate genes in glucose cultures of both *E. coli* (data not shown) and *P. putida*, as discussed below.

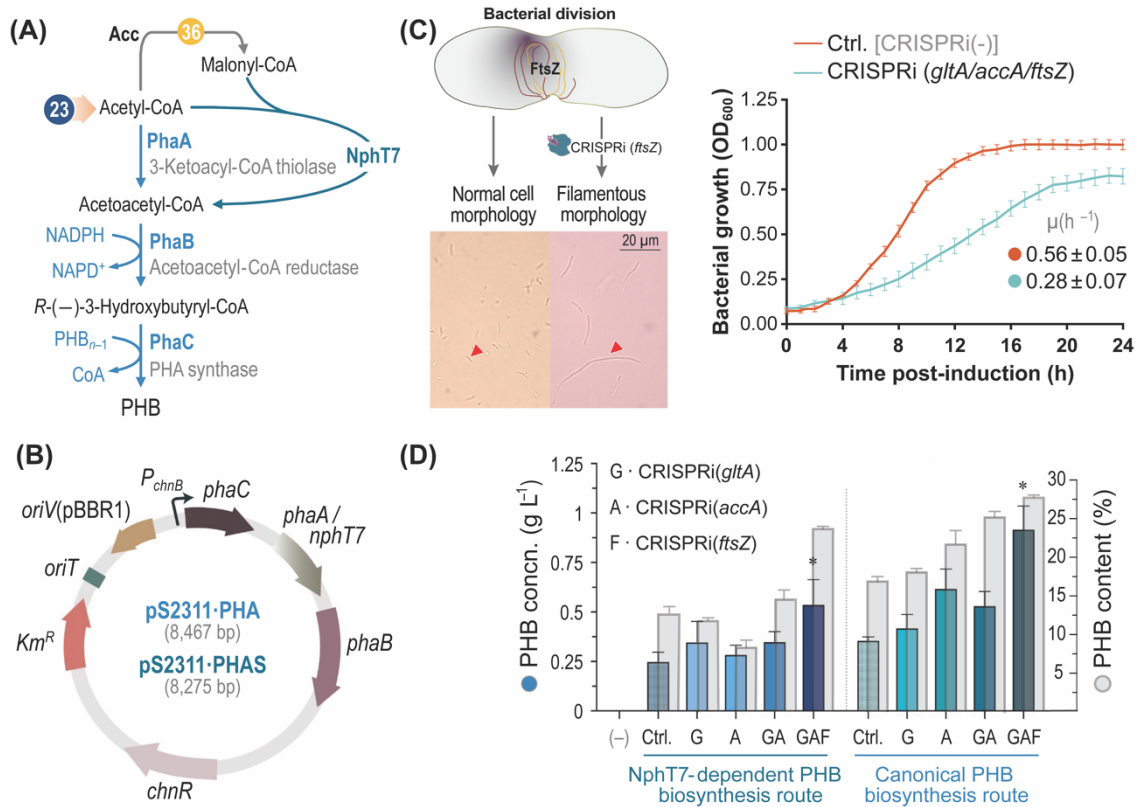


Figure 5.4. Engineering synthetic pathways for poly(3-hydroxybutyrate) (PHB) biosynthesis in *P. putida*. (A) Canonical and NphT7-dependent PHB biosynthesis routes. In the alternative route, NphT7 mediates the malonyl-CoA-dependent synthesis of acetoacetyl-CoA. The two key reactions producing or consuming acetyl-CoA (citrate synthase, *v*₂₃, and acetyl-CoA carboxylase, *v*₃₆, respectively) are identified with their code numbers as in **Figure 5.1** and were targeted by CRISPRi-mediated knock-down. (B) Scheme of plasmids constructed for acetyl-CoA-dependent PHB biosynthesis. The two synthetic pathways differ in the second gene (either *phaA* from *C. necator* in the canonical route or *nphT7* from *Streptomyces* sp. in the alternative route). In either case, the expression of the cognate genes, under control of the ChnR/*P_{chnB}* system, is triggered by addition of cyclohexanone to the culture medium. *Km^R*, kanamycin-resistance determinant. (C) FtsZ is involved in septum formation during bacterial division and was targeted for manipulating the architecture of PHB-producing *P. putida* cells. *P. putida* SEM1.3 was transformed with the empty pMCRi vector [non-target spacer, indicated as CRISPRi(-) and used as a control (Ctrl.)] or with pMCRi plasmids carrying spacers against the *gltA*, *accA* and *ftsZ* sequences. The resulting strains were grown in de Bont minimal medium

supplemented with 1% (w/v) glucose, 100 $\mu\text{g mL}^{-1}$ Sm and 1 mM 3-*mBz* as inducer of the CRISPRi system. Specific growth rates (μ) were calculated during exponential growth based on the optical density at 600 nm (OD_{600}) profiles. Pictures were taken after 15 h of induction with a Leica 2000 LED microscopy system at 100 \times resolution (F1 type immersion oil), and slanted red arrowheads indicate cells displaying a normal morphology or a filamentous phenotype bestowed by transcriptional repression of *ftsZ*. **(D)** PHB production experiments in shaken-flask cultures. *P. putida* SEM1.3 was transformed with a combination of PHB production- and CRISPRi-plasmids as indicated in the figure and grown in de Bont minimal medium supplemented with 1% (w/v) glucose, 50 $\mu\text{g mL}^{-1}$ Km, 100 $\mu\text{g mL}^{-1}$ Sm, 1 mM 3-*mBz* as inducer of the CRISPRi system and 1 mM cyclohexanone as trigger of PHB accumulation. *P. putida* SEM1.3 transformed with empty vectors (pSEVA2311 and pMCRi) was used as a negative control of accumulation (-), and *P. putida* SEM1.3 transformed with the corresponding PHB production plasmid and the empty pMCRi vector was used as a control of CRISPRi-mediated effects (Ctrl.). The PHB concentration (concn.) was calculated after 24 h of incubation by GC-FID analysis of methanolysed samples. The polymer content, expressed as the % (w/w) of CDW, is represented as grey columns. Bars represent the mean value of the PHB concn. or content \pm standard deviations of triplicate measurements from at least three independent experiments, and the asterisk symbol (*) identifies significant differences ($P < 0.01$) between cells carrying the triple-target CRISPRi system and the corresponding Ctrl. experiment.

Building on the use of CRISPRi as an approach to increase acetyl-CoA availability in rewired *P. putida* strains, we added an additional target to boost PHB accumulation. In this case, the knock-down strategy was directed towards cell shape, rather than metabolic targets, in order to tune synthetic morphologies of engineered bacteria⁹⁴. The bacterial fission ring protein FtsZ is a key player in the formation of the cell septum during the bacterial division process. Down-regulation of *ftsZ* results in the emergence of filamentous cells, which can be beneficial for compounds accumulating inside the cell, e.g., PHB and other polymers^{95,96}. Plasmid pMCRi_ *ftsZ* was constructed to target this gene (**Table 5.1**) and *P. putida* SEM1.3/pMCRi_ *ftsZ* cells acquired a long shape (up to 10-fold longer than normally shaped bacteria), filamentous phenotype upon induction of the CRISPRi with 3-*mBz* (**Figure 5.4, C**). The *ftsZ*-specific spacer was further introduced in plasmid pMCRi_ *gltA_accA_ftsZ*, which can be used to repress all three targets simultaneously. Following the trend observed for single- and dually-repressed genes, *P. putida* SEM1.3/pMCRi_ *gltA_accA_ftsZ* had a reduction in μ of 50% as compared to the control strain in glucose cultures added with 3-*mBz*, with final OD₆₀₀ values ranging around 70-80% of those for the control cultures (**Figure 5.4, C**). Cells sampled from these experiments showed an altered morphology, where most bacteria had a filamentous morphology (data not shown).

With these metabolic- and morphology engineering CRISPRi system at hand, the next objective was to validate their use for enhanced PHB biosynthesis in rewired *P. putida*. To this end, *P. putida* SEM1.3 was transformed with different combinations of plasmids conferring PHB biosynthesis and mediating CRISPRi of *gltA*, *accA* and *ftsZ* as indicated in **Figure 5.4, D**. Shaken-flask cultures of these rewired strains were run in de Bont minimal medium containing glucose as the only carbon source, and biomass and PHB production were measured after 24 h. No PHB accumulation could be detected in strain SEM1.3 carrying the empty pSEVA2311 and pMCRi vectors, used as a negative control here. In contrast, both the NphT7-dependent and the canonical pathways for PHB biosynthesis were effective for polymer accumulation in *P. putida* SEM1.3, with final PHB titers of 0.25 and 0.36 g L⁻¹, respectively. These figures correspond to a PHB content on biomass (on a CDW basis) of 13 and 18%,

respectively. Repressing single metabolic targets in *P. putida* SEM1.3 expressing the canonical pathway boosted PHB accumulation by ca. 30% (in the case of *accA* repression), and a combination of the two (i.e., *P. putida* SEM1.3/pS2311·PHA + pMCRi_*gltA_accA_ftsZ*) further increased the polymer titers by 1.4-fold as compared to those in the control experiment. Addition of the third spacer to the pMCRi plasmids (i.e., repressing *gltA*, *accA* and *ftsZ* simultaneously) further boosted PHB titers by 2.6-fold (reaching a final concentration of ca. 1 g L⁻¹) when compared with the strain without any CRISPRi intervention. A similar qualitative trend was observed in strains carrying the NphT7-dependent route (i.e., *P. putida* SEM1.3/pS2311·PHAS). In this case, the largest impact on PHB titers was brought about by repressing *gltA* that, together with the negligible effect of targeting *accA* on bioproduction, highlights the dual dependence of the NphT7 pathway on acetyl-CoA and malonyl-CoA. Furthermore, *P. putida* SEM1.3/pS2311·PHAS + pMCRi_*gltA_accA_ftsZ* had a 2.2-fold increase in the final PHB titer as compared to its control strain. These results underscore the positive impact of combining metabolic and morphology determinants as targets for CRISPRi—and they show that PHB accumulation can be adopted as a sensitive indicator of acetyl-CoA availability in *P. putida*. On this background, our next task was to study if the rewired strains can be used for acetyl-CoA-dependent biosynthesis in an industrially-relevant cultivation setup.

3.5. CRISPRi-assisted PHB production by rewired *P. putida* strains in an automated fermentation platform

Considering that few studies have demonstrated the use of CRISPRi as a strategy for increasing product titers and yields in bioreactor cultures, we tested the behavior of the rewired *P. putida* strains in a fully automated, multiplex bioreactor platform. The motivation was assessing if these strains can support consistent PHB biosynthesis during process upscaling while omitting irregularities caused by standard laboratory cultivation formats—where poorly controlled environmental conditions, e.g., pH, temperature drops and aeration, can contribute to significant variations in strain performance⁹⁷. To this end, we used the commercial Ambr™ 250 system for process development as a high-throughput, automated bioreactor

platform with 12 single-use, 250-mL mini-bioreactors (**Figure 5.5, A**)—maintaining the dissolved O_2 tension (dO_2) $>40\%$ and controlling the pH at 7 by automatic base addition. Five *P. putida* strains, derived from SEM1.3 and equipped with different plasmid combinations (i.e., pS2311·PHA and CRISPRi plasmids, **Figure 5.5, A**), were cultivated in batch-mode in de Bont minimal medium containing 1% (w/v) glucose as the sole carbon source. In these bioreactor experiments, all PHB-producing *P. putida* strains harbored the canonical biosynthesis pathway, selected according to the higher polymer titers it mediated in shaken-flask cultures (**Figure 5.4, D**). The dO_2 and carbon evolution rates (CER) trajectories were followed online during the entire cultivation period, and the resulting cultures were harvested after 24–48 h of fermentation for CDW and PHB analysis.

All strains followed a similar qualitative trend in terms of dO_2 and CER curves, indicative of bacterial growth and substrate consumption. The trajectories of *P. putida* SEM1.3 transformed with the empty vectors and the fully rewired strain (SEM1.3/pS2311·PHA + pMCRi_ *gltA_accA_fts*) illustrate this behavior (**Figure 5.5, B**). Cells started to grow exponentially upon inoculation, marked by a sharp drop in dO_2 accompanied by an increase in CER. Carbon exhaustion at ca. 12 h was signaled by the opposite trend— dO_2 spiked rapidly afterwards, and CO_2 was produced at very low CERs. Biomass and PHB were likewise determined in samples of these cultures (**Figure 5.5, C**). On one hand, *P. putida* SEM1.3/pS2311·PHA + empty pMCRi vector, the control strain, produced 0.27 g L^{-1} of PHB, which corresponds to a biopolymer accumulation of 17% (w/w) on a CDW basis—similarly to the results obtained in shaken-flask cultures (**Figure 5.4, D**). The rewired *P. putida* strains, on the other hand, featured increased PHB titers and polymer accumulation profiles. *P. putida* SEM1.3/pS2311·PHA + pMCRi_ *gltA_accA* reached a PHB concentration of 0.94 g L^{-1} , with a polymer accumulation of 28% (w/w). When synthetic morphology was also targeted by CRISPRi (i.e., cells carrying plasmid pMCRi_ *gltA_accA_fts*), the rewired strain *P. putida* produced 1.12 g L^{-1} of PHB—reaching the highest polymer accumulation of 32% (w/w), which corresponds to a 5-fold increase with respect to the control, non-CRISPRi strain.

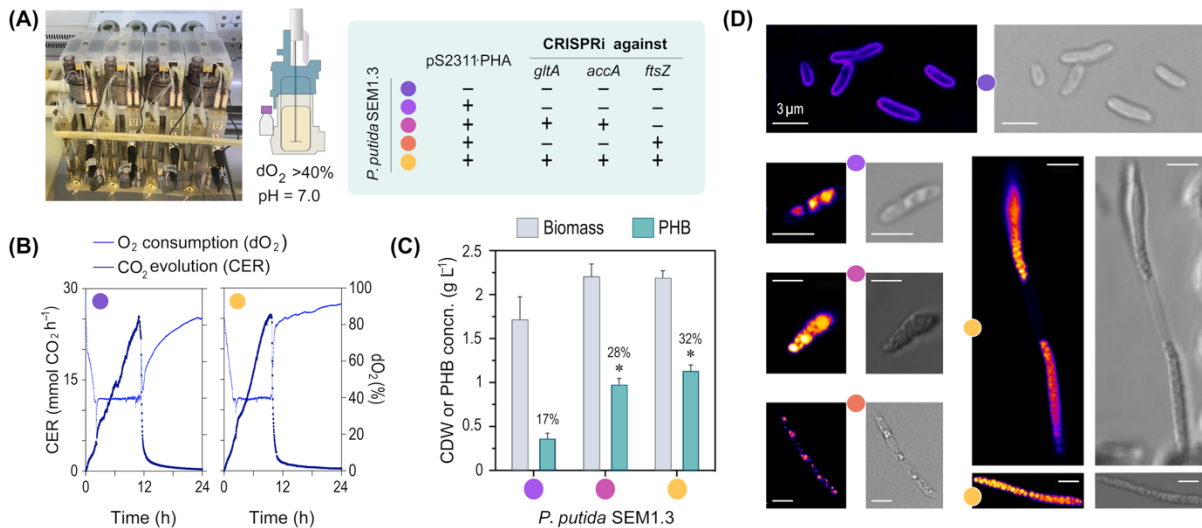


Figure 5.5. Poly(3-hydroxybutyrate) (PHB) biosynthesis in rewired *P. putida* strains in automated bioreactor cultures. (A) The Ambr™ 250 bioreactor system was used for controlled cultivation of the *P. putida* strains (derived from *P. putida* SEM1.3) indicated in the table. The same color code identifies the different strains in all panels of this figure. Batch-mode fermentations were carried out in de Bont minimal medium with 1% (w/v) glucose as the carbon source, 1 mM 3-*m*Bz for induction of the CRISPRi system, 1 mM cyclohexanone as a trigger of PHB biosynthesis, 100 μg mL⁻¹ streptomycin and 50 μg mL⁻¹ kanamycin. All fermentations were performed in independent biological triplicates, and the dissolved O₂ tension (dO₂) and pH were automatically controlled during the runs as indicated. (B) Representative fermentation profiles for two of the *P. putida* strains analyzed (control strain, and fully rewired *P. putida* SEM1.3). O₂ consumption (represented as the dO₂) and CO₂ evolution rates (CER) were recorded online with the built-in Ambr™ 250 bioreactor system software. (C) Biomass (cell dry weight, CDW) and PHB concentration (concn.) in cultures of rewired *P. putida* SEM1.3 at 24 h. Polymer accumulation is also shown as the PHB content in % (w/w) of the cell dry weight. Bars represent the mean value of either the CDW or PHB concns. ± standard deviations of triplicate measurements from at least three independent bioreactor experiments, the asterisk symbol (*) identifies significant differences ($P < 0.01$) with respect to *P. putida* SEM1.3/pS2311-PHA + empty pMCRi vector. (D) Morphology phenotypes of rewired *P. putida* SEM1.3 cells sampled from bioreactor cultures after 24 h. Representative pictures were taken in a high-resolution laser scanning confocal microscopy system after staining the cells with a 0.5 μg mL⁻¹ Nile Red solution to detect intracellular PHB granules⁷⁵. The scale of the microscopy pictures is shown with a white line and represents 3 μm in all cases.

High-resolution laser scanning confocal microscopy of *P. putida* cells harvested from these bioreactor cultures exposed bacterial phenotypes upon PHB accumulation (**Figure 5.5, D**). Intracellular PHB granules were dyed *in vivo* by using a viable-staining procedure. Expectedly, no PHB accumulation was observed in strain SEM1.3 carrying the empty pSEVA2311 and pMCRi vectors, used here as a negative control. Cells carrying plasmid pS2311-PHA, in contrast, accumulated amorphous PHB inclusions (easily discernable as bright orange spots in the cytoplasm). The effect of targeting the two metabolic enzymes (i.e., CS and ACCOAC) was clearly discernable in *P. putida* SEM1.3/pS2311-PHA + pMCRi_ *gltA_accA* cells, as the number and size of intracellular PHB inclusions was significantly increased when compared to the non-CRISPRi strain. Suppressing *ftsZ* expression had a strong impact on bacterial shape—as we could observe the elongated, filamentous cell phenotype previously detected by simpler, contrast-phase microscopy observation (**Figure 5.4, C**). Finally, fully rewired *P. putida* cells exhibited an altered morphology and were essentially filled with PHB inclusions—in agreement with the direct determination of PHB accumulation in samples from these cultures (**Figure 5.5, C**).

4. CONCLUSION

The unavoidable competition between biomass accumulation and production of target compounds is a well-recognized challenge in biomanufacturing—and such trade-off impacts (often, limiting) both product titers and bioprocess scalability⁹⁸. Such problem becomes particularly relevant for products derived from central metabolites, which could be either converted to biomass components or the compound(s) of interest. Thus, manipulating metabolic nodes to redirect fluxes from these central precursor metabolites towards bioproduction is key towards establishing robust cell factories⁴. Canonical approaches for prediction of potential targets for manipulation include flux balance analysis-guided methods based on genome-scale or kinetic models^{21,99-101}. Kinetic ensemble modelling has been recently shown to be very useful in predicting the impact of metabolic perturbations in *P. putida* KT2440¹⁰². The authors created a near-genome

scale kinetic model capable of capturing complex phenotypes (e.g., ATP demand and redox homeostasis) under different growth conditions and *via* the *in silico* implementation of key knock-outs. In this work, we focused on developing a kinetic model with focus on central carbon metabolism containing a detailed description of kinetic parameters. Our core kinetic model of central carbon metabolism of *P. putida* was developed by rationally integrating fluxomics, thermodynamics and metabolomics datasets in addition to manually-curated information of enzyme mechanisms, number of composing subunits, inhibitors and activators. The modelling strategy adopted herein highlighted the (surprisingly few) crucial reactions of central carbon metabolism that should be targeted to improve acetyl-CoA availability in *P. putida*. Knock-down of essential genes—e.g., *accA*, as suggested by the model—can only be performed by dynamic regulation of gene transcription¹⁰³. In this sense, CRISPRi emerged as a powerful technique to establish balanced metabolic networks with rerouted fluxes towards desired products, especially when genome-wide transcriptional regulation is required²³. In recent years, a variety of metabolic engineering applications leveraged CRISPRi to increase the titer and productivity of several primary and secondary bioproducts, e.g. terpenes¹⁰⁴, organic acids¹⁰⁵ and amino acids¹⁰⁶. We followed a similar approach by rewiring the acetyl-CoA node *via* CRISPRi—not only at the level of metabolic enzymes, but also to establish synthetic morphologies that facilitated the accumulation of an intracellular polymer (i.e. PHB, produced *via* two synthetic pathways). Our approach adds to some studies that showed how the manipulation of cell morphologies in engineered *E. coli* and *Halomonas* had a significant and positive effect on PHA accumulation^{107,108}. In these examples, CRISPRi was adopted to tamper with cell wall synthesis- or cell shape-determining proteins, as loosening the cells rigidity improved PHB accumulation^{109,110}. From a broader perspective, repressing the transcription of genes that encode key enzymes or structural proteins can be used to assess the interplay between essentiality towards decoupling growth from production of the desired compound(s). Strategies of this sort will also support the development of efficient bioprocesses at scale when using microbial species that are difficult to grow in high-cell-density (e.g., fed-batch) culture setups. Moreover, this type of combined, *in silico*-guided approaches will enable access to non-biological, added-value products^{111,112} as the expanding synthetic biology

toolbox facilitates the engineering of non-traditional cell factories towards *neo*-metabolism.

ACKNOWLEDGMENTS

We are thankful to Ivan Kulik, Suresh Sudarsan, Christoffer Knudsen and Milica Randelovic for experimental support, fruitful discussions and technical assistance. The financial support from The Novo Nordisk Foundation through grants NNF20CC0035580, *LiFe* (NNF18OC0034818) and *TARGET* (NNF21OC0067996), the Danish Council for Independent Research (*SWEET*, DFF-Research Project 8021-00039B), and the European Union's Horizon 2020 Research and Innovation Programme under grant agreement No. 814418 (*SinFonia*) to P.I.N. is gratefully acknowledged. E.K. and S.V. were supported by the Novo Nordisk Foundation (grant NNF17CC0026768) as part of the Copenhagen Bioscience Ph.D. Programme. M.P.M. acknowledges the support of the Novo Nordisk Foundation through a post-doctoral fellowship (grant NNF18OC0032314).

REFERENCES

- 1 Choi, K. R. *et al.* Systems metabolic engineering strategies: Integrating systems and synthetic biology with metabolic engineering. *Trends Biotechnol.* **37**, 817-837, doi:10.1016/j.tibtech.2019.01.003 (2019).
- 2 Ko, Y. S. *et al.* Tools and strategies of systems metabolic engineering for the development of microbial cell factories for chemical production. *Chem. Soc. Rev.* **49**, 4615-4636, doi:10.1039/D0CS00155D (2020).
- 3 Smanski, M. J. *et al.* Synthetic biology to access and expand nature's chemical diversity. *Nat. Rev. Microbiol.* **14**, 135-149, doi:10.1038/nrmicro.2015.24 (2016).
- 4 Nielsen, J. & Keasling, J. D. Engineering cellular metabolism. *Cell* **164**, 1185-1197, doi:10.1016/j.cell.2016.02.004 (2016).
- 5 Calero, P. & Nikel, P. I. Chasing bacterial *chassis* for metabolic engineering: A perspective review from classical to non-traditional microorganisms. *Microb. Biotechnol.* **12**, 98-124, doi:10.1111/1751-7915.13292 (2019).
- 6 Becker, J. & Wittmann, C. From systems biology to metabolically engineered cells—An omics perspective on the development of industrial microbes. *Curr. Opin. Microbiol.* **45**, 180-188, doi:10.1016/j.mib.2018.06.001 (2018).
- 7 Volkova, S., Matos, M. R. A., Mattanovich, M. & Marín de Mas, I. Metabolic modelling as a framework for metabolomics data integration and analysis. *Metabolites* **10**, 303, doi:10.3390/metabo10080303 (2020).
- 8 Fang, X., Lloyd, C. J. & Palsson, B. Ø. Reconstructing organisms *in silico*: genome-scale models and their emerging applications. *Nat. Rev. Microbiol.* **18**, 731-743, doi:10.1038/s41579-020-00440-4 (2020).
- 9 Nishida, K. & Kondo, A. CRISPR-derived genome editing technologies for metabolic engineering. *Metab. Eng.* **63**, 141-147, doi:10.1016/j.ymben.2020.12.002 (2020).
- 10 Shen, X., Wang, J., Li, C., Yuan, Q. & Yan, Y. Dynamic gene expression engineering as a tool in pathway engineering. *Curr. Opin. Biotechnol.* **59**, 122-129, doi:10.1016/j.copbio.2019.03.019 (2019).
- 11 Chen, Y., Banerjee, D., Mukhopadhyay, A. & Petzold, C. J. Systems and synthetic biology tools for advanced bioproduction hosts. *Curr. Opin. Biotechnol.* **64**, 101-109, doi:10.1016/j.copbio.2019.12.007 (2020).

- 12 Young, R., Haines, M., Storch, M. & Freemont, P. S. Combinatorial metabolic pathway assembly approaches and toolkits for modular assembly. *Metab. Eng.* **63**, 81-101, doi:10.1016/j.ymben.2020.12.001 (2021).
- 13 Lammens, E. M., Nickel, P. I. & Lavigne, R. Exploring the synthetic biology potential of bacteriophages for engineering non-model bacteria. *Nat. Commun.* **11**, 5294, doi:10.1038/s41467-020-19124-x (2020).
- 14 Jakočiūnas, T., Jensen, M. K. & Keasling, J. D. System-level perturbations of cell metabolism using CRISPR/Cas9. *Curr. Opin. Biotechnol.* **46**, 134-140, doi:10.1016/j.copbio.2017.03.014 (2017).
- 15 Zhao, D. *et al.* CRISPR-based metabolic pathway engineering. *Metab. Eng.* **63**, 148-159, doi:10.1016/j.ymben.2020.10.004 (2021).
- 16 Tarasava, K., Oh, E. J., Eckert, C. A. & Gill, R. T. CRISPR-enabled tools for engineering microbial genomes and phenotypes. *Biotechnol. J.* **13**, e1700586, doi:10.1002/biot.201700586 (2018).
- 17 Batianis, C. *et al.* An expanded CRISPRi toolbox for tunable control of gene expression in *Pseudomonas putida*. *Microb. Biotechnol.* **13**, 368-385, doi:10.1111/1751-7915.13533 (2020).
- 18 Weimer, A., Kohlstedt, M., Volke, D. C., Nickel, P. I. & Wittmann, C. Industrial biotechnology of *Pseudomonas putida*: Advances and prospects. *Appl. Microbiol. Biotechnol.* **104**, 7745-7766, doi:10.1007/s00253-020-10811-9 (2020).
- 19 Tan, S. Z., Reisch, C. R. & Prather, K. L. J. A robust CRISPR interference gene repression system in *Pseudomonas*. *J. Bacteriol.* **200**, e00575-00517, doi:10.1128/JB.00575-17 (2018).
- 20 Kim, S. K. *et al.* CRISPR interference-mediated gene regulation in *Pseudomonas putida* KT2440. *Microb. Biotechnol.* **13**, 210-221, doi:10.1111/1751-7915.13382 (2020).
- 21 Banerjee, D. *et al.* Genome-scale metabolic rewiring improves titers rates and yields of the non-native product indigoidine at scale. *Nat. Commun.* **11**, 5385, doi:10.1038/s41467-020-19171-4 (2020).
- 22 Schultenkämper, K., Brito, L. F. & Wendisch, V. F. Impact of CRISPR interference on strain development in biotechnology. *Biotechnol. Appl. Biochem.* **67**, 7-21, doi:10.1002/bab.1901 (2020).
- 23 Larson, M. H. *et al.* CRISPR interference (CRISPRi) for sequence-specific control of gene expression. *Nat. Protoc.* **8**, 2180-2196, doi:10.1038/nprot.2013.132 (2013).
- 24 Zhang, R., Xu, W., Shao, S. & Wang, Q. Gene silencing through CRISPR interference in bacteria: current advances and future

- prospects. *Front. Microbiol.* **12**, 635227, doi:10.3389/fmicb.2021.635227 (2021).
- 25 Xu, X. & Qi, L. S. A CRISPR-dCas toolbox for genetic engineering and synthetic biology. *J. Mol. Biol.* **431**, 34-47, doi:10.1016/j.jmb.2018.06.037 (2019).
- 26 Domínguez, A. A., Lim, W. A. & Qi, L. S. Beyond editing: repurposing CRISPR-Cas9 for precision genome regulation and interrogation. *Nat. Rev. Mol. Cell Biol.* **17**, 5-15, doi:10.1038/nrm.2015.2 (2016).
- 27 Gauttam, R., Mukhopadhyay, A., Simmons, B. A. & Singer, S. W. Development of dual-inducible duet-expression vectors for tunable gene expression control and CRISPR interference-based gene repression in *Pseudomonas putida* KT2440. *Microb. Biotechnol.*, doi:<https://doi.org/10.1111/1751-7915.13832> (2021).
- 28 Nikel, P. I. & de Lorenzo, V. *Pseudomonas putida* as a functional chassis for industrial biocatalysis: From native biochemistry to trans-metabolism. *Metab. Eng.* **50**, 142-155, doi:10.1016/j.ymben.2018.05.005 (2018).
- 29 Bitzenhofer, N. L. *et al.* Towards robust *Pseudomonas* cell factories to harbour novel biosynthetic pathways. *Essays Biochem.*, doi:10.1042/ebc20200173 (2021).
- 30 Akkaya, Ö., Pérez-Pantoja, D., Calles, B., Nikel, P. I. & de Lorenzo, V. The metabolic redox regime of *Pseudomonas putida* tunes its evolvability toward novel xenobiotic substrates. *mBio* **9**, e01512-01518, doi:10.1128/mBio.01512-18 (2018).
- 31 Volke, D. C., Calero, P. & Nikel, P. I. *Pseudomonas putida*. *Trends Microbiol.* **28**, 512-513, doi:10.1016/j.tim.2020.02.015 (2020).
- 32 Loeschcke, A. & Thies, S. *Pseudomonas putida*—A versatile host for the production of natural products. *Appl. Microbiol. Biotechnol.* **99**, 6197-6214, doi:10.1007/s00253-015-6745-4 (2015).
- 33 Bentley, G. J. *et al.* Engineering glucose metabolism for enhanced muconic acid production in *Pseudomonas putida* KT2440. *Metab. Eng.* **59**, 64-75, doi:10.1016/j.ymben.2020.01.001 (2020).
- 34 Eng, T. *et al.* Engineering *Pseudomonas putida* for efficient aromatic conversion to bioproduct using high throughput screening in a bioreactor. *Metab. Eng.* **66**, 229-238, doi:<https://doi.org/10.1016/j.ymben.2021.04.015> (2021).
- 35 Mezzina, M. P., Manoli, M. T., Prieto, M. A. & Nikel, P. I. Engineering native and synthetic pathways in *Pseudomonas putida* for the production of tailored polyhydroxyalkanoates. *Biotechnol. J.* **16**, 2000165, doi:10.1002/biot.202000165 (2021).

- 36 Prieto, M. A. *et al.* A holistic view of polyhydroxyalkanoate metabolism in *Pseudomonas putida*. *Environmental microbiology* **18**, 341-357, doi:10.1111/1462-2920.12760 (2016).
- 37 Salvachúa, D. *et al.* Metabolic engineering of *Pseudomonas putida* for increased polyhydroxyalkanoate production from lignin. *Microb. Biotechnol.* **13**, 290-298, doi:10.1111/1751-7915.13481 (2020).
- 38 Beckers, V., Poblete-Castro, I., Tomasch, J. & Wittmann, C. Integrated analysis of gene expression and metabolic fluxes in PHA-producing *Pseudomonas putida* grown on glycerol. *Microb. Cell Fact.* **15**, 73, doi:10.1186/s12934-016-0470-2 (2016).
- 39 Poblete-Castro, I., Wittmann, C. & Nikel, P. I. Biochemistry, genetics, and biotechnology of glycerol utilization in *Pseudomonas* species. *Microb. Biotechnol.* **13**, 32-53, doi:10.1111/1751-7915.13400 (2020).
- 40 Sudarsan, S., Dethlefsen, S., Blank, L. M., Siemann-Herzberg, M. & Schmid, A. The functional structure of central carbon metabolism in *Pseudomonas putida* KT2440. *Appl. Environ. Microbiol.* **80**, 5292-5303, doi:10.1128/AEM.01643-14 (2014).
- 41 Belda, E. *et al.* The revisited genome of *Pseudomonas putida* KT2440 enlightens its value as a robust metabolic chassis. *Environmental microbiology* **18**, 3403-3424, doi:10.1111/1462-2920.13230 (2016).
- 42 Chohnan, S., Furukawa, H., Fujio, T., Nishihara, H. & Takamura, Y. Changes in the size and composition of intracellular pools of nonesterified coenzyme A and coenzyme A thioesters in aerobic and facultatively anaerobic bacteria. *Appl. Environ. Microbiol.* **63**, 553-560 (1997).
- 43 Gläser, L. *et al.* A common approach for absolute quantification of short chain CoA thioesters in prokaryotic and eukaryotic microbes. *Microb. Cell Fact.* **19**, 160, doi:10.1186/s12934-020-01413-1 (2020).
- 44 Kiefer, D., Merkel, M., Lilge, L., Henkel, M. & Hausmann, R. From acetate to bio-based products: Underexploited potential for industrial biotechnology. *Trends Biotechnol.* **39**, 397-411, doi:<https://doi.org/10.1016/j.tibtech.2020.09.004> (2021).
- 45 Barajas, J. F., Blake-Hedges, J. M., Bailey, C. B., Curran, S. & Keasling, J. D. Engineered polyketides: Synergy between protein and host level engineering. *Synth. Syst. Biotechnol.* **2**, 147-166, doi:10.1016/j.synbio.2017.08.005 (2017).
- 46 Chavarria, M., Nikel, P. I., Pérez-Pantoja, D. & de Lorenzo, V. The Entner-Doudoroff pathway empowers *Pseudomonas putida* KT2440 with a high tolerance to oxidative stress. *Environmental microbiology* **15**, 1772-1785, doi:10.1111/1462-2920.12069 (2013).

- 47 Nikel, P. I., Chavarría, M., Fuhrer, T., Sauer, U. & de Lorenzo, V. *Pseudomonas putida* KT2440 strain metabolizes glucose through a cycle formed by enzymes of the Entner-Doudoroff, Embden-Meyerhof-Parnas, and pentose phosphate pathways. *J. Biol. Chem.* **290**, 25920-25932, doi:10.1074/jbc.M115.687749 (2015).
- 48 Sánchez-Pascuala, A., Fernández-Cabezón, L., de Lorenzo, V. & Nikel, P. I. Functional implementation of a linear glycolysis for sugar catabolism in *Pseudomonas putida*. *Metab. Eng.* **54**, 200-211, doi:10.1016/j.ymben.2019.04.005 (2019).
- 49 Ku, J. T., Chen, A. Y. & Lan, E. I. Metabolic engineering design strategies for increasing acetyl-CoA flux. *Metabolites* **10**, 166, doi:10.3390/metabo10040166 (2020).
- 50 Choi, S. Y. *et al.* Metabolic engineering for the synthesis of polyesters: A 100-year journey from polyhydroxyalkanoates to non-natural microbial polyesters. *Metab. Eng.* **58**, 47-81, doi:10.1016/j.ymben.2019.05.009 (2020).
- 51 Anderson, A. J. & Dawes, E. A. Occurrence, metabolism, metabolic role, and industrial uses of bacterial polyhydroxyalkanoates. *Microbiol. Rev.* **54**, 450-472 (1990).
- 52 Hartmans, S., Smits, J. P., van der Werf, M. J., Volkering, F. & de Bont, J. A. Metabolism of styrene oxide and 2-phenylethanol in the styrene-degrading *Xanthobacter* strain 124X. *Appl. Environ. Microbiol.* **55**, 2850-2855, doi:10.1128/aem.55.11.2850-2855.1989 (1989).
- 53 Cavaleiro, A. M., Kim, S. H., Seppälä, S., Nielsen, M. T. & Nørholm, M. H. Accurate DNA assembly and genome engineering with optimized uracil excision cloning. *ACS Synth. Biol.* **4**, 1042-1046, doi:10.1021/acssynbio.5b00113 (2015).
- 54 Genee, H. J. *et al.* Software-supported *USER* cloning strategies for site-directed mutagenesis and DNA assembly. *ACS Synth. Biol.* **4**, 342-349, doi:10.1021/sb500194z (2015).
- 55 Choi, Y. J. *et al.* Bestowing inducibility on the cloned methanol dehydrogenase promoter (P_{mxoF}) of *Methylobacterium extorquens* by applying regulatory elements of *Pseudomonas putida* F1. *Appl. Environ. Microbiol.* **72**, 7723-7729, doi:10.1128/AEM.02002-06 (2006).
- 56 Volke, D. C., Turlin, J., Mol, V. & Nikel, P. I. Physical decoupling of XylS/*Pm* regulatory elements and conditional proteolysis enable precise control of gene expression in *Pseudomonas putida*. *Microb. Biotechnol.* **13**, 222-232, doi:10.1111/1751-7915.13383 (2020).
- 57 Volke, D. C., Friis, L., Wirth, N. T., Turlin, J. & Nikel, P. I. Synthetic control of plasmid replication enables target- and self-curing of vectors

- and expedites genome engineering of *Pseudomonas putida*. *Metab. Eng. Commun.* **10**, e00126, doi:10.1016/j.mec.2020.e00126 (2020).
- 58 Wirth, N. T., Kozaeva, E. & Nikel, P. I. Accelerated genome engineering of *Pseudomonas putida* by I-SceI—mediated recombination and CRISPR-Cas9 counterselection. *Microb. Biotechnol.* **13**, 233-249, doi:10.1111/1751-7915.13396 (2020).
- 59 Saa, P. & Nielsen, L. K. A general framework for thermodynamically consistent parameterization and efficient sampling of enzymatic reactions. *PLoS Comput. Biol.* **11**, e1004195, doi:10.1371/journal.pcbi.1004195 (2015).
- 60 Cleland, W. W. The kinetics of enzyme-catalyzed reactions with two or more substrates or products. III. Prediction of initial velocity and inhibition patterns by inspection. *Biochim. Biophys. Acta* **67**, 188-196, doi:10.1016/0006-3002(63)91816-x (1963).
- 61 Tran, L. M., Rizk, M. L. & Liao, J. C. Ensemble modeling of metabolic networks. *Biophys. J.* **95**, 5606-5617, doi:10.1529/biophysj.108.135442 (2008).
- 62 Nikel, P. I. *et al.* Reconfiguration of metabolic fluxes in *Pseudomonas putida* as a response to sub-lethal oxidative stress. *ISME J.* **15**, 1751-1766, doi:10.1038/s41396-020-00884-9 (2021).
- 63 Flamholz, A., Noor, E., Bar-Even, A. & Milo, R. *eQuilibrator*—The biochemical thermodynamics calculator. *Nucleic Acids Res.* **40**, D770-775, doi:10.1093/nar/gkr874 (2012).
- 64 Rabinowitz, J. D. & Kimball, E. Acidic acetonitrile for cellular metabolome extraction from *Escherichia coli*. *Anal. Chem.* **79**, 6167-6173, doi:10.1021/ac070470c (2007).
- 65 McCloskey, D., Young, J. D., Xu, S., Palsson, B. Ø. & Feist, A. M. MID Max: LC-MS/MS method for measuring the precursor and product mass isotopomer distributions of metabolic intermediates and cofactors for metabolic flux analysis applications. *Anal. Chem.* **88**, 1362-1370, doi:10.1021/acs.analchem.5b03887 (2016).
- 66 Hunter, J. D. Matplotlib: A 2D graphics environment. *Computing Sci. Eng.* **9**, 90-95, doi:10.1109/MCSE.2007.55 (2007).
- 67 Bongers, M. *et al.* Adaptation of hydroxymethylbutenyl diphosphate reductase enables volatile isoprenoid production. *eLife* **9**, e48685, doi:10.7554/eLife.48685 (2020).
- 68 Ferreira, J. A. The Benjamini-Hochberg method in the case of discrete test statistics. *Int. J. Biostat.* **3**, Article 11, doi:10.2202/1557-4679.1065 (2007).
- 69 Nogales, J. *et al.* High-quality genome-scale metabolic modelling of *Pseudomonas putida* highlights its broad metabolic capabilities.

- Environmental microbiology* **22**, 255-269, doi:10.1111/1462-2920.14843 (2020).
- 70 Karp, P. D. *et al.* Computational Metabolomics Operations at BioCyc.org. *Metabolites* **5**, 291-310, doi:10.3390/metabo5020291 (2015).
- 71 Braunegg, G., Sonnleitner, B. & Lafferty, R. M. A rapid gas chromatographic method for the determination of poly- β -hydroxybutyric acid in microbial biomass. *Eur. J. Appl. Microbiol. Biotechnol.* **6**, 29-37, doi:10.1007/BF00500854 (1978).
- 72 Ruiz, J. A., Fernández, R. O., Nickel, P. I., Méndez, B. S. & Pettinari, M. J. *dye (arc)* Mutants: insights into an unexplained phenotype and its suppression by the synthesis of poly(3-hydroxybutyrate) in *Escherichia coli* recombinants. *FEMS Microbiol. Lett.* **258**, 55-60, doi:10.1111/j.1574-6968.2006.00196.x (2006).
- 73 Martínez-García, E., Aparicio, T., de Lorenzo, V. & Nickel, P. I. New transposon tools tailored for metabolic engineering of Gram-negative microbial cell factories. *Front. Bioeng. Biotechnol.* **2**, 46, doi:10.3389/fbioe.2014.00046 (2014).
- 74 Nickel, P. I., Pettinari, M. J., Galvagno, M. A. & Méndez, B. S. Poly(3-hydroxybutyrate) synthesis by recombinant *Escherichia coli arcA* mutants in microaerobiosis. *Appl. Environ. Microbiol.* **72**, 2614-2620, doi:10.1128/AEM.72.4.2614-2620.2006 (2006).
- 75 Spiekermann, P., Rehm, B. H., Kalscheuer, R., Baumeister, D. & Steinbüchel, A. A sensitive, viable-colony staining method using Nile red for direct screening of bacteria that accumulate polyhydroxyalkanoic acids and other lipid storage compounds. *Arch. Microbiol.* **171**, 73-80, doi:10.1007/s002030050681 (1999).
- 76 Thompson, M. G. *et al.* Fatty acid and alcohol metabolism in *Pseudomonas putida*: Functional analysis using random barcode transposon sequencing. *Appl. Environ. Microbiol.* **86**, e01665-01620, doi:10.1128/aem.01665-20 (2020).
- 77 Lewis, N. E. *et al.* Omic data from evolved *E. coli* are consistent with computed optimal growth from genome-scale models. *Mol. Syst. Biol.* **6**, 390, doi:<https://doi.org/10.1038/msb.2010.47> (2010).
- 78 Polyak, S. W., Abell, A. D., Wilce, M. C. J., Zhang, L. & Booker, G. W. Structure, function and selective inhibition of bacterial acetyl-CoA carboxylase. *Appl. Microbiol. Biotechnol.* **93**, 983-992, doi:10.1007/s00253-011-3796-z (2012).
- 79 Tovilla-Coutiño, D. B., Momany, C. & Eiteman, M. A. Engineered citrate synthase alters acetate accumulation in *Escherichia coli*. *Metab. Eng.* **61**, 171-180, doi:10.1016/j.ymben.2020.06.006 (2020).

- 80 Tokuyama, K. *et al.* Magnesium starvation improves production of malonyl-CoA-derived metabolites in *Escherichia coli*. *Metab. Eng.* **52**, 215-223, doi:10.1016/j.ymben.2018.12.002 (2019).
- 81 Udaondo, Z., Molina, L., Segura, A., Duque, E. & Ramos, J. L. Analysis of the core genome and pangenome of *Pseudomonas putida*. *Environmental microbiology* **18**, 3268-3283, doi:10.1111/1462-2920.13015 (2016).
- 82 Martínez-García, E., Nickel, P. I., Aparicio, T. & de Lorenzo, V. *Pseudomonas* 2.0: genetic upgrading of *P. putida* KT2440 as an enhanced host for heterologous gene expression. *Microb. Cell Fact.* **13**, 159, doi:10.1186/s12934-014-0159-3 (2014).
- 83 Feist, C. F. & Hegeman, G. D. Phenol and benzoate metabolism by *Pseudomonas putida*: regulation of tangential pathways. *J. Bacteriol.* **100**, 869-877, doi:10.1128/JB.100.2.869-877.1969 (1969).
- 84 Jiménez, J. I., Miñambres, B., García, J. L. & Díaz, E. Genomic analysis of the aromatic catabolic pathways from *Pseudomonas putida* KT2440. *Environmental microbiology* **4**, 824-841, doi:10.1046/j.1462-2920.2002.00370.x (2002).
- 85 Jiménez, J. I., Pérez-Pantoja, D., Chavarría, M., Díaz, E. & de Lorenzo, V. A second chromosomal copy of the *catA* gene endows *Pseudomonas putida* mt-2 with an enzymatic safety valve for excess of catechol. *Environmental microbiology* **16**, 1767-1778, doi:10.1111/1462-2920.12361 (2014).
- 86 Smith, A. C. & Cronan, J. E. Dimerization of the bacterial biotin carboxylase subunit is required for acetyl coenzyme A carboxylase activity *in vivo*. *J. Bacteriol.* **194**, 72-78, doi:10.1128/JB.06309-11 (2012).
- 87 Abdel-Hamid, A. M. & Cronan, J. E. Coordinate expression of the acetyl coenzyme A carboxylase genes, *accB* and *accC*, is necessary for normal regulation of biotin synthesis in *Escherichia coli*. *J. Bacteriol.* **189**, 369-376, doi:10.1128/JB.01373-06 (2007).
- 88 Zhou, S., Lama, S., Jiang, J., Sankaranarayanan, M. & Park, S. Use of acetate for the production of 3-hydroxypropionic acid by metabolically-engineered *Pseudomonas denitrificans*. *Bioresour. Technol.* **307**, 123194, doi:10.1016/j.biortech.2020.123194 (2020).
- 89 Volke, D. C., Olavarría, K. & Nickel, P. I. Cofactor specificity of glucose-6-phosphate dehydrogenase isozymes in *Pseudomonas putida* reveals a general principle underlying glycolytic strategies in bacteria. *mSystems* **6**, e00014-00021, doi:10.1128/mSystems.00014-21 (2021).

- 90 Patel, M. S., Nemeria, N. S., Furey, W. & Jordan, F. The pyruvate dehydrogenase complexes: structure-based function and regulation. *J. Biol. Chem.* **289**, 16615-16623, doi:10.1074/jbc.R114.563148 (2014).
- 91 Chavarria, M., Kleijn, R. J., Sauer, U., Pflüger-Grau, K. & de Lorenzo, V. Regulatory tasks of the phosphoenolpyruvate-phosphotransferase system of *Pseudomonas putida* in central carbon metabolism. *mBio* **3**, e00028-00012, doi:10.1128/mBio.00028-12 (2012).
- 92 Okamura, E., Tomita, T., Sawa, R., Nishiyama, M. & Kuzuyama, T. Unprecedented acetoacetyl-coenzyme A synthesizing enzyme of the thiolase superfamily involved in the mevalonate pathway. *Proc. Natl. Acad. Sci. USA* **107**, 11265-11270, doi:10.1073/pnas.1000532107 (2010).
- 93 Benedetti, I., de Lorenzo, V. & Nikel, P. I. Genetic programming of catalytic *Pseudomonas putida* biofilms for boosting biodegradation of haloalkanes. *Metab. Eng.* **33**, 109-118, doi:10.1016/j.ymben.2015.11.004 (2016).
- 94 Volke, D. C. & Nikel, P. I. Getting bacteria in shape: Synthetic morphology approaches for the design of efficient microbial cell factories. *Adv. Biosyst.* **2**, 1800111, doi:10.1002/adbi.201800111 (2018).
- 95 Tao, W., Lv, L. & Chen, G. Q. Engineering *Halomonas* species TD01 for enhanced polyhydroxyalkanoates synthesis via CRISPRi. *Microb. Cell Fact.* **16**, 48, doi:10.1186/s12934-017-0655-3 (2017).
- 96 Zhang, X., Lin, Y., Wu, Q., Wang, Y. & Chen, G. Q. Synthetic biology and genome-editing tools for improving PHA metabolic engineering. *Trends Biotechnol.* **38**, 689-700, doi:10.1016/j.tibtech.2019.10.006 (2020).
- 97 Hecht, A., Filliben, J., Munro, S. A. & Salit, M. A minimum information standard for reproducing bench-scale bacterial cell growth and productivity. *Commun. Biol.* **1**, 219, doi:10.1038/s42003-018-0220-6 (2018).
- 98 Fernández-Cabezón, L., Cros, A. & Nikel, P. I. Evolutionary approaches for engineering industrially-relevant phenotypes in bacterial cell factories. *Biotechnol. J.* **14**, 1800439, doi:10.1002/biot.201800439 (2019).
- 99 Lloyd, C. J. *et al.* COBRAME: A computational framework for genome-scale models of metabolism and gene expression. *PLoS Comput. Biol.* **14**, e1006302, doi:10.1371/journal.pcbi.1006302 (2018).

- 100 Maia, P., Rocha, M. & Rocha, I. *In silico* constraint-based strain optimization methods: The quest for optimal cell factories. *Microbiol. Mol. Biol. Rev.* **80**, 45-67, doi:10.1128/MMBR.00014-15 (2016).
- 101 Gopalakrishnan, S., Dash, S. & Maranas, C. K-FIT: An accelerated kinetic parameterization algorithm using steady-state fluxomic data. *Metab. Eng.* **61**, 197-205, doi:<https://doi.org/10.1016/j.ymben.2020.03.001> (2020).
- 102 Tokic, M., Hatzimanikatis, V. & Miskovic, L. Large-scale kinetic metabolic models of *Pseudomonas putida* KT2440 for consistent design of metabolic engineering strategies. *Biotechnol. Biofuels* **13**, 33, doi:10.1186/s13068-020-1665-7 (2020).
- 103 Brockman, I. M. & Prather, K. L. J. Dynamic knockdown of *E. coli* central metabolism for redirecting fluxes of primary metabolites. *Metab. Eng.* **28**, 104-113, doi:10.1016/j.ymben.2014.12.005 (2015).
- 104 Tao, S. *et al.* Regulation of ATP levels in *Escherichia coli* using CRISPR interference for enhanced pinocembrin production. *Microb. Cell Fact.* **17**, 147, doi:10.1186/s12934-018-0995-7 (2018).
- 105 Woolston, B. M., Emerson, D. F., Currie, D. H. & Stephanopoulos, G. Rediverting carbon flux in *Clostridium ljungdahlii* using CRISPR interference (CRISPRi). *Metab. Eng.* **48**, 243-253, doi:10.1016/j.ymben.2018.06.006 (2018).
- 106 Cleto, S., Jensen, J. V., Wendisch, V. F. & Lu, T. K. *Corynebacterium glutamicum* metabolic engineering with CRISPR interference (CRISPRi). *ACS Synth. Biol.* **5**, 375-385, doi:10.1021/acssynbio.5b00216 (2016).
- 107 Jiang, X. R. & Chen, G. Q. Morphology engineering of bacteria for bio-production. *Biotechnol. Adv.* **34**, 435-440, doi:<https://doi.org/10.1016/j.biotechadv.2015.12.007> (2016).
- 108 Jiang, X. R., Wang, H., Shen, R. & Chen, G. Q. Engineering the bacterial shapes for enhanced inclusion bodies accumulation. *Metab. Eng.* **29**, 227-237, doi:<https://doi.org/10.1016/j.ymben.2015.03.017> (2015).
- 109 Zhang, X. C. *et al.* Engineering cell wall synthesis mechanism for enhanced PHB accumulation in *E. coli*. *Metab. Eng.* **45**, 32-42, doi:10.1016/j.ymben.2017.11.010 (2018).
- 110 Chen, G. Q. & Jiang, X. R. Engineering microorganisms for improving polyhydroxyalkanoate biosynthesis. *Curr. Opin. Biotechnol.* **53**, 20-25, doi:10.1016/j.copbio.2017.10.008 (2017).
- 111 Nieto-Domínguez, M. & Nikel, P. I. Intersecting xenobiology and *neo*-metabolism to bring novel chemistries to life. *ChemBioChem* **21**, 2551-2571, doi:10.1002/cbic.202000091 (2020).

- 112 Calero, P. *et al.* A fluoride-responsive genetic circuit enables *in vivo* biofluorination in engineered *Pseudomonas putida*. *Nat. Commun.* **11**, 5045, doi:10.1038/s41467-020-18813-x (2020).
- 113 Hanahan, D. & Meselson, M. Plasmid screening at high colony density. *Methods Enzymol.* **100**, 333-342 (1983).
- 114 Worsey, M.J. & Williams, P. A. Metabolism of toluene and xylenes by *Pseudomonas putida (arvilla)* mt-2: evidence for a new function of the TOL plasmid. *J. Bacteriol.* **124**, 7-13 (1975).
- 115 Bagdasarian, M. *et al.* Specific purpose plasmid cloning vectors. II. Broad host range, high copy number, RSF1010-derived vectors, and a host-vector system for gene cloning in *Pseudomonas*. *Gene* **16**, 237-247, doi:10.1016/0378-1119(81)90080-9 (1981).
- 116 Silva-Rocha, R. *et al.* The Standard European Vector Architecture (SEVA): a coherent platform for the analysis and deployment of complex prokaryotic phenotypes. *Nucleic Acids Res.* **41**, D666-D675, doi:10.1093/nar/gks1119 (2013).

Supplementary Data

Table S1. Composition of de Bont minimal medium.

Component	Final concentration
K_2HPO_4	3.88 g L ⁻¹
NaH_2PO_4	1.63 g L ⁻¹
$(NH_4)_2SO_4$	2 g L ⁻¹
$MgCl_2 \cdot 6H_2O$	0.1 g L ⁻¹
EDTA	10 mg L ⁻¹
$ZnSO_4 \cdot 7H_2O$	2 mg L ⁻¹
$CaCl_2 \cdot 2H_2O$	1 mg L ⁻¹
$FeSO_4 \cdot 7H_2O$	5 mg L ⁻¹
$Na_2MoO_4 \cdot 2H_2O$	0.2 mg L ⁻¹
$CuSO_4 \cdot 5H_2O$	0.2 mg L ⁻¹
$CoCl_2 \cdot 6H_2O$	0.4 mg L ⁻¹
$MnCl_2 \cdot 2H_2O$	1 mg L ⁻¹

Table S2. Oligonucleotides used in this work.

Number	Name	Sequence (5'→3')	Application
1	HR1-PHA_F	AGA TCC UCC TGC AGT TCG GCA AGA TCA ACG T	Verifying the deletion of the <i>phaC1ZC2DFI</i> cluster in <i>P. putida</i> SEM1.3
2	HR1-PHA_R	ATG CAT CUA CGA CGC TCC GTT GTC CTG AGA	
3	HR2-PHA_F	AGA TGC AUG CTG TGT ACC TCA TGC TCA T	
4	HR2-PHA_R	AGG TCG ACU AAC ACA TGG GGT GGG CTG AT	
5	HR1_ <i>benABCD</i> _F	ACC CTG GCC AUG TGA ACC GCA ACC TCA AGG CAA A	Verifying the deletion of the <i>benABCD</i> cluster in <i>P. putida</i> SEM1.3
6	HR1_ <i>benABCD</i> _R	ACT TAT UCG TTC ATC AGT GCC ACG GC	
7	HR2_ <i>benABCD</i> _F	AGG CGG UTT ATT TAC CAA GCG ATG GGG A	
8	HR2_ <i>benABCD</i> _R	AGC GTC ACA UGG CCA GGG TCT CCC TTG T	
9	pGNW2_ <i>benABC</i> <i>D</i> _F	AAT AAG UCG ACC TGC AGG CAT GCA A	Constructing the suicide plasmid for deletion of the <i>benABCD</i> cluster
10	pGNW2_ <i>benABC</i> <i>D</i> _R	ACC GCC UAG AGG ATC CCC GGG TAC CG	
11	<i>phaCAB</i> _pSEVA_ F	AAA AAC AUA TGG CGA CCG GCA AAG GC	USER cloning of <i>phaC</i> , <i>phaA</i> and <i>phaB</i> in vector pSEVA2311; synthetic RBSs for each gene were added in the oligonucleotide sequences
12	<i>phaC</i> _R	ATG TTT TTC CUC CTG AAT TCT CAT GCC TTG GCT TTG ACG TAT CGC	
13	<i>phaA</i> _F	AGG AAA AAC AUA TGA CTG ACG TTG TCA TCG TAT C	
14	<i>phaA</i> _R	ATG TTT TUC CTC CTG AAT TCT TAT TTG CGC TCG ACT GCC	
15	<i>phaB</i> _F	AAA AAC AUA TGA CTC AGC GCA TTG CGT AT	

16	<i>phaCAB_pSEVA_R</i>	AGG ATC CUC AGC CCA TAT GCA GGC CG	
17	<i>nphT7_F</i>	AGG AAA AAC AUA TGA CGG ATG TGC GGT TCC GTA T	USER cloning of <i>nphT7</i> , amplified from a synthetic gene
18	<i>nphT7_R</i>	ATG TTT TUC CTC CTG AAT TCC TAC CAT TCG ATC AGG GCG AAG G	
19	pS2311:: <i>phaB_F</i>	AAA AAC AUA TGA CTC AGC GCA TTG CGT AT	USER cloning of <i>phaB</i> , <i>nphT7</i> and <i>phaC</i> in vector pSEVA2311
20	pS2311:: <i>phaC_R</i>	ATG TTT TTC CUC CTG AAT TCT CAT GCC TTG GCT TTG ACG TAT CGC	
21	<i>accA-spacer_F</i>	GCG CGG TTC GAA GTC GAG GAA ATT C	Cloning of spacers for sgRNA in pMCRI-based vectors with overhangs for <i>Bsal</i> -assisted restriction-ligation
22	<i>accA-spacer_R</i>	AAA CGA ATT TCC TCG ACT TCG AAC C	
23	<i>accC-spacer_F</i>	GCG CGT TTC CCC GCG GTT GGC GAT C	
24	<i>accC-spacer_R</i>	AAA CGA TCG CCA ACC GCG GGG AAA C	
25	<i>gltA-spacer_F</i>	GCG CGT AAA ATG GGC AGC TCG ACG G	
26	<i>gltA-spacer_R</i>	AAA CCC GTC GAG CTG CCC ATT TTA C	

Table S3. Components of the biochemical network of *Pseudomonas putida* KT2440^a.

Block	Code	Reaction	Enzyme(s)	Name(s) and PP number(s)
Peripheral pathways	1	Glucose + Ubiquinone → Glucono-1,5-lactone + Ubiquinol	Glucose dehydrogenase	Gcd (PP_1444)
		Glucono-1,5-lactone + H ₂ O → Gluconate + H ⁺	Gluconolactonase	Gnl (PP_1170)
	2	Gluconate + Ubiquinone → 2-Ketogluconate + Ubiquinol	Gluconate 2-dehydrogenase	PP_3382 PP_3383 PP_3384
	4	Gluconate + ATP → 6PG + ADP + H ⁺	Gluconate kinase	GnuK (PP_3416)
	5	2-Ketogluconate + ATP → 2K6PG + ADP + H ⁺	2-Ketogluco- kinase	KguK (PP_3378)
	6	2K6PG + NADPH + H ⁺ → 6PG + NADP ⁺	2-Ketogluconate-6- phosphate reductase	KguD (PP_3376)
Pentose phosphate pathway	7	G6P + NADP ⁺ → 6-Phosphoglucono-1,5-lactone + NADPH + H ⁺	Glucose-6-phosphate 1-dehydrogenase	ZwfA (PP_1022) ZwfB (PP_4042) Zwf (PP_5351)
		6-Phosphoglucono-1,5-lactone + H ₂ O → 6PG + H ⁺	6-Phospho- gluconolactonase	Pgl (PP_1023)
	10	6PG + NADP ⁺ → Ru5P + NADPH + CO ₂	6-Phosphogluconate dehydrogenase	GntZ (PP_4043)
	11	Ru5P ↔ Xu5P	Ribulose-5-phosphate 3-epimerase	Rpe (PP_0415)
	12	Ru5P ↔ Ri5P	Ribose-5-phosphate isomerase	RpiA (PP_5150)
	13	Xu5P + R5P ↔ S7P + G3P	Transketolase	TktA (PP_4965)
	14	Xu5P + E4P ↔ G3P + F6P		
15	S7P + G3P ↔ E4P + F6P	Transaldolase	Tal (PP_2168)	
Entner-Doudoroff pathway	8	6PG → KDPG + H ₂ O	6-Phosphogluconate dehydratase	Edd (PP_1010)
	9	KDPG → G3P + Pyr	2-Keto-3-deoxy-6- phosphogluconate aldolase	Eda (PP_1024)

Embden-Meyerhof-Parnas pathway	3	$\text{Glucose} + \text{ATP} \rightarrow \text{G6P} + \text{ADP} + \text{H}^+$	Glucokinase	Glk (PP_1011)
	16	$\text{G6P} \rightarrow \text{F6P}$	Glucose-6-phosphate isomerase	Pgi-I (PP_1808) Pgi-II (PP_4701)
	17	$\text{FBP} + \text{H}_2\text{O} + \text{ADP} \rightarrow \text{F6P} + \text{ATP}$	Fructose-1,6-bisphosphatase	Fbp (PP_5040)
	18	$\text{DHAP} + \text{G3P} \leftrightarrow \text{FBP}$	Fructose-1,6-bisphosphate aldolase	Fda (PP_4960) PP_2871 PP_3224
	19	$\text{G3P} \leftrightarrow \text{DHAP}$	Triose phosphate isomerase	TpiA (PP_4715)
	20	$\text{G3P} + \text{NAD}^+ + \text{Pi} \rightarrow$ $1,3\text{-Bisphosphoglycerate} + \text{NADH} + \text{H}^+$	Glyceraldehyde-3-phosphate dehydrogenase	GapA (PP_1009) GapB (PP_2149) PP_0665 PP_3443
		$1,3\text{-Bisphosphoglycerate} + \text{ADP} \rightarrow$ $3\text{PG} + \text{ATP}$	Phosphoglycerate kinase	Pgk (PP_4963)
	21	$3\text{PG} \rightarrow 2\text{PG}$	Phosphoglycerate mutase	Gpml (PP_5056) PP_2243 PP_3923 PP_4450
		$2\text{PG} \rightarrow \text{PEP} + \text{H}_2\text{O}$	Enolase	Eno (PP_1612)
	22	$\text{PEP} + \text{ADP} + \text{H}^+ \rightarrow \text{Pyr} + \text{ATP}$	Pyruvate kinase	PykA (PP_1362) Pyk (PP_4301)
Tricarboxylic acid cycle / Glyoxylate shunt	23	$\text{Pyr} + \text{NAD}^+ + \text{Coenzyme A} \rightarrow$ $\text{AcCoA} + \text{NADH} + \text{CO}_2$	Pyruvate dehydrogenase	AcoA (PP_0555) AcoC (PP_0553) AceF (PP_0338) AceE (PP_0339)
	24	$\text{OAA} + \text{AcCoA} + \text{H}_2\text{O}$ $\rightarrow \text{CIT} + \text{Coenzyme A} + \text{H}^+$	Citrate synthase	GlhA (PP_4194)

Tricarboxylic acid cycle / Glyoxylate shunt	26	$ICT + NADP^+ \rightarrow KG + CO_2 + NADPH + H^+$	Isocitrate dehydrogenase	Icd (PP_4011) Idh (PP_4012)
	27	$KG + \text{Coenzyme A} + NAD^+ \rightarrow$ $\text{Succinyl-Coenzyme A} + NADH + H^+ + CO_2$	α -Ketoglutarate dehydrogenase	Lpd (PP_5366) LpdG (PP_4187) LpdV (PP_4404) SucA (PP_4189) SucB (PP_4188) PP2652 PP3662
		$\text{Succinyl-Coenzyme A} + ADP + Pi \rightarrow$ $SUC + \text{Coenzyme A} + ATP$	Succinyl-coenzyme A synthetase	SucC (PP_4186) SucD (PP_4185) ScpC (PP_0154)
	28	$SUC + \text{Ubiquinone} \rightarrow FUM + \text{Ubiquinol}$	Succinate dehydrogenase	SdhA (PP_4191) SdhB (PP_4190) SdhC (PP_4193) SdhD (PP_4192)
	29	$FUM + H_2O \rightarrow MAL$	Fumarate hydratase	FumC-I (PP_0944) FumC-II (PP_1755) PP_0897
	30	$MAL + NAD^+ (\text{quinone}) \rightarrow$ $OAA + NADH (\text{quinol}) + H^+$	Malate dehydrogenase / Malate:quinone oxidoreductase	Mdh (PP_0654, PP_3591) Mqo-1 (PP_0751) Mqo-2 (PP_1251) Mqo-3 (PP2925)

	31	$\text{ICT} \rightarrow \text{SUC} + \text{Glyoxylate}$	Isocitrate lyase	AceA (PP_4116)
Anaplerosis / Gluconeogenesis	33	$\text{Pyr} + \text{CO}_2 \rightarrow \text{OAA} + \text{H}^+$	Pyruvate carboxylase	PycA (PP_5347) PycB (PP_5346)
	34	$\text{OAA} + \text{Pi} \rightarrow \text{PEP} + \text{CO}_2$	Phosphoenol- pyruvate carboxylase ^d	Ppc (PP_1505)
	35	$\text{MAL} + \text{NADP}^+ \rightarrow \text{Pyr} + \text{CO}_2 + \text{NADPH}$	Malic enzyme	MaeB (PP_5085)
Fatty acids biosynthesis	3	$\text{Acetyl-CoA} + \text{HCO}_3^- + \text{ATP} \rightarrow$ $\text{Malonyl-CoA} + \text{ADP} + \text{Pi}$	Acetyl-CoA carboxylase complex	AccA (PP_1607) AccB (PP_0559) AccC (PP_0558) AccD (PP_1996)
	37	$\text{Malonyl-CoA} + \text{ACP-SH} \rightarrow$ $\text{Malonyl-ACP} + \text{CoA}$	Malonyl-CoA-ACP transacylase	FabD (PP_1913)
	38	$\text{Malonyl-ACP} \rightarrow \text{Fatty acid biosynthesis}$		

^a Information compiled from the *Pseudomonas* Genome Database (Winsor et al., 2016; 2011), MetaCyc (Caspi et al., 2018) and the literature (Nikel et al., 2015; 2021; 2014; Nogales et al., 2020). Biochemical reactions are coded according to seven functional blocks. In the instances in which no gene name has been assigned, the PP number is given for each open reading frame. The reaction catalyzed by the pyruvate dehydrogenase complex (v_{23}) has been assigned to the TCA cycle for the sake of simplicity. Pi, inorganic orthophosphate; ACP, acyl carrier protein; the rest of abbreviations are defined in the legend to **Figure 1**.

Table S4. Reaction IDs, names and abbreviations used in the model.

Reaction ID	Reaction name	Reaction abbreviation
R_GLCabcpp	D-glucose transport <i>via</i> ABC system (periplasm)	GLCabcpp
R_GLK	Glucokinase	GLK
R_GLCNt2rpp	D-gluconate transport <i>via</i> H ⁺ symport, reversible (periplasm)	GLCNt2rpp
R_GNK	Gluconokinase	GNK
R_2DHGLCNkt_tp	Ketogluconate transporter	2DHGLCNkt tp
R_2DHGLCK	Dehydroglucokinase	2DHGLCK
R_PGLCNDH_NAD	Phosphogluconate 2-dehydrogenase	PGLCNDH NAD
R_PGLCNDH_NADP	Phosphogluconate 2-dehydrogenase	PGLCNDH NADP
R_GLCDpp	Glucose dehydrogenase (ubiquinone-8 as acceptor) (periplasm)	GLCDpp
R_GAD2ktp	Gluconate 2-dehydrogenase periplasm	GAD2ktp
R_G6PDH2_NAD	Glucose-6-phosphate dehydrogenase with NAD ⁺	G6PDH2 NAD
R_G6PDH2_NADP	Glucose-6-phosphate dehydrogenase with NADP ⁺	G6PDH2 NADP
R_PGL	6-Phosphogluconolactonase	PGL
R_GND_NAD	Phosphogluconate dehydrogenase	GND NAD
R_GND_NADP	Phosphogluconate dehydrogenase	GND NADP

R_RPI	Ribose-5-phosphate isomerase	RPI
R_RPE	Ribulose-5-phosphate 3-epimerase	RPE
R_TKT1	Transketolase 1	TKT1
R_TKT2	Transketolase 2	TKT2
R_TALA	Transaldolase	TALA
R_EDD	6-Phosphogluconate dehydratase	EDD
R_EDA	2-Dehydro-3-deoxy-phosphogluconate aldolase	EDA
R_PGI	Glucose-6-phosphate isomerase	PGI
R_FBP	Fructose biphosphatase	FBP
R_FBA	Fructose-bisphosphate aldolase	FBA
R_TPI	Triose phosphate isomerase	TPI
R_GAPD_NAD	Glyceraldehyde-3-phosphate dehydrogenase with NAD ⁺	GAPD NAD
R_GAPD_NADP	Glyceraldehyde-3-phosphate dehydrogenase with NADP ⁺	GAPD NADP
R_PGK	Phosphoglycerate kinase	PGK
R_PGM	Phosphoglycerate mutase	PGM
R_ENO	Enolase	ENO
R_PYK	Pyruvate kinase	PYK
R_PDH	Pyruvate dehydrogenase	PDH
R_OAADC	Oxaloacetate decarboxylase	OAADC
R_PPC	Phosphoenolpyruvate carboxylase	PPC
R_ME2_NADP	Malic enzyme nadp	ME2_NADP
R_ME2_NAD	Malic enzyme nad	ME2_NAD

R_MDH_NAD	Malate dehydrogenase nad	MDH_NAD
R_MDH_NADP	Malate dehydrogenase nadp	MDH_NADP
R_FUM	Fumarase	FUM
R_SUCDi	Succinate dehydrogenase	SUCDi
R_SUCOAS	Succinyl CoA synthetase (ADP forming)	SUCOAS
R_AKGDH	2-oxoglutarate dehydrogenase	AKGDH
R_ICDHyr_NADP	Isocitrate dehydrogenase nadp	ICDHyr_NADP
R_ICDHyr_NAD	Isocitrate dehydrogenase nad	ICDHyr_NAD
R_ACONTa	Aconitase A	ACONTa
R_ACONTb	Aconitase B	ACONTb
R_CS	Citrate synthase	CS
R_ACCOAC	Acetyl-CoA carboxylase	ACCOAC
R_KAS15	Beta-ketoacyl-ACP synthase	KAS15
R_MCOATA	Malonyl-CoA-ACP transacylase	MCOATA

Lumped* reactions of the model

R_OPNAD	Lump reaction of ATP production from NADH in oxidative phosphorylation	OPNAD
R_OPQ8	Lump reaction of ATP production from Q8H2 on oxidative phosphorylation	OPQ8
R_AXPr	ATP-and ADP regeneration	AXPr
R_NADHr	NAD-and NADH regeneration	NADHr
R_NADPHr	NADPH regeneration	NADPHr
R_ACCOAr	CoA regeneration	ACCOAr
R_Q8H2r	Q8H2 to G8 regeneration	Q8H2r

R_GLCtex	Glucose transport via diffusion (extracellular to periplasm)	GLCtex
R_EX_pyr	Pyruvate exchange	EX_pyr
R_EX_pep	Phosphoenolpyruvate exchange	EX_pep
R_EX_g6p	G6P exchange	EX_g6p
R_EX_r5p	R5P exchange	EX_r5p
R_EX_g3p	G3P exchange	EX_g3p
R_EX_e4p	E4P exchange	EX_e4p
R_EX_f6p	F6P exchange	EX_f6p
R_EX_3pg	3PG exchange	EX_3pg
R_EX_oaa	Oxaloacetate exchange	EX_oaa
R_EX_malL	Malate exchange	EX_malL
R_EX_akg	2-oxoglutarate exchange	EX_akg
R_EX_succ	Succinate exchange	EX_succ
R_EX_ru5p_D	Ru5P__D exchange	EX_ru5p_D
R_EX_fum	Fumarate exchange	EX_fum
R_EX_s7p	S7P exchange	EX_s7p
R_EX_13dpg	1,3-DPG exchange	EX_13dpg
R_EX_dhap	DHAP exchange	EX_dhap
R_EX_amp_in	AMP exchange (in)	EX_amp_in
R_EX_amp_out	AMP exchange (out)	EX_amp_out

*Lumped reaction captures the overall stoichiometry of the multiple reactions, while preserving the elemental balance

Table S5. Enzyme mechanisms used in the model.

Reaction	Mechanism ^a	Reference
GLCabcpp	Ordered BiTer	
GLK	Random BiBi	Burns et al. (1988)
GLCNt2rpp	uniUni	
GNK	Random BiBi	Anderson et al. (2014)
2DHGLCNkt_tpp	uniUni	
2DHGLCK	Ordered BiBi	
PGLCNDH	Ordered BiBi	
GLCDpp	pingPong BiBi	Davidson and Chen (2004)
GAD2ktp	Ordered BiBi	
G6PDH	Ordered BiBi	Coffee and Hu (1972)
PGL	uniUni	
GND	Ordered BiBi	Olsthoorn and Duine (1996)
RPI	uniUni	
RPE	uniUni	
TKT1	pingPong BiBi	Levy et al. (1983)
TKT2	pingPong BiBi	Levy et al. (1983)
TALA	pingPong BiBi	Chen et al. (2010)
EDD	uniUni	
EDA	Random UniBi	Asztalos et al. (2007)
PGI	uniUni	

FBP	Ordered UniBi	
FBA	Ordered BiUni	Jia et al. (1996)
TPI	uniUni	
GAPD	Ordered TerBi	Wang et al. (2010)
PGK	Random BiBi	Rutter and Ling (1958)
PGM	uniUni	
ENO	uniUni	
PYK	Ordered BiBi	Lai et al. (1965)
PDH	Ordered BiBi	
OAADC	uniUni	
PPC	Ordered BiUni	
ME2	Ordered BiBi	
MDH	Ordered BiBi	
FUM	uniUni	
SUCDi	Ordered BiBi	
SUCOAS	Ordered TerTer	
AKGDH	Ordered TerBi	
ICDHyr	Ordered BiBi	
ACONTa	uniUni	
ACONTb	uniUni	
CS	Ordered BiBi	
ACETYL-COAC	Ordered BiBi	
KAS15	uniUni	

MCOATA**uniUni**

^a The nomenclature originally proposed by Cleland (1963) was adopted here to describe enzymatic mechanisms. Shortly, the notation describes the order of binding and release of substrates and products as **Ordered** (where the order of substrate binding is defined) or **Random** (where it is not). Next to this, the mechanism can be classified to be either **sequential** or **ping-pong** (i.e. double-displacement reaction). The number of products and substrates intervening in the reaction is also taken into account, e.g. the UniUni mechanism describes a reaction with one substrate and one product, UniBi represents a reaction with one substrate and two products, UniTer involves a reaction with one substrate and three products, etc. All remaining reactions, mostly exchange reactions, were modeled with a simple mass action rate law (Saa and Nielsen, 2017).

Table S6. Patterns of enzyme regulation considered in the dynamic model.

Reaction	Regulation	Reference
G6PDH (Zwf)	Allosterically inhibited by NADH and NADPH	Ben-Bassat and Goldberg (1980); Larsson-Raznikiewicz and Arvidsson (1971); Lessmann et al. (1975); Vander Wyk and Lessie (1974); Wang and Alaupovic (1980)
GND (GntZ)	Allosterically inhibited by NADPH	Ben-Bassat and Goldberg (1980)
EDD	Allosterically activated by NADPH	Lee and Lessie (1974)
PYK	Allosterically activated by 2-dehydro-3-deoxy-D-gluconate-6-phosphate (2ddg6p), α -D-ribose 5-phosphate (r5p) and D-fructose-6-phosphate (f6p)	Chuang and Utter (1979)
ME2	Allosterically inhibited by oxaloacetate and NADPH, activated by fumarate and succinate	Garrido-Pertierra et al. (1983)
ICDH	Allosterically activated by pyruvate and oxaloacetate	Molina et al. (2019)
CS	Allosterically inhibited by NADH, activated by AMP	Mitchell and Weitzman (1986)

Table S7. Metabolite IDs, names and abbreviations used in the model.

Metabolite ID	Metabolite name (compartment)	Metabolite abbreviation
m_glc__D_p	D-glucose (periplasm)	GLC-D
m_atp_c	Adenosine-triphosphate (cytoplasm)	ATP
m_h2o_c	Water (cytoplasm)	H2O
m_glc__D_c	D-glucose (cytoplasm)	GLC-D
m_adp_c	Adenosine-diphosphate (cytoplasm)	ADP
m_pi_c	Phosphate (cytoplasm)	PI
m_g6p_c	α -D-glucose 6 phosphate (cytoplasm)	G6P
m_glc_n_p	D-gluconate (periplasm)	GLCN
m_glc_n_c	D-gluconate (cytoplasm)	GLCN
m_6pgc_c	6-phospho-D-gluconate (cytoplasm)	6PGC
m_2dhgln_p	2-Dehydro-D-gluconate (periplasm)	2DHGLCN
m_2dhgln_c	2-Dehydro-D-gluconate cytosol	2DHGLCN
m_6p2dhgln_c	6-Phospho-2-dehydro-D-gluconate cytosol	6P2DHGLCN
m_nadh_c	Nicotinamide adenine dinucleotide reduced (cytoplasm)	NADH
m_nad_c	Nicotinamide adenine dinucleotide (cytoplasm)	NAD
m_nadph_c	Nicotinamide adenine dinucleotide phosphate reduced (cytoplasm)	NADPH
m_nadp_c	Nicotinamide adenine dinucleotide phosphate (cytoplasm)	NADP

m_q8_c	Ubiquinone-8 (cytoplasm)	Q8
m_q8h2_c	Ubiquinol-8 (cytoplasm)	Q8H2
m_6pgl_c	6-phospho-D-glucono-1,5-lactone (cytoplasm)	6PGL
m_co2_c	Carbon dioxide (cytoplasm)	CO2
m_ru5p__D_c	D-ribulose-5-phosphate (cytoplasm)	RU5P-D
m_r5p_c	α -D-ribose-5-phosphate (cytoplasm)	R5P
m_xu5p__D_c	D-xylulose-5-phosphate (cytoplasm)	XU5P-D
m_g3p_c	D-glyceraldehyde 3-phosphate (cytoplasm)	G3P
m_s7p_c	Sedoheptulose-7-phosphate (cytoplasm)	S7P
m_e4p_c	D-erythrose-4-phosphate (cytoplasm)	E4P
m_f6p_c	D-fructose-6-phosphate (cytoplasm)	F6P
m_2ddg6p_c	2-Dehydro-3-deoxy-D-gluconate 6-phosphate (cytoplasm)	2DDG6P
m_pyr_c	Pyruvate (cytoplasm)	PYR
m_fdp_c	D-fructose-1,6-bisphosphate (cytoplasm)	FDP
m_dhap_c	Dihydroxyacetone-phosphate (cytoplasm)	DHAP
m_13dpg_c	3-Phospho-D-glyceroyl-phosphate (cytoplasm)	13DPG
m_3pg_c	3-Phospho-D-glycerate (cytoplasm)	3PG
m_2pg_c	2-Phospho-D-glycerate (cytoplasm)	2PG
m_pep_c	Phosphoenolpyruvate (cytoplasm)	PEP
m_coa_c	Coenzyme A (cytoplasm)	COA
m_accoa_c	Acetyl-CoA (cytoplasm)	ACCOA

m_oaa_c	Oxaloacetate (cytoplasm)	OAA
m_mal__L_c	Malate (cytoplasm)	MAL-L
m_fum_c	Fumarate (cytoplasm)	FUC
m_succ_c	Succinate (cytoplasm)	SUCC
m_succoa_c	Succinyl-CoA (cytoplasm)	SUCCOA
m_akg_c	2-oxoglutarate (cytoplasm)	AKG
m_icit_c	Isocitrate (cytoplasm)	ICIT
m_cit_c	Citrate (cytoplasm)	CIT
m_acon_C_c	Cis-aconitate (cytoplasm)	ACON
m_hco3_c	Bicarbonate (cytoplasm)	HCO3
m_malcoa_c	Malonyl-CoA (cytoplasm)	MALCOA
m_malACP_c	Malonyl-acyl carrier protein (ACP) (cytoplasm)	MALACP
m_actACP_c	Acetoacetyl-ACP (cytoplasm)	ACTACP
m_ACP_c	Acyl carrier protein (cytoplasm)	ACP
m_o2_c	Oxygen (cytoplasm)	O2
m_glc__D_e	D-glucose (extracellular)	GLC-D
m_pyr_e	Pyruvate (extracellular)	PYR
m_pep_e	Phosphoenolpyruvate (extracellular)	PEP
m_g6p_e	α -D-Glucose 6 phosphate (extracellular)	G6P
m_r5p_e	α -D-Ribose-5-phosphate (extracellular)	R5P
m_g3p_e	D-Glyceraldehyde 3-phosphate (extracellular)	G3P
m_e4p_e	D-Erythrose-4-phosphate (extracellular)	E4P

m_f6p_e	D-Fructose-6-phosphate (extracellular)	F6P
m_3pg_e	3-Phospho-D-glycerate (extracellular)	3PG
m_oaa_e	Oxaloacetate (extracellular)	OAA
m_mal__L_e	Malate (extracellular)	MAL-L
m_akg_e	2-Oxoglutarate (extracellular)	AKG
m_succ_e	Succinate (extracellular)	SUCC
m_ru5p__D_e	D-Ribulose 5-phosphate (extracellular)	RU5P-D
m_fum_e	Fumarate (extracellular)	FUE
m_s7p_e	Sedoheptulose-7-phosphate (extracellular)	S7P
m_13dpg_e	3-Phospho-D-glyceroyl-phosphate (extracellular)	13DPG
m_dhap_e	Dihydroxyacetone-phosphate (extracellular)	DHAP
m_amp_i	Adenosine-monophosphate (cytoplasm)	AMP
m_amp_c	Adenosine-monophosphate (cytoplasm)	AMP
m_amp_e	Adenosine-monophosphate (extracellular)	AMP

Table S8. Substrate binding and product unbinding order of reactions with non-random mechanisms.

Reaction ID	Substrate order	Product order
GLCABCPP	GLC-D ATP	ADP PI GLC-D
2DHGLCK	ATP 2DHGLCN	6P2DHGLCN ADP
PGLCNDH_NAD	NADH 6P2DHGLCN 6P2DHGLCN	NADPH NAD+ NADP 6PGC 6PGC
PGLCNDH_NAD P	NADH 6P2DHGLCN 6P2DHGLCN	NADPH NAD+ NADP 6PGC 6PGC
GLCDPP	GLC-D Q8	GLCN Q8H2
GAD2KTPP	Q8 GLCN	2DHGLCN Q8H2
G6PDH2_NAD*	NAD+ G6P NADP G6P	6PGL 6PGL NADH NADPH
G6PDH2_NADP*	NAD+ G6P NADP G6P	6PGL 6PGL NADH NADPH
GND_NAD*	6PGC NAD+ 6PGC NADP	NADH NADPH RU5P-D RU5P-D
GND_NADP*	6PGC NAD+ 6PGC NADP	NADH NADPH RU5P-D RU5P-D
TKT1	R5P XU5P-D	G3P S7P
TKT2	XU5P-D E4P	G3P F6P
TALA	S7P G3P	E4P F6P
FBP	FDP	F6P PI
FBA	DHAP G3P	FDP
GAPD_NAD*	NAD+ G3P PI NADP G3P PI	13-DPG 13-DPG NADH NADPH
GAPD_NAD*	NAD+ G3P PI NADP G3P PI	13-DPG 13-DPG NADH NADPH
PGK	ADP 13-DPG	3PG ATP
PYK	ADP PEP	ATP PYC

PDH	NAD+ CoA PYC	ACCOA NADH
PPC	OAA Pi	PEP
ME2_NADP*	NADP MAL-L NAD+ MAL-L	PYC PYC NADPH NADH
ME2_NAD*	NADP MAL-L NAD+ MAL-L	PYC PYC NADPH NADH
MDH_NAD*	NAD+ MAL-L NAD+P MAL-L	OAA OAA NADH NADPH
MDH_NADP*	NAD+ MAL-L NAD+P MAL-L	OAA OAA NADH NADPH
SUCDI	Q8 SUCC	FUC Q8H2
SUCOAS	ADP SUCCOA Pi	SUCC CoA ATP
AKGDH	NAD+ CoA AKG	SUCCOA NADH
ICDHYNADP*	NADP ICIT NAD+ ICIT	AKG AKG NADPH NAH
ICDHYNAD*	NADP ICIT NAD+ ICIT	AKG AKG NADPH NADH
CS	OAA ACCoA	CIT CoA
ACCOAC	ATP ACCoA	MALCoA ADP

* For promiscuous reactions, all reactants are specified.

** References are the same as in the table describing the reaction mechanisms.

Table S9. Gibbs energy for the reactions used in the model.

Reaction ID	$\Delta G_r'$ Minimum (kJ mol ⁻¹)	$\Delta G_r'$ Maximum (kJ mol ⁻¹)
GLCabcpp	-27.01	-25.77
GLK	-18.15	-16.39
GLCNt2rpp	-5	5
GNK	-16.57	-3.49
2DHGLCNkt_tpp	-5	5
2DHGLCK	-18.86	-4.74
PGLCNDH NAD	-20.59	-12.95
PGLCNDH NADP	-21.46	-13.7
GLCDpp	-124.6	-107.6
GAD2ktp	-72.7	-60.3
G6PDH2 NAD	-5.93	-0.41
G6PDH2 NADP	-5.07	0.33
PGL	-24.45	-17.69
GND_NAD	3.81	16.73
GND_NADP	4.6	17.56
RPI	-3.48	-0.36
RPE	-5.73	-1.01
TKT1	-7.81	0.03
TKT2	-13.8	-6.2
TALA	-3.49	2.27
EDD	-48.22	-37.74

EDA	11.31	19.75
PGI	-3.3	-1.74
FBP	-12.86	-10.02
FBA	-35.88	-18.72
TPI	-21.58	-4.34
GAPD NAD	7	8.64
GAPD NADP	7.57	9.69
PGK	-19.35	-17.55
PGM	3.49	4.97
ENO	-24.71	-3.47
PYK	-28.51	-26.79
PDH	-41.56	-28.44
OAADC	-3.99	23.73
PPC	0.33	43.01
ME2 NADP	7.54	20.34
ME2 NAD	6.77	19.49
MDH NAD	9.89	31.13
MDH NADP	10.42	32.22
FUM	-4	-2.88
SUCDi	-28.6	-14.4
SUCOAS	-5.86	4.58
AKGDH	-35.3	-19.46
ICDH _{Hy} NADP	-0.14	12.86

ICDH _{Hy} NAD	-0.95	12.05
ACONT _a	6.01	10.65
ACONT _b	-3.02	1.62
CS	-35.73	-33.93
ACCOAC	-11.9	1.1
KAS15	-348.6	-304.8
MCOATA	-5	5
OPNAD	-41.2	-29.2
OPQ8	-102.4	-88.8
AXPr	-185.45	-182.25
NADH _r	-65.39	-63.15
NADPH _r	-66.3	-63.86

* For the exchange and mass action reactions, a default constraint of -5 kJ mol⁻¹ to 5 kJ⁻¹ was used in order allow for small adjustment in the calculation of feasible Gibbs free range.

Table S10. Metabolic pathways enriched in the set of proteins with decreased abundance in CRISPRi-mediated AccA depletion.

AccA		Down	
Pathways		P-values	Matches
Pyrimidine degradation	nucleotide	0.002216137	PP_2531 // rdgB // hyuC // pydX // pydA
Pyrimidine degradation	nucleobase	0.002217697	hyuC // pydX // pydA
Reductant biosynthesis		0.010813462	gshB // trxB // PP_1686
Two-component alkanesulfonate monooxygenase		0.011382705	ssuD // ssuE
Carrier biosynthesis		0.015278612	ubiG // gshB // metK // folD-I // glyA-I // fau // purU-III // nadE // trxB // PP_2531 // PP_1686
Nucleoside and nucleotide degradation	nucleotide	0.020337237	PP_2531 // rdgB // hyuC // pydX // pydA
Folate polyglutamylation		0.021836216	glyA-I // folD-I
Folate transformations I		0.022896051	glyA-I // folD-I // purU-III // fau
C1 compound utilization and assimilation		0.027646376	folD-I // fdoG // purU-III // frmA
Formaldehyde oxidation (THF pathway)	VII	0.034915227	purU-III // folD-I
Superpathway of acetate utilization and formation	acetate	0.034915227	pta // acsA-II
L-citrulline degradation		0.034915227	arcC // arcB
β -Alanine Biosynthesis		0.03538174	hyuC // pydX // pydA
Formaldehyde oxidation		0.03538174	purU-III // folD-I // frmA
Folate transformations		0.03880267	glyA-I // folD-I // fau // purU-III
Electron carrier biosynthesis		0.039719667	ubiG // gshB // nadE // trxB // PP_2531 // PP_1686

Table S11. Metabolic pathways enriched in the set of proteins with increased abundance in CRISPRi-mediated AccA depletion.

AccA	Up		
Pathways	P-values	Matches	
Glucose degradation (oxidative)	2.16E-04	PP_3382 // PP_3383 // PP_3384 // kguD // kguK	
L-lysine degradation	2.27E-04	PP_4108 // dpkA // amaD // alr // davT // davD // davA	
Amino acid biosynthesis	0.001971679	argJ // argB // argG // ilvA-I // ilvA-II // PP_3365 // ilvE // leuA // lysC // dapA-II // dapC // gatC // hisH // asnB // hisZ // PP_3724 // lpdG // proC // ltaE // alr // PP_3190 // metX // PP_2528 // cysI // trpE // alaA // glnA	
Proteinogenic amino acid biosynthesis	0.002210446	argJ // argB // argG // lysC // dapA-II // dapC // gatC // hisH // asnB // hisZ // leuA // ilvE // ilvA-I // ilvA-II // PP_3365 // lpdG // proC // ltaE // PP_3190 // cysI // metX // PP_2528 // trpE // alaA // glnA	
Sugar acid degradation	0.007888692	PP_3382 // PP_3383 // PP_3384 // kguD // kguK // eda	
L-lysine degradation V	0.009866621	PP_4108 // dpkA // amaD // alr	
L-lysine degradation IV	0.009870843	davT // davD // davA	
Carbohydrate degradation	0.011034243	algC // PP_3443 // gapA // eda // PP_3382 // PP_3383 // PP_3384 // kguD // kguK // glgP	
Amino acid fermentation (Stickland reactions)	0.011129538	PP_4635 // ilvE	
L-homocysteine biosynthesis	0.011129538	metX // PP_2528	
Sugar degradation	0.01660269	algC // PP_3443 // gapA // eda // PP_3382 // PP_3383 // PP_3384 // kguD // kguK	
Lipid IVA biosynthesis	0.018227478	lpxA // lpxD // lpxH	
L-Threonine degradation	0.018227478	ltaE // ilvA-I // ilvA-II	
Superpathway of branched chain amino acid biosynthesis	0.020461915	ilvA-I // ilvA-II // PP_3365 // ilvE // leuA	
Proteinogenic amino acid degradation	0.021782137	ilvE // speA // proC // ansA // ltaE // ilvA-I // ilvA-II // lpdG // PP_4108 // dpkA // amaD // alr // gatC // hisH // asnB // davT // davD // davA // PP_4635 // PP_3190	
Other amino acid biosynthesis	0.027289184	PP_3724 // alr // metX // PP_2528 // lysC // gatC // hisH // asnB // argB // argJ	

Lipopolysaccharide biosynthesis	0.02946399	lpxA // lpxD // lpxH
L-Isoleucine biosynthesis I (from threonine)	0.030146621	ilvA-I // ilvA-II // PP_3365 // ilvE
D-Galacturonate degradation I	0.031069959	eda // kguK
Urate degradation	0.031069959	pucL // puuD
Carboxylate degradation	0.037750833	eda // PP_2217 // gcdH // aceE // lpdG // PP_3382 // PP_3383 // PP_3384 // kguD // kguK // PP_3724 // glcB
Amino acid degradation	0.0384817	ilvE // speA // proC // ansA // ltaE // ilvA-I // ilvA-II // PP_3190 // lpdG // PP_4108 // dpkA // amaD // alr // gatC // hisH // asnB // davT // davD // davA // PP_4635
Polysaccharide degradation	0.043563962	algC // glgP // kguK

Table S12. Metabolic pathways enriched in the set of proteins with increased abundance in CRISPRi-mediated GltA depletion.

GltA	Up	
Pathways	P-values	Matches
Carbohydrate degradation	4.80E-05	pgm // pykA // pgl // eda // PP_3382 // PP_3383 // PP_3384 // kguD // kguK // aacs // bktB // malQ // glgP
Glucose degradation (oxidative)	1.03E-04	PP_3382 // PP_3383 // PP_3384 // kguD // kguK
Sugar degradation	3.88E-04	pgm // pykA // pgl // eda // PP_3382 // PP_3383 // PP_3384 // kguD // kguK // aacs // bktB
Carboxylate degradation	4.45E-04	eda // acsA-I // bktB // pcal // aceE // lpdG // aceF // PP_3382 // PP_3383 // PP_3384 // kguD // kguK // mmgF // pykA // PP_2036
Sugar acid degradation	5.75E-04	PP_3382 // PP_3383 // PP_3384 // kguD // kguK // PP_2036 // eda
Glucose metabolism	0.0017916 9	eda // pgl // PP_3382 // PP_3383 // PP_3384 // kguD // kguK // rpiA // pykA
Glycolysis	0.0017916 9	eda // pgl // PP_3382 // PP_3383 // PP_3384 // kguD // kguK // rpiA // pykA
Generation of precursor metabolites and energy	0.0018007	eda // pgl // PP_3382 // PP_3383 // PP_3384 // kguD // kguK // rpiA // pykA // nuol // aceE // lpdG // aceF // icd // mqp1 // sucB // fumC2 // aceA // tal
Acetyl-CoA biosynthesis	0.0027395 1	aceE // lpdG // aceF
Pyruvate decarboxylation to acetyl-CoA	0.0027395 1	aceE // lpdG // aceF
Polymeric compound degradation	0.0033985 2	malQ // pgm // glgP // kguK
Polysaccharide degradation	0.0033985 2	malQ // pgm // glgP // kguK
L-Glutamine degradation I	0.0040222 8	gatB // gatC // guaA // carA // gltD
L-Glutamine degradation	0.0040222 8	gltD // gatB // gatC // guaA // carA
S-Adenosyl-L-methionine cycle II	0.0063965 9	metE // ahcY // metK

S-Adenosyl-L-methionine biosynthesis	0.0063965	9	metE // ahcY // metK
Glycogen degradation II	0.0063965	9	malQ // pgm // glgP
Glycogen degradation	0.0063965	9	malQ // pgm // glgP
tRNA processing	0.0063965	9	rne // rnd // rnr
L-Citrulline degradation	0.0063965	9	arcC // carA // arcB
Glycan degradation	0.0063965	9	malQ // pgm // glgP
L-Citrulline biosynthesis	0.0065858	2	arcB // gatB // gatC // guaA // carA // gltD
L-Citrulline biosynthesis	0.0065858	2	arcB // gatB // gatC // guaA // carA // gltD
L-Asparagine biosynthesis	0.0080966		gatB // gatC // guaA // carA // gltD
L-Asparagine biosynthesis III (tRNA-dependent)	0.0080966		gatB // gatC // guaA // carA // gltD
L-Methionine degradation I (to L-homocysteine)	0.0082151	7	ahcY // metK
Secondary metabolite degradation	0.0104437	3	vdh // PP_3382 // PP_3383 // PP_3384 // kguD // kguK // PP_2036 // eda
Glutaminyl-tRNA ^{Gln} biosynthesis via transamidation	0.0109407	3	gatB // gatC // guaA // carA // gltD
Degradation/utilization/assimilation	0.0114970	4	bktB // eda // fadD1 // acsA-I // pcal // aceE // lpdG // aceF // davA // glnA // malQ // pgm // glgP // PP_0596 // gltD // kguK // ssuD // aruH // arcC // carA // arcB // gloA // PP_2036 // proC // proI // pykA // vdh // argG // mmgF // pcaC // icd // mqo1 // sucB // fumC2 // pgl // PP_1389 // ahcY // metK // PP_1143 // betA-II // betB // gatB // gatC // guaA // puuD // PP_3382 // PP_3383 // PP_3384 // kguD // aacs
L-Arginine degradation V (arginine deiminase pathway)	0.0119519	5	arcC // carA // arcB
Nitrogen compound metabolism	0.0144010	1	carA // argG // arcB // gltD // glnA
Sugar derivative degradation	0.0147185	8	PP_3382 // PP_3383 // PP_3384 // kguD // kguK // PP_2036 // eda

Proteinogenic amino acid biosynthesis	0.0148487	5	carA // arcB // argG // pheA // PP_2036 // gatB // gatC // guaA // gltD // hisE // leuD // leuB // lpdG // proC // prol // PP_2528 // metE // trpA // iscS-I // glnA
Urea cycle	0.0195463	2	carA // argG // arcB
Amino acid biosynthesis	0.0215806	5	carA // arcB // argG // pheA // leuD // leuB // PP_2036 // gatB // gatC // guaA // gltD // hisE // PP_0596 // lpdG // proC // prol // PP_2528 // metE // trpA // iscS-I // glnA
L-Methionine degradation	0.0231785	2	ahcY // metK
L-Proline biosynthesis III (from L-ornithine)	0.0231785	2	proC // prol
D-Galacturonate degradation I	0.0231785	2	eda // kguK
2-Oxoglutarate decarboxylation to succinyl-CoA	0.0231785	2	lpdG // sucB
Choline degradation I	0.0231785	2	betA-II // betB
Betaine biosynthesis	0.0231785	2	betB // betA-II
Glycine betaine biosynthesis I	0.0231785	2	betB // betA-II
TCA cycle	0.0353471	5	icd // mqo1 // sucB // lpdG // fumC2
Pentose phosphate pathway	0.0410058	1	pgl // rpiA // tal
L-arginine degradation (arginase 2 pathway)	0.0436175	4	proC // prol
L-proline biosynthesis I	0.0436175	4	proC // prol
Choline degradation	0.0436175	4	betA-II // betB

Table S13. Metabolic pathways enriched in the set of proteins with decreased abundance in CRISPRi-mediated GltA depletion.

GltA	Down	
Pathways	P-values	Matches
Degradation/Utilization/ Assimilation	5.97E-08	folD-I // fdoG // fadA // fadBA // PP_2213 // PP_2215 // PP_3732 // hyuC // ydcJ // PP_4108 // amaB // amaA // dpkA // peaD // peaC // peaA // hpd // mmsA-II // mvaB // liuC // cysK // PP_3190 // astA-I // pedE // vanA // argH // mdh // gltA // lpdV // bkdB // bkdAA // mmsB // purU-III // fdhA // ltaE // amiC
Proteinogenic amino acid degradation	5.43E-07	mvaB // liuC // hpd // ltaE // PP_2215 // mmsA-II // lpdV // bkdB // bkdAA // mmsB // cysK // ydcJ // PP_4108 // amaB // amaA // dpkA // PP_3190 // astA-I
Amino acid degradation	1.33E-06	mvaB // liuC // hpd // ltaE // PP_2215 // mmsA-II // lpdV // bkdB // bkdAA // mmsB // PP_3190 // cysK // ydcJ // PP_4108 // amaB // amaA // dpkA // astA-I
L-Lysine degradation V	1.38E-05	ydcJ // PP_4108 // amaB // amaA // dpkA
L-Valine degradation I	4.75E-05	mmsA-II // lpdV // bkdB // bkdAA // mmsB
L-Valine Degradation	4.75E-05	mmsA-II // lpdV // bkdB // bkdAA // mmsB
Methylamine degradation	7.74E-05	peaD // peaC // peaA
L-Lysine degradation	1.87E-04	ydcJ // PP_4108 // amaB // amaA // dpkA
2-oxoisovalerate decarboxylation to isobutanoyl-CoA	3.00E-04	lpdV // bkdB // bkdAA
Fatty acid β -oxidation I	0.00301591	PP_3732 // PP_2213 // fadA // fadBA
Fatty acid degradation	0.00491181	PP_3732 // fadA // fadBA // PP_2213 // PP_2215
C1 Compound utilization and assimilation	0.00753291	purU-III // folD-I // fdhA // fdoG
Fatty acid and lipid degradation	0.00786009	PP_3732 // fadA // fadBA // PP_2213 // PP_2215
Formaldehyde oxidation	0.01289365	purU-III // folD-I // fdhA
Formaldehyde oxidation VII (THF pathway)	0.01706519	purU-III // folD-I
1-Butanol degradation	0.02006703	PP_2215 // fadBA // pedE
Fatty acid salvage	0.02904573	fadBA // fadA // PP_2213
Glyoxylate cycle	0.03389312	mdh // gltA

L-Leucine degradation I	0.03389312	mvaB // liuC
L-Cysteine degradation II	0.04356436	cysK
L-Cysteine Degradation	0.04356436	cysK
Bis(guanylyl molybdenum cofactor) biosynthesis	0.04356436	mobA
L-Threonine degradation IV	0.04356436	ltaE
Guanylyl molybdenum cofactor biosynthesis	0.04356436	mobA
Glycine biosynthesis IV	0.04356436	ltaE
Glutaryl-CoA degradation	0.04395372	fadBA // PP_2215
L-Leucine degradation	0.04395372	mvaB // liuC

Table S14. Metabolic pathways enriched in the set of proteins with decreased abundance in CRISPRi-mediated GltA and AccA depletion.

AccA GltA	Down	
Pathways	P-values	Matches
Degradation/Utilization/ Assimilation	3.09E-07	folD-I // fdoG // fadA // fadB // PP_0368 // PP_3732 // PP_3726 // pta // maeB // acsA-II // hyuC // pydB // pydX // pydA // PP_4108 // amaB // dpkA // peaD // peaC // peaA // hpd // gcvT-I // PP_1944 // mmsA-I // mmsA-II // mvaB // liuC // mcca // ssuD // ssuE // quiC // cysK // PP_3190 // aldA // pedI // PP_3602 // pedE // puuB // gcl // argH // PP_3646 // mdh // gltA // lpdV // bkdB // bkdAA // mmsB // purU-III // frmA // fdhA // PP_3191 // rbsK // amiC
L-valine degradation I	4.73E-05	mmsA-I // mmsA-II // lpdV // bkdB // bkdAA // mmsB
L-valine degradation	4.73E-05	mmsA-I // mmsA-II // lpdV // bkdB // bkdAA // mmsB
Formaldehyde oxidation	8.90E-05	purU-III // folD-I // frmA // fdhA // aldA // pedI
Pyrimidine nucleobase degradation	1.33E-04	hyuC // pydB // pydX // pydA
Uracil degradation	1.33E-04	hyuC // pydB // pydX // pydA
Thymine degradation	1.33E-04	hyuC // pydB // pydX // pydA
Uracil degradation I (reductive)	1.33E-04	hyuC // pydB // pydX // pydA
C1 Compound utilization and assimilation	2.31E-04	purU-III // folD-I // frmA // fdhA // aldA // pedI // fdoG
Methylamine degradation I	3.94E-04	peaD // peaC // peaA
Methylamine degradation	3.94E-04	peaD // peaC // peaA
Amino acid degradation	4.97E-04	mvaB // liuC // mcca // hpd // puuB // PP_3602 // PP_3191 // mmsA-I // mmsA-II // lpdV // bkdB // bkdAA // mmsB // PP_3190 // gcvT-I // PP_1944 // cysK // PP_4108 // amaB // dpkA
Proteinogenic amino acid degradation	6.71E-04	mvaB // liuC // mcca // hpd // puuB // PP_3191 // mmsA-I // mmsA-II // lpdV // bkdB // bkdAA // mmsB // gcvT-I // PP_1944 // cysK // PP_4108 // amaB // dpkA // PP_3190
2-Oxoisovalerate decarboxylation to isobutanoyl- CoA	0.0014930 2	lpdV // bkdB // bkdAA
Ethylene glycol degradation	0.003533	pedE // pedI // aldA

Superpathway of acetate utilization and formation	0.003533	pta // maeB // acsA-II
Fatty acid β -oxidation III (unsaturated, odd number)	0.003533	fadB // PP_3726 // PP_3732
Formaldehyde oxidation IV (thiol-independent)	0.003533	fdhA // aldA // pedI
Ethanol degradation	0.0066893	acsA-II // aldA // pedI
	8	
β -Alanine biosynthesis	0.0087944	hyuC // pydB // pydX // pydA
	6	
L-Leucine degradation I	0.0110844	mvaB // liuC // mccA
	2	
Unsaturated, even numbered fatty acid β -oxidation	0.0110844	fadB // PP_3726 // PP_3732
	2	
Superpathway of glycol metabolism and degradation	0.0119963	pedE // pedI // aldA // gcl
	3	
Acetate and ATP formation from acetyl-CoA I	0.0155493	pta // maeB
β -alanine degradation II	0.0155493	mmsA-I // mmsA-II
Two-component alkanesulfonate monooxygenase	0.0155493	ssuD // ssuE
Fermentation to short-chain fatty acids	0.0155493	pta // maeB
β -Alanine degradation	0.0155493	mmsA-I // mmsA-II
Fermentation to Acetate	0.0155493	pta // maeB
Alcohol degradation	0.0164494	acsA-II // aldA // pedI // fadB // pedE // gcl
	8	
L-Leucine degradation	0.0167957	mvaB // liuC // mccA
	8	
Fatty acid β -oxidation I	0.0204319	fadB // PP_3726 // PP_3732 // fadA
	7	
L-Lysine degradation V	0.0238637	PP_4108 // amaB // dpkA
	3	
Pyrimidine nucleotide degradation	0.0257364	hyuC // pydB // pydX // pydA
	1	
Fatty acid biosynthesis initiation	0.0296055	accA // accD
	7	
Folate polyglutamylation	0.0296055	glyA-I // folD-I
	7	
Biotin-carboxyl carrier protein assembly	0.0296055	accA // accD
	7	

Acyl-CoA hydrolysis	0.0296055	estP // PP_2308
	7	
Propanoyl-CoA degradation II	0.0296055	mmsA-I // mmsA-II
	7	
Amine and polyamine degradation	0.0305688	pta // maeB // peaD // peaC // peaA // puuB // hyuC
	4	
Other amino acid degradation	0.0317986	PP_3602 // mmsA-I // mmsA-II // PP_3190
	4	
Oleate β -oxidation	0.0378327	fadB // fadA // PP_0368 // PP_3732 // PP_3726
	4	
Folate transformations I	0.0386335	glyA-I // folD-I // purU-III // gcvT-I
	7	
Glycine biosynthesis	0.0420805	glyA-I // gcvT-I // PP_1944
	9	
Fatty acid degradation	0.0438053	fadB // PP_3726 // PP_3732 // fadA // PP_0368
	4	
Formaldehyde oxidation VII (THF pathway)	0.0469872	purU-III // folD-I
	8	
Fermentation	0.0469872	pta // maeB
	8	
Carboxylate degradation	0.0484748	pta // maeB // acsA-II // fadB // PP_3602 // fadA // mmsA-I // mmsA-II // gcl
	6	

Table S15. Metabolic pathways enriched in the set of proteins with decreased abundance in CRISPRi-mediated GltA and AccA depletion.

AccA GltA	Up	
Pathways	p-values	Matches
Purine ribonucleotide <i>De novo</i> biosynthesis	3.08E-04	gmk // guaA // guaB // adk // purB // purE // purH // purC
Carbohydrate degradation	3.93E-04	PP_1776 // algC // pgm // pykA // eno // pgk // PP_3443 // gapB // pgl // PP_3382 // PP_3383 // PP_3384 // kguD // kguK // aacs // PP_2215 // bktB // glgP // nagZ
Carboxylate degradation	8.50E-04	purT // acsA-I // PP_2217 // PP_2215 // bktB // lvaB // aceE // lpdG // aceF // PP_3382 // PP_3383 // PP_3384 // kguD // kguK // acnB // mmgF // prpC // PP_3724 // PP_2213 // glcB // pykA // eno // glxR // PP_2036 // gudD
Sugar degradation	9.83E-04	PP_1776 // algC // pgm // pykA // eno // pgk // PP_3443 // gapB // pgl // PP_3382 // PP_3383 // PP_3384 // kguD // kguK // aacs // PP_2215 // bktB
Amino acid biosynthesis	0.001606582	argJ // argA // carA // argB // argC // astC // argG // pheA // glyA-II // serC // ilvA-II // PP_3365 // ilvE // leuD // leuB // lysC // asd2 // PP_2036 // dapD // dapF // gatC // asnB // guaA // serS // hisG // hisE // PP_0596 // PP_3724 // PP_2213 // lpdG // gcvT-II // proC // prol // alr // metX // PP_2528 // trpA // trpE // trpD // trpF // trpC // iscS-I // cysM // cysE // PP_3148 // glnA
Purine nucleotide <i>de novo</i> biosynthesis	0.00161483	gmk // guaA // guaB // adk // purB // purE // purH // purC
Proteinogenic amino acid biosynthesis	0.002296617	argJ // argA // carA // argB // argC // astC // argG // pheA // lysC // asd2 // PP_2036 // dapD // dapF // gatC // asnB // guaA // serS // hisG // hisE // serC // leuD // ilvE // leuB // glyA-II // ilvA-II // PP_3365 // lpdG // gcvT-II // proC // prol // metX // PP_2528 // trpA // trpE // trpD // trpF // trpC // iscS-I // cysM // cysE // PP_3148 // glnA
Purine nucleotide biosynthesis	0.003175203	gmk // xpt // guaA // guaB // adk // purB // purT // purF // purN // purE // purH // purC
Glucose degradation (oxidative)	0.005660584	PP_3382 // PP_3383 // PP_3384 // kguD // kguK

L-Tryptophan biosynthesis	0.005660584	trpA // trpE // trpD // trpF // trpC
Inosine-5'-phosphate biosynthesis	0.007920012	purE // purH // purB // purC
L-Isoleucine degradation	0.007920012	acd // PP_2215 // bktB // ilvE
tRNA processing	0.007920012	rne // rnd // rnpA // rnr
Inosine-5'-phosphate biosynthesis I	0.007920012	purE // purH // purB // purC
L-isoleucine degradation I	0.007920012	acd // PP_2215 // bktB // ilvE
L-arginine biosynthesis II (acetyl cycle)	0.008804983	argJ // argA // carA // argB // argC // astC // argG
Urate degradation	0.009144597	pucM // pucL // puuD
UDP- α -D-glucose biosynthesis I	0.009144597	algC // pgm // galU
Urate conversion to allantoin I	0.009144597	pucM // pucL // puuD
Glucose metabolism	0.011064811	pgl // gntZ // PP_3382 // PP_3383 // PP_3384 // kguD // kguK // rpiA // pykA // eno // pgk // PP_3443 // gapB
Glycolysis	0.011064811	pgl // gntZ // PP_3382 // PP_3383 // PP_3384 // kguD // kguK // rpiA // pykA // eno // pgk // PP_3443 // gapB
2-Methylcitrate cycle	0.012531084	acnB // mmgF // prpC // PP_3724 // PP_2213
Polymeric compound degradation	0.012531084	algC // pgm // glgP // kguK // nagZ
2-Methylcitrate cycle I	0.012531084	acnB // mmgF // prpC // PP_3724 // PP_2213
Polysaccharide degradation	0.012531084	algC // pgm // glgP // kguK // nagZ
Other amino acid biosynthesis	0.016163075	PP_0596 // PP_3724 // PP_2213 // alr // metX // PP_2528 // asd2 // lysC // gatC // asnB // guaA // carA // astC // argC // argB // argJ // argA
Lipid IV A biosynthesis (<i>P. putida</i>)	0.019859303	lpxA // lpxD // lpxH // lpxB
Sugar acid degradation	0.02058967	PP_3382 // PP_3383 // PP_3384 // kguD // kguK // PP_2036 // gudD // glxR
L-Arginine biosynthesis I (via L-ornithine)	0.022454944	astC // argC // argB // argJ // argA // carA // argG
L-ornithine biosynthesis I	0.023433374	astC // argC // argB // argJ // argA
Guanosine ribonucleotides <i>de novo</i> biosynthesis	0.03088458	gmk // guaA // guaB
Acetyl-CoA biosynthesis	0.03088458	aceE // lpdG // aceF

Pyruvate decarboxylation to acetyl-CoA	0.03088458	aceE // lpdG // aceF
Sugar derivative degradation	0.033394706	PP_3382 // PP_3383 // PP_3384 // kguD // kguK // mupP // amiD // nagZ // PP_2036 // gudD // glxR
Sugar biosynthesis	0.033810347	algC // pgm // galU // prs // PP_1776 // ppsA // eno // pgk // PP_3443 // gapB // glmS // glmU // rmlC // kdsD // kdsB
Glycolate degradation	0.038790926	glcB // pykA // eno // glxR
Pyridoxal 5'-phosphate biosynthesis I	0.038790926	pdxA // serC // pdxB // pdxJ
Lipopolysaccharide biosynthesis	0.038790926	lpxA // lpxD // lpxH // lpxB
UDP-sugar biosynthesis	0.03899936	algC // pgm // galU // glmS // glmU
Nucleoside and nucleotide biosynthesis	0.04098957	pyrR // gmk // xpt // pyrB // carA // guaA // guaB // adk // purB // purT // purF // purN // purE // purH // purC
Amino acid fermentation (Stickland reactions)	0.043894064	PP_4635 // ilvE
Cyclitol biosynthesis	0.043894064	PP_3157 // suhB
Lipoate biosynthesis	0.043894064	lipB // lipA
Sugar derivative biosynthesis	0.043894064	PP_3157 // suhB
Sugar alcohol biosynthesis	0.043894064	PP_3157 // suhB
Lipoate biosynthesis and incorporation I	0.043894064	lipB // lipA
L-homocysteine biosynthesis	0.043894064	metX // PP_2528
Myoinositol biosynthesis	0.043894064	PP_3157 // suhB
Secondary metabolite degradation	0.044997934	vdh // PP_3382 // PP_3383 // PP_3384 // kguD // kguK // mupP // amiD // nagZ // PP_2036 // gudD // glxR

Supplementary Methods

S1. *P. putida* KT2440 core metabolism kinetic model reconstruction

S1.2. Integration of omics data

Allosteric regulation was modeled using the generalized MWC model (Popova and Sel'kov, 1975, 1976, 1979), where the reaction flux is represented as the product of a catalytic and a regulatory function:

$$v = \Phi_{catalytic} \Psi_{regulatory}$$

The original omics data had units of mol · g cell dry weight (CDW)⁻¹, which were converted to mol L⁻¹, since $\Delta_r G'$ values are calculated based on concentrations of mol L⁻¹. Cell dry weight and volume values were calculated in comparison with the respective values for *E. coli* (Nyström and Neidhardt, 1996) and the conversion was made as follows:

$$[met]_{mol/L} = \frac{[met]_{mol/gCDW} \times gCDW}{V_{cell,water}}$$

where $[met]_{mol/L}$ is the metabolite concentration in mol L⁻¹, $[met]_{mol/gCDW}$ is the metabolite amount in mol · g CDW⁻¹, $gCDW$ is the single cell dry weight, 2.8×10^{-13} g and $V_{cell,water}$ is the volume of water in the cell, defined as 74% of the total cell volume (Cayley et al., 1991), where the total cell volume is set to 4.96×10^{-16} L (Ishii et al., 2007). Flux values were converted in the same way.

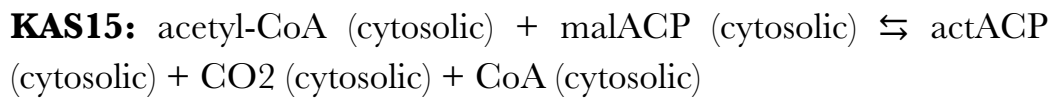
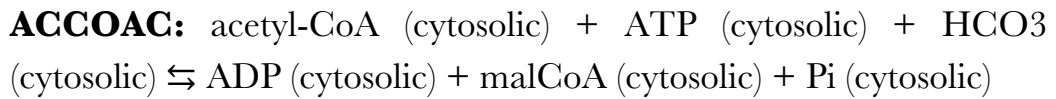
S1.2. Parsimonious enzyme usage flux balance analysis (pFBA)

pFBA (Lewis et al., 2010) was performed on the genome-scale model *i*JN1463 (Nogales et al., 2020) to find the fluxes for reactions that were not yet reported. To perform pFBA the fluxes for all reactions (Nikel et al., 2015;

2021) they were constrained to their mean value (the same used to build the kinetic model ensemble) and biomass production was maximized.

S1.3. Fatty acid synthesis reactions

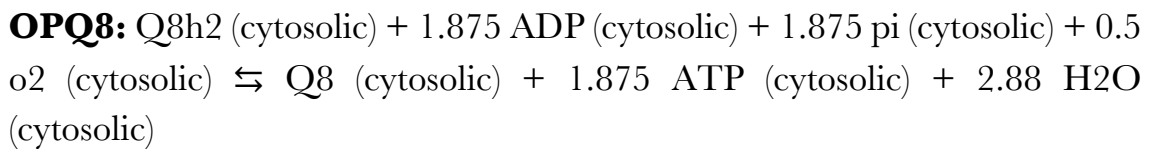
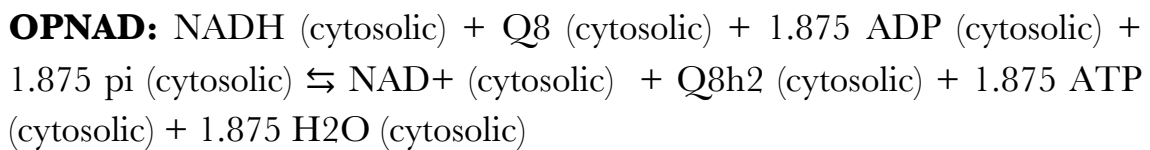
Three reactions from fatty acid synthesis were included in the model as follows:



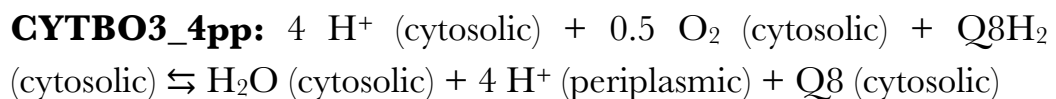
The fluxes for these reactions were calculated using pFBA on the genome-scale model *i*JN1463 as described above.

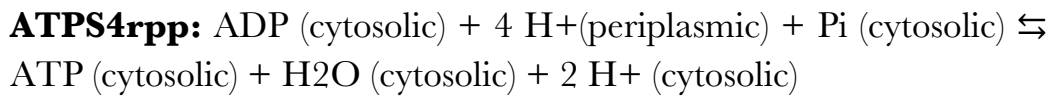
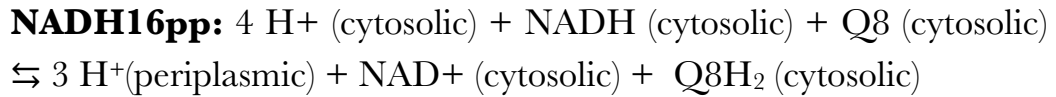
S1.4. Oxidative phosphorylation reactions

Oxidative phosphorylation was modeled by introducing the following two lumped reactions:



We decided on these reactions by checking the fluxes of all oxidative phosphorylation reactions in the genome-scale model *i*JN1463 after performing pFBA. In particular, we found the reactions with non-zero flux:





The protons were removed, since these are hard to balance, and the P/O ratio in *P. putida* (Kohlstedt and Wittmann, 2019) was used to summarize these three reactions into the two lumped reactions above. Once we had the two lumped reactions, we used *eQuilibrator* (Flamholz et al., 2012) to find their standard Gibbs energies, $\Delta_r G'^0$, which led to a rebalancing by adding water on the product side of each reaction.

To define the flux values of each reaction, we took the flux for ATPS4rpp as given by pFBA, divided it by the P/O ratio to find what the sum of the fluxes for OPNAD and OPQ8 should be. Since the sum of the individual fluxes of CYTBO3_4pp and NADH16pp is higher than the sum of the fluxes for OPNAD and OPQ8 should be, we removed roughly an equal percentage from both CYTBO3_4pp and NADH16pp fluxes, and set OPNAD flux to be the same as NADH16pp and OPQ8 the same as CYTBO3_4pp. As an example, if we have the following fluxes:

$$\mathbf{ATPS4rpp} = 16,052$$

$$\mathbf{CYTBO3_4pp} = 12,971$$

$$\mathbf{NADH16pp} = 4,398$$

then the sum of the fluxes through OPNAD and OPQ8 (and consequently CYTBO3_4pp and NADH16pp) should be $16,052/1.875 \approx 8,561$, and the fluxes through CYTBO3_4pp and NADH16pp are reduced by roughly 50% each, so we have

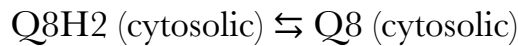
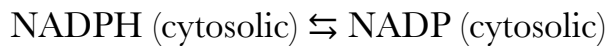
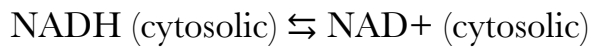
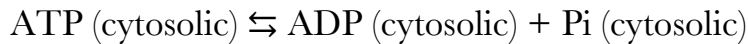
$$\mathbf{CYTBO3_4pp} = 6,381 = \text{OPQ8}$$

and

$$\mathbf{NADH16pp} = 2,190 = \text{OPNAD}.$$

S1.5. Balancing metabolite concentrations and cofactors

To achieve steady-state, exchange reactions were added to the model so that individual metabolites would be balanced: pyruvate (pyr), phosphoenolpyruvate (pep), D-glucose 6-phosphate (g6p), α -D-ribose 5-phosphate (r5p), glyceraldehyde 3-phosphate (g3p), D-erythrose 4-phosphate (e4p), D-fructose-6-phosphate (f6p), 3-phospho-D-glycerate (3pg), oxaloacetate (oaa), L-malate (mal__L), 2-oxoglutarate (akg), succinate (succ), D-ribulose 5-phosphate (ru5p__D), fumarate (fum), sedoheptulose-7-phosphate (s7p), 3-phospho-D-glyceroyl phosphate (13dpg) and dihydroxyacetone phosphate (dhap). To balance cofactors, the following reactions were added to interconvert cofactor pairs:



The fluxes for each reaction were defined such that the whole system would be at steady-state.

S1.6. Promiscuous enzymes

All enzymes that use either NAD^+ or NADP^+ as a substrate/product were assumed to be able to catalyze the same reaction using both cofactors. The flux proportion for each reaction was defined based on the measurements of cofactor specificity under non-saturating quasi *in vivo* conditions (Fuhrer and Sauer, 2009; Nikel et al., 2015).

S1.7. Metabolic control analysis

The concentration control coefficients were calculated as follows, based on Kacser et al. (1990):

$$C_E^M = C_v^M \Pi$$

where C_E^M are the concentration control coefficients when enzyme concentrations are perturbed and Π is parameter elasticity matrix:

$$\pi_{ij} = \frac{p_j}{v_i} \left(\frac{\partial v_i}{\partial p_j} \right)$$

C_v^M are the concentration control coefficients when reaction fluxes are perturbed:

$$C_v^M = \frac{v}{M} \frac{\partial M}{\partial v} = \frac{\partial \ln M}{\partial \ln v}$$

which is equivalent to Sauro and Kacser (1990):

$$C_v^M = - \left[S \frac{\partial v}{\partial M} \right]^{-1} S = -J^{-1} S$$

where M represents the metabolite concentrations at steady-state, E represents enzyme concentrations, v represents reaction fluxes, S is the stoichiometric matrix, and J is the Jacobian matrix. If a change in an enzyme perturbation leads to a proportional change in the respective reaction's flux and enzyme perturbations are independent, i.e. if perturbing enzyme i has no impact on the local rate of enzyme j , then $\Pi = 1$ and $C_E^M = C_v^M$. However, if promiscuous enzymes are part of the system, perturbing the concentration of enzyme i will have an impact in the flux of two or more reactions and $\Pi \neq 1$. In our model, there are several enzymes that can use both NAD⁺ and NADP⁺, thus $\Pi \neq 1$ in this case.

S2. Analytical PHB determinations

PHB, dissolved in CHCl_3 at 0.25 mg mL^{-1} , 0.5 mg mL^{-1} , 1 mg mL^{-1} , 1.5 mg mL^{-1} and 2 mg mL^{-1} was used as a standard. The acidic methanolysis reaction is well-known (Braunegg et al., 1978):



The chromatogram peak area (A) was taken as a measure for molar concentration. Using the values of internal standard (IS), molar concentration of the methanolized monomer C_x was calculated as:

$$[C_x] = \frac{A_{C_x}}{A_{IS}} \cdot \frac{MW_{IS}}{MW_{C_x}} [IS]$$

Where MW_{C_x} is a molar mass of the monomeric unit (PHB). The PHB mass in the original 2 mL sample was calculated as:

$$PHA = 2 \cdot \sum [C_x] \cdot MW_{C_x}$$

The polymer standards provided information about the methanolysis conversion X :

$$X = \frac{(\text{PHB in the assay})}{(\text{PHB originally present in the standard})}$$

and

$$(\text{PHB in the sample}) = \frac{(\text{PHB in the assay})}{X}$$

The resulting yields for PHB content in the cells were calculated normalizing obtained results by CDW values.

Supplementary Figures

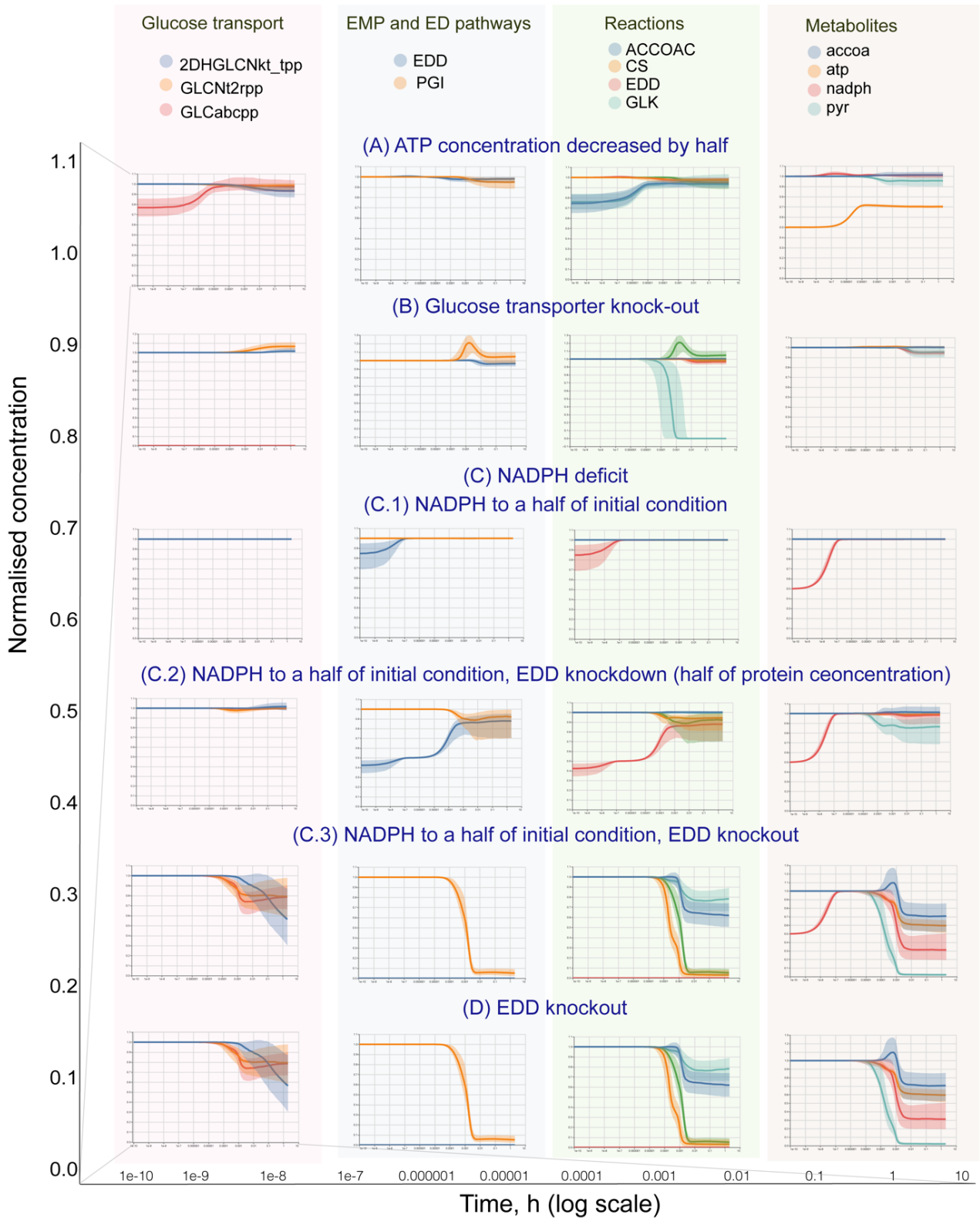


Figure S1 Consistency check for the kinetic model: time course simulations implemented in GRASP. In brief, the system of differential equations was integrated with a solver for stiff problems based on numerical differentiation (ode15s MATLAB® R2018a, MathWorks). The reference metabolites concentration was used as initial concentrations for all simulations. Knock outs are simulated by specifying the enzyme amount as 0 in order to change maximum reaction rate. For EDD knock down simulation 0.5 enzyme amount was used. All plots show median value of the ensemble model prediction in bold line and interquartile range in shaded area. Abbreviations for each reaction and metabolite are listed in **Tables S4** and **S7**, respectively.

Figure S2. MCA (*metabolite control analysis*) modelling using *P. putida* KT2440 core metabolism kinetic model reconstruction. Concentration control coefficient (CCC) values are shown as a heatmap for key metabolites and reactions of central carbon metabolism (top), and CCC distribution for the acetyl-CoA metabolite and citrate synthase (CS) reaction is presented for each of the 10,000 models in the ensemble (bottom). Abbreviations for each reaction and metabolite are listed in **Tables S4** and **S7**, respectively.

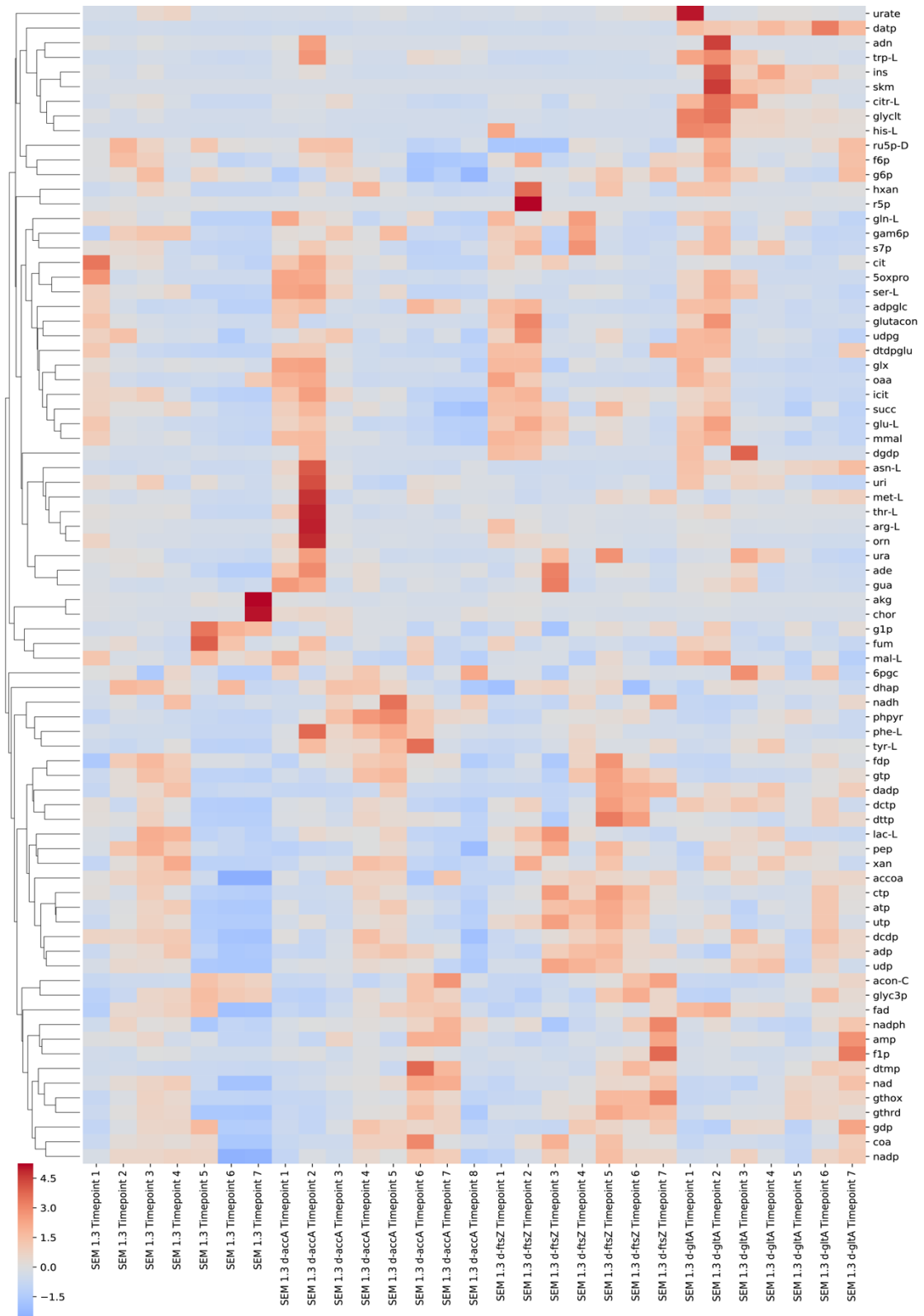


Figure S3. MCA (*metabolite control analysis*) metabolomics during time-course LS-MS measurements for *P. putida* SEM1.3 carrying pMCRi vectors (non-target, *accA*, *gltA*, *ftsZ*). Timepoints are indicated as: **1.** – 0.1 h (pre-induction); **2.** 0 h, **3.** 3 h, **4.** 5 h, **5.** 6 h, **6.** 6 h and **7.** 9 h post-induction. Data were normalized across samples before analysis by subtracting the mean and dividing by the standard deviation. Euclidean distance between the samples was used to perform clustering (*y*-axis). Abbreviations for metabolites are indicated in **Table S4.**

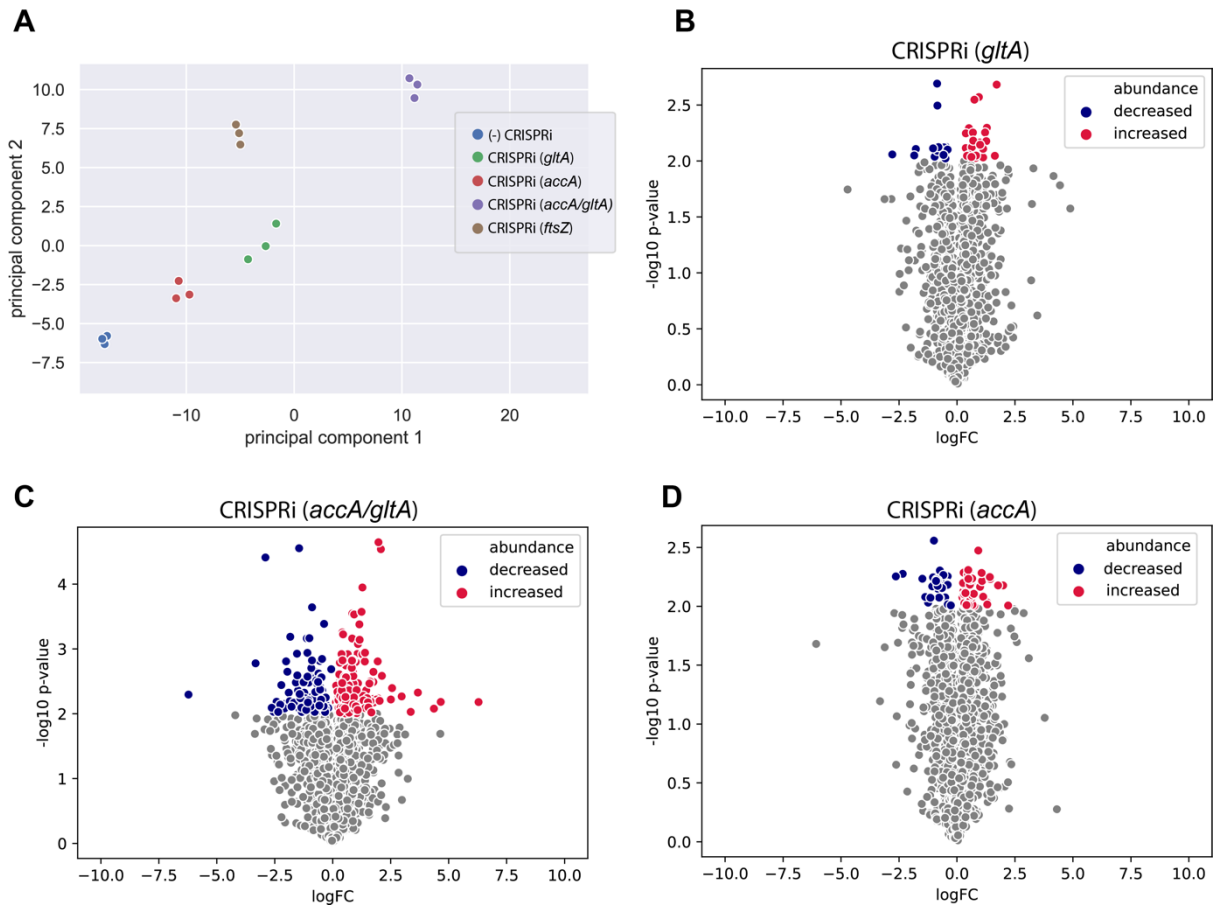


Figure S4. Statistical analysis of proteomics. **(A)** PCA (principal component analysis) was performed for quality control purposes. All the samples from the same group cluster together. The percentage of the explained variance by component 1 is 69.53%; the percentage of the explained variance by component 2 is 15.87%. The percentage of the explained variance by two first components is 85.40%. sklearn PCA was used for this analysis; data was normalized before analysis by subtracting the mean and dividing by the standard deviation. Volcano plots of proteome comparison between *P. putida* SEM1.3 transformed with an empty pMCRi vector [non-target spacer, indicated as (-)CRISPRi] and strains with CRISPRi-mediated downregulation of target genes: *gltA* **(B)**; *accA* and *gltA* **(C)**; and *accA* **(D)**. Proteins with decreased abundance are shown in blue, proteins with increased abundance shown in red. False discovery rate (FDR) of 0.01% was used as a threshold for significance. FDR was calculated according to the Benjamini and Hochberg procedure. A logFC [log₁₀ fold change, where fold change is calculated as abundance in a group divided to the abundance in the (-)CRISPRi group] threshold of 1.5 was chosen to highlight the number proteins which abundance changed the most.

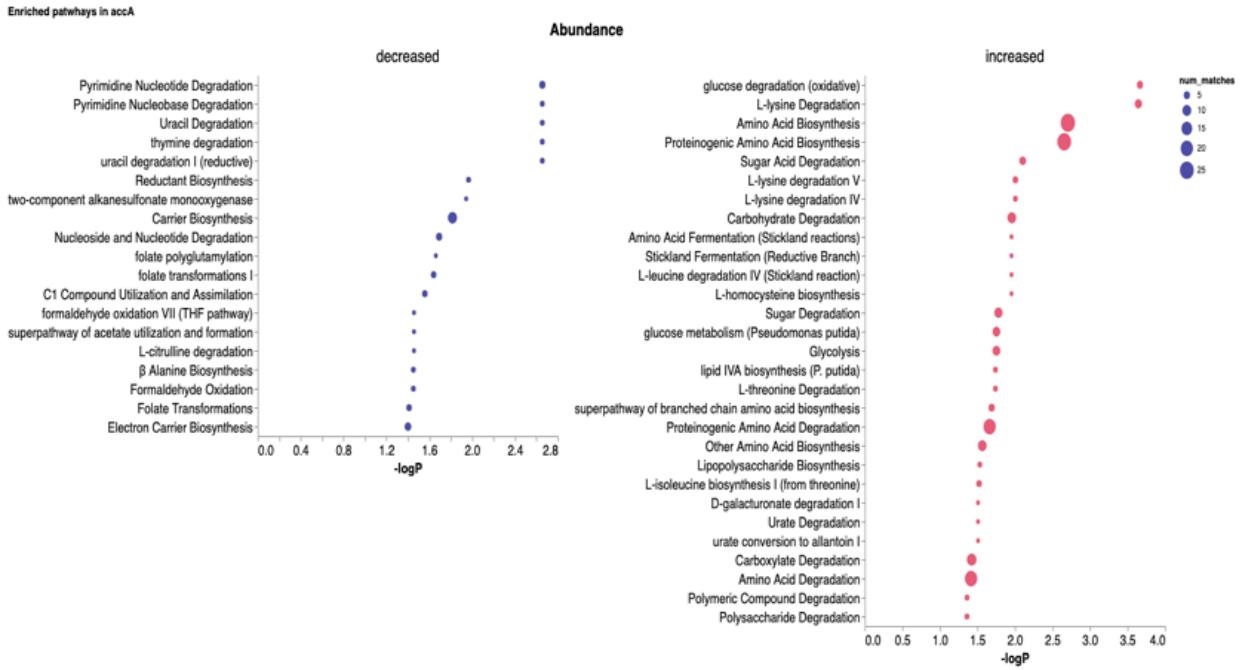


Figure S5. Metabolic pathway enrichment analysis of proteins with changed abundance. The significantly enriched pathways (P -value < 0.05) in the proteome of CRISPRi mediated depletion targeting *accA*. The position of the marker represents the $-\log P$ -values and the size of the node represents the matched proteins. On the left panel, the pathways enriched with proteins with decreased abundances are shown (in blue), on the right panel, the pathways with proteins with increased abundances are shown (in red).

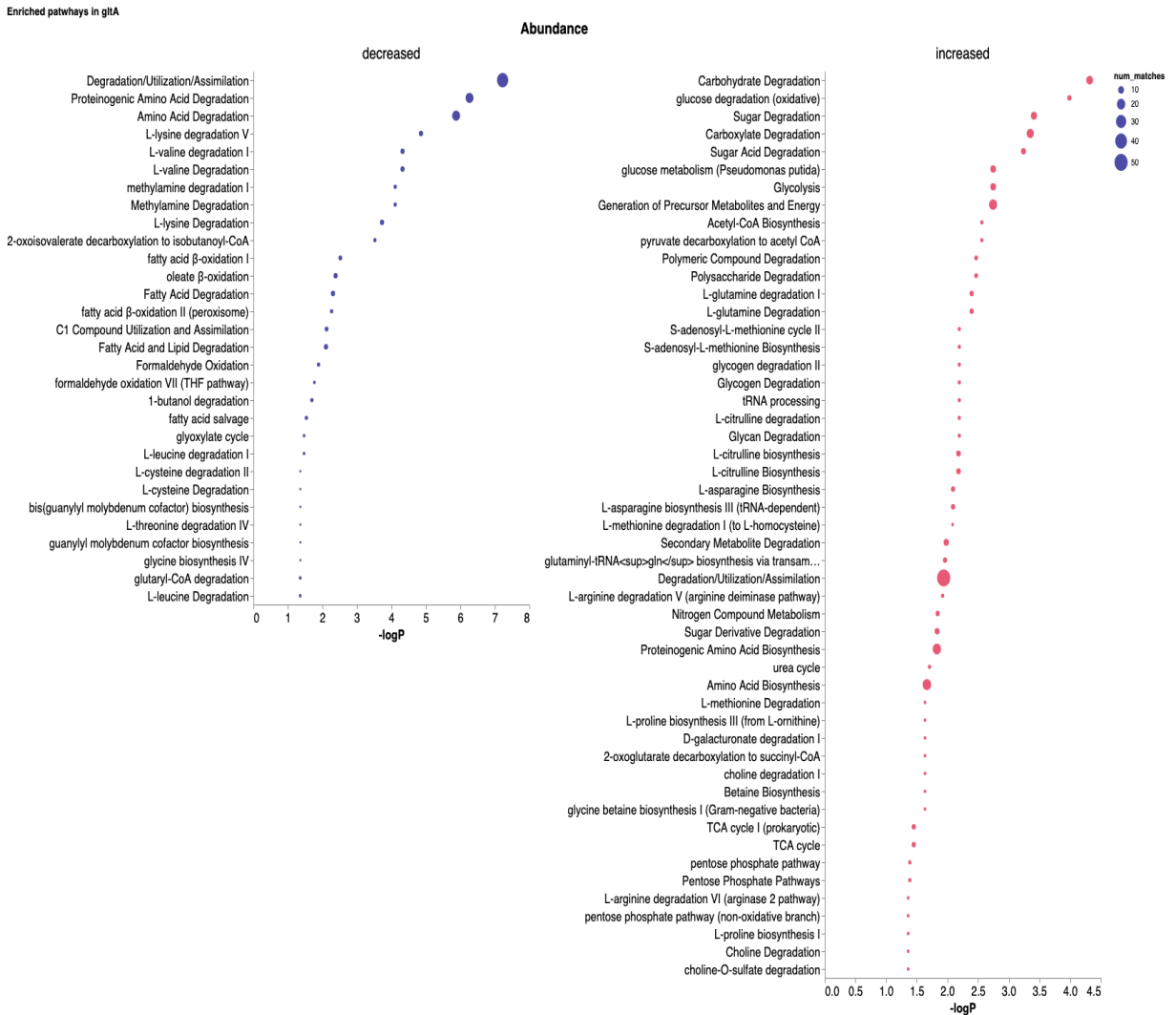


Figure S6. Metabolic pathway enrichment analysis of proteins with changed abundance. The significantly enriched pathways (P -value < 0.05) in the proteome of CRISPRi mediated depletion targeting *gltA*. The position of the marker represents the $-p$ -values and the size of the node represents the matched proteins. On the left panel, the pathways enriched with proteins with decreased abundances are shown (in blue), on the right panel, the pathways with proteins with increased abundances are shown (in red).

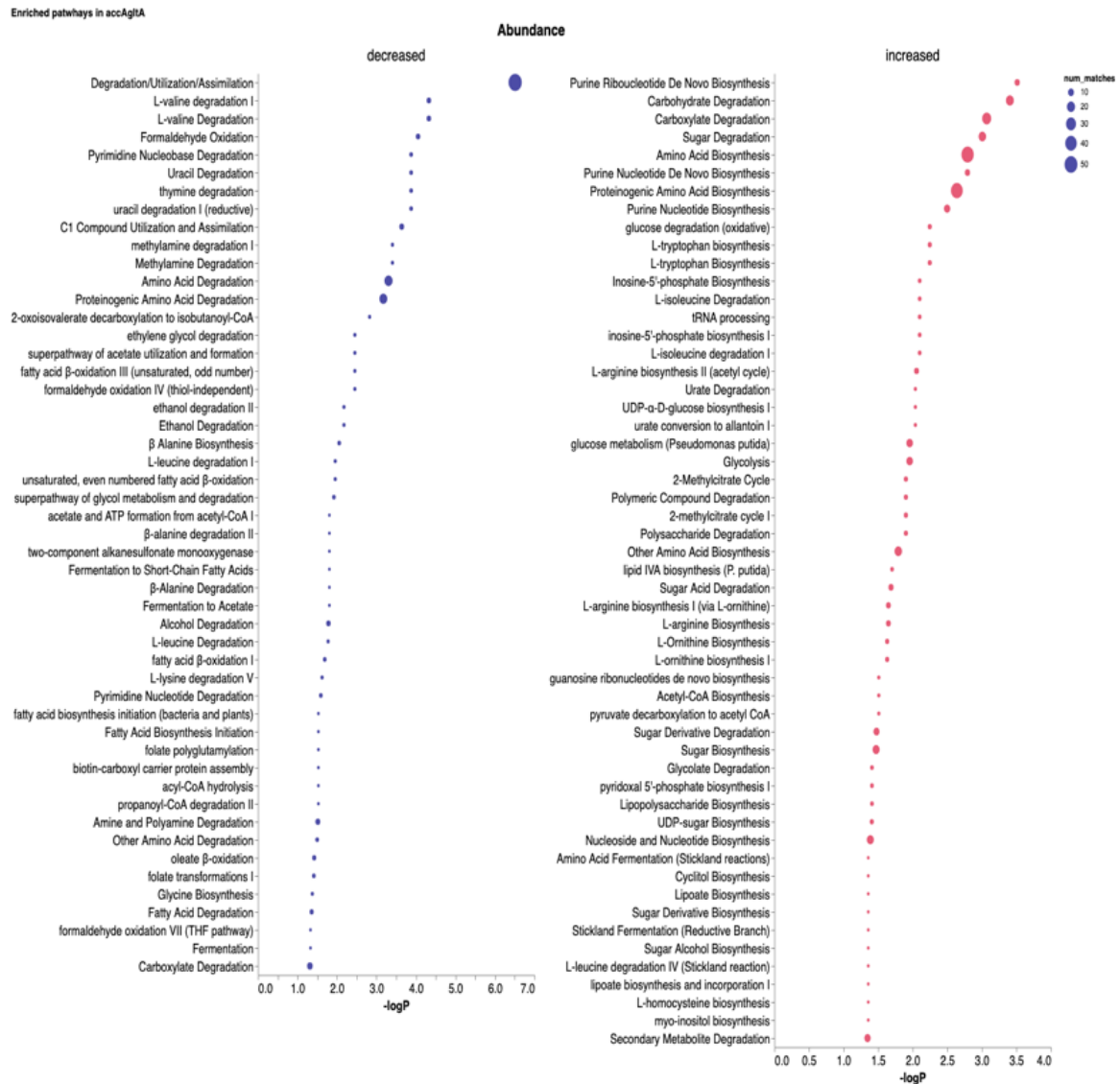


Figure S7. Metabolic pathway enrichment analysis of proteins with changed abundance. The significantly enriched pathways (P -value < 0.05) in the proteome of CRISPRi mediated depletion targeting *accA* and *gltA*. The position of the marker represents the $-p$ -values and the size of the node represents the matched proteins. On the left panel, the pathways enriched with proteins with decreased abundances are shown (in blue), on the right panel, the pathways with proteins with increased abundances are shown (in red).

References

1. Anderson, R. F., Shinde, S. S., Hille, R., Rothery, R. A., Weiner, J. H., Rajagukguk, S., Maklashina, E., Cecchini, G., 2014. Electron-transfer pathways in the heme and quinone-binding domain of complex II (succinate dehydrogenase). *Biochemistry*. 53, 1637-1646.
2. Asztalos, P., Parthier, C., Golbik, R., Kleinschmidt, M., Hubner, G., Weiss, M. S., Friedemann, R., Wille, G., Tittmann, K., 2007. Strain and near attack conformers in enzymic thiamin catalysis: X-ray crystallographic snapshots of bacterial transketolase in covalent complex with donor ketoses xylulose 5-phosphate and fructose 6-phosphate, and in noncovalent complex with acceptor aldose ribose 5-phosphate. *Biochemistry*. 46, 12037-12052.
3. Ben-Bassat, A., Goldberg, I., 1980. Purification and properties of glucose-6-phosphate dehydrogenase (NADP⁺/NAD⁺) and 6-phosphogluconate dehydrogenase (NADP⁺/NAD⁺) from methanol-grown *Pseudomonas C*. *Biochim. Biophys. Acta*. 611, 1-10.
4. Braunegg, G., Sonnleitner, B., Lafferty, R. M., 1978. A rapid gas chromatographic method for the determination of poly-β-hydroxybutyric acid in microbial biomass. *Eur. J. Appl. Microbiol. Biotechnol.* 6, 29-37.
5. Burns, G., Brown, T., Hatter, K., Sokatch, J. R., 1988. Comparison of the amino acid sequences of the transacylase components of branched chain oxoacid dehydrogenase of *Pseudomonas putida*, and the pyruvate and 2-oxoglutarate dehydrogenases of *Escherichia coli*. *Eur. J. Biochem.* 176, 165-169.
6. Caspi, R., Billington, R., Fulcher, C. A., Keseler, I. M., Kothari, A., Krummenacker, M., Latendresse, M., Midford, P. E., Ong, Q., Ong, W. K., Paley, S., Subhraveti, P., Karp, P. D., 2018. The MetaCyc database of metabolic pathways and enzymes. *Nucleic Acids Res.* 46, D633-D639.
7. Cayley, S., Lewis, B. A., Guttman, H. J., Record, M. T., 1991. Characterization of the cytoplasm of *Escherichia coli* K-12 as a function of external osmolarity. Implications for protein-DNA interactions *in vivo*. *J. Mol. Biol.* 222, 281-300.
8. Chen, Y. Y., Ko, T. P., Chen, W. H., Lo, L. P., Lin, C. H., Wang, A. H., 2010. Conformational changes associated with cofactor/substrate binding of 6-phosphogluconate dehydrogenase from *Escherichia coli* and *Klebsiella pneumoniae*: Implications for enzyme mechanism. *J. Struct. Biol.* 169, 25-35.
9. Chuang, D. T., Utter, M. F., 1979. Structural and regulatory properties of pyruvate kinase from *Pseudomonas citronellolis*. *J. Biol. Chem.* 254, 8434-8441.

10. Cleland, W. W., 1963. The kinetics of enzyme-catalyzed reactions with two or more substrates or products. I. Nomenclature and rate equations. *Biochim. Biophys. Acta.* 67, 104-137.
11. Coffee, C. J., Hu, A. S., 1972. The kinetic characterization of gluconokinase from a pseudomonad. *Arch. Biochem. Biophys.* 149, 549-559.
12. Davidson, A. L., Chen, J., 2004. ATP-binding cassette transporters in bacteria. *Annu. Rev. Biochem.* 73, 241-268.
13. Flamholz, A., Noor, E., Bar-Even, A., Milo, R., 2012. *eQuilibrator*—The biochemical thermodynamics calculator. *Nucleic Acids Res.* 40, D770-775.
14. Fuhrer, T., Sauer, U., 2009. Different biochemical mechanisms ensure network-wide balancing of reducing equivalents in microbial metabolism. *J. Bacteriol.* 191, 2112-2121.
15. Garrido-Pertierra, A., Martínez Marcos, C., Martín Fernández, M., Ruiz-Amil, M., 1983. Properties and function of malate enzyme from *Pseudomonas putida*. *Biochimie.* 65, 629-635.
16. Ishii, N., Nakahigashi, K., Baba, T., Robert, M., Soga, T., Kanai, A., Hirasawa, T., Naba, M., Hirai, K., Hoque, A., Ho, P. Y., Kakazu, Y., Sugawara, K., Igarashi, S., Harada, S., Masuda, T., Sugiyama, N., Togashi, T., Hasegawa, M., Takai, Y., Yugi, K., Arakawa, K., Iwata, N., Toya, Y., Nakayama, Y., Nishioka, T., Shimizu, K., Mori, H., Tomita, M., 2007. Multiple high-throughput analyses monitor the response of *E. coli* to perturbations. *Science.* 316, 593-597.
17. Jia, J., Huang, W., Schorcken, U., Sahm, H., Sprenger, G. A., Lindqvist, Y., Schneider, G., 1996. Crystal structure of transaldolase B from *Escherichia coli* suggests a circular permutation of the alpha/beta barrel within the class I aldolase family. *Structure.* 4, 715-724.
18. Kacser, H., Sauro, H. M., Acerenza, L., 1990. Enzyme-enzyme interactions and control analysis. 1. The case of non-additivity: monomer-oligomer associations. *Eur. J. Biochem.* 187, 481-491.
19. Kohlstedt, M., Wittmann, C., 2019. GC-MS-based ¹³C metabolic flux analysis resolves the parallel and cyclic glucose metabolism of *Pseudomonas putida* KT2440 and *Pseudomonas aeruginosa* PAO1. *Metab. Eng.* 54, 35-53.
20. Lai, C. Y., Tchola, O., Cheng, T., Horecker, B. L., 1965. The mechanism of action of aldolases. 8. The number of combining sites in fructose diphosphate aldolase. *J. Biol. Chem.* 240, 1347-1350.
21. Larsson-Raznikiewicz, M., Arvidsson, L., 1971. Inhibition of phosphoglycerate kinase by products and product homologues. *Eur. J. Biochem.* 22, 506-512.

22. Lee, Y. N., Lessie, T. G., 1974. Purification and characterization of the two 6-phosphogluconate dehydrogenase species from *Pseudomonas multivorans*. *J. Bacteriol.* 120, 1043-1057.
23. Lessmann, D., Schimz, K. L., Kurz, G., 1975. D-glucose-6-phosphate dehydrogenase (Entner-Doudoroff enzyme) from *Pseudomonas fluorescens*. Purification, properties and regulation. *Eur. J. Biochem.* 59, 545-559.
24. Levy, H. R., Christoff, M., Ingulli, J., Ho, E. M., 1983. Glucose-6-phosphate dehydrogenase from *Leuconostoc mesenteroides*: revised kinetic mechanism and kinetics of ATP inhibition. *Arch. Biochem. Biophys.* 222, 473-488.
25. Lewis, N. E., Hixson, K. K., Conrad, T. M., Lerman, J. A., Charusanti, P., Polpitiya, A. D., Adkins, J. N., Schramm, G., Purvine, S. O., López-Ferrer, D., Weitz, K. K., Eils, R., König, R., Smith, R. D., Palsson, B. Ø., 2010. Omic data from evolved *E. coli* are consistent with computed optimal growth from genome-scale models. *Mol. Syst. Biol.* 6, 390.
26. Mitchell, C. G., Weitzman, P. D., 1986. Molecular size diversity of citrate synthases from *Pseudomonas* species. *J. Gen. Microbiol.* 132, 737-742.
27. Molina, L., La Rosa, R., Nogales, J., Rojo, F., 2019. *Pseudomonas putida* KT2440 metabolism undergoes sequential modifications during exponential growth in a complete medium as compounds are gradually consumed. *Environ. Microbiol.* 0.
28. Nickel, P. I., Chavarría, M., Fuhrer, T., Sauer, U., de Lorenzo, V., 2015. *Pseudomonas putida* KT2440 strain metabolizes glucose through a cycle formed by enzymes of the Entner-Doudoroff, Embden-Meyerhof-Parnas, and pentose phosphate pathways. *J. Biol. Chem.* 290, 25920-25932.
29. Nickel, P. I., Fuhrer, T., Chavarría, M., Sánchez-Pascuala, A., Sauer, U., de Lorenzo, V., 2021. Reconfiguration of metabolic fluxes in *Pseudomonas putida* as a response to sub-lethal oxidative stress. *ISME J.*, In press, DOI: 10.1038/s41396-41020-00884-41399.
30. Nickel, P. I., Martínez-García, E., de Lorenzo, V., 2014. Biotechnological domestication of pseudomonads using synthetic biology. *Nat. Rev. Microbiol.* 12, 368-379.
31. Nogales, J., Mueller, J., Gudmundsson, S., Canalejo, F. J., Duque, E., Monk, J., Feist, A. M., Ramos, J. L., Niu, W., Palsson, B. Ø., 2020. High-quality genome-scale metabolic modelling of *Pseudomonas putida* highlights its broad metabolic capabilities. *Environ. Microbiol.* 22, 255-269.
32. Nyström, T., Neidhardt, F. C., 1996. Effects of overproducing the universal stress protein, UspA, in *Escherichia coli* K-12. *J. Bacteriol.* 178, 927-930.
33. Olsthoorn, A. J., Duine, J. A., 1996. Production, characterization, and reconstitution of recombinant quinoprotein glucose dehydrogenase

- (soluble type; EC 1.1.99.17) apoenzyme of *Acinetobacter calcoaceticus*. Arch. Biochem. Biophys. 336, 42-48.
34. Popova, S. V., Sel'kov, E. E., 1975. Generalization of the model by Monod, Wyman and Changeux for the case of a reversible monosubstrate reaction SR, TP. FEBS Lett. 53, 269-273.
35. Popova, S. V., Sel'kov, E. E., 1976. Generalization of the Monod-Wyman-Changeux model for the case of multisubstrate reactions. Mol. Biol. 10, 1116-1126.
36. Popova, S. V., Sel'kov, E. E., 1979. Description of the kinetics of the two substrate reactions S_1+S_2 goes to and comes from S_3+S_4 by a generalized Monod, Wyman, Changeux model. Mol. Biol. 13, 129-139.
37. Rutter, W. J., Ling, K. H., 1958. The mechanism of action of fructose diphosphate aldolase. Biochim. Biophys. Acta. 30, 71-79.
38. Saa, P. A., Nielsen, L. K., 2017. Formulation, construction and analysis of kinetic models of metabolism: A review of modelling frameworks. Biotechnol. Adv. 35, 981-1003.
39. Sauro, H. M., Kacser, H., 1990. Enzyme-enzyme interactions and control analysis. 2. The case of non-independence: heterologous associations. Eur. J. Biochem. 187, 493-500.
40. Vander Wyk, J. C., Lessie, T. G., 1974. Purification and characterization of the *Pseudomonas multivorans* glucose-6-phosphate dehydrogenase active with nicotinamide adenine dinucleotide. J. Bacteriol. 120, 1033-1042.
41. Wang, C. S., Alaupovic, P., 1980. Glyceraldehyde-3-phosphate dehydrogenase from human erythrocyte membranes. Kinetic mechanism and competitive substrate inhibition by glyceraldehyde 3-phosphate. Arch. Biochem. Biophys. 205, 136-145.
42. Wang, W., Baker, P., Seah, S. Y., 2010. Comparison of two metal-dependent pyruvate aldolases related by convergent evolution: substrate specificity, kinetic mechanism, and substrate channeling. Biochemistry. 49, 3774-3782.
43. Winsor, G. L., Griffiths, E. J., Lo, R., Dhillon, B. K., Shay, J. A., Brinkman, F. S., 2016. Enhanced annotations and features for comparing thousands of *Pseudomonas* genomes in the *Pseudomonas* Genome Database. Nucleic Acids Res. 44, D646-D653.
44. Winsor, G. L., Lam, D. K. W., Fleming, L., Lo, R., Whiteside, M. D., Yu, N. Y., Hancock, R. E. W., Brinkman, F. S. L., 2011. *Pseudomonas* Genome Database: improved comparative analysis and population genomics capability for *Pseudomonas* genomes. Nucleic Acids Res. 39, D596-D600.

Chapter 6

PATHWAY AND MORPHOLOGY ENGINEERING TOWARDS 2-PENTANONE BIOSYNTHESIS IN WHOLE- AND MINI-CELLS OF *PSEUDOMONAS PUTIDA*

Ekaterina Kozaeva¹, Kent K. Y. Tang², and Pablo I. Nikel^{1*}

1. The Novo Nordisk Foundation Center for Biosustainability, Technical University of Denmark, 2800 Kgs. Lyngby, Denmark
2. Novo Nordisk A/S, Novo Allé, 2880 Bagsvaerd, Denmark

* Correspondence to:

Pablo I. Nikel
(pabnik@biosustain.dtu.dk)
The Novo Nordisk Foundation Center for
Biosustainability
Technical University of Denmark
Kgs Lyngby 2800, Denmark
Tel: (+45) 93 51 19 18

INTRODUCTION

The pathway towards green manufacturing calls for a broad expansion of the biochemical repertoire in living cells beyond the trivial, endogenous molecules that form part of the extant metabolism. To this end, microorganisms have been engineered to produce a wide spectrum of chemicals¹. Ketones, for instance, form an important class of structurally-diverse molecules produced in large quantities using traditional, oil-dependent synthetic chemistry². Methyl ketones (MK), a subset of this family of compounds where one ligand on the carbonyl carbon is a CH₃ group, play an important commercial role. Because of their strong solvent properties and generally high evaporation rates, MKs are used as building-blocks in the fragrance, flavor, textiles, pesticide and agrochemical industries³⁻⁵, as well as being components in pharmacological synthesis^{6,7}. 2-Pentanone is a prominent member of the MK family, which, besides applications in the fragrance sector, is recognized as an inhibitor of prostaglandin production associated with colon carcinogenesis. In fact, 2-pentanone shows potential as a treating agent of colon cancer as it can mediate a 2-fold inhibition of COX-2 protein production in TNF- α stimulated cells⁸. Greener alternatives for MK production are needed to fulfil market demands, and the adoption of robust microbial cell factories emerge as an attractive option to this end.

The only 2-pentanone bioproduction approach reported so far involves an engineered *Escherichia coli* strain in a process that uses glucose as a carbon source. The engineered strain contained two plasmids: one of them, carrying three genes, encodes proteins for coenzyme A (CoA)-dependent chain elongation, while the other harbors four genes encoding the actual ketone production pathway⁹. The CoA-dependent pathway allows ketoacid chain elongation, yielding butyryl-CoA (C₄) from acetyl-CoA (C₂) extender units. The ketone production pathway is inspired by the well-described fermentation process to produce acetone in *Clostridium acetobutylicum* ATCC 824, also known as the “Weizmann organism”¹⁰. Adapting this pathway to produce 2-pentanone (C₅) involves the condensation of acetyl-CoA and butyryl-CoA (forming 3-ketohexanoyl-

CoA) followed by decarboxylation to yield the final product. Toxicity issues, imposed either by the intermediates or the products of the MK biosynthesis pathway on the producer cells, continue to be a major hurdle that impairs the development of robust bioprocesses. This occurrence also leads to the loss of plasmids encoding the components of the MK biosynthesis pathway or the accumulation of mutations in the genes thereof, resulting in non-producing phenotypes.

While several strategies have been implemented towards extending the lifespan of actively producing cell factories, growth-coupled bioprocesses involving harsh, reactive products tend to display limited yields due to the stability issues mentioned above. An alternative to *in vivo*, whole-cell bioproduction is the use of anucleated vesicles as catalysts^{11,12}. Chromosome-free mini-cells, for instance, are natural occurrences within bacterial populations. Under normal conditions, the tubulin-like FtsZ protein assembles into a ring-like structure (ζ ring) at the middle of the cell, determining the future bacterial division site. During the cell division process, the ζ ring constricts and recruits the peptidoglycan synthesis machinery in combination with associated proteins^{13,14}. FtsZ unit assembly is controlled by the Min system, which includes the MinC, MinD and MinE structural proteins. MinC and MinD inhibit FtsZ assembly, while MinE is a negative regulator of MinCD. Mini-cells are formed when there is a limited abundance of MinC and MinD, whereupon FtsZ promotes asymmetric cell division¹⁵.

Mini-cells do not contain nucleic acids and are thus unable to further divide; for this reason, they have historically been exploited as a model for visualizing molecular machinery by cryo-electron tomography. Remarkably, these chromosome-less vesicles have not been extensively exploited for bioproduction, in spite of their potential for stable bioproduction of chemicals¹⁶. For instance, plasmids are preferentially located at the poles and enter mini-cells *via* active partitioning or random distribution¹⁷, enabling enhanced protein production. Moreover, mini-cells are expected to allocate resources to biotechnological goals instead to housekeeping processes, e.g. genome duplication¹⁸.

Building on the well-known solvent tolerance of *Pseudomonas putida*¹⁹ and its ability of using a wide range of carbon sources, in this work we adapted genome-reduced *P. putida* strains for 2-pentanone bioproduction. The product toxicity was compared in *E. coli* and *P. putida*, and optimized production conditions were explored by using butyrate as main carbon source. Different synthetic pathway designs were likewise tested, analyzing expression system performance across production conditions. Moreover, we extended the range of MK production setups by engineering *P. putida*-derived chromosome-free mini-cells containing the selected pathway enzymes. This programmable *chassis*, relevant for handling toxic intermediates, was examined for its ability to stably produce 2-pentanone over extended timeframes—a first case example of an ‘off-the-shelf’ bacterial cell factory for MK biosynthesis.

Materials and methods

2.1. Bacterial strains, plasmids, and culture conditions

All bacterial strains and plasmids used in this study presented in **Table 6.1**. *E. coli* cultures were incubated at 37°C, *P. putida* cultures were grown at 30°C. For cloning procedures and during genome engineering manipulations, lysogeny broth (LB) medium was used (10 g L⁻¹ tryptone, 5 g L⁻¹ yeast extract and 10 g L⁻¹ NaCl; solid culture media additionally contained 15 g L⁻¹ agar). For other experiments, the minimal medium de Bont was used, with the composition as follows: 3.88 g L⁻¹ K₂HPO₄, 1.63 g L⁻¹ NaH₂PO₄, 2 g L⁻¹ (NH₄)₂SO₄, 0.1 g L⁻¹ MgCl₂ · 6H₂O, 10 mg L⁻¹ EDTA, 2 mg L⁻¹ ZnSO₄ · 7H₂O, 1 mg L⁻¹ CaCl₂ · 2H₂O, 5 mg L⁻¹ FeSO₄ · 7H₂O, 0.2 mg L⁻¹ Na₂MoO₄ · 2H₂O, 0.2 mg L⁻¹ CuSO₄ · 5H₂O, 0.4 mg L⁻¹ CoCl₂ · 6H₂O, 1 mg L⁻¹ MnCl₂ · 2H₂O. For whole-cell 2-pentanone production assays, cultures were initiated from a saturated inoculum at a starting optical density measured at 600 nm (OD₆₀₀) of 0.05. Cells were grown for 24 h at 30 °C with rotary agitation at 200 rpm (MaxQ™ 8000 incubator; ThermoFisher Scientific, Waltham, MA, USA) in 10 mL of de Bont minimal medium with

the corresponding antibiotics and chemical inducers needed for induction of the pathway genes as indicated in the figure legends. Streptomycin (Str), and kanamycin (Km) were added whenever needed at 100 $\mu\text{g mL}^{-1}$ and 50 $\mu\text{g mL}^{-1}$, respectively. OD₆₀₀ was recorded in a Genesys 20 spectrophotometer (Thermo Fisher Scientific) to estimate bacterial growth. After 24 h, cultures were incubated for 1 h at 4°C and then centrifuged at 5,000 $\times g$ for 15 min at 4°C, and the presence of substrates and products in the resulting supernatant was analyzed by HPLC or GC-FID (as indicated in *Section 2.4* below). During physiological characterization of engineered strains, growth kinetics were followed at OD₆₀₀ with light path correction in a Synergy™ MX microtiter plate reader (BioTek Instruments Inc., Winooski, VT, USA).

2.2. General cloning procedures and construction of plasmids and mutant strains

Oligonucleotides and gene fragments used in this work are listed in **Table S7.1** and **S7.2** in the Supplemental Material. Unless stated otherwise, uracil-excision (*USER*) cloning²⁰ was used for the construction of all plasmids. The *AMUSER* tool was employed for designing oligonucleotides²¹. Phusion™ *U* high-fidelity DNA polymerase (ThermoFisher Scientific) was used according to the manufacturer's specifications in amplifications intended for *USER* cloning. For colony PCR, the commercial *OneTaq*™ master mix (New England BioLabs, Ipswich, MA, USA) was used according to the supplier's instructions. *E. coli* DH5 α λ *pir* (**Table 6.1**) was employed as a host for general cloning purposes. Chemically competent *E. coli* cells were prepared and transformed with plasmids using the Mix and Go™ commercial kit (Zymo Research, Irvin, CA, USA) according to the manufacturer's indications. The sequence of all used plasmids and strains was verified by Mix2Seq sequencing (Eurofins Genomics, Ebersberg, Germany).

Table 6.1. Bacterial strains and plasmids used in this study.

Bacterial strain	Relevant characteristics^a	Reference or source
<i>Escherichia coli</i>		
DH5α λ pir	Cloning host; F ⁻ λ - <i>endA1 glnX44(AS) thiE1 recA1 relA1 spoT1 gyrA96(Nal^R) rfbC1 deoR nupG Φ80(lacZΔM15) Δ(<i>argF-lac</i>)UI169 <i>hsdR17</i>(<i>r_K⁻ m_K⁺</i>), λpir lysogen</i>	Hanahan and Meselson ²²
<i>Pseudomonas putida</i>		
KT2440	Wild-type strain; derivative of <i>P. putida</i> mt-2 ²³ cured of the catabolic TOL plasmid pWW0	Bagdasarian, et al. ²⁴
EM42	Reduced-genome derivative of strain KT2440; Δ prophage1 Δ prophage4 Δ prophage3 Δ prophage2 Δ Tn7 Δ endA-1 Δ endA-2 Δ hsdRMS Δ flagellum Δ Tn4652	Martínez-García, et al. ²⁵
SEM1.3	Reduced-genome derivative of strain EM42; Δ phaC1ZC2DFI (Δ PP_5003-PP_5008) Δ benABCD (Δ PP_3161-PP_3164)	Kozaeva, et al. ²⁶
Plasmid	Relevant characteristics^a	Reference or source
pSEVA2313	Standard vector for constitutive gene expression; P _{EM7} promoter; <i>oriV</i> (pBBR1); Km ^R	Wirth, et al. ²⁷
pS2313 MKc	Derivative of vector pSEVA2313 harboring the genes encoding the canonical acetone production pathway from <i>Clostridium acetobutylicum</i> ; P _{EM7} → <i>thl^{Ca}</i> , <i>ctfAB^{Ca}</i> , <i>adc^{Ca}</i> ; Km ^R	This work

pS2313 ·MKs1	Derivative of vector pSEVA2313 harboring the genes encoding a synthetic MK production pathway; $P_{EM7} \rightarrow thl^{Ca}, atoDA^{Ec}, adc^{Ca}; Km^R$	This work
pS2313 ·MKs2	Derivative of vector pSEVA2313 harboring the genes encoding a synthetic MK production pathway; $P_{EM7} \rightarrow thl^{Ca}, pcaI^{Jp}, adc^{Ca}; Km^R$	This work
pS2313 ·MKs3	Derivative of vector pSEVA2313 harboring the genes encoding a synthetic MK production pathway; $P_{EM7} \rightarrow phaA^{Ca}, ctfAB^{Ca}, adc^{Ca}; Km^R$	This work
pSEVA438	Standard expression vector carrying a 3-mBz ⁻ inducible expression system; $oriV(pBBR1); xylS, Pm; Sm^R/Sp^R$	Silva-Rocha, et al. ²⁸
pS438 ·MKc	Derivative of vector pSEVA2313 harboring the genes encoding the canonical acetone production pathway from <i>C. acetobutylicum</i> ; $XylS/Pm \rightarrow thl^{Ca}, ctfAB^{Ca}, adc^{Ca}; Sm^R/Sp^R$	This work
pS438 ·MKs1	Derivative of vector pSEVA438 harboring the genes encoding a synthetic MK production pathway; $XylS/Pm \rightarrow thl^{Ca}, atoDA^{Ec}, adc^{Ca}; Sm^R/Sp^R$	This work
pSEVA4318	Standard expression vector carrying a rhamnose-inducible expression system; $oriV(pBBR1); rhaR, rhaS, P_{rhaBAD}; Sm^R/Sp^R$	This work
pS4318 ·MKc	Derivative of vector pSEVA43R harboring the genes encoding the canonical acetone production pathway from <i>C. acetobutylicum</i> ; $RhaRS/P_{rhaBAD} \rightarrow thl^{Ca}, ctfAB^{Ca}, adc^{Ca}; Sm^R/Sp^R$	This work

pS4318 ·MKs1	Derivative of vector pSEVA43R harboring the genes encoding a synthetic MK production pathway; RhaRS/ <i>P_{rhaBAD}</i> → <i>thl^{Ca}</i> , <i>atoDA^{Ec}</i> , <i>adc^{Ca}</i> ; Sm ^R /Sp ^R	This work
pS4318 ·MKc-Acs	Derivative of vector pSEVA43R harboring the genes encoding the canonical acetone production pathway from <i>C. acetobutylicum</i> and an acetyl-CoA synthase gene from <i>Bacillus subtilis</i> ; RhaRS/ <i>P_{rhaBAD}</i> → <i>thl^{Ca}</i> , <i>ctfAB^{Ca}</i> , <i>adc^{Ca}</i> , <i>acs^{Bs}</i> ; Sm ^R /Sp ^R	This work
pS4318 ·MKs1-Acs	Derivative of vector pSEVA43R harboring the genes encoding a synthetic MK production pathway and an acetyl-CoA synthase gene from <i>Bacillus subtilis</i> ; RhaRS/ <i>P_{rhaBAD}</i> → <i>thl^{Ca}</i> , <i>atoDA^{Ec}</i> , <i>adc^{Ca}</i> , <i>acs^{Bs}</i> ; Sm ^R /Sp ^R	This work
pCasso	Plasmid for cytidine base editing; <i>xyIS</i> (cured of <i>BsaI</i> -sites), <i>Pm</i> → <i>SpRY</i> (engineered Cas9 ^{Sp} nickase variant), <i>P_{EM7}</i> →non-specific sgRNA; <i>oriV</i> (pRO1600/ColE1); Sm ^R /Sp ^R	Kozaeva <i>et al.</i> , in preparation
pCasso <i>minD^{Q71}</i>	Plasmid for cytidine base editing; <i>P_{EM7}</i> → <i>minD_Q71</i> sgRNA; Sm ^R /Sp ^R	This work

^a Antibiotic markers and abbreviations are identified as follows: Km, kanamycin; Nal, nalidixic acid; Sm, streptomycin; Sp, spectinomycin; and MK, methyl ketone. The source of relevant genes is indicated with a superscript abbreviation as follows: *Ca*, *Clostridium acetobutylicum*; *Cn*, *Cupriavidus necator*; *Ec*, *Escherichia coli*; *Pp*, *Pseudomonas putida*; *Sp*, *Streptococcus pyogenes*; and *Bs*, *Bacillus subtilis*.

2.3. 2-Pentanone toxicity tests

The tolerance limit towards 2-pentanone of *P. putida* strains was assessed in two experimental setups, either in 50-mL test tubes or in microtiter plate cultures, with samples taken approximately every 1 h or at 15-min intervals, respectively, over 72 h. Experiments were performed using LB medium and minimal medium de Bont containing 1% (w/v) glucose in biological triplicates. Microtiter plates were covered with a Breath-Easy™ sealing membrane (Sigma-Aldrich Co., St. Louis, MO, USA) and OD₆₀₀ readings were recorded automatically under continuous shaking in an Elx808™ absorbance microplate reader (Biotek Instruments Inc.).

2.4. Detection and quantification of ketones and organic acids with GC-FID and HPLC

Culture samples (10 mL) were cooled down in an ice bath and transferred into pre-chilled, 50-mL conical tubes. Supernatants, obtained as indicated in Section 2.1., were extracted with hexane (200 µL), and the organic phase was separated by centrifugation for 10 min at 4,500×g at 4°C. The organic phase samples were analyzed by gas chromatography (GC) with flame-ionization detection (FID) in a Trace™ 1300 gas chromatograph (Thermo Fisher Scientific). The separation of products was carried out using an Agilent HP-INNOWax capillary column. The results were analyzed using the Chromeleon™ chromatography data system software 7.1.3 (Thermo Fisher Scientific). Quantification was performed by generating a standard calibration curve from the integrated area of spiked samples and calculating the corresponding concentration(s) in experimental samples by the integrated area of their respective peaks. The concentration of acetone was measured in a Dionex UltiMate 3000 HPLC system equipped with an Aminex™ HPX-87X ion exclusion (300×7.8 mm) column (BioRad, Hercules, CA) coupled to RI-150 refractive index and UV (260, 277, 304 and 210 nm) detectors. The column was maintained at 30°C, the mobile phase was comprised of 5 mM H₂SO₄ in Milli-Q water at a flow rate of 0.6 mL min⁻¹, with a run length of 30 min. The eluted compounds were detected

by a HPLC Waters 481 UV-visible detector at 214 nm. This detector was connected in series to an RI detector (model 410). HPLC data were processed using the Chromeleon™ chromatography data system software 7.1.3 (Thermo Fisher Scientific). The detection of acetone was monitored at RI and compound concentrations were calculated from peak areas using a calibration curve prepared with acetone (99% HPLC standard, Sigma-Aldrich Co.).

2.5. *Preparation and storage of P. putida mini cells*

Preculture for minicells production was grown overnight in LB medium with 100 µg mL⁻¹ of streptomycin, and the next day inoculated in LB medium with 100 µg mL⁻¹ of streptomycin and 10 mM of rhamnose for the pathway induction. After 24h, cells were harvested for minicell purification (**Figure 6.1**): (i) centrifugation at 1000 g for 5 min allows to precipitate parent cells, (ii) supernatant is further centrifugated at 17000g to precipitate minicells, (iii) resulting pellet is resuspended in the buffer of choice, containing 15% of glycerol to store the samples at -20C; additionally, 100 µg mL⁻¹ of ampicillin can be added to prevent bacterial contamination. As a result, purified minicell fraction was carefully resuspended in the 30 mM of phosphate buffer and aliquoted for further storage at -20C.

2.6. *Data and statistical analysis*

All the experiments reported were independently repeated at least in three independent biological replicates (as indicated in the corresponding figure legend), and the mean value of the corresponding parameter ± standard deviation is presented. When relevant, the level of significance of differences when comparing results was evaluated by ANOVA (Barlett's test, Prism 8, GraphPad software, San Diego, CA, USA) with a *P* value = 0.01, as indicated in the figure legends.

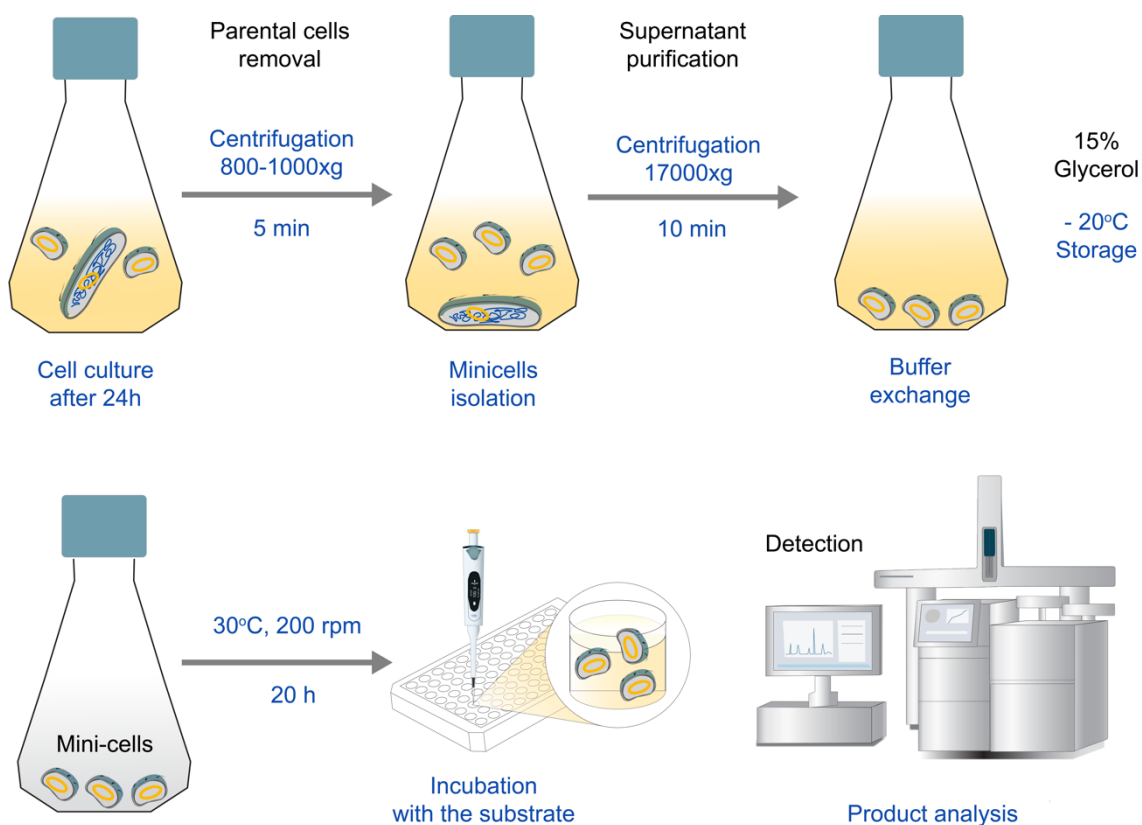


Figure 6.1. Schematic representation of the protocol for mini-cells production and purification. The resulting mini-cell fraction can be either used immediately or stored for at least a month -20°C. The product is detected after 20 h incubation with the substrate.

Results and discussion

3.1. *P. putida* is endowed with high tolerance towards 2-pentanone and butyrate

One of the challenges for MK production in bacterial cell factories is the stress caused by the endogenously produced chemicals, which could inhibit bacterial growth or even cause cell death. So far, the only bio-based approach for 2-pentanone production has been reported in engineered *E. coli* strains, where the toxicity issue was clearly noted. Growth of *E. coli* JCL299, one of such engineered strains, was reported to be inhibited by 50% in the presence of 0.6 g L⁻¹ 2-pentanone, and bacterial growth was fully arrested⁹ when the concentration of the MK increased to 5 g L⁻¹. Thus, we selected *P. putida* as a solvent-tolerant host¹⁹ towards 2-pentanone biosynthesis. As a first step in testing the performance of *P. putida* as a production platform of MKs, the effect of 2-pentanone addition on bacterial growth was evaluated in cultures of *P. putida* SEM1.3²⁶. Strain SEM1.3 (**Table 6.1**) is a refactored derivative of *P. putida* EM42, a reduced-genome version of the platform strain KT2440²⁵. Specifically, the modifications introduced in *P. putida* SEM1.3 comprise (i) deletion of the *benABCD* gene cluster to abolish oxidation of 3-methylbenzoate, allowing the use of this molecule as a gratuitous (i.e., non-metabolizable) inducer of the XylS/*P_m* expression system without the interference to OD₆₀₀ measurements typically caused by brown-colored catechols and products of benzoate metabolism, and (ii) elimination of the native *pha* gene cluster, comprising *phaC1ZC2DFI*, to avoid any potential metabolic cross-talk that could compete for acetyl-CoA, the key precursor for 2-pentanone biosynthesis. *P. putida* SEM 1.3 was grown either on rich LB medium or minimal de Bont medium supplemented with 1% (w/v) glucose as the main carbon source and spiked with 2-pentanone at different concentrations (1, 2.5, 5, 10, 25 and 50 g L⁻¹). Under all conditions, the impact of 2-pentanone on the cell physiology was more evident when cells grew in a minimal medium than in rich broth cultures. Bacterial growth, assessed as the final OD₆₀₀ after 24 h, started to be affected at MK concentrations above 2.5 g L⁻¹, but growth was still observed with up to 25 or 50 g L⁻¹ 2-pentanone both in de Bont minimal medium (32%) or LB medium (40%), respectively (**Figure 6.2, A**).

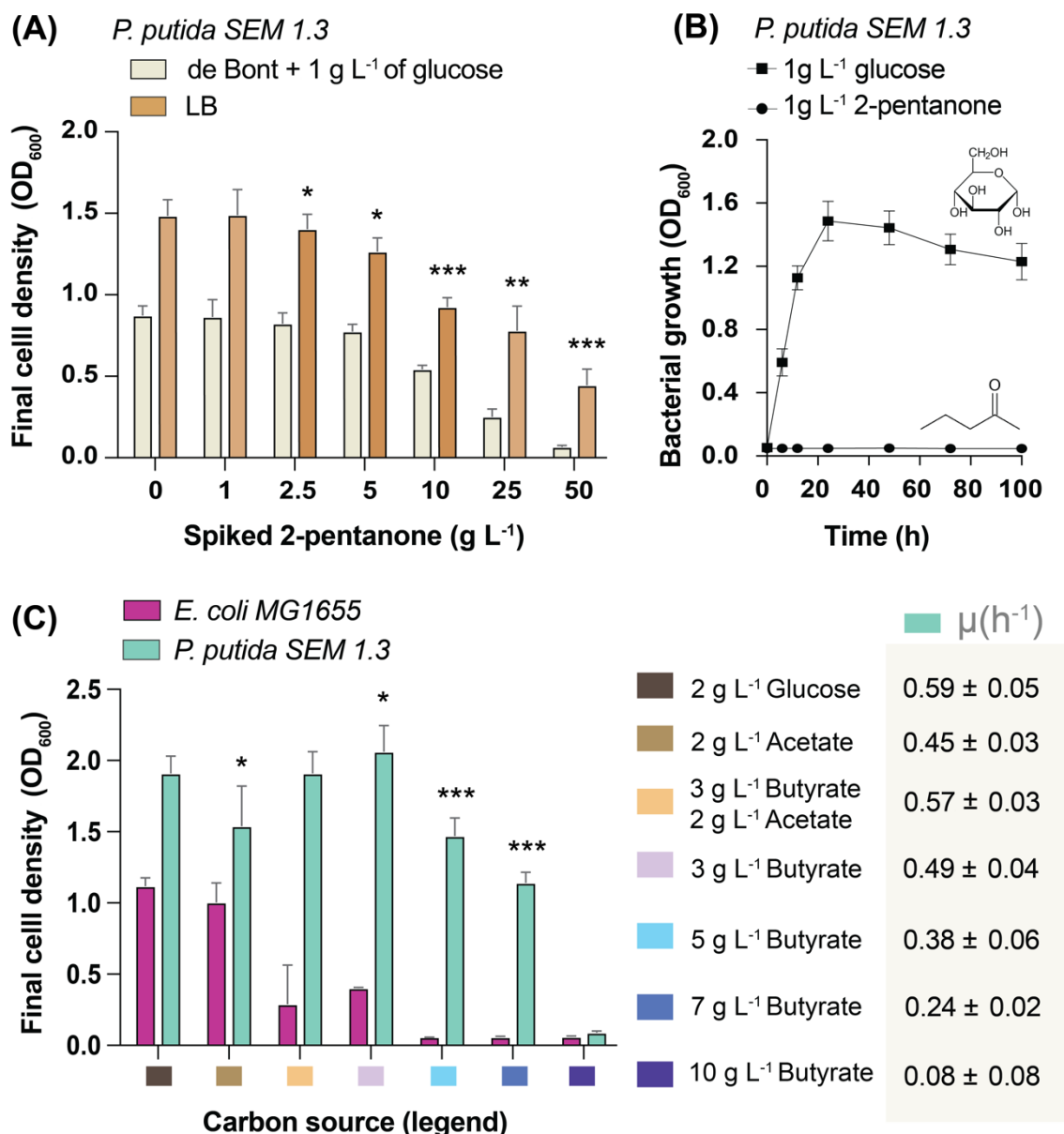


Figure 6.2. Bacterial growth analysis upon 2-pentanone or organic acids supplementation. **(A)** Increasing concentrations of 2-pentanone added to the minimal de Bont medium, containing 1 g L⁻¹ of glucose and rich LB medium affect growth of *P. putida* SEM 1.3, shown as drop in final cell density after 24 h. **(B)** Strain *P. putida* SEM 1.3 is not able to utilize 2-pentanone as a sole source of carbon. **(C)** Comparison of *E. coli* MG1655 and *P. putida* SEM 1.3 bacterial growth in the de Bont minimal medium with different carbon sources added: 2 g L⁻¹ glucose, a combination of 3 g L⁻¹ butyrate and 2 g L⁻¹ acetate or increasing concentrations of butyrate (3 g L⁻¹, 5 g L⁻¹, 7 g L⁻¹, and 10 g L⁻¹). Averages are made as biological triplicates, with individual replicates and standard deviations shown.

In general, *P. putida* SEM1.3 fared significantly better under these conditions as compared with data reported for *E. coli* JCL299⁹. These results illustrate the ability of *P. putida* to adapt to high solvent concentrations, a phenotype that could be mediated by modifications in the surface properties of the outer membrane and other natural stress response mechanisms¹⁹. Furthermore, we explored if 2-pentanone can be utilized as a carbon source by *P. putida* by incubating strain SEM1.3 in de Bont minimal medium supplemented with 1 g L⁻¹ of 2-pentanone as the sole carbon source and assessing bacterial growth over 100 h (**Figure 6.2, B**). Control cultures with glucose were used to benchmark bacterial growth, reaching full saturation within 24 h of incubation under similar conditions (**Figure 6.2, B**). No growth was detected under these conditions, indicating that *P. putida* is unable to utilize 2-pentanone as a substrate.

Owing the ability of *P. putida* to utilize organic acids as sole carbon sources, we examined the possibility of using butyrate as a substrate supporting 2-pentanone production. Butyrate, a C₄ carboxylic acid, can be processed by *Pseudomonas* by the canonical β -oxidation pathway to yield acetyl-CoA units. Even though it has not been actively investigated as a feedstock for bacterial fermentations, butyrate is a promising building block that can be obtained from renewable resources²⁹ and it has been shown to be the substrate of choice for high-cell-density cultures of *P. putida*³⁰. While these properties position butyrate as an interesting substrate for bioprocesses, osmotic shock caused by the carboxylate results in toxicity issues even at relatively low concentrations³¹. To test this scenario, the tolerance of *P. putida* SEM1.3 and *E. coli* MG1655 to increasing butyrate concentrations was evaluated in the absence or presence of different co-substrates (**Figure 6.2, C**). Glucose or acetate were selected as the primary carbon feedstock as a representative example of a glycolytic and a gluconeogenic substrate, respectively. *P. putida* SEM1.3 tolerated up to 7 g L⁻¹ butyrate with a reduction of 42-46% of the final OD₆₀₀, while the growth of *E. coli* MG1655 was almost abolished at any butyrate concentration above 3 g L⁻¹. Neither bacterial species could grow on de Bont minimal medium containing 10 g L⁻¹ butyrate, which marks the practical upper concentration that can be used in production experiments. Interestingly, *P. putida* reached similar final OD₆₀₀ values when butyrate was

either used as the sole carbon substrate or added at 3 g L⁻¹ to glucose or acetate cultures. This observation indicates that butyrate is not a preferred carbon source in the presence of a co-substrate. Growth rates of the *P. putida* strain for every tested substrate are presented in **Figure 6.2, C**. Taken together, these results led us to adopt reduced-genome *P. putida* SEM1.3 for establishing a butyrate-dependent biosynthesis pathway for 2-pentanone.

3.1. Design and implementation of a 2-pentanone biosynthesis pathway and optimization of culture conditions of MKs production from butyrate

The canonical acetone biosynthesis pathway of *C. acetobutylicum* ATCC 824 was implemented as the basis for 2-pentanone production. This route starts with the condensation of acetyl-CoA and butyryl-CoA mediated by a thiolase (Thl; acetyl-CoA acetyltransferase, EC 2.3.1.9) to generate 3-ketohexanoyl-CoA. Next, a butyrate-acetoacetate CoA transferase (CtfAB; EC 2.8.3.9) relocates a CoA moiety from 3-ketohexanoyl-CoA to acetate, thereby forming 3-ketohexanoate. Finally, this molecule is reduced to 2-pentanone by an acetoacetate decarboxylase (Adc; EC 4.1.1.4), releasing CO₂ (**Figure 6.3, A**). Since all the enzymes within the pathway stem from a Gram-positive bacterium, we expanded the biochemical toolset by harnessing activities from bacterial species phylogenetically closer to our host. Hence, the PhaA thiolase from *Cupriavidus necator* and the AtoDA and PcaIJ CoA transferases from *E. coli* MG1655 and *P. putida* KT2440, respectively, were also considered for pathway designs. Plasmids pS2313-MK(c,s1-s3), harboring different combinations of the genes encoding all relevant pathway enzymes (**Figure 6.3, B**), were constructed to this end (**Table 6.1**). Note the plasmid nomenclature indicates whether the pathway for MK biosynthesis is composed by the canonical enzyme components (c) or synthetic versions thereof (s).

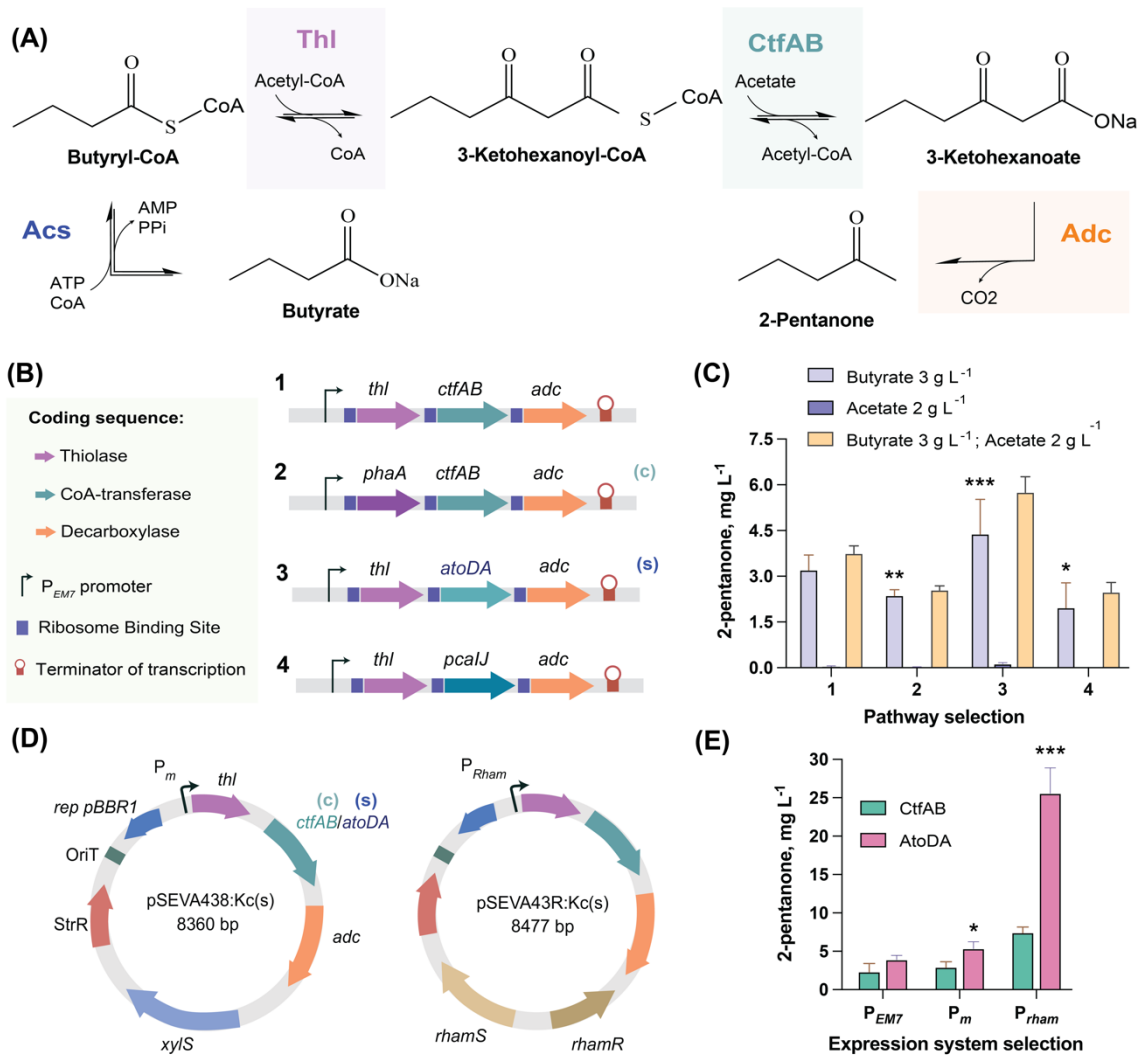


Figure 6.3. Pathway engineering and optimization for 2-pentanone bioproduction. **(A)** Biosynthetic pathway overview for the 2-pentanone production from butyrate, reliant on the native *C. acetobutylicum* pathway for acetone biosynthesis (Thl – thiolase; CtfAB – CoA transferase; Adc – decarboxylase). **(B)** Overview of the alternative combinations of genes, encoding the enzymes for 2-pentanone production pathway. **(C)** Examinations of the constructed variants after growing *P. putida* SEM 1.3 with pS2313-MK(c, s1-s3) plasmids for 24h in 10 mL of minimal de Bont medium. Different combinations of the carbon source were tested: 3 g L⁻¹ butyrate; 2 g L⁻¹ acetate or combination of 3 g L⁻¹ butyrate and 2 g L⁻¹ acetate. **(D)** Vectors carrying XylS/ P_m expression system inducible by 1 mM of 3-mBz₃, and RhamRS/ P_{rham} expression system inducible by 5 mM of rhamnose. **(E)** Examination of the strain production performance after growing *P. putida* SEM 1.3 with the selected plasmid for 24h in 10 mL of minimal de Bont medium, containing 3 g L⁻¹ butyrate. 2-pentanone content is quantified using GC-FID. Averages are made as biological triplicates, with individual replicates and standard deviation shown.

To examine the pathway performance, we inoculated *P. putida* SEM1.3 cultures transformed with the constructed vectors and performed 30 h fermentation in 10 mL of minimal de Bont medium containing 3 g L⁻¹ of butyrate or 2 g L⁻¹ of acetate, or the combination of 3 g L⁻¹ of butyrate and 2 g L⁻¹ of acetate as a carbon source, as well as 50 µg mL⁻¹ of kanamycin (**Figure 6.3, C**).

In each case, there were no carbon source detected in the supernatant, indicating full consumption of the substrate in all tested conditions. 2-pentanone biosynthesis shown to be more efficient when constructs 1 (genes *thl*, *ctfAB*, *adc*) and 3 (genes *thl*, *atoDA*, *adc*) were used for production: comprising of 3.5 mg L⁻¹ and 4.5 mg L⁻¹, respectively. The pathway with butyrate-acetoacetate CoA transferase AtoDA, which transfers a CoA from 3-ketohexanoyl-CoA to acetate, is the most efficient for 2-pentanone production. This is expected, as AtoDA is reported to have a 22.6-fold higher substrate affinity ($K_m = 53.1 \mu\text{M}$) than CtfAB ($K_m = 1,200 \mu\text{M}$)³². Interestingly, 2-pentanone was not produced when 3 g L⁻¹ of acetate was used as a sole source of carbon, however its supplementation to 3 g L⁻¹ butyrate resulted in slight improvement in the yield with up to 6 mg L⁻¹ of 2-pentanone for the construct 3 (genes *thl*, *atoDA*, *adc*) (**Figure 6.3, C**). We then chose those constructs for further optimization.

Selection of promoters for expression of heterologous enzymes is a crucial parameter to ensure efficient bioproduction of chemicals. A number of expression systems are available for use in *P. putida*, among them are native *Pseudomonas* systems like XylS/*P_m*, AlkS/*P_{alkB}*, and NahR/*P_{sal}*, as well as heterologous AraC/*P_{araB}* and RhaRS/*P_{rhaB}*^{33,34}. To improve 2-pentanone synthesis in *P. putida* we have tested constitutive promoter *P_{EM7}* as well as inducible XylS/*P_m* and RhaRS/*P_{rhaB}* expression systems, shown to have tight inducer-dependent regulation, and high levels of expression³³.

Hence, we have constructed vectors pS438·MK(c,s1) and pS4318·MK(c,s1), with two previously described pathway designs, representing either combination genes: *thl*, *ctfAB*, *adc* (c) or : *thl*, *atoDA*, *adc* (s) (**Table 1**). The

details on the vector architecture for inducible XylS/ P_m and RhaRS/ P_{rhaB} expression systems are shown in **Figure 6.3, D**. We have further examined *P. putida* SEM 1.3 cultures transformed with the vectors pS438·MK(c,s1), pS4318·MK(c, s1) and pS2313·MK(c, s1). Inoculated cultures were grown for 30 h in 10 mL of minimal de Bont medium containing 3 g L⁻¹ of butyrate, as well as 100 µg mL⁻¹ of streptomycin for the inducible system, or 50 µg mL⁻¹ of kanamycin for constitutive expression. The best 2-pentanone production: 90 mg L⁻¹ from 3 g L⁻¹ of butyrate (full substrate consumption verified by HPLC) was achieved while expressing the pathway enzymes under the control of P_{rhaB} , induced with 5 mM of rhamnose (**Figure 6.3, E**), the highest expression under tested conditions³⁵.

As acetyl-CoA synthetase (Asc) is needed for the butyryl-CoA generation, we constructed additional vectors pS4318·MK(c,s)-acs, carrying the gene, encoding well-studied heterologous Acs³⁶ from *Bacillus subtilis* (**Table 6.1**). We observed no effect on the 2-pentanone content after 24h of bacterial growth in 10 mL of minimal de Bont medium containing 3 g L⁻¹ of butyrate, and 5 mM of rhamnose (data not shown). This indicates that endogenous Asc-I, Acs-II are sufficient and do not limit the pathway performance.

3.3. *P. putida* mini-cells as platform for stable MKs bioproduction

The Min system has been thoroughly characterized in *E. coli* and *Bacillus subtilis* but is also present in diverse bacterial species³⁷, including Pseudomonads. Min proteins, MinC, MinD, and MinE, synergistically mediate the cell division machinery, and depletion of one of the protein complex components (such as MinD) results in assembly of the Z-ring near the poles, followed by chromosome-less minicell formation (**Figure 6.4, AB**). As a result, minicells cannot grow and duplicate, but they can continue other cellular processes, such as ATP synthesis, replication and transcription of plasmid DNA, and translation of mRNA¹⁵. In this work we created a MinD-deficient strain, *P. putida* SEM1.3 $\Delta minD$, which is able to generate minicells constitutively (**Figure 6.4, A**).

It was created by integrating premature stop codon into the reading frame of the *minD* gene using the previously established cytosine base-editing approach presented in **Chapter 3**. We constructed vector pCasso *minD*^{Q71} (**Table 6.1, Figure 6.4, C**), expressing target-specific sgRNA (converting Q71 CAG codon into stop TAG codon) as well as cytidine deaminase fused to a nickase nCas9 variant. The editing in *minD* gene was verified by sequencing and the mutant strain was cured from the plasmid according to the developed protocol (**Chapter 3**).

A minicell can be associated with a miniature factory full of a variety of molecular machines, orchestrating chemistry of the cell. If we want to start a new process, such as 2-pentanone synthesis, we bring in an additional machine - new-to-cell biochemical pathway (**Figure 6.3, A**). Thus, resulting strain *P. putida* SEM1.3 Δ *minD* was transformed with pS4318 MKs1 plasmid (**Table 6.1**), previously tested to yield the most efficient 2-pentanone production (**Figure 6.3, E**). Samples used for biosynthesis of 2-pentanone were taken at different timepoints after the storage to examine minicell viability: 2 h, 24 h, 9 days and 18 days. Methyl-ketone was detected in all samples, ranging from 6 to 9 mg L⁻¹ 2-pentanone (**Figure 6.4, D**) without any statistically significant difference in the production efficiency. In the tested conditions 35-40% of substrate was consumed by mini cells fraction, with the estimated yield of 10 mg L⁻¹ of 2-pentanone per 1 g L⁻¹ of butyrate. This result for the first time explores formation of *P. putida*-derived minicells as well as their ability to exploit new-to-cell biochemistries in a stable manner, demonstrating their potential for bioproduction applications.

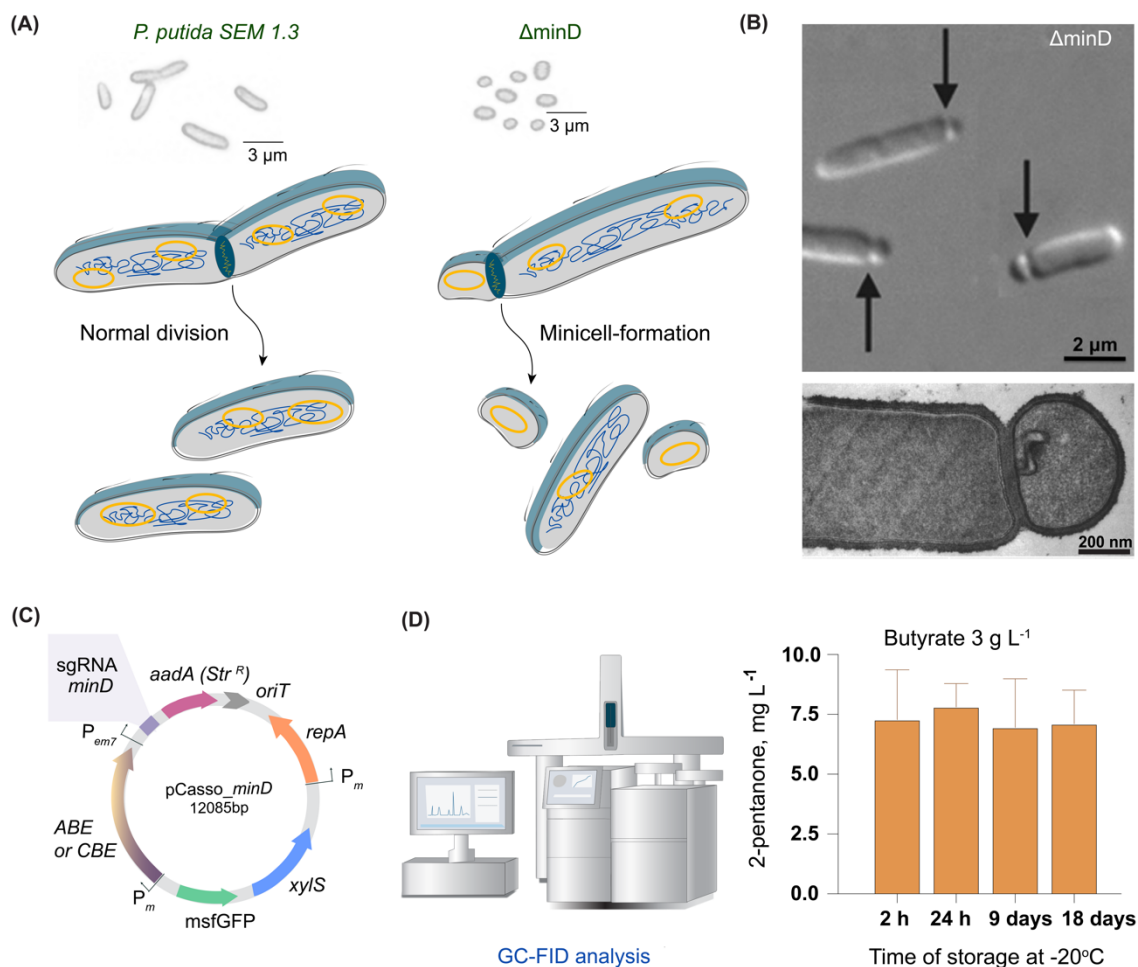


Figure 6.4. Mini-cells production, purification, and application for 2-pentanone synthesis. **(A)** Schematic representation of the normal cell division in the strain *P. putida SEM.1.3* and mini-cell formation after functional *minD* knockout. **(B)** Cryo-Electron tomography photograph of the mini-cell morphology, reprinted with a permission of the publisher³⁸. **(C)** pCasso *minD*^{Q71} vector used for creating of the *P. putida SEM.1.3* Δ *minD* strain **(D)** 2-pentanone synthesis in mini-cells, containing pS4318 MKs1 plasmid, harboring production pathway (**Figure 6.3, A**). Mini-cells were used after different time of storage at -20C (2h, 24h, 9 days and 18 days), and after 20 h incubation with the substrate (3 g L⁻¹ butyrate) resulting supernatant was analyzed by GC-FID.

4. CONCLUSION AND OUTLOOK

Here, we adapted genome-reduced *P. putida* SEM 1.3 strains for 2-pentanone production owing to the abilities of this bacterium for solvent tolerance and utilization of organic acids as a carbon source¹⁹. The product and substrate toxicity were examined in both *E. coli* and *P. putida*, demonstrating desirable properties of the selected host. Optimized production conditions were explored by using butyrate as main carbon source. Several 2-pentanone production pathway designs and expression systems were tested and compared, suggesting the best combination: Thl^{Ca} thiolase, AtoDA^{Ec} CoA-transferase and Adc^{Ca} decarboxylase under the control of the P_{phaB} promoter.

Previous studies reported titers of 240 mg L⁻¹ 2-pentanone in the rich Terrific Broth (TB) medium with 40 g L⁻¹ glucose. This bioprocess encompassed a 3-day fermentation of engineered *E. coli* strain JCL299 (derivative of BW25113 with multiple gene knockouts: *IdhA*, *adhE*, *frdBC*, *pta* - to minimize side product formation), transformed with 2 plasmids carrying 8 genes for 2-pentanone synthesis⁹. It was shown to rely on CoA-dependent chain elongation pathway of two rounds of acyl-CoA condensation; and one of the steps to improve the production, was introducing the CoA-transferase enzyme from *P. putida*. Moreover, the concentration of 2-pentanone from 600 mg L⁻¹ to 5 g L⁻¹ in the described strain showed dramatic reduction of growth (from 50% to 100%, respectively)⁹.

Here, we were able to achieve 90 mg L⁻¹ of 2-pentanone from 3 g L⁻¹ of butyrate (full substrate consumption verified by HPLC) in the minimal medium after 30 h of fermentation in *P. putida* SEM 1.3 (without targeted genome engineering to further reduce crosstalk with competing pathways), expressing only 3 enzymes from one plasmid. We have also shown that the toxicity of 2-pentanone is not critical for up to 25 g L⁻¹. This study provides solid evidence that *P. putida* is a suitable host for production of ketones, and further genetic engineering of the host (which was not performed during the scope of this work) as well as fed-batch fermentation approaches can be done to improve titer and yield.

We further engineered chromosome-free *P. putida*-derived mini cells to explore the alternative approach for bioproduction of MK. We demonstrated that those vesicles, containing the selected pathway enzymes, are able to convert provided substrate towards product formation. Such nanoparticles could be highly promising for targeted drug delivery in such biomedical applications as tumor therapy, as 2-pentanone shown to inhibit the colon carcinogenesis⁸. In our experiments, the purified mini cell fraction remained the stable activity after several weeks of storage, but most likely, the time can be extended up to months^{15,18}. To this end, more tests are needed to further characterize and optimize this chromosome-less bioproduction *chassis* for medium-chain ketones using alternative carbon sources.

ACKNOWLEDGMENTS

The financial support from The Novo Nordisk Foundation (NNF10CC1016517) and from the European Union's *Horizon2020* Research and Innovation Programme under grant agreement No. 814418 (*SinFonia*) to P.I.N. is gratefully acknowledged. E.K. is the recipient of a fellowship from the Novo Nordisk Foundation as part of the Copenhagen Bioscience Ph.D. Programme, supported through grant NNF 18CC0033664. The authors declare that there are no competing interests associated with the contents of this article.

References

- 1 Calero, P. & Nikel, P. I. Chasing bacterial *chassis* for metabolic engineering: A perspective review from classical to non-traditional microorganisms. *Microb. Biotechnol.* **12**, 98-124, doi:10.1111/1751-7915.13292 (2019).
- 2 Goh, E. B., Baidoo, E. E., Keasling, J. D. & Beller, H. R. Engineering of bacterial methyl ketone synthesis for biofuels. *Appl Environ Microbiol* **78**, 70-80, doi:10.1128/AEM.06785-11 (2012).
- 3 Park, J. *et al.* Synthesis of methyl ketones by metabolically engineered *Escherichia coli*. *J. Ind. Microbiol. Biotechnol.* **39**, 1703-1712, doi:10.1007/s10295-012-1178-x (2012).
- 4 Scognamiglio, J., Letizia, C. S. & Api, A. M. Fragrance material review on cyclohexyl methyl pentanone. *Food Chem Toxicol* **62 Suppl 1**, S138-143, doi:10.1016/j.fct.2013.07.056 (2013).
- 5 Smit, B. A., Engels, W. J. & Smit, G. Branched chain aldehydes: production and breakdown pathways and relevance for flavour in foods. *Appl. Microbiol. Biotechnol.* **81**, 987-999, doi:10.1007/s00253-008-1758-x (2009).
- 6 He, Z. T. & Hartwig, J. F. Enantioselective alpha-functionalizations of ketones via allylic substitution of silyl enol ethers. *Nat Chem* **11**, 177-183, doi:10.1038/s41557-018-0165-x (2019).
- 7 Rodriguez, G. M. & Atsumi, S. Toward aldehyde and alkane production by removing aldehyde reductase activity in *Escherichia coli*. *Metab Eng* **25**, 227-237, doi:10.1016/j.ymben.2014.07.012 (2014).
- 8 Pettersson, J., Karlsson, P. C., Goransson, U., Rafter, J. J. & Bohlin, L. The flavouring phytochemical 2-pentanone reduces prostaglandin production and COX-2 expression in colon cancer cells. *Biol Pharm Bull* **31**, 534-537, doi:10.1248/bpb.31.534 (2008).
- 9 Lan, E. I., Dekishima, Y., Chuang, D. S. & Liao, J. C. Metabolic engineering of 2-pentanone synthesis in *Escherichia coli*. *AIChE J.* **59**, 3167-3175, doi:<https://doi.org/10.1002/aic.14086> (2013).
- 10 Weizmann, C. & Rosenfeld, B. The activation of the butanol-acetone fermentation of carbohydrates by *Clostridium acetobutylicum* (Weizmann). *Biochem. J.* **31**, 619-639, doi:10.1042/bj0310619 (1937).
- 11 Fan, C. *et al.* Chromosome-free bacterial cells are safe and programmable platforms for synthetic biology. *Proc. Natl. Acad. Sci. USA* **117**, 6752-6761, doi:10.1073/pnas.1918859117 (2020).

- 12 Rampley, C. P. N. *et al.* Development of *SimCells* as a novel *chassis* for functional biosensors. *Sci. Rep.* **7**, 7261, doi:10.1038/s41598-017-07391-6 (2017).
- 13 Rothfield, L., Taghbalout, A. & Shih, Y. L. Spatial control of bacterial division-site placement. *Nat Rev Microbiol* **3**, 959-968, doi:10.1038/nrmicro1290 (2005).
- 14 Rowlett, V. W. & Margolin, W. The Min system and other nucleoid-independent regulators of Z ring positioning. *Front Microbiol* **6**, 478, doi:10.3389/fmicb.2015.00478 (2015).
- 15 Farley, M. M., Hu, B., Margolin, W. & Liu, J. Minicells, Back in Fashion. *J Bacteriol* **198**, 1186-1195, doi:10.1128/JB.00901-15 (2016).
- 16 Volke, D. C. & Nikel, P. I. Getting bacteria in shape: Synthetic morphology approaches for the design of efficient microbial cell factories. *Adv. Biosyst.* **2**, 1800111, doi:10.1002/adbi.201800111 (2018).
- 17 Million-Weaver, S. & Camps, M. Mechanisms of plasmid segregation: have multicopy plasmids been overlooked? *Plasmid* **75**, 27-36, doi:10.1016/j.plasmid.2014.07.002 (2014).
- 18 Yu, H. *et al.* Minicells from highly genome reduced *Escherichia coli*: cytoplasmic and surface expression of recombinant proteins and incorporation in the minicells. *ACS Synth. Biol.* **10**, 2465-2477, doi:10.1021/acssynbio.1c00375 (2021).
- 19 Bitzenhofer, N. L. *et al.* Towards robust *Pseudomonas* cell factories to harbour novel biosynthetic pathways. *Essays Biochem.* **65**, 319-336, doi:10.1042/ebc20200173 (2021).
- 20 Cavaleiro, A. M., Kim, S. H., Seppälä, S., Nielsen, M. T. & Nørholm, M. H. Accurate DNA assembly and genome engineering with optimized uracil excision cloning. *ACS Synth. Biol.* **4**, 1042-1046, doi:10.1021/acssynbio.5b00113 (2015).
- 21 Genee, H. J. *et al.* Software-supported *USER* cloning strategies for site-directed mutagenesis and DNA assembly. *ACS Synth. Biol.* **4**, 342-349, doi:10.1021/sb500194z (2015).
- 22 Hanahan, D. & Meselson, M. Plasmid screening at high colony density. *Methods Enzymol.* **100**, 333-342 (1983).
- 23 Worsey, M. J. & Williams, P. A. Metabolism of toluene and xylenes by *Pseudomonas putida (arvilla)* mt-2: evidence for a new function of the TOL plasmid. *J. Bacteriol.* **124**, 7-13 (1975).
- 24 Bagdasarian, M. *et al.* Specific purpose plasmid cloning vectors. II. Broad host range, high copy number, RSF1010-derived vectors, and a host-vector system for gene cloning in *Pseudomonas*. *Gene* **16**, 237-247, doi:10.1016/0378-1119(81)90080-9 (1981).

- 25 Martínez-García, E., Nikel, P. I., Aparicio, T. & de Lorenzo, V. *Pseudomonas* 2.0: genetic upgrading of *P. putida* KT2440 as an enhanced host for heterologous gene expression. *Microb. Cell Fact.* **13**, 159, doi:10.1186/s12934-014-0159-3 (2014).
- 26 Kozaeva, E. *et al.* Model-guided dynamic control of essential metabolic nodes boosts acetyl-coenzyme A-dependent bioproduction in rewired *Pseudomonas putida*. *Metab. Eng.* **67**, 373-386 (2021).
- 27 Wirth, N. T., Kozaeva, E. & Nikel, P. I. Accelerated genome engineering of *Pseudomonas putida* by I-SceI—mediated recombination and CRISPR-Cas9 counterselection. *Microb. Biotechnol.* **13**, 233-249, doi:10.1111/1751-7915.13396 (2020).
- 28 Silva-Rocha, R. *et al.* The Standard European Vector Architecture (SEVA): a coherent platform for the analysis and deployment of complex prokaryotic phenotypes. *Nucleic Acids Res.* **41**, D666-D675, doi:10.1093/nar/gks1119 (2013).
- 29 Zhang, C., Yang, H., Yang, F. & Ma, Y. Current progress on butyric acid production by fermentation. *Curr Microbiol* **59**, 656-663, doi:10.1007/s00284-009-9491-y (2009).
- 30 Cerrone, F. *et al.* Fed-batch strategies using butyrate for high cell density cultivation of *Pseudomonas putida* and its use as a biocatalyst. *Appl. Microbiol. Biotechnol.* **98**, 9217-9228, doi:10.1007/s00253-014-5989-8 (2014).
- 31 Cheung, H. N., Huang, G. H. & Yu, H. Microbial-growth inhibition during composting of food waste: effects of organic acids. *Bioresour Technol* **101**, 5925-5934, doi:10.1016/j.biortech.2010.02.062 (2010).
- 32 Bermejo, L. L., Welker, N. E. & Papoutsakis, E. T. Expression of *Clostridium acetobutylicum* ATCC 824 genes in *Escherichia coli* for acetone production and acetate detoxification. *Appl Environ Microbiol* **64**, 1079-1085, doi:10.1128/AEM.64.3.1079-1085.1998 (1998).
- 33 Calero, P., Jensen, S. I. & Nielsen, A. T. Broad-host-range *ProUSER* vectors enable fast characterization of inducible promoters and optimization of *p*-coumaric acid production in *Pseudomonas putida* KT2440. *ACS Synth. Biol.* **5**, 741-753, doi:10.1021/acssynbio.6b00081 (2016).
- 34 Nikel, P. I. & de Lorenzo, V. *Pseudomonas putida* as a functional chassis for industrial biocatalysis: From native biochemistry to *trans*-metabolism. *Metab. Eng.* **50**, 142-155, doi:10.1016/j.ymben.2018.05.005 (2018).
- 35 Calero, P., Jensen, S. I. & Nielsen, A. T. Broad-Host-Range ProUSER Vectors Enable Fast Characterization of Inducible Promoters and Optimization of *p*-Coumaric Acid Production in *Pseudomonas putida*

- KT2440. *ACS Synth Biol* **5**, 741-753, doi:10.1021/acssynbio.6b00081 (2016).
- 36 Gardner, J. G. & Escalante-Semerena, J. C. In *Bacillus subtilis*, the sirtuin protein deacetylase, encoded by the srtN gene (formerly yhdZ), and functions encoded by the acuABC genes control the activity of acetyl coenzyme A synthetase. *J Bacteriol* **191**, 1749-1755, doi:10.1128/JB.01674-08 (2009).
- 37 Frazer, A. C. & Curtiss, R., 3rd. Production, properties and utility of bacterial minicells. *Curr Top Microbiol Immunol* **69**, 1-84, doi:10.1007/978-3-642-50112-8_1 (1975).
- 38 Liu, J., Chen, C. Y., Shiomi, D., Niki, H. & Margolin, W. Visualization of bacteriophage P1 infection by cryo-electron tomography of tiny *Escherichia coli*. *Virology* **417**, 304-311, doi:10.1016/j.virol.2011.06.005 (2011).

Supplementary Data

Table S7.1. Oligonucleotides used in this work.

	Name	Sequence (5'→3')	Application
1	U-SEVA43-F	ATCGCCCUAGGCCGCGGCCGC GCGAATTCGA	USER cloning of elements of the rhamnose expression system (RhaS-RhaR/P _{rhaBAD}), to build the vector pSEVA43R
2	U-SEVA43-R	AAAGGCAUCAAAATAAAACGAAA GGCTCAGTC	
3	U- <i>rhaSR</i> -F	ATGCCTTUAATTAAAGCGGATA ACAATTTTCAC	
4	U- <i>rhaSR</i> -R	AGGGCGAUCGCCTCAGCGAAT TTCATTACGA	
5	U-SEVA43R-F	AGGCGTCGUGACTGGGAAAAC CCTGGCG	USER cloning to assemble a canonical production pathway. Oligonucleotides used for assembly of the <i>thl</i> , <i>ctfAB</i> , <i>adc</i> genes in vector pSEVA43R; synthetic RBSs for each gene were added in the oligonucleotide sequences
6	U-SEVA43R-R	ACCTCCUACCGCGGCCTAGGG CGA	
7	U- <i>thl</i> -F	AGGAGGUTAGTTAGAATGAAA GAAG	
8	U- <i>thl</i> -R	TTCAUTTTAATCCCTCCTTTTC TAGC	
9	U- <i>ctfAB</i> -F	AAAUGAACTCTAAAATAATTA GATT	
10	U- <i>ctfAB</i> -R	ACAGCCAUGGGTCTAAGTTCA TTGG	
11	U- <i>adc</i> -F	ATGGCTGUTTAGTTTAGGAAG GTGACT	
12	U- <i>adc</i> -R	ACGACGCCUTACTTAAGATAAT CATATATAA	
13	U-SEVA43R- <i>adc</i> -F	ATTTATGAUTTAGGAAGGTGA CTTTT	
14	U-SEVA43R- <i>thl</i> -R	AGCACTTUTCTAGCAATATTGC TGT	
15	U- <i>atoDA</i> -for	ATCATAAAUCACCCCGTTGCG TATT	USER cloning to exchange <i>ctfAB</i> with <i>atoDA</i> genes to build a synthetic production pathway
16	U- <i>atoDA</i> -rev	AGAAAAGUGCTAGAAAAGGAG GGATTA	
17	U-SEVA43-F	ATCGCCCUAGGCCGCGGCCGC GCGAATTCGA	USER cloning of elements of the rhamnose

18	U-SEVA43-R	AAAGGCAUCAAAATAAAAACGAAA GGCTCAGT	expression system (RhaS- RhaR/P _{rhaBAD}), to build the vector pSEVA43R
19	U- <i>rhaSR</i> -F	ATGCCTTUAATTAAAGCGGATA ACATCAC	
20	U- <i>rhaSR</i> -R	AGGGCGAUCGCCTCAGCGAAT TTCATTACG	
21	U-SEVA23-F	ATCGCCCUAGGCCGCGGCCGC GCGAATCGA	USER cloning to assemble production pathway with constitutive expression.
22	U-SEVA23-R	AAAGGCAUCAAAATAAAAACGAAA GGCTCAGTC	
23	U-Pem7-F	ATGCCTTUAATTAAAGCGGATA ACAATCAC	
24	U-Pem7-R	AGGGCGAUCGCCTCAGCGAAT TTCATTACG	
25	U-SEVA43-F	ATCGCCCUAGGCCGCGGCCGC GCGAA	USER cloning to assemble production pathway with XylS/Pm expression system
26	U-SEVA43-R	AAAGGCAUCAAAATAAAAACGAAA GGCTCAGTC	
27	U- <i>xylS</i> -F	ATGCCTTUAATTAAAGCGGATA ACTTCAC	
28	U- <i>xylS</i> -R	AGGGCGAUCGCCTCAGCGAAT TTCTACGA	
29	U- <i>phaA</i> -F	ATCGCCCUAGGCCGCGGCCGC GCGAATCGA	USER cloning to exchange <i>thl</i> with <i>phaA</i> genes
30	U- <i>phaA</i> -R	AAAGGCAUCAAAATAAAAACGAAA GGCTCA	

Table S7.2. Gene fragments used in this work.

Description	Sequence (5'→3')
Sequence encoding the <i>thl</i> gene	<p>ATGAAAGAAGTTGTAATAGCTAGTGCAGTAAGAACAGCGATTGGATCCTTATGGAAAG TCTCTTAAGGATGTACCAGCAGTAGATTTAGGAGCTACAGCTATAAAGGAAGCAGTT AAAAAAGCAGGAATAAAACCAGAGGATGTTAATGAAGTCATTTTAGGAAATGTTCTT CAAGCAGGTTTAGGACAGAATCCAGCAAGACAGGCATCTTTTAAAGCAGGATTACCA GTTGAAATCCAGCTATGACTATTAATAAGGTTTGTGGTTCAGGACTTAGAACAGTT AGCTTAGCAGCACAAAATTATAAAAGCAGGAGATGCTGACGTAATAATAGCAGGTGGT ATGGAAAATATGTCTAGAGCTCCTTACTTAGCGAATAACGCTAGATGGGGATATAGA ATGGGAAACGCTAAATTTGTTGATGAAATGACTGACGGATGCTGAGAGATGGAACATTTT CAAGAGAACAAGATGAGTTTGTCTTTCATCACAAAAAAGCTGAAGAAGCTATA AAATCAGGTCAATTTAAAGATGAAATAGTTCCTGTAGTAATTAAGGCAGAAAGGGA GAAACTGTAGTTGATACAGATGAGCACCTAGATTTGGATCAACTATAGAAGGACTT GCAAAATTTAAACCTGCCTTCAAAAAAGATGGAACAGTTACAGCTGGTAATGCATCA GGATTAATGACTGTGCAGCAGTACTTGTAAATCATGAGTGCAGAAAAAGCTAAAGAG CTTGGAGTAAAACCACTTGCTAAGATAGTTCTTATGGTTCAGCAGGAGTTGACCCA GCAATAATGGGATATGGACCTTTCTATGCAACAAAAGCAGCTATTGAAAAAGCAGGT TGGACAGTTGATGAATFAGATTTAATAGAATCAAATGAAGCTTTTGCAGCTCAAAGT TTAGCAGTAGCAAAAGATTTAAAATTTGATATGAATAAAGTAAATGTAAATGGAGGA GCTATTGCCCTTGGTCATCCAATTGGAGCATCAGGTGCAAGAATACTCGTTACTCTT GTACACGCAATGCAAAAAAGAGATGCAAAAAAGGCTTAGCAACTTTATGTATAGGT GGCGGACAAGGAACAGCAATATTGCTAGAAAAGTGCTAG</p>
Sequence encoding the <i>ctfAB</i> genes	<p>ATGATTAATGATAAAAACCTAGCGAAAGAAATAATAGCCAAAAGAGTTGCAAGAGAA TTAAAAAATGGTCAACTTGTAACTTAGGTGTAGGTCTTCCCTACCATGGTTGCAGAT TATATACCAAAAAATTTCAAATTACTTTCCAATCAGAAAACGGAATAGTTGGAATGG GCGCTAGTCCTAAAATAAATGAGGCAGATAAAGATGTAGTAAATGCAGGAGGAGACT ATACAACAGTACTTCCCTGACGGCACATTTTTTCGATAGCTCAGTTTCGTTTTACTAA TCCGTGGTGGTCACGTAGATGTTACTGTTTTAGGGGCTCTCCAGGTAGATGAAAAG GGTAATATAGCCAATTGGATTGTTCCCTGAAAAATGCTCTCTGGTATGGGTGGAGC TATGGATTTAGTAAATGGAGCTAAGAAAGTAATAATTGCAATGAGACATACAAATAA AAGTCAACCTAAAATTTAAAAAATGTACACTTCCCTCACGGCAAAGTCTCAAGC AAATCTAATTGTAACAGAACTTGGAGTAATTGAGGTTATTAATGATGGTTTACTTCT CACTGAAATTAATAAAAACACAACCATTGATGAAATAAGGTCTTTAACTGCTGCAGAT TTACTCATATCCAATGAACTTAGACCCATGGCTGTTTAG</p>
Sequence encoding the <i>atoDA</i> genes	<p>ATGGATGCGAAACAACGTATTGCGCGCCGTGTGGCGCAAGAGCTTCGTGATGGTGA CATCGTTAACTTAGGGATCGGTTTACCACAATGGTCGCCAATTTATTTACCGGAGG GTATTTCATATCACTCTGCAATCGGAAAACGGCTTCCCTCGGTTTAGGCCCGGTCACG ACAGCGCATCCAGATCTGGTGAACGCTGGCGGGCAACCGTGCGGTGTTTTACCGG TGCAGCCATGTTTGATAGCGCCATGTCATTTGCGCTAATCCGTGGCGGTCATATTG ATGCCTGCGTGCTCGGCGGTTTGCAAGTAGACGAAGAAGCAAACCTCGCGAACTGG GTAGTGCCTGGGAAAATGGTGCCCGGTATGGGTGGCGCGATGGATCTGGTGACCG GGTGCGCAAAGTGATCATCGCCATGGAACATTGCGCAAAGATGGTTCAGCAAAAA TTTTGCGCCGCTGCACCATGCCACTCACTGCGCAACATGCGGTGCATATGCTGGTT ACTGAACTGGCTGTCTTTTCGTTTTATTGACGGCAAATGTGGCTCACCGAAATGCG GACGGGTGTGATTTAGCCACCGTGCCTGCCAAAACAGAAGCTCGGTTTGAAGTCGC CGCCGATCTGAATACGCAACGGGGTGATTTTGA</p>

Chapter 7

A HIGH-THROUGHPUT COLORIMETRIC ASSAYS OPTIMIZED FOR KETONE AND ALDEHYDE DETECTION PRODUCED BY MICROBIAL CELL FACTORIES

Ekaterina Kozaeva^{1§}, Viviënne Mol^{1§}, Pablo I. Nikel^{1*}, and Alex T. Nielsen^{1*}

1. The Novo Nordisk Foundation Center for Biosustainability, Technical University of Denmark, 2800 Kgs. Lyngby, Denmark

§ These authors made equal contributions and should be considered joint first authors

* Correspondence to:

Alex T. Nielsen

(atn@biosustain.dtu.dk)

The Novo Nordisk Foundation

Center for Biosustainability

Technical University of Denmark

Kgs Lyngby 2800, Denmark

Tel: (+45) 21 79 89 06

INTRODUCTION

With increased pressure on society to replace fossil-based production with more sustainable alternatives, interest in biomanufacturing is at an all-time high. Ketones and aldehydes are a class of valuable molecules to consider for biomanufacturing as they have widespread applications in industry. Their solvent properties and high evaporation rates play an important commercial role in the fragrance, flavor, textiles, and agrochemical industries¹⁻³, as well as components in pharmacological and plastics syntheses^{4,5}.

To date, these compounds are predominantly relying on chemical production based on the oil-derived industry. Replacement of these processes with biosynthesis through cell factory engineering is gaining a growing interest as demonstrated by production of various ketones⁶⁻⁸ and aldehydes⁹ using metabolic engineering approaches in different hosts. Bioproduction of acetone, for example, was achieved at quite promising rates, reported to be up to 122 mM in 48 h in *E. coli*¹⁰. Where initial strain development is done in a rational, human-designed manner, novel approaches relying on computer aided strain design and randomized strain engineering allow tapping into the space of non-understood metabolism through a systems metabolic engineering approach¹¹.

Through iterative rounds of systems analysis and engineering, possibly combined with machine learning, significant strain optimization aimed to near theoretical maxima and industrial applicability can be achieved¹². Critical to such strategies, reliant on the generation of large libraries of strains, is an effective method to screen or select improved strains for baseline starting strains. Various methods have been developed to this end, relying on intracellular response elements such as biosensors or high-throughput analysis¹³ of produced metabolites, such as high-throughput High Pressure Liquid Chromatography (HPLC).

Though these approaches may be effective, development of biosensors is complex, whereas high-throughput HPLC have a heavy reliance on expensive hardware making its use limited. As an alternative to equipment-

heavy analytical techniques, spectrophotometric methods can provide quantitative determination in various sample types of interest, for the determination of a wide range of target molecules such as metabolites, nucleotides, and proteins. In the early 20th century, several spectrophotometric methods to determine ketone and aldehyde concentrations were developed before gas or liquid analytic chromatography became available in most laboratories. These methods include the use of 2,4-dinitrophenylhydrazine, or DNPH¹⁴ and vanillin¹⁵. Here we optimized two spectrophotometric methods of ketone and aldehyde determination with further potential for high throughput screening of microbial production strains. We rely on the use of a vanillin- and DNPH assay for quantifying the amounts of various ketones and aldehydes from crude cell-culture broth, allowing easy determination of strain performance for iterative rounds of cell factory optimization.

Materials and methods

2.1. Bacterial strains, plasmids, and culture conditions

Bacterial strains and plasmids used in this study are presented in **Table 7.1**. *E. coli* cultures were incubated at 37°C. For cloning procedures and during genome engineering manipulations, cells were grown in lysogeny broth (LB) medium (10 g L⁻¹ tryptone, 5 g L⁻¹ yeast extract and 10 g L⁻¹ NaCl; solid culture media additionally contained 15 g L⁻¹ agar). All cultures were agitated at 200 rpm (MaxQ™ 8000 incubator; ThermoFisher Scientific, Waltham, MA, USA). Streptomycin (Str) was added whenever needed at 100 µg mL⁻¹. The optical density measured at 600 nm (OD₆₀₀) was recorded in a Genesys 20 spectrophotometer (Thermo Fisher Scientific) to estimate bacterial growth. During physiological characterization of engineered strains, growth kinetics were followed at OD₆₀₀ with light path correction in a Synergy™ MX microtiter plate reader (BioTek Instruments Inc., Winooski, VT, USA).

2.2. General cloning procedures and construction of plasmids and strains

Oligonucleotides and gene fragments used in this study are listed in **Tables S7.1, S7.2**, respectively. Unless stated otherwise, uracil-excision (*USER*) cloning¹⁶ was used for the construction of all plasmids. The *AMUSER* tool was employed for designing oligonucleotides¹⁷. Phusion™ *U* high-fidelity DNA polymerase (ThermoFisher Scientific) was used according to the manufacturer's specifications in amplifications intended for *USER* cloning. For colony PCR, the commercial *OneTaq*™ master mix (New England BioLabs, Ipswich, MA, USA) was used according to the supplier's instructions. *E. coli* DH5 α λ pir (Table 1) was employed as a host for general cloning purposes. Chemically competent *E. coli* cells were prepared and transformed with plasmids using the *Mix and Go*™ commercial kit (Zymo Research, Irvin, CA, USA) according to the manufacturer's indications. The sequence of all used plasmids and strains was verified by Mix2Seq sequencing (Eurofins Genomics, Ebersberg, Germany).

2.3. Characterization of the production strains

Overnight pre-cultures of *E. coli* MG1655 transformed with plasmids pSEVA43R (non-production control), pS43R·MKc (canonical MK production pathway) or pS43R·MKs1 (synthetic MK production pathway) were grown in 5 mL of M9 minimal medium (detailed composition in **Table S7.3**) added with Str at 100 $\mu\text{g mL}^{-1}$ and 10 g L^{-1} glucose as a carbon source. These cultures were used as the inoculum for acetone production experiments by dilution in fresh medium at a starting $\text{OD}_{600} = 0.05$. Cells were grown for 24 h at 37°C with agitation at 200 rpm in 10 mL of M9 minimal medium with Str at 100 $\mu\text{g mL}^{-1}$, and 1 mM of rhamnose for the pathway induction. 10 g L^{-1} glucose, 2 g L^{-1} sodium acetate (pH 7) or their combination were added in the medium as a carbon source. After 24 h cells were incubated for 1 h at 4°C, then centrifugated at 5000g for 15 min, and the supernatant was analyzed by HPLC or colorimetry assays for the acetone content.

2.4. HPLC analysis of acetone biosynthesis

The concentration of acetone was measured in a Dionex UltiMate 3000 HPLC system equipped with an Aminex™ HPX-87X ion exclusion (300×7.8 mm) column (BioRad, Hercules, CA) coupled to RI-150 refractive index and UV (260, 277, 304 and 210 nm) detectors. The column was maintained at 30°C, the mobile phase was comprised of 5 mM H₂SO₄ in Milli-Q water at a flow rate of 0.6 mL min⁻¹, with a run length of 30 min. The eluted compounds were detected by a HPLC Waters 481 UV-visible detector at 214 nm. This detector was connected in series to an RI detector (model 410). HPLC data were processed using the Chromeleon™ chromatography data system software 7.1.3 (Thermo Fisher Scientific). The detection of acetone was monitored at RI and compound concentrations were calculated from peak areas using a calibration curve prepared with acetone (99% HPLC standard, Sigma-Aldrich Co.).

2.5. Data and statistical analysis

All the experiments reported were independently repeated at least twice in three independent biological replicates (as indicated in the corresponding figure or table legend), and the mean value of the corresponding parameter ± standard deviation is presented. The data analysis and visualization were done using Adobe Illustrator and Prism 9 (GraphPad).

Table 7.1. Bacterial strains and plasmids used in this study.

Bacterial strain	Relevant characteristics^a	Reference or source
<i>Escherichia coli</i>		
DH5 α λ pir	Cloning host; F ⁻ λ ⁻ <i>endA1 glnX44(AS) thiE1 recA1 relA1 spoT1 gyrA96(Nal^R) rfbC1 deoR nupG</i> Φ 80(<i>lacZ</i> Δ M15) Δ (<i>argF-lac</i>)U169 <i>hsdR17(r_K⁻ m_K⁺)</i> , λ pir lysogen	Hanahan and Meselson ¹⁸
MG1655	Wild-type strain; F ⁻ λ ⁻ <i>rph-1</i>	Blattner, et al. ¹⁹
Plasmid	Relevant characteristics^a	Reference or source
pSEVA43R	Standard expression vector carrying a rhamnose-inducible expression system; <i>oriV</i> (pBBR1); <i>rhaR</i> , <i>rhaS</i> , <i>P_{rhaBAD}</i> ; Sm ^R /Sp ^R	Kozaeva <i>et al.</i> , <i>in preparation</i>
pS43R :MKc	Derivative of vector pSEVA43R harboring the genes encoding the canonical acetone production pathway from <i>C. acetobutylicum</i> ; <i>RhaRS/P_{rhaBAD}→thl^{Ca}</i> , <i>ctfAB^{Ca}</i> , <i>adc^{Ca}</i> ; Sm ^R /Sp ^R	Kozaeva <i>et al.</i> , <i>in preparation</i>
pS43R :MKs1	Derivative of vector pSEVA43R harboring the genes encoding a synthetic MK production pathway; <i>RhaRS/P_{rhaBAD}→thl^{Ca}</i> , <i>atoDA^{Ec}</i> , <i>adc^{Ca}</i> ; Sm ^R /Sp ^R	Kozaeva <i>et al.</i> , <i>in preparation</i>

^aAntibiotic markers and abbreviations are identified as follows: Km, kanamycin; Nal, nalidixic acid; Sm, streptomycin; Sp, spectinomycin; and MK, methyl ketone. The source of relevant genes is indicated with a superscript abbreviation as follows: *Ca*, *Clostridium acetobutylicum*; and *Ec*, *Escherichia coli*.

Results and discussion

3.1. Vanillin assay guidelines for acetone detection

To specifically quantify acetone, a spectrophotometric method previously described in 1990¹⁵ used for clinical and environmental samples was adapted to a high-throughput 96-well plate format for both *in vivo* and *in vitro* screening. Reliant on the specific reaction of acetone with vanillin, the optimized protocol is presented in **Figure 7.1, A**. In brief, (i) an aliquot of the sample of interest (100 μ l) with unknown concentration of acetone is carefully mixed with (60 μ l) 130mM vanillin, followed by addition of 40 μ l 500 mM sodium hydroxide. (ii) The plate with the resulting solution is transferred to 60°C for 10 min, and afterwards cooled to room temperature for 10 min. Acetone reacts with vanillin in alkaline medium forming 4-(4-hydroxyphenyl-3-methoxy)-3-buten-2-one (**Figure 7.1, B**), a yellow compound visible by eye (**Figure 7.1, C**). (iii) The absorbance can be measured at 430 nm in a plate reader and remains stable for 1 h. The reagent blank (with water, buffer, or production medium, depending on the type of experiment) as well as calibration curve should be done in parallel. The blank shows negligible absorbance values, which can be extracted from the absolute value of the sample for more precise compound concentration determination. Through optimization of the protocol, sensitivity ranges from 50 mg L⁻¹ to 2000 mg L⁻¹ were observed, which is suitable for evaluating microbial strain performance in iterative rounds of strain development.

Additionally, we have verified that the developed vanillin assay is specific to acetone and observed no formation of colorful product with neither 2-butanone, 2-pentanone, 2-nonanone or acetaldehyde (**Figure S7.1**). This enables specific detection of acetone, especially useful during microbial production *in vivo*¹⁰ where the side activity of the enzymes may result in the production of a range of other compounds, specifically ketones, by the cell.

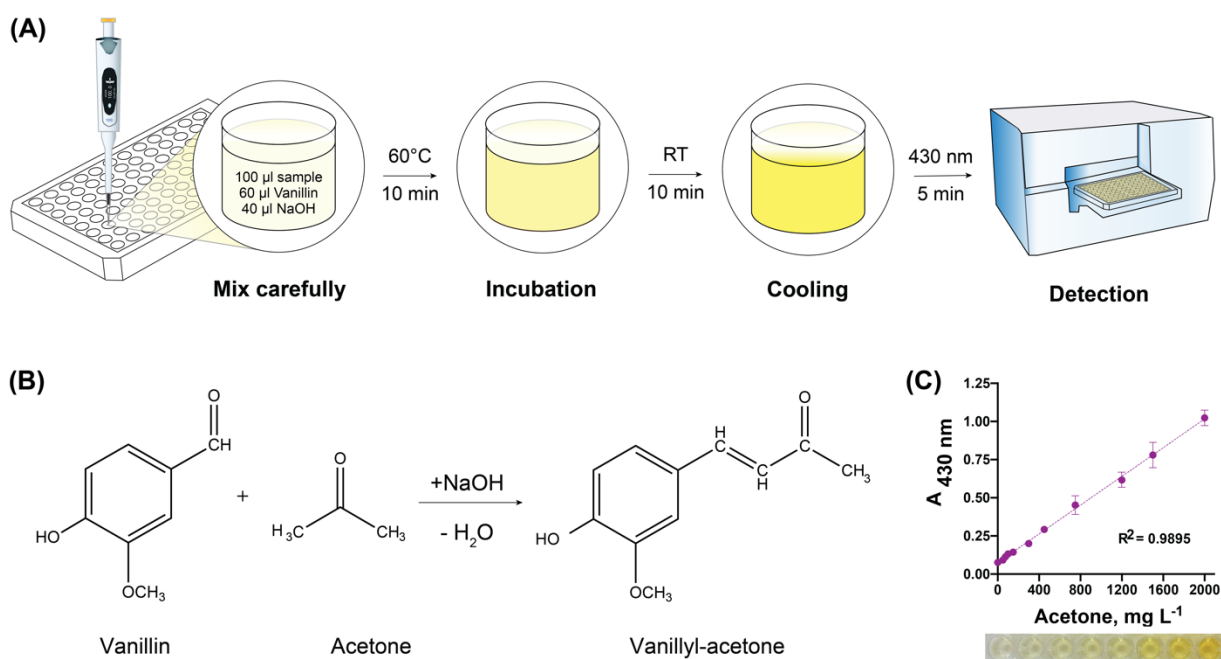


Figure 7.1. Vanillin-acetone based colorimetric assay guidelines.

- (A)** Scheme of the protocol. Carefully mix 60 μl of 130 mM vanillin, 40 μl of 5M NaOH with 100 μl of sample with unknown concentration of acetone or calibration standard. Incubate for 10 min at 60C. After cooling at room temperature for 10 min, measure the absorbance of analyzed sample at 430 nm.
- (B)** Vanillin-acetone simplified chemical reaction. Formation of colorful vanillyl-acetone under strong basic conditions.
- (C)** Calibration standard curve and an example visual representation. Regression over the linear range is shown, with the R^2 value of the fit indicated. Presented values are an average of three technical triplicates, with standard deviation represented as error bars.

3.2. *The vanillin assay is specific to acetone and can be used for vanillin detection.*

Considering that vanillin itself is an industrially relevant aldehyde, we established a protocol with optimized conditions for vanillin quantification, which allows sensitive detection of vanillin. The procedure is described in **Figure 7.1.** with the difference of acetone used at the fixed concentration. (i) An aliquot of the sample of interest (100 μ l) with unknown concentration of vanillin is carefully mixed with (60 μ l) 100mM acetone, followed by addition of (40 μ l) 500 mM sodium hydroxide. (ii) The plate with the resulting solution is transferred to 60°C for 10 min, and afterwards cooled to room temperature for 10 min. Acetone reacts with vanillin in alkaline medium forming 4-(4-Hydroxyphenyl-3-methoxy)-3-buten-2-one (**Figure 7.1., B**), a yellow compound visible by eye. (iii) The absorbance can be measured at 430 nm in the plate reader and remains reliable for 1 h. The example calibration for vanillin with acetone assay is presented at the **Figure S7.2.** The reagent blank (with water, buffer, or production medium, depending on the type of experiment) as well as calibration curve should be done in parallel. The protocol established here can for example be used during strain development for vanillin production and characterization ²⁰ or protein engineering ²¹.

3.3. *2,4 - DNPH assay guidelines for acetone detection*

Though the vanillin assay is well suited for specific detection of acetone, to expand the pallet of ketones and aldehydes that can be detected, an optimized assay based on 2, 4 - Dinitrophenylhydrazine (DNPH) was developed. DNPH contains a benzene ring, two nitro groups, and a hydrazine functional group that is dissolved in a solution of phosphoric acid and can be used for the detection of ketones and aldehydes in solution. DNPH does not react with amides, esters, carboxylic acids, or alcohols, making it sufficiently selective in complex fermentation broth, yet flexible enough to detect a variety of ketones and aldehydes^{22,23}. To allow effective use in 96-well plate format, optimization of the setup was performed leading to a suitable protocol for detection in cell culture broth. The protocol describing key steps for acetone determination (as an example) is presented

in **Figure 7.2, A**: (i) An aliquot of the sample of interest (195 μl) with unknown concentration of acetone (or other aldehyde/ketone) is carefully mixed with (5 μl) 200mM 2,4-dinitrophenylhydrozine phosphoric acid solution (Sigma-Aldrich, St. Louis, MO, USA). (ii) The plate with the resulting mixture is incubated for 2 min at room temperature (RT). Acetone reacts with 2,4-dinitrophenylhydrozine forming acetone 2,4-dinitrophenylhydrozone (**Figure 7.2, B**), an orange compound visible by eye. (iii) The absorbance can be measured at 490 nm (optimized for acetone) in a plate reader and remains reliable for 30 minutes (**Figure 7.2, C**). The reagent blank (with water, buffer, or production medium, depending on the type of experiment) should be done in parallel as well as calibration curve. The developed DNPH assay presented here, shows a linear range of 25-500 mg mL^{-1} and 10-200 mg mL^{-1} in milliQ and rich (LB) media, respectively. Though the response differs depending on background media, this can be accounted for through appropriate calibration curves. This also indicates that the presence of complex media components in rich medium, often present in fermentation broth, does influence but doesn't prohibit quantifiable output.

3.4. The DNPH assay allows for the detection of a variety of aldehydes and ketones

Contrary to vanillin, the condensation reaction between DNPH and the functional ketone or aldehyde group, is insensitive to the rest of the groups present in the molecule, thus allowing this assay to be used for quantification of other ketones and aldehydes of interest. Depending on the ketone or aldehyde present, the resulting 2,4-dinitrophenylhydrozone conjugate will have different absorbance wavelengths, also visible as a different color by eye ranging from yellow to orange or red. To enable the DNPH assay described here to be used for the detection of a panel of different ketones and aldehydes, we have optimized the detection wavelength and determined the corresponding linear range and fit, presented in **Table 7.2**. This highlights the wide applicability of such an assay to use in optimization of cell factories to produce a wide range of compounds, including cyclic ketones and lactones.

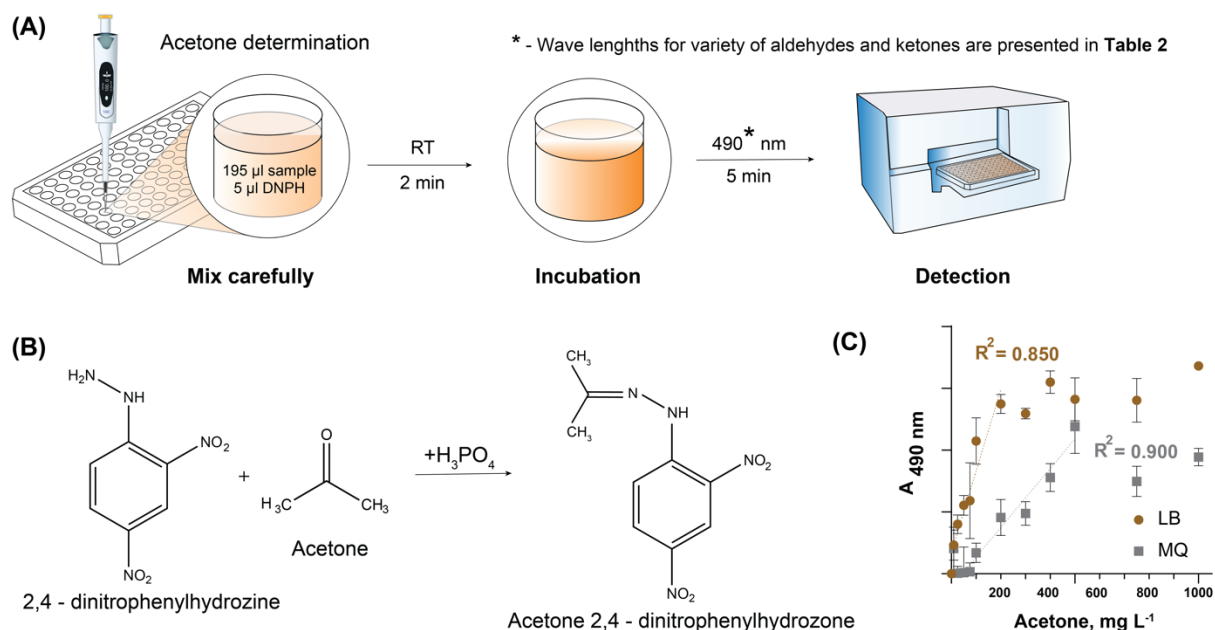


Figure 7.2. · 2,4 - dinitrophenylhydrazine assay guideline with optimized conditions.

(A) Scheme of the protocol. Carefully mix 5 µl of the 0.2 M DNP phosphoric acid solution and 195 µl of sample. Incubate 2 min at room temperature and measure the absorbance of analyzed sample at 490 nm. **Table 7.2** contains optimized wavelengths for absorbance detection of other ketones and aldehydes.

(B) Acetone 2,4-dinitrophenylhydrazone simplified chemical reaction. Formation of colorful 2,4-dinitrophenylhydrazone in the acidic conditions.

(C) Calibration acetone standard in lysogeny broth (LB) medium and MilliQ-deionized water (MQ). Regression over the linear range is shown, with R^2 values indicated. Presented values are an average of three technical triplicates, with standard deviation represented as error bars.

Table 7.2. Overview of optimum wavelength, with corresponding linear detection ranges and observed fit for various ketones and aldehydes detected with the DNPH assay in a milliQ background.

Compound	λ_{opt} (nm)	Concn. range of linear detection (mg mL ⁻¹)	Fit (R^2)
Aldehydes			
Acetaldehyde	500	50-300	0.99
Formaldehyde	550	10-100	0.77
D-Glyceraldehyde	470	10-1,000	0.84
Isobutyraldehyde	500	10-500	0.97
2-Phenyl Acetaldehyde	500	10-200	0.98
Propionaldehyde	510	25-500	0.92
Vanillin	570	10-750	0.98
Ketones			
Acetone	490	10-500	0.79
Acetyl-acetone	490	10-200	0.83
2-Butanone	520	75-1,000	0.92
γ -Butyrolactone	420	10-200	0.88
Cyclohexanone	520	25-200	0.91
2-Nonanone	420	25-500	0.77
2-Pentanone	520	10-500	0.92
3-Pentanone	510	10-750	0.97

3.5. Application of assays for *in vivo* production of acetone

To demonstrate the ease of use and application of the assays, they were used to assay the *in vivo* production of acetone in *Escherichia coli*. Biological production of acetone predominantly relies on the canonical (c) pathway from *Clostridium acetobutylicum* ATCC 824. In this pathway (**Figure 7.3, A**): (i) acetate is first converted into acetyl-CoA through acetyl-CoA synthetase (Acs). Then, (ii) 2 mol of acetyl-CoA are condensed by thiolase (Thl) to generate 1 mol of acetoacetyl-CoA. (iii) Acetoacetyl-CoA transferase (CtfAB) transfers the CoA moiety from acetoacetyl-CoA to acetate, and forms acetoacetate, which is (iv) catalyzed by acetoacetate carboxylase (Adc) to form acetone and carbon dioxide. This pathway has been improved through the establishment of a synthetic (s) alternative to one step in the pathway: using an acetoacetyl-CoA transferase (AtoDA) from *E. coli* MG1655 where the concentration of acetone after 24 h of fermentation of modified *E. coli* strain reached up to 20 mM from 120 mM of acetate using acetate as carbon source¹⁰ (**Figure 7.3, A**).

To this end, we used pSEVA43R:Kc(s) plasmids (**Table 7.1**), harboring genes encoding the canonical (c, Thl, CtfAB, Adc from *C. acetobutylicum*) or synthetic (s, Thl, Adc from *C. acetobutylicum* and AtoDA from *E. coli*) acetone production pathway, with a detailed vector scheme illustrated at **Figure 7.3, B**. To compare the pathway performance, we have inoculated *E. coli* DH5 α cultures with the constructed vectors and performed 24h fermentation in 10 mL of minimal M9 medium containing 10 g/L of glucose as a carbon source, streptomycin at 100 $\mu\text{g mL}^{-1}$, and 1 mM of rhamnose for pathway induction. After 24 h, cultures were cooled down at 4°C for 1h, and then centrifuged at 5000 g for 15 min. We evaluated acetone concentration in the resultant supernatant using the vanillin assay presented in Section 3.1 of this paper. As expected, we observed 3.5-fold improvement of acetone synthesis in the strain containing the synthetic pathway (**Figure 7.3, C**) which corresponds to previously published data¹⁰. Thus, we decided to further validate the assay performance using this synthetic pathway for acetone bioproduction.

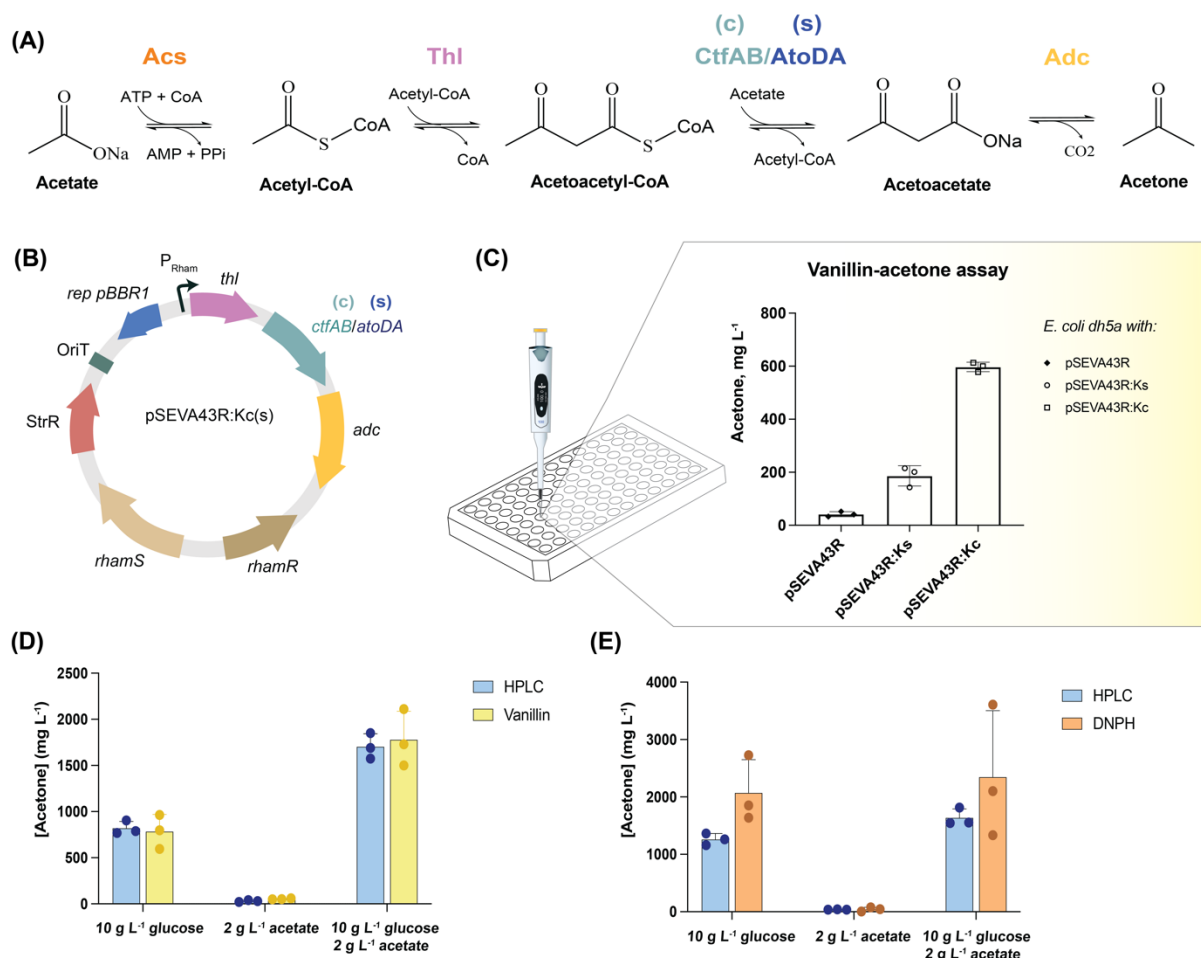


Figure 7.3 · Assay application for acetone bioproduction. **(A)** Biosynthetic pathway overview for the acetone production from acetate, reliant on the canonical (c) or synthetic (s) pathway. **(B)** Overview of the rhamnose-inducible expression vector used for the acetone biosynthesis. **(C)** Choosing the best acetone synthesis vector. *E. coli dh5a* strains harboring vectors pSEVA43R:Kc(s) were grown for 24 h in 10 mL of minimal M9 medium, containing 10 g L⁻¹ of glucose as a carbon source. Acetone concentration was defined by vanillin reaction, according to protocol established herein. **(D, E)** Acetone production and determination after fermentation of *E. coli* MG1655 strain containing synthetic pathway. 10 g L⁻¹ of glucose, 2 g L⁻¹ of acetate, or the combination of 10 g L⁻¹ of glucose and 2 g L⁻¹ of acetate was added to the medium as a carbon source. Assay performance was compared with HPLC acetone determination (Section 2.4 of Materials and Methods). **(D)** Vanillin assay. Bacterial growth was performed in M9 minimal medium. **(E)** DNPH assay. Bacterial growth was performed in LB medium. Averages are made as biological triplicates, with individual replicates and standard deviation shown.

Since *E. coli* MG1655 is considered a workhorse host strain for industrial bioprocesses^{24,25}, this K-12 strain was chosen for the next round of production experiments. In particular, vector pSEVA43R:Ks was transformed into *E. coli* MG1655, and the resulting strain was used to demonstrate vanillin (**Figure 3, D**) and the DHPH (**Figure 3, E**) assays, as well as their comparison with HPLC detection. The production of acetone in an engineered *E. coli* strain from either glucose or acetate as carbon source was previously shown¹⁰. In a wild-type *E. coli*, aerobic growth on acetate is achieved through the ATP demanding conversion of the substrate into acetyl-CoA, respiring, and assimilating this further into energy and biomass respectively. Here, we investigated if the co-feeding of glucose and acetate would improve acetone yields, through the rationale that energy can be generated through glucose metabolism, allowing a more efficient conversion of acetate into acetone. As expected, we observe no acetone accumulation when fed sole acetate, as this is expected to be used for energy and biomass assimilation. Interestingly, when 2 g L⁻¹ acetate is supplied as co-substrate to 10 g L⁻¹ glucose, we observed 2.2-fold increase in acetone titer.

Taken together, the developed approaches enable accurate detection of acetone in both minimal M9 medium through the vanillin assay, as well as in rich LB medium through the DNPH assay, resolving high, medium, and low levels of production similarly to HPLC results.

Conclusion

Microbial strain optimization to move cell factories from lab-scale to industrially-relevant titers and productivities depends on the development of high-throughput assays and systems-level technologies. These are facilitated by computer-aided design and automation principles. However, a critical factor often hampering the application of these approaches is an effective strain screening and selection strategy. Recently, methods for ketone^{26,27} and aldehyde²⁸ determination were also described based on other chemical reactions, and optimized either for one chemical species or the other. Application of these assays was shown for engineering one specific enzyme in whole (resting) cells, or in an *in vitro*, purified enzyme system. Though critical for improving specific enzymatic steps in production pathways, the ability to screen *in vivo* whole-cell functionality by assaying the sole culture broth is valuable due to increased ease of use, and more translatable outputs to observed fermentation profiles. A critical difference between these two parameters is the sensitivity range with which products should be detected accurately. Conversely to enzymatic studies, optimization of cell factories relies on wider and higher sensitivity ranges to prevent the needed additional step of multiple dilutions of fermentation samples. The complexity of fermentation broth also can interfere with assay output, when compared to enzymatic buffer conditions. Thus, the developed assays presented here are suitable and optimized for indicated purposes. In this work, we have presented high-throughput strain screening approaches for (i) specific acetone detection (vanillin-based assay), and (ii) various ketones and aldehydes screening (DNPH-based assay).

The vanillin-acetone assay can be used to determine acetone or vanillin titers with high precision, comparable to HPLC detection and quantification. With no response in the presence of other ketones, this assay can be used to accurately distinguish acetone in minimal media, in a range of 50-2000 mg L⁻¹. This can be especially relevant even when ketones and aldehydes are concomitantly produced by the cell factory, a typical feature of production pathways of this sort.

When the product of interest is another ketone or aldehyde, the presented DNPH assay can be used. Optimized for a total of 15 structurally-unrelated

ketones and aldehydes, this shows the versatility of the proposed assay, with the application likely being translatable to an even wider number of compounds. Additionally, the DNPH assay works even in the presence of complex media, often used in further production steps and so beneficial to screen small scale productivity in.

Finally, to demonstrate how the assays can be applied to explore strain productivity, *E. coli* was equipped with a synthetic acetone production pathway. Acetone titers in response to glucose, acetate and the combination of both was determined through both assays and HPLC, in both minimal and rich medium. The assay titers showed good correlation to HPLC-determined titers, for low, medium, and high production ranges, making it possible to distinguish the best producers from others in a 96-wells format. The availability of an assay to determine acetone concentration through simple culture supernatant analysis opens the possibility for further genome and pathway engineering in randomized approaches. Additionally, it can be used to further optimize media components of substrates, as indicated through the co-supply of glucose and acetate to further improve acetone titer. Altogether, this facilitates the use of fully automated pipelines for the iterative improvement of production strains and conditions, allowing society to transition towards biomanufacturing.

ACKNOWLEDGMENTS

We thank Ivan Pogrebnyakov for the fruitful discussions and support through the project. The financial support from The Novo Nordisk Foundation (NNF10CC1016517) and from the European Union's *Horizon2020* Research and Innovation Programme under grant agreement No. 814418 (*SinFonia*) to **P.I.N.** is gratefully acknowledged. **E.K.** and **V.M.** are the recipients of a fellowship from the Novo Nordisk Foundation as part of the Copenhagen Bioscience Ph.D. Programme, supported through grant NNF 18CC0033664. The authors declare that there are no competing interests associated with the contents of this article.

References

- 1 Park, J. *et al.* Synthesis of methyl ketones by metabolically engineered *Escherichia coli*. *J Ind Microbiol Biotechnol* **39**, 1703-1712, doi:10.1007/s10295-012-1178-x (2012).
- 2 Scognamiglio, J., Letizia, C. S. & Api, A. M. Fragrance material review on cyclohexyl methyl pentanone. *Food Chem Toxicol* **62 Suppl 1**, S138-143, doi:10.1016/j.fct.2013.07.056 (2013).
- 3 Smit, B. A., Engels, W. J. & Smit, G. Branched chain aldehydes: production and breakdown pathways and relevance for flavour in foods. *Appl Microbiol Biotechnol* **81**, 987-999, doi:10.1007/s00253-008-1758-x (2009).
- 4 He, Z. T. & Hartwig, J. F. Enantioselective alpha-functionalizations of ketones via allylic substitution of silyl enol ethers. *Nat Chem* **11**, 177-183, doi:10.1038/s41557-018-0165-x (2019).
- 5 Rodriguez, G. M. & Atsumi, S. Toward aldehyde and alkane production by removing aldehyde reductase activity in *Escherichia coli*. *Metab Eng* **25**, 227-237, doi:10.1016/j.ymben.2014.07.012 (2014).
- 6 Srirangan, K. *et al.* Engineering *Escherichia coli* for Microbial Production of Butanone. *Appl Environ Microbiol* **82**, 2574-2584, doi:10.1128/AEM.03964-15 (2016).
- 7 May, A. *et al.* A modified pathway for the production of acetone in *Escherichia coli*. *Metab Eng* **15**, 218-225, doi:10.1016/j.ymben.2012.08.001 (2013).
- 8 Walker, V. & Mills, G. A. 2-Pentanone production from hexanoic acid by *Penicillium roqueforti* from blue cheese: is this the pathway used in humans? *ScientificWorldJournal* **2014**, 215783, doi:10.1155/2014/215783 (2014).
- 9 Kunjapur, A. M. & Prather, K. L. Microbial engineering for aldehyde synthesis. *Appl Environ Microbiol* **81**, 1892-1901, doi:10.1128/AEM.03319-14 (2015).
- 10 Yang, H. *et al.* Metabolic engineering of *Escherichia coli* carrying the hybrid acetone-biosynthesis pathway for efficient acetone biosynthesis from acetate. *Microb Cell Fact* **18**, 6, doi:10.1186/s12934-019-1054-8 (2019).

- 11 Choi, K. R. *et al.* Systems Metabolic Engineering Strategies: Integrating Systems and Synthetic Biology with Metabolic Engineering. *Trends Biotechnol* **37**, 817-837, doi:10.1016/j.tibtech.2019.01.003 (2019).
- 12 Zhou, Y. *et al.* MiYA, an efficient machine-learning workflow in conjunction with the YeastFab assembly strategy for combinatorial optimization of heterologous metabolic pathways in *Saccharomyces cerevisiae*. *Metab Eng* **47**, 294-302, doi:10.1016/j.ymben.2018.03.020 (2018).
- 13 Zeng, W., Guo, L., Xu, S., Chen, J. & Zhou, J. High-Throughput Screening Technology in Industrial Biotechnology. *Trends Biotechnol* **38**, 888-906, doi:10.1016/j.tibtech.2020.01.001 (2020).
- 14 G. R. Lappin, L. C. Colorimetric Method for Determination of Traces of Carbonyl Compounds. *Analytical Chemistry* **23**, 541-542, doi:<https://doi.org/10.1021/ac60051a050> (1951).
- 15 Amlathe, S. & Gupta, V. K. Spectrophotometric determination of acetone using vanillin. *Analyst* **115**, 1385-1387, doi:10.1039/an9901501385 (1990).
- 16 Cavaleiro, A. M., Kim, S. H., Seppälä, S., Nielsen, M. T. & Nørholm, M. H. Accurate DNA assembly and genome engineering with optimized uracil excision cloning. *ACS Synth. Biol.* **4**, 1042-1046, doi:10.1021/acssynbio.5b00113 (2015).
- 17 Genee, H. J. *et al.* Software-supported *USER* cloning strategies for site-directed mutagenesis and DNA assembly. *ACS Synth. Biol.* **4**, 342-349, doi:10.1021/sb500194z (2015).
- 18 Hanahan, D. & Meselson, M. Plasmid screening at high colony density. *Methods Enzymol.* **100**, 333-342 (1983).
- 19 Blattner, F. R. *et al.* The complete genome sequence of *Escherichia coli* K-12. *Science* **277**, 1453-1462 (1997).
- 20 Banerjee, G. & Chattopadhyay, P. Vanillin biotechnology: the perspectives and future. *J Sci Food Agric* **99**, 499-506, doi:10.1002/jsfa.9303 (2019).
- 21 Luziatelli, F., Brunetti, L., Ficca, A. G. & Ruzzi, M. Maximizing the Efficiency of Vanillin Production by Biocatalyst Enhancement and Process Optimization. *Front Bioeng Biotech* **7**, doi:ARTN 279 10.3389/fbioe.2019.00279 (2019).
- 22 Lawrence, R. C. Use of 2,4-Dinitrophenylhydrazine for Estimation of Micro Amounts of Carbonyls. *Nature* **205**, 1313-&, doi:DOI 10.1038/2051313a0 (1965).

- 23 Lewis, S. A., Connatser, R. M., Olarte, M. V. & Keiser, J. R. Determining aromatic and aliphatic carboxylic acids in biomass-derived oil samples using 2,4-dinitrophenylhydrazine and liquid chromatography-electrospray injection-mass spectrometry/mass spectrometry. *Biomass Bioenerg* **108**, 198-206, doi:10.1016/j.biombioe.2017.10.043 (2018).
- 24 Soupene, E. *et al.* Physiological studies of Escherichia coli strain MG1655: Growth defects and apparent cross-regulation of gene expression. *Journal of Bacteriology* **185**, 5611-5626, doi:10.1128/Jb.185.18.5611-5626.2003 (2003).
- 25 Wang, J. G. *et al.* Converting Escherichia coli MG1655 into a chemical overproducer through inactivating defense system against exogenous DNA. *Syn Syst Biotechnol* **5**, 333-342, doi:10.1016/j.synbio.2020.10.005 (2020).
- 26 Mei, Z. *et al.* High-Throughput Fluorescence Assay for Ketone Detection and Its Applications in Enzyme Mining and Protein Engineering. *ACS Omega* **5**, 13588-13594, doi:10.1021/acsomega.0c00245 (2020).
- 27 Zhou, J. Y. *et al.* Carbonyl group-dependent high-throughput screening and enzymatic characterization of diaromatic ketone reductase. *Catal Sci Technol* **6**, 6320-6327, doi:10.1039/c6cy00922k (2016).
- 28 Ressmann, A. K. *et al.* Substrate-Independent High-Throughput Assay for the Quantification of Aldehydes. *Adv Synth Catal* **361**, 2538-2543, doi:10.1002/adsc.201900154 (2019).

Supplementary Data

Table S7.1. Oligonucleotides used in this work.

	Name	Sequence (5'→3')	Application	
1	U-SEVA43-F	ATCGCCCUAGGCCGCGGCCGCGCGA ATTCGA	USER cloning of elements of the rhamnose expression system (RhaS-RhaR/P _{rhaBAD}), to build the vector pSEVA43R	
2	U-SEVA43-R	AAAGGCAUCAAAATAAAACGAAAGGCT CAGTC		
3	U- <i>rhaSR</i> -F	ATGCCTTUAATTAAAGCGGATAACAA TTTCAC		
4	U- <i>rhaSR</i> -R	AGGGCGAUCGCCTCAGCGAATTTCA TTACGA		
5	U-SEVA43R-F	AGGCGTCGUGACTGGGAAAACCCTG GCG	USER cloning to assemble a canonical acetone production pathway. Oligonucleotides used for assembly of the <i>thl</i> , <i>ctfAB</i> , <i>adc</i> genes in vector pSEVA43R; synthetic RBSs for each gene were added in the oligonucleotide sequences	
6	U-SEVA43R-R	ACCTCCUACCGCGGCCTAGGGCGA		
7	U- <i>thl</i> -F	AGGAGGUTAGTTAGAATGAAAGAAG		
8	U- <i>thl</i> -R	TTCAUTTTAATCCCTCCTTTTCTAGC		
9	U- <i>ctfAB</i> -F	AAA AUGAACTCTAAAATAATTAGATT		
10	U- <i>ctfAB</i> -R	ACAGCCAUGGGTCTAAGTTCATTGG		
11	U- <i>adc</i> -F	ATGGCTGUTTAGTTT TAGGAAGGTGA CT		
12	U- <i>adc</i> -R	ACGACGCCUTACTTAAGATAATCATA TATAA		
13	U-SEVA43R- <i>adc</i> -F	ATTTATGAUTTAGGAAGGTGACTTTT		USER cloning to exchange <i>ctfAB</i> with <i>atoDA</i> genes to build a synthetic acetone production pathway
14	U-SEVA43R- <i>thl</i> -R	AGCACTTUTCTAGCAATATTGC TGT		
15	U- <i>atoDA</i> -for	ATCATAAAUCACCCCGTTGCGT ATT		
16	U- <i>atoDA</i> -rev	AGAAAAGUGCTAGAAAAGGAGG GATTA		

Table S7.2. Gene fragments used in this work.

Description	Sequence (5'→3')
Sequence encoding the <i>thl</i> gene	<p>ATGAAAGAAGTTGTAATAGCTAGTGCAGTAAGAACAGCGATTGGATCCTTATGGAAAGTCTCTTAAGGATGTACCAGCAGTAGATTTAGGAGCTACAGCTATAAAGGAAGCAGTTAAAAAGCAGGAATAAAACCAGAGGATGTTAATGAAGTCATTTTAGGAAATGTTCTTCAAGCAGGTTTAGGACAGAATCCAGCAAGACAGGCATCTTTTAAAGCAGGATTACCA GTTGAAATCCAGCTATGACTATTAATAAGGTTTGTGGTTCAGGACTTAGAACAGTTAGCTTAGCAGCACAAAATTATAAAAGCAGGAGATGCTGACGTAATAATAGCAGGTGGTATGGAAAATATGTCTAGAGCTCCTTACTTAGCGAATAACGCTAGATGGGGATATAGAATGGGAAACGCTAAATTTGTTGATGAAATGACTGACGCTGAGAGATGTTGGGATGCATTTAATGATTACCACATGGGAATAACAGCAGAAAACATAGCTGAGAGATGGAACATTTTCAAGAGAACAAGATGAGTTTGTCTTTCATCACAAAAAAGCTGAAGAAGCTATAAAATCAGGTCAATTTAAAGATGAAATAGTTCCTGTAGTAATTAAGGCAGAAAGGGA GAAACTGTAGTTGATACAGATGAGCACCTAGATTTGGATCAACTATAGAAGGACTTGCAAAATTAACCTGCCTTCAAAAAAGATGGAACAGTTACAGCTGGTAATGCATCAGGATTAATGACTGTGCAGCAGTACTTGTAAATCATGAGTGCAGAAAAAGCTAAAGAGCTTTGGAGTAAAACCACTTGCTAAGATAGTTTCTTATGGTTCAGCAGGAGTTGACCCA GCAATAATGGGATATGGACCTTTCTATGCAACAAAAGCAGCTATTGAAAAAGCAGGT TGGACAGTTGATGAATFAGATTTAATAGAATCAAATGAAGCTTTTGCAGCTCAAAGT TTAGCAGTAGCAAAAGATTTAAAATTTGATATGAATAAAGTAAATGTAAATGGAGGA GCTATTGCCCTTGGTCATCCAATTGGAGCATCAGGTGCAAGAATACTCGTTACTCTTGTACACGCAATGCAAAAAAGAGATGCAAAAAAGGCTTAGCAACTTTATGTATAGGT GGCGGACAAGGAACAGCAATATTGCTAGAAAAGTGCTAG</p>
Sequence encoding the <i>ctfAB</i> genes	<p>ATGATTAATGATAAAAACCTAGCGAAAGAAATAATAGCCAAAAGAGTTGCAAGAGAA TTAAAAAATGGTCAACTTGTAACTTAGGTGTAGGTCTTCCCTACCATGGTTGCAGAT TATATACCAAAAAATTTCAAATTACTTTCCAATCAGAAAACGGAATAGTTGGAATGG GCGCTAGTCCTAAAAATAATGAGGCAGATAAAGATGTAGTAAATGCAGGAGGAGACT ATACAACAGTACTTCCCTGACGGCACATTTTTTCGATAGCTCAGTTTCGTTTTCACTAA TCCGTGGTGGTCACGTAGATGTTACTGTTTTAGGGGCTCTCCAGGTAGATGAAAAG GGTAATATAGCCAATTGGATTGTTCCCTGAAAAATGCTCTCTGGTATGGGTGGAGC TATGGATTTAGTAAATGGAGCTAAGAAAGTAATAATTGCAATGAGACATACAAATAA AAGTCAACCTAAAATTTAAAAAATGTACACTTCCCTCACGGCAAAGTCTCAAGC AAATCTAATTGTAACAGAACTTGGAGTAATTGAGGTTATTAATGATGGTTTACTTCT CACTGAAATTAATAAAAACACAACCATTGATGAAATAAGGTCTTTAACTGCTGCAGAT TTACTCATATCCAATGAACTTAGACCCATGGCTGTTTAG</p>
Sequence encoding the <i>atoDA</i> genes	<p>ATGGATGCGAAACAACGTATTGCGCGCCGTGTGGCGCAAGAGCTTCGTGATGGTGA CATCGTTAACTTAGGGATCGGTTTACCACAATGGTCGCCAATTAATTTACCGGAGG GTATTTCATATCACTCTGCAATCGGAAAACGGCTTCCCTCGGTTTAGGCCCGGTCACG ACAGCGCATCCAGATCTGGTGAACGCTGGCGGGCAACCGTGCGGTGTTTTACCGG TGCAGCCATGTTTGATAGCGCCATGTCATTTGCGCTAATCCGTGGCGGTCATATTG ATGCCTGCGTGCTCGGCGGTTTGCAAGTAGACGAAGAAGCAAACCTCGCGAACTGG GTAGTGCCTGGGAAAATGGTGCCCGGTATGGGTGGCGCGATGGATCTGGTGACCG GGTGCGGCAAAGTGATCATCGCCATGGAACATTGCGCCAAAGATGGTTCAGCAAAAA TTTTGCGCCGCTGCACCATGCCACTCACTGCGCAACATGCGGTGCATATGCTGGTT ACTGAACTGGCTGTCTTTCGTTTTATTGACGGCAAATGTGGCTCACCGAAATGCGG GACGGGTGTGATTTAGCCACCGTGCCTGCCAAAACAGAAGCTCGGTTTGAAGTCGG CGCCGATCTGAATACGCAACGGGGTGATTTATGA</p>

Table S7.3. Composition of the M9 minimal medium.

Component	Final concentration
Na ₂ HPO ₄ ·7H ₂ O	12.8 g L ⁻¹
KH ₂ PO ₄	3 g L ⁻¹
NaCl	0.5 g L ⁻¹
NH ₄ Cl	1 g L ⁻¹
MgSO ₄	2 mM
CaCl ₂	0.1 mM
Carbon source	As indicated in the text

Procedure to prepare M9 minimal medium

1. Prepare solution of M9 salts (10×).

To make M9 salts, to 800 mL of H₂O add:

- 128 g Na₂HPO₄·7H₂O
- 30 g KH₂PO₄
- 5 g NaCl
- 10 g NH₄Cl

Stir until dissolved, adjust to 1000 mL with distilled H₂O, and sterilize by autoclaving.

2. Measure ~800 mL of distilled H₂O (sterile).
3. Add 100 mL of M9 salts.
4. Add 2 mL of 1 M MgSO₄ (sterile).
5. Add 50 mL of 20% (w/v) glucose (or other carbon source, as indicated).
6. Add 100 μL of 1 M CaCl₂ (sterile).
7. Adjust to 1,000 mL with distilled H₂O.

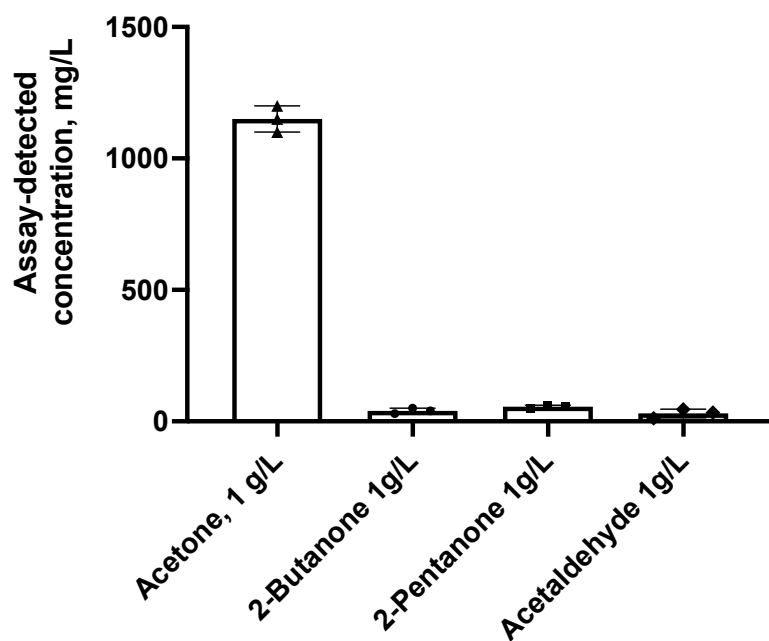


Figure S7.1. Vanillin-based detection of acetone, 2-butanone, 2-pentanone, and acetaldehyde. The average of three independent experiments is shown along the individual measurement. Bars represent standard deviation.

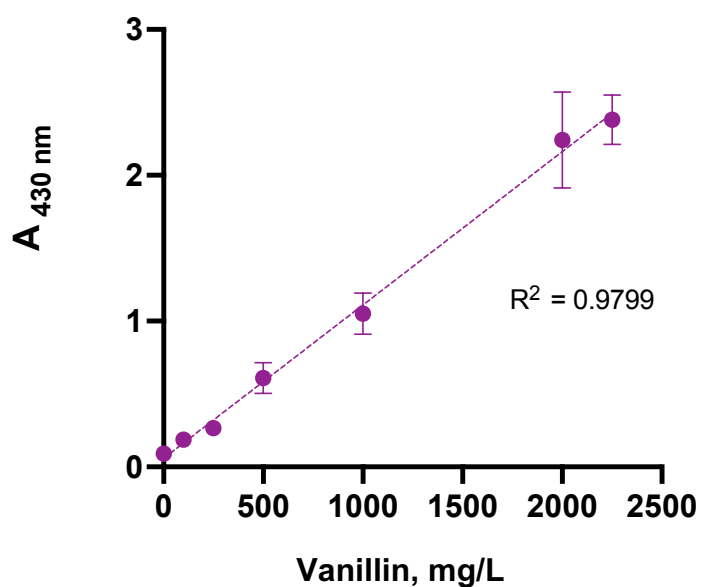


Figure S7.2. Acetone-based detection of vanillin. The average of three independent experiments is shown along the individual measurement. Bars represent standard deviation.

CONCLUSIONS AND OUTLOOK

Closing remarks

As a global society, our most urgent goal is to re-think, re-design, re-invent and adapt the industrial advances from the last century to novel sustainable production platforms. Microbial cell factories provide an opportunity to establish alternative processes towards consolidating a circular bioeconomy, which can be unlocked by concerted research and optimization efforts. Advances in automation, standardization, DNA synthesis and genome engineering, as well as high-throughput screening methods, enabled the implementation of systematic metabolic engineering. Improved computational algorithms and the raise of machine learning are expected to further reduce the time and costs for the design-build-test-learn circle, paving the way towards green manufacturing (**Chapter 1**). The projects presented in this Ph.D. thesis contribute to the field of metabolic engineering by making a step towards empowering sustainable bioproduction.

The work of this thesis was focused on developing CRISPR-Cas9 technologies to explore and manipulate the metabolism of the soil bacterium *Pseudomonas putida* towards establishing robust cell factories for bioproduction. The scope of these synthetic biology tools reaches into other environmental bacteria besides *Pseudomonas*, helping to improve bio-based chemical synthesis, and providing insights on engineering metabolism. The toolset developed includes: (i) genome-engineering approaches based on I-SceI-mediated homologous recombination assisted by CRISPR-Cas9 counterselection, **Chapter 2**; (ii) an expanded CRISPRi toolbox for tuning gene expression, **Chapter 3**; and (iii) unconstrained genome editing approach of nucleotide substitution using CRISPR-nCas9-guided deamination and DNA repair, **Chapter 4**. This Ph.D. thesis also demonstrated potential applications of the toolset. In **Chapter 5**, model-guided dynamic CRISPRi control of metabolic fluxes improved acetyl-CoA-dependent accumulation poly(3-hydroxybutyrate) as biopolymer precursor.

By manipulating the cell morphology (adapting the CRISPRi system presented in **Chapter 3**) of the engineered strains (with the help of the genome engineering approach presented in **Chapter 2**), biopolymer accumulation was further increased in these cell factories. These efforts illustrated how CRISPRi technologies benefit strain development programmes. Balancing growth, resources and competing essential pathways is an important strategy to increase product titres, yields and productivities. In **Chapter 5**, bioproduction upscaling under controlled conditions in the commercial Ambr²⁵⁰ fermentation system resulted in improved yields and titres compared to shaken flask-fermentations. Further exploration of CRISPR-Cas9 technologies will provide access to industrial large-scale processes applications.

Another application of the tools is presented in **Chapter 6** by providing insights on bioproduction alternatives. Using the developed base editor (**Chapter 4**), strains of *P. putida* were engineered to produce catalytically active mini-cells. Combined efforts of synthetic morphology and pathway engineering resulted in chromosome-free vesicles which were able to produce 2-pentanone, a commercially relevant methyl-ketone. CRISPR-mediated nucleotide editing has only recently been developed and established in bacteria but is already widely adapted for multiple purposes. This strategy enables efficient integration of single-nucleotide resolution mutations or even simultaneous multiplex editing without introducing (lethal) double-stranded DNA breaks. In this way, one can generate, for example, loss-of-function mutations by integrating premature translational stop codon into coding sequences. Importantly, nucleotide editing can also be used along with CRISPRi for manipulating bacterial transcription levels: changing promoter strength towards in(de)creased transcription or integrating an alternative start codon into the reading frame (**Chapter 4**).

The vast landscape of engineering opportunities afforded by base editors is yet to be fully explored and characterized (e.g. creating complex phenotypes and building libraries to remodel transcription, among many other exciting prospects). Additionally, **Chapter 7** describes the development of colorimetric assays to further improve bioproduction titers of industrially-relevant ketones and aldehydes, which is not only critical for designed strains in **Chapter 6**, but also important for characterizing bioproduction in mini-

cells as well as biosynthesis *in vitro*. High-throughput screening and selection systems play a key role to further improve microbial cell factory performance.

While CRISPR-based strategies provide a range powerful tool for genome-wide regulation, there are some challenges to address towards industrial bioproduction. The main ones are (i) system stability, (ii) Cas9 enzyme toxicity, (iii) restricted target scope due to narrow PAM sequence requirements, and (iv) potential off-target effect. Thus, CRISPR-based systems should be carefully designed with respect to targets and the host organism.

In this sense, (i) multiplexing of gRNA towards desired targets and integration of the CRISPR-d(n)Cas9 module into the chromosome is a way to ensure system stability. When the desired goal is reached, d(n)Cas9 expression can be dynamically regulated. (ii) Fine-tuning of dCas9 production in a host of choice (weak promoters or inducible expression) can be used to overcome the toxicity. (iii) The requirement of a PAM sequence limits the number of potential target sequences, but target flexibility can be addressed either by expanding the scope of alternative enzyme variants or by directed evolution of Cas9 to recognize non-canonical PAM sequences. (iv) Off-target effect is a common bottleneck of CRISPR technologies. In most cases, the careful design of the gRNA containing specific 5-nucleotide seed sequences can reduce the impact of off-target effects, and there are multiple bioinformatic tools available to navigate the choice of the correct sequence. A machine-learning approach, combined with structural biology advances can reveal even more insights on the seed sequence requirements and improve further spacer design. It is worth mentioning that off-target effects are certainly more prominent in organisms containing large genomes (e.g. higher eukaryotes, such as humans). Industrial biotechnology can benefit from the smaller size of bacterial genomes. Regardless, further improvement to overcome the challenges mentioned is needed for feasible, widespread application of the CRISPR-Cas9 technologies.

One way or the other, the continuous contributions to the field of metabolic engineering and cell factory development, assisted by CRISPR-Cas9 approaches and other emerging synthetic biology technologies, will help building reliable cell factories. May this scenario bring a Sustainable Revolution already in the XXI century? Answering this question, and addressing the exciting prospect it represents, will be the subject of intense research efforts over the years to come.

Declaration of co-authorship at DTU

If a PhD thesis contains articles (i.e. published journal and conference articles, unpublished manuscripts, chapters, etc.) written in collaboration with other researchers, a co-author statement verifying the PhD student's contribution to each article should be made.

If an article is written in collaboration with three or less researchers (including the PhD student), all researchers must sign the statement. However, if an article has more than three authors the statement may be signed by a representative sample, cf. article 12, section 4 and 5 of the Ministerial Order No. 1039, 27 August 2013. A representative sample consists of minimum three authors, which is comprised of the first author, the corresponding author, the senior author, and 1-2 authors (preferably international/non-supervisor authors).

DTU has implemented the Danish Code of Conduct for Research Integrity, which states the following regarding attribution of authorship:

"Attribution of authorship should in general be based on criteria a-d adopted from the Vancouver guidelines¹, and all individuals who meet these criteria should be recognized as authors:

- a. Substantial contributions to the conception or design of the work, or the acquisition, analysis, or interpretation of data for the work, *and*
- b. drafting the work or revising it critically for important intellectual content, *and*
- c. final approval of the version to be published, *and*
- d. agreement to be accountable for all aspects of the work in ensuring that questions related to the accuracy or integrity of any part of the work are appropriately investigated and resolved."²

For more information regarding definition of co-authorship and examples of authorship conflicts, we refer to DTU Code of Conduct for Research Integrity (pp. 19-22).

By signing this declaration, co-authors permit the PhD student to reuse whole or parts of co-authored articles in their PhD thesis, under the condition that co-authors are acknowledged in connection with the reused text or figure.

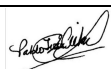
It is **important** to note that it is the responsibility of the PhD student to obtain permission from the publisher to use the article in the PhD thesis³

¹ International Committee of Medical Journal Editors – Recommendations for the Conduct, Reporting, Editing, and Publication of Scholarly Work in Medical Journals, updated December 2016

² DTU Code of Conduct for Research Integrity (E-book p. 19)

³ Many journals will allow you to use only the post-print version of your article, meaning the accepted version of the article, without the publisher's final formatting. In the event that your article is submitted, but still under review, you should of course use the latest submitted version of your article in your thesis. Always remember to check your publisher's guidelines on reuse of published articles. Most journals, unless open access, have an embargo period on published articles, meaning that within this period you cannot freely use the article. Check your publisher's rules on this issue.

Title of article		
pAblo pCasso vectors for unconstrained CRISPR-SpRY cytidine and adenosine base-editing <i>and</i> self-curing in <i>Pseudomonas putida</i>		
Journal/conference		
Manuscript in preparation		
Author(s)		
Ekaterina Kozaeva, Zacharias Søgaard Nielsen, Pablo I. Nikel		
Name (capital letters) and signature of PhD student		
EKATERINA KOZAEVA 		
PhD student's date of birth		
27.08.1993		
Declaration of the PhD student's contribution		
<i>For each category in the table below, please specify the PhD student's contribution to the article as appropriate (please do not fill in with names or x's)</i>		
Category	Minor contribution to the work <i>(please specify the nature of the PhD student's contribution)</i>	Substantial contribution to the work <i>(please specify the nature of the PhD student's contribution)</i>
Formulation of the conceptual framework and/or planning of the design of the study including scientific questions		The work presented in this manuscript was conceptualized and planned mainly by the PhD student.
Carrying out of experiments/data collection and analysis/interpretation of results		Most experimental results were collected, analyzed, and interpreted by PhD student including the data gathered by Z. S. Nielsen during the Master thesis under the supervision of PhD student.
Writing of the article/revising the manuscript for intellectual content		The manuscript draft and data visualization were prepared by the PhD student.
Signatures		

Title of article			
pAblO pCasso vectors for unconstrained CRISPR-SpRY cytidine and adenosine base-editing <i>and</i> self-curing in <i>Pseudomonas putida</i>			
Journal/conference			
Manuscript in preparation			
Author(s)			
Ekaterina Kozaeva, Zacharias Søgaard Nielsen, Pablo I. Nikel			
Name (capital letters) and signature of PhD student			
EKATERINA KOZAEVA			
PhD student's date of birth			
27.08.1993			
Date	Name	Title	Signature
14.11.21	Zacharias S. Nielsen	MSc	
26.11.21	Pablo Ivan Nikel	Sr Researcher	

Please note that by signing this declaration, co-authors permit the PhD student to reuse whole or parts of co-authored articles in their PhD thesis, under the condition that co-authors are acknowledged in connection with the reused text or figure.

Declaration of co-authorship at DTU

If a PhD thesis contains articles (i.e. published journal and conference articles, unpublished manuscripts, chapters, etc.) written in collaboration with other researchers, a co-author statement verifying the PhD student's contribution to each article should be made.

If an article is written in collaboration with three or less researchers (including the PhD student), all researchers must sign the statement. However, if an article has more than three authors the statement may be signed by a representative sample, cf. article 12, section 4 and 5 of the Ministerial Order No. 1039, 27 August 2013. A representative sample consists of minimum three authors, which is comprised of the first author, the corresponding author, the senior author, and 1-2 authors (preferably international/non-supervisor authors).

DTU has implemented the Danish Code of Conduct for Research Integrity, which states the following regarding attribution of authorship:

"Attribution of authorship should in general be based on criteria a-d adopted from the Vancouver guidelines¹, and all individuals who meet these criteria should be recognized as authors:

- a. Substantial contributions to the conception or design of the work, or the acquisition, analysis, or interpretation of data for the work, *and*
- b. drafting the work or revising it critically for important intellectual content, *and*
- c. final approval of the version to be published, *and*
- d. agreement to be accountable for all aspects of the work in ensuring that questions related to the accuracy or integrity of any part of the work are appropriately investigated and resolved."²

For more information regarding definition of co-authorship and examples of authorship conflicts, we refer to DTU Code of Conduct for Research Integrity (pp. 19-22).

By signing this declaration, co-authors permit the PhD student to reuse whole or parts of co-authored articles in their PhD thesis, under the condition that co-authors are acknowledged in connection with the reused text or figure.

It is **important** to note that it is the responsibility of the PhD student to obtain permission from the publisher to use the article in the PhD thesis³

¹ International Committee of Medical Journal Editors – Recommendations for the Conduct, Reporting, Editing, and Publication of Scholarly Work in Medical Journals, updated December 2016

² DTU Code of Conduct for Research Integrity (E-book p. 19)

³ Many journals will allow you to use only the post-print version of your article, meaning the accepted version of the article, without the publisher's final formatting. In the event that your article is submitted, but still under review, you should of course use the latest submitted version of your article in your thesis. Always remember to check your publisher's guidelines on reuse of published articles. Most journals, unless open access, have an embargo period on published articles, meaning that within this period you cannot freely use the article. Check your publisher's rules on this issue.

Title of article		
Pathway and morphology engineering towards 2-pentanone biosynthesis in whole- and mini-cells of <i>Pseudomonas putida</i>		
Journal/conference		
Manuscript in preparation		
Author(s)		
Ekaterina Kozaeva, Kent K. Y. Tang, Pablo I. Nickel		
Name (capital letters) and signature of PhD student		
EKATERINA KOZAEVA 		
PhD student's date of birth		
27.08.1993		
Declaration of the PhD student's contribution		
<i>For each category in the table below, please specify the PhD student's contribution to the article as appropriate (please do not fill in with names or x's)</i>		
Category	Minor contribution to the work <i>(please specify the nature of the PhD student's contribution)</i>	Substantial contribution to the work <i>(please specify the nature of the PhD student's contribution)</i>
Formulation of the conceptual framework and/or planning of the design of the study including scientific questions		The work presented in this manuscript was conceptualized and planned mainly by the PhD student.
Carrying out of experiments/data collection and analysis/interpretation of results		Most experimental results were collected, analyzed, and interpreted by PhD student including the data gathered by K.K.Y. Tang during the Master thesis under the supervision of PhD student.
Writing of the article/revising the manuscript for intellectual content		The manuscript draft and data visualization were prepared by the PhD student.
Signatures		



Title of article			
Pathway and morphology engineering towards stable 2-pentanone biosynthesis in whole- and mini-cells of <i>Pseudomonas putida</i>			
Journal/conference			
Manuscript in preparation			
Author(s)			
Ekaterina Kozaeva, Kent K. Y. Tang, Pablo I. Nickel			
Name (capital letters) and signature of PhD student			
EKATERINA KOZAEVA			
PhD student's date of birth			
27.08.1993			
Date	Name	Title	Signature
2021.11.15	Kent Kang Yong Tang	Mr.	
26.11.2021	Pablo Ivan Nickel	Sr Researcher	

Please note that by signing this declaration, co-authors permit the PhD student to reuse whole or parts of co-authored articles in their PhD thesis, under the condition that co-authors are acknowledged in connection with the reused text or figure.



Declaration of co-authorship at DTU

If a PhD thesis contains articles (i.e. published journal and conference articles, unpublished manuscripts, chapters, etc.) written in collaboration with other researchers, a co-author statement verifying the PhD student's contribution to each article should be made.

If an article is written in collaboration with three or less researchers (including the PhD student), all researchers must sign the statement. However, if an article has more than three authors the statement may be signed by a representative sample, cf. article 12, section 4 and 5 of the Ministerial Order No. 1039, 27 August 2013. A representative sample consists of minimum three authors, which is comprised of the first author, the corresponding author, the senior author, and 1-2 authors (preferably international/non-supervisor authors).

DTU has implemented the Danish Code of Conduct for Research Integrity, which states the following regarding attribution of authorship:

"Attribution of authorship should in general be based on criteria a-d adopted from the Vancouver guidelines¹, and all individuals who meet these criteria should be recognized as authors:

- a. Substantial contributions to the conception or design of the work, or the acquisition, analysis, or interpretation of data for the work, *and*
- b. drafting the work or revising it critically for important intellectual content, *and*
- c. final approval of the version to be published, *and*
- d. agreement to be accountable for all aspects of the work in ensuring that questions related to the accuracy or integrity of any part of the work are appropriately investigated and resolved."²

For more information regarding definition of co-authorship and examples of authorship conflicts, we refer to DTU Code of Conduct for Research Integrity (pp. 19-22).

By signing this declaration, co-authors permit the PhD student to reuse whole or parts of co-authored articles in their PhD thesis, under the condition that co-authors are acknowledged in connection with the reused text or figure.

It is **important** to note that it is the responsibility of the PhD student to obtain permission from the publisher to use the article in the PhD thesis³

¹ International Committee of Medical Journal Editors – Recommendations for the Conduct, Reporting, Editing, and Publication of Scholarly Work in Medical Journals, updated December 2016

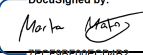
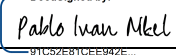
² DTU Code of Conduct for Research Integrity (E-book p. 19)

³ Many journals will allow you to use only the post-print version of your article, meaning the accepted version of the article, without the publisher's final formatting. In the event that your article is submitted, but still under review, you should of course use the latest submitted version of your article in your thesis. Always remember to check your publisher's guidelines on reuse of published articles. Most journals, unless open access, have an embargo period on published articles, meaning that within this period you cannot freely use the article. Check your publisher's rules on this issue.



Title of article		
Model-guided dynamic control of essential metabolic nodes boosts acetyl-coenzyme A-dependent bioproduction in rewired <i>Pseudomonas putida</i>		
Journal/conference		
Metabolic Engineering		
Author(s)		
Ekaterina Kozaeva, Svetlana Volkova, Marta RA Matos, Mariela P Mezzina, Tune Wulff, Daniel C Volke, Lars K Nielsen, Pablo I Nikel		
Name (capital letters) and signature of PhD student		
EKATERINA KOZAEVA 		
PhD student's date of birth		
27.08.1993		
Declaration of the PhD student's contribution		
<i>For each category in the table below, please specify the PhD student's contribution to the article as appropriate (please do not fill in with names or x's)</i>		
Category	Minor contribution to the work <i>(please specify the nature of the PhD student's contribution)</i>	Substantial contribution to the work <i>(please specify the nature of the PhD student's contribution)</i>
Formulation of the conceptual framework and/or planning of the design of the study including scientific questions		The work presented in this article was conceptualized mainly by the PhD student.
Carrying out of experiments/data collection and analysis/interpretation of results		Most experimental results in the article were gathered, analyzed, and interpreted by PhD student. Kinetic modelling development and omics analysis was done by Svetlana Volkova and Marta R.A. Matos.
Writing of the article/revising the manuscript for intellectual content		Initial draft and the figures were made by PhD student, the article was written, edited, and assembled by the PhD student with the help of co-authors.
Signatures		



Title of article			
Model-guided dynamic control of essential metabolic nodes boosts acetyl-coenzyme A-dependent bioproduction in rewired <i>Pseudomonas putida</i>			
Journal/conference			
Metabolic Engineering			
Author(s)			
Ekaterina Kozaeva, Svetlana Volkova, Marta RA Matos, Mariela P Mezzina, Tune Wulff, Daniel C Volke, Lars K Nielsen, Pablo I Nikel			
Name (capital letters) and signature of PhD student			
EKATERINA KOZAEVA			
PhD student's date of birth			
27.08.1993			
Date	Name	Title	Signature
11/10/2021	Svetlana Volkova	MSc	
11/16/2021	Marta Matos	PhD	
11/16/2021	Pablo Ivan Nikel	Sr Researcher	
11/16/2021	Lars Nielsen	Professor	

Please note that by signing this declaration, co-authors permit the PhD student to reuse whole or parts of co-authored articles in their PhD thesis, under the condition that co-authors are acknowledged in connection with the reused text or figure.



Declaration of co-authorship at DTU

If a PhD thesis contains articles (i.e. published journal and conference articles, unpublished manuscripts, chapters, etc.) written in collaboration with other researchers, a co-author statement verifying the PhD student's contribution to each article should be made.

If an article is written in collaboration with three or less researchers (including the PhD student), all researchers must sign the statement. However, if an article has more than three authors the statement may be signed by a representative sample, cf. article 12, section 4 and 5 of the Ministerial Order No. 1039, 27 August 2013. A representative sample consists of minimum three authors, which is comprised of the first author, the corresponding author, the senior author, and 1-2 authors (preferably international/non-supervisor authors).

DTU has implemented the Danish Code of Conduct for Research Integrity, which states the following regarding attribution of authorship:

"Attribution of authorship should in general be based on criteria a-d adopted from the Vancouver guidelines¹, and all individuals who meet these criteria should be recognized as authors:

- a. Substantial contributions to the conception or design of the work, or the acquisition, analysis, or interpretation of data for the work, *and*
- b. drafting the work or revising it critically for important intellectual content, *and*
- c. final approval of the version to be published, *and*
- d. agreement to be accountable for all aspects of the work in ensuring that questions related to the accuracy or integrity of any part of the work are appropriately investigated and resolved."²

For more information regarding definition of co-authorship and examples of authorship conflicts, we refer to DTU Code of Conduct for Research Integrity (pp. 19-22).

By signing this declaration, co-authors permit the PhD student to reuse whole or parts of co-authored articles in their PhD thesis, under the condition that co-authors are acknowledged in connection with the reused text or figure.

It is **important** to note that it is the responsibility of the PhD student to obtain permission from the publisher to use the article in the PhD thesis³

¹ International Committee of Medical Journal Editors – Recommendations for the Conduct, Reporting, Editing, and Publication of Scholarly Work in Medical Journals, updated December 2016

² DTU Code of Conduct for Research Integrity (E-book p. 19)

³ Many journals will allow you to use only the post-print version of your article, meaning the accepted version of the article, without the publisher's final formatting. In the event that your article is submitted, but still under review, you should of course use the latest submitted version of your article in your thesis. Always remember to check your publisher's guidelines on reuse of published articles. Most journals, unless open access, have an embargo period on published articles, meaning that within this period you cannot freely use the article. Check your publisher's rules on this issue.



Title of article		
High-throughput colorimetric assays optimized for ketone and aldehyde detection produced by microbial cell factories		
Journal/conference		
Manuscript in preparation		
Author(s)		
Ekaterina Kozaeva*, Viviënne Mol*, Pablo I Nickel, Alex T. Nielsen *Co-first authors		
Name (capital letters) and signature of PhD student		
EKATERINA KOZAEVA 		
PhD student's date of birth		
27.08.1993		
Declaration of the PhD student's contribution		
<i>For each category in the table below, please specify the PhD student's contribution to the article as appropriate (please do not fill in with names or x's)</i>		
Category	Minor contribution to the work <i>(please specify the nature of the PhD student's contribution)</i>	Substantial contribution to the work <i>(please specify the nature of the PhD student's contribution)</i>
Formulation of the conceptual framework and/or planning of the design of the study including scientific questions		The work presented in this article was conceptualized by the PhD student.
Carrying out of experiments/data collection and analysis/interpretation of results		Experimental results in the article were gathered, analyzed, and interpreted by PhD student. DNPH assay optimization, application and characterization was done by Viviënne Mol.
Writing of the article/revising the manuscript for intellectual content		Initial draft and the figures were made by PhD student. The article was further written, edited, and assembled by the PhD student with the help of co-authors.



Title of article			
High-throughput colorimetric assays optimized for ketone and aldehyde detection produced by microbial cell factories			
Journal/conference			
Manuscript in preparation			
Author(s)			
Ekaterina Kozaeva*, Viviënne Mol*, Pablo I Nickel, Alex T. Nielsen *Co-first authors			
Name (capital letters) and signature of PhD student			
EKATERINA KOZAEVA			
PhD student's date of birth			
27.08.1993			
Signatures			
Date	Name	Title	Signature
11/15/2021	vivienne Mol	MSc	
11/15/2021	Alex T. Nielsen	Professor	
11/15/2021	Pablo Ivan Nickel	Sr Researcher	

Please note that by signing this declaration, co-authors permit the PhD student to reuse whole or parts of co-authored articles in their PhD thesis, under the condition that co-authors are acknowledged in connection with the reused text or figure.



Declaration of co-authorship at DTU

If a PhD thesis contains articles (i.e. published journal and conference articles, unpublished manuscripts, chapters, etc.) written in collaboration with other researchers, a co-author statement verifying the PhD student's contribution to each article should be made.

If an article is written in collaboration with three or less researchers (including the PhD student), all researchers must sign the statement. However, if an article has more than three authors the statement may be signed by a representative sample, cf. article 12, section 4 and 5 of the Ministerial Order No. 1039, 27 August 2013. A representative sample consists of minimum three authors, which is comprised of the first author, the corresponding author, the senior author, and 1-2 authors (preferably international/non-supervisor authors).

DTU has implemented the Danish Code of Conduct for Research Integrity, which states the following regarding attribution of authorship:

"Attribution of authorship should in general be based on criteria a-d adopted from the Vancouver guidelines¹, and all individuals who meet these criteria should be recognized as authors:

- a. Substantial contributions to the conception or design of the work, or the acquisition, analysis, or interpretation of data for the work, *and*
- b. drafting the work or revising it critically for important intellectual content, *and*
- c. final approval of the version to be published, *and*
- d. agreement to be accountable for all aspects of the work in ensuring that questions related to the accuracy or integrity of any part of the work are appropriately investigated and resolved."²

For more information regarding definition of co-authorship and examples of authorship conflicts, we refer to DTU Code of Conduct for Research Integrity (pp. 19-22).

By signing this declaration, co-authors permit the PhD student to reuse whole or parts of co-authored articles in their PhD thesis, under the condition that co-authors are acknowledged in connection with the reused text or figure.

It is **important** to note that it is the responsibility of the PhD student to obtain permission from the publisher to use the article in the PhD thesis³

¹ International Committee of Medical Journal Editors – Recommendations for the Conduct, Reporting, Editing, and Publication of Scholarly Work in Medical Journals, updated December 2016

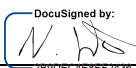
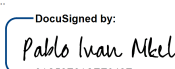
² DTU Code of Conduct for Research Integrity (E-book p. 19)

³ Many journals will allow you to use only the post-print version of your article, meaning the accepted version of the article, without the publisher's final formatting. In the event that your article is submitted, but still under review, you should of course use the latest submitted version of your article in your thesis. Always remember to check your publisher's guidelines on reuse of published articles. Most journals, unless open access, have an embargo period on published articles, meaning that within this period you cannot freely use the article. Check your publisher's rules on this issue.



Title of article		
Accelerated genome engineering of <i>Pseudomonas putida</i> by I- Sce I—mediated recombination and CRISPR - Cas9 counterselection		
Journal/conference		
Microbial Biotechnology		
Author(s)		
Nicolas T. Wirth, Ekaterina Kozaeva, Pablo I. Nikel		
Name (capital letters) and signature of PhD student		
EKATERINA KOZAEVA 		
PhD student's date of birth		
27.08.1993		
Declaration of the PhD student's contribution		
<i>For each category in the table below, please specify the PhD student's contribution to the article as appropriate (please do not fill in with names or x's)</i>		
Category	Minor contribution to the work <i>(please specify the nature of the PhD student's contribution)</i>	Substantial contribution to the work <i>(please specify the nature of the PhD student's contribution)</i>
Formulation of the conceptual framework and/or planning of the design of the study including scientific questions		CRISPR-Cas9 counter-selection system and previous characterization of fluorescent proteins were developed and designed by PhD student.
Carrying out of experiments/data collection and analysis/interpretation of results		The construction of CRISPR-Cas9 plasmids, prior tests of the system performance with different targets, protocol development and previous establishment of fluorescent reporter genes was carried out by the PhD student.
Writing of the article/revising the manuscript for intellectual content		The article was revised, edited, and approved by the PhD student, while the initial draft was made by N. Wirth.
Signatures		



Title of article			
Accelerated genome engineering of <i>Pseudomonas putida</i> by I- Sce I—mediated recombination and CRISPR - Cas9 counterselection			
Journal/conference			
Microbial Biotechnology			
Author(s)			
Nicolas T. Wirth, Ekaterina Kozaeva, Pablo I. Nikel			
Name (capital letters) and signature of PhD student			
EKATERINA KOZAEVA 			
PhD student's date of birth			
27.08.1993			
Date	Name	Title	Signature
11/10/2021	Nicolas T. Wirth	Ph.D.	
11/10/2021	Pablo Ivan Nikel	Sr Researcher	

Please note that by signing this declaration, co-authors permit the PhD student to reuse whole or parts of co-authored articles in their PhD thesis, under the condition that co-authors are acknowledged in connection with the reused text or figure.



Declaration of co-authorship at DTU

If a PhD thesis contains articles (i.e. published journal and conference articles, unpublished manuscripts, chapters, etc.) written in collaboration with other researchers, a co-author statement verifying the PhD student's contribution to each article should be made.

If an article is written in collaboration with three or less researchers (including the PhD student), all researchers must sign the statement. However, if an article has more than three authors the statement may be signed by a representative sample, cf. article 12, section 4 and 5 of the Ministerial Order No. 1039, 27 August 2013. A representative sample consists of minimum three authors, which is comprised of the first author, the corresponding author, the senior author, and 1-2 authors (preferably international/non-supervisor authors).

DTU has implemented the Danish Code of Conduct for Research Integrity, which states the following regarding attribution of authorship:

"Attribution of authorship should in general be based on criteria a-d adopted from the Vancouver guidelines¹, and all individuals who meet these criteria should be recognized as authors:

- a. Substantial contributions to the conception or design of the work, or the acquisition, analysis, or interpretation of data for the work, *and*
- b. drafting the work or revising it critically for important intellectual content, *and*
- c. final approval of the version to be published, *and*
- d. agreement to be accountable for all aspects of the work in ensuring that questions related to the accuracy or integrity of any part of the work are appropriately investigated and resolved."²

For more information regarding definition of co-authorship and examples of authorship conflicts, we refer to DTU Code of Conduct for Research Integrity (pp. 19-22).

By signing this declaration, co-authors permit the PhD student to reuse whole or parts of co-authored articles in their PhD thesis, under the condition that co-authors are acknowledged in connection with the reused text or figure.

It is **important** to note that it is the responsibility of the PhD student to obtain permission from the publisher to use the article in the PhD thesis³

¹ International Committee of Medical Journal Editors – Recommendations for the Conduct, Reporting, Editing, and Publication of Scholarly Work in Medical Journals, updated December 2016

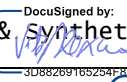
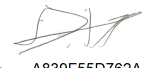
² DTU Code of Conduct for Research Integrity (E-book p. 19)

³ Many journals will allow you to use only the post-print version of your article, meaning the accepted version of the article, without the publisher's final formatting. In the event that your article is submitted, but still under review, you should of course use the latest submitted version of your article in your thesis. Always remember to check your publisher's guidelines on reuse of published articles. Most journals, unless open access, have an embargo period on published articles, meaning that within this period you cannot freely use the article. Check your publisher's rules on this issue.



Title of article		
An expanded CRISPRi toolbox for tunable control of gene expression in <i>Pseudomonas putida</i>		
Journal/conference		
Microbial Biotechnology		
Author(s)		
Christos Batianis*, Ekaterina Kozaeva*, Stamatios G Damalas*, María Martín-Pascual, Daniel C Volke, Pablo I Nikel, Vitor A P Martins Dos Santos		
* Joint first authours		
Name (capital letters) and signature of PhD student		
EKATERINA KOZAEVA 		
PhD student's date of birth		
27.08.1993		
Declaration of the PhD student's contribution		
<i>For each category in the table below, please specify the PhD student's contribution to the article as appropriate (please do not fill in with names or x's)</i>		
Category	Minor contribution to the work <i>(please specify the nature of the PhD student's contribution)</i>	Substantial contribution to the work <i>(please specify the nature of the PhD student's contribution)</i>
Formulation of the conceptual framework and/or planning of the design of the study including scientific questions		The work presented in this article was conceptualized by the PhD student in collaboration with co-authors.
Carrying out of experiments/data collection and analysis/interpretation of results	Experiments of C. Batianis were based on previous work of S. G. Damalas.	Most experimental results in the article were gathered, analyzed, and interpreted by PhD student. Vectors pGCRI-R, pGCRI_yfp, pGCRI_ftsZ, pGCRI_pyrF, pCRIMc were constructed and tested by C. Batianis.
Writing of the article/revising the manuscript for intellectual content	Figure 4 was done by C. Batianis based on previous work of S. G. Damalas.	The article was drafted by the PhD student as well as Figures 1, 2, 3, 5, 6, 7 with revisions from co-authors. crRNA-based CRISPRi protocol were drafted by C. Batianis.



Title of article			
An expanded CRISPRi toolbox for tunable control of gene expression in <i>Pseudomonas putida</i>			
Journal/conference			
Microbial Biotechnology			
Author(s)			
Christos Batianis*, Ekaterina Kozaeva*, Stamatios G Damalas*, María Martín-Pascual, Daniel C Volke, Pablo I Nikel, Vitor A P Martins Dos Santos			
* Joint first authours			
Name (capital letters) and signature of PhD student			
EKATERINA KOZAEVA 			
PhD student's date of birth			
27.08.1993			
Signatures			
Date	Name	Title	Signature
October 10th, 2021	Pablo Ivan Nikel	Senior Researcher /Group Leader	
10/26/2021	Prof. Dr. Vitor Martins dos Santos	Professor Systems & Synthetic Biology	 DocuSigned by: 3D88269165254F8
10/26/2021	Christos Batianis	PhD Candidate	 DocuSigned by: C471511161EE4C5
10/26/2021	Stamatios Dalamas	PhD Candidate	 DocuSigned by: A830F55D762A403...

Please note that by signing this declaration, co-authors permit the PhD student to reuse whole or parts of co-authored articles in their PhD thesis, under the condition that co-authors are acknowledged in connection with the reused text or figure.

© **PhD Thesis 2021 Ekaterina Kozaeva**
Novo Nordisk Center for Biosustainability
Technical University of Denmark
All rights reserved



**Technical
University of
Denmark**